An evaluation of the therapeutic potential of human amniotic epithelial cells during ex-vivo donor lung perfusion

Chelsea Paige Griffiths

Abstract

Introduction: *Ex Vivo* Lung Perfusion (EVLP) provides a normothermic isolated environment for the evaluation and reconditioning of donor lungs deemed unsuitable for immediate transplantation and offers a unique opportunity to administer advanced therapeutics, such as cell-based therapies. Human Amniotic Epithelial Cells (hAECs) have been shown to have immunomodulatory properties that could reduce injury in donor lungs. Our aim was to assess the anti-inflammatory actions of hAECs when administered during EVLP to lungs declined for transplant due to poor organ function.

Methods: hAECs were isolated from term placenta through enzymatic digestion. In *in vitro* studies, THP-1 derived macrophage phagocytosis and activation was determined after treatment with hAECs for 6 hours. Neutrophils were migrated through an IL-1β activated Human Microvascular Endothelial Cells (HMEC)-1 monolayer, after treatment of hAECs. In *ex vivo* perfusion studies; human lungs declined for transplant were split, with 150 x 10^6 hAECs or the HTR-8/SVneo cell line administered to each single lung and perfused concurrently for up to 4 hours (n=3). Serial samples of perfusate and tissue biopsies were collected for ELISA, qPCR and immunofluorescence (IF).

Results: hAECs were isolated with 94 $\pm$ 4% purity, with an average isolation yielding 134.2 x 10^6 with viability >90%. hAECs reduced neutrophil transendothelial migration (p=0.0128). hAEC treatment of macrophages led to an increase in phagocytosis observed *in vitro* and a decrease in CXCL8 (p=0.0465) and TNFα (p=0.0158) expression. hAEC-treated lungs had significantly reduced TNFα expression in the tissue (p=0.0415). IF staining demonstrated reduced expression of CXCL8 and 3-nitrotyrosine in the hAEC-treated lungs compared to the HTR cell treated lungs.

Conclusion: *In vitro* assays demonstrated the potential of hAECs to minimise pro-inflammatory macrophage activation and neutrophil migration. hAEC-treated lungs led to a reduction in pro-inflammatory cytokine production and oxidative stress. hAECs may offer a therapeutic approach to reduce inflammation in donor lungs during EVLP.

Acknowledgements

On a more personal note, I would like to give a huge thank you to my loving family, you've always been there to provide encouragement when it was needed. Finally, thank you to my partner, Harvey Morgan, for putting up with my grumpiness and for providing endless support and cups of tea. Without you all I would not have been able to complete this project.

Contents

Table of Figures

Table of Tables

Abbreviations

3-NT	3-nitrotryosine
A1AT	Alpha-1 antitrypsin
AdhIL-10	Adenoviral interleukin-10
AM	Amnion membrane
APES	3-aminopropyltriethoxysilane
ATP	Adenosine triphosphate
BASCs	Bronchioalveolar stem cells
BCA	Bicinchoninic acid
BMI	Body mass index
BPD	Bronchopulmonary dysplasia
BSA	Bovine serum albumin
cDNA	Complementary deoxyribonucleic acid
CF	Cystic fibrosis
cGMP	Current Good Manufacturing Practice regulations
CK	Cytokeratin
CM	Conditioned media
CO	Cardiac output
COPD	Chronic pulmonary obstructive disease
CPB	Cardiopulmonary bypass
C-section	Caesarean section
CT	Cycle threshold
CV	Coefficient of variance
DAB	3, 3'-diaminobenzidine
DAMPs	Damage-associated molecular patterns
DBD	Donation after brain death
DCD	Donation after circulatory death
DI	Deionised water
DiO	3,3'-Dioctadecyloxacarbocyanine perchlorate
DLS	Dynamic light scattering
DMEM	Dulbecco's Modified Eagle Medium
DMSO	Dimethyl sulfoxide
ECMO	Extracorporeal membrane oxygenation
EDTA	Ethylenediaminetetraacetic acid
ELISA	Enzyme linked immunosorbent assay
ET	Endotracheal tube
EVLP	*Ex vivo* lung perfusion
EVs	Extracellular vesicles
FACS	Fluorescence activated cell sort
FasL	Fas ligand
FBS	Fetal bovine serum
FiO_2	Fraction of inspired oxygen
FSC	Forward scatter
H&E	Haemotoxylin and eosin
hAECs	Human amniotic epithelial cells

HBSS	Hanks balanced salt solution
HLA	Human leukocyte antigens
HMEC-1	Human microvascular endothelial cells-1
HMGB1	High mobility group box protein 1
HRP	Horseradish peroxidase
ICAM-1	Intracellular adhesion molecule-1
IF	Immunofluorescence
IFNγ	Interferon gamma
IHC	Immunohistochemistry
IL	Interleukin
IPF	Idiopathic pulmonary fibrosis
IRI	Ischemia reperfusion injury
ISEV	International Society for Extracellular Vesicles
ISHLT	The International Society of Heart and Lung Transplantation
LA	Left atrium
LPS	Lipopolysaccharide
LTx	Lung transplantation
MAPCs	Multipotent adult progenitor cells
MCP-1	Monocyte chemoattractant protein-1
MFI	Mean fluorescence intensity
MHC	Major histocompatibility complex
MIF	Migration inhibitory factor
MIP-2	Macrophage inflammatory protein-2
miRNA	microRNA
MMP9	Matrix metalloproteinase-9
MRC1	Mannose receptor phosphate 1
MSCs	Mesenchymal stem cells
MSD	Meso scale discovery
NADPH	Nicotinamide adenine dinucleotide phosphate
NF-κB	Nuclear factor kappa B
NHSBT	NHS Blood and Transplant Unit
NK	Natural killer
NTA	Nanoparticle tracking analysis
OCS	Organ care system
PA	Pulmonary artery
PaCO$_2$	Partial pressure of carbon dioxide
PaO$_2$	Partial pressure of oxygen
PAP	Pulmonary arterial pressure
PBS	Phosphate buffered saline
PES	Polyethersulfone
PFA	Paraformaldehyde
PGD	Primary Graft dysfunction
PMA	Phorbol 12-myristate 13-acetate
qPCR	Quantitative polymerase chain reaction
RBC	Red blood cells

ROS	Reactive oxygen species
RPMI	Roswell Park Memorial Institute
RVI	Royal Victoria Infirmary
SCS	Static cold storage
sICAM	Soluble ICAM
SIP	Sphingosine 1 phosphate
SSC	Side scatter
TBS	Tris buffered saline
TEM	Transmission electron microscopy
TGF-β	Transforming growth factor beta
THAM	Tromethamine
TLC	Total lung capacity
TLR	Toll like receptor
TNFα	Tumour nercrosis factor alpha
Tregs	Regulatory T cells
VCAM-1	Vascular cell adhesion molecule-1
VEGF	Vascular endothelial growth factor

1 Introduction

1.1 Lung transplantation

The first reported successful lung transplant was performed by James Hardy *et al,* in 1963, where they carried out a single lung transplant on a 58-year-old man with advanced lung cancer. The patient survived 18 days post-transplant but subsequently died of renal failure and infection (Hardy et al., 1963). More attempts were made to carry out single lung transplants with limited long-term success until the Toronto lung transplant group reported two cases of successful unilateral lung transplants with post-transplant survival rates beyond 26 months, after making improvements in immunosuppression and surgical techniques (Toronto Lung Transplant Group, 1986). The Toronto group also reported the first double lung transplant in 1988, after extensive research on canines and primates, with the patient showing excellent lung function post-transplant (Patterson et al., 1988). Lung transplant techniques have improved since these initial reports and now lung transplantation offers the only viable treatment option for selected patients with end-stage lung disease, such as chronic obstructive pulmonary disease (COPD), idiopathic pulmonary fibrosis (IPF) or cystic fibrosis (CF) (Diamond et al., 2017). These initial reports used donation after circulatory death (DCD) donors; but nowadays, donation after brain death (DBD) donors are more widely utilised for lung transplantation (LTx) than DCD (Krutsinger et al., 2015). In the UK, the NHS Blood and Transplant (NHSBT) reported 165 lung transplants were performed between 2018-2019 (NHSBT, 2019).

LTx is now a lifesaving treatment option which can extend and improve the quality of life of lung transplant recipients. However, currently the field of lung transplantation is facing two critical issues: the first involving a shortage of donor lungs available and secondly the occurrence of primary graft dysfunction (PGD) post-transplant.

1.1.1 Clinical utility of lung transplantation

A major challenge facing the field of LTx involves a shortage of donor lungs available compared to the number of patients on the active transplant waiting list (Figure 1-1). In 2018-2019 there was a 22% drop in the number of lung transplants occurring compared to 2017-2018 despite the number of patients on the transplant waiting list

staying relatively stagnant. The transplant rate for lungs is one of the lowest compared to the other organs, with only 13% of potential lungs from DBD organ donors and only 6% of potential lungs from DCD organ donors being transplanted in 2018-2019 (Figure 1-2) (NHSBT, 2019).
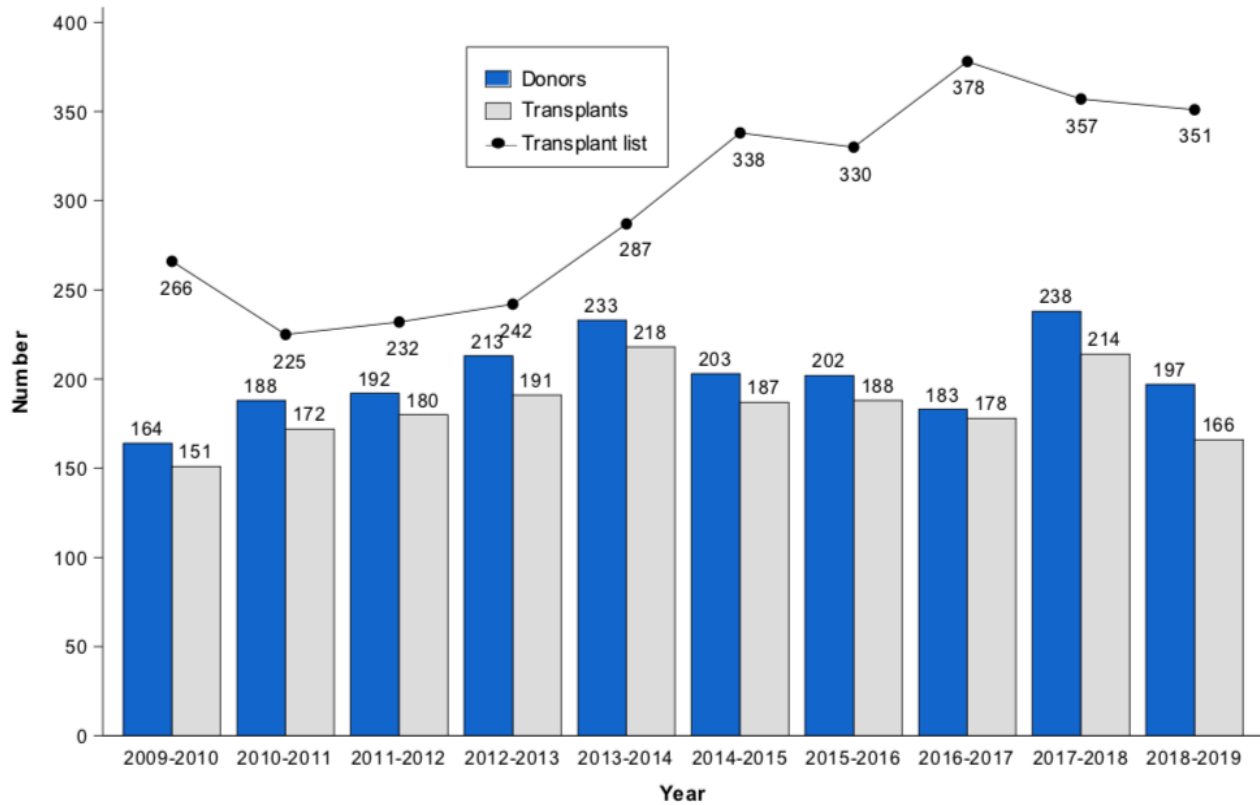
Figure 1-1 The number of lung donors, transplants and patients on the active transplant waiting list in the UK from April 2009 – March 2019.

There is an increasing number of lung donors however, the number of transplants occurring has decreased from previous years. The lung transplant waiting list is considerably higher than the number of transplants occurring (NHSBT, 2019).
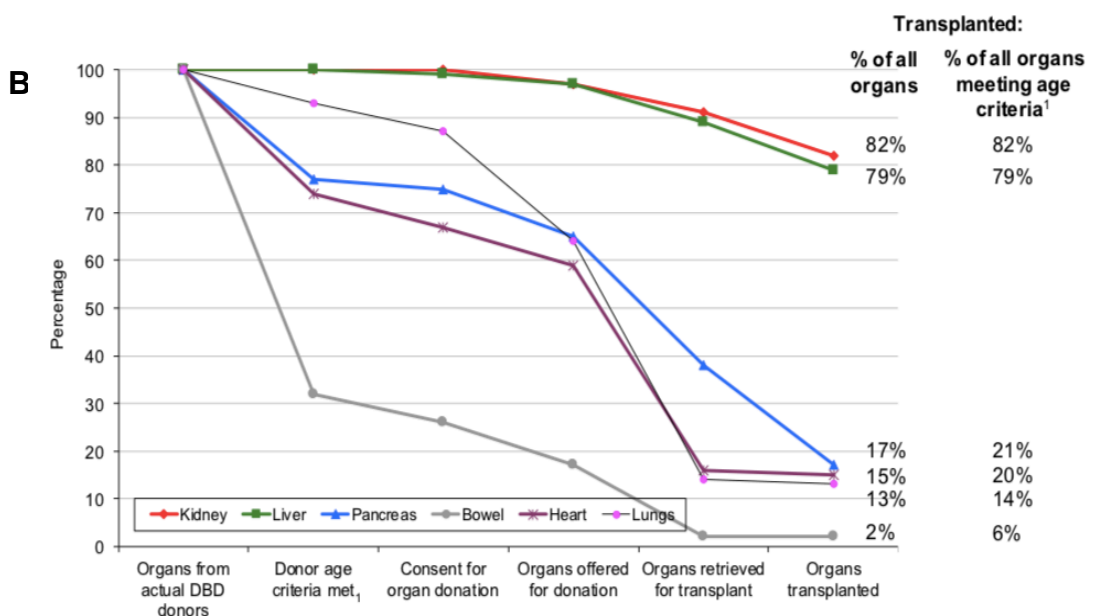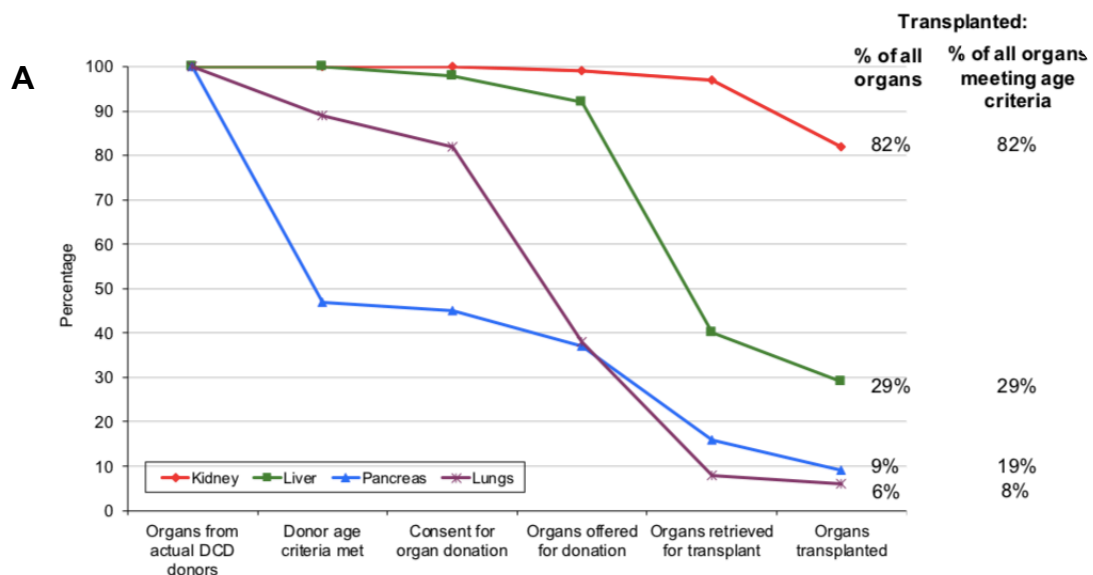
Figure 1-2 Donation and Transplantation rates from (A) DCD and (B) DBD organ donors in the UK between April 2018 – March 2019.

Organ donation pathway from point of offer to transplantation. Each stage presents an opportunity at which an organ may not be accepted or transplanted for (A) DCD donors (lungs highlighted with purple line) and (B) DBD donors (lungs highlighted with black/pink line). Transplantation rates are highest for kidney and liver, while other organs, particularly lungs, are one of the lowest despite consent being given (NHSBT, 2019).

One reason for the shortage of donor lungs available could be due to the strict "ideal" lung donor acceptance criteria set out by The International Society of Heart and Lung Transplantation (ISHLT), which limits the number of donor lungs that can be accepted for transplant (Table 1-1). However, due to the high numbers of patients on the transplant waiting list, there is a need to expand the donor pool of usable donor lungs for transplant (Orens et al., 2003). Therefore, most transplant centres agree that these acceptance criteria are too strict and so are more recently turning to the use of "marginal" or extended criteria donors. These extended criteria donors include those with a smoking history, aged over 55, donor lungs with an arterial partial pressure of oxygen (PaO_2) of 250-300 mmHg or a DCD donor. Use of these extended criteria donors is considered to be more of a risk but does not appear to impact lung transplant survival (Reyes et al., 2010). The ultimate judgment on whether extended criteria lungs are used for transplant is made based on the donor and recipient factors in that specific instance (Orens et al., 2003). Despite this effort, there is still a shortage of donor lungs suitable for transplant, leading to long active transplant waiting lists which increases the likelihood of mortality occurring in that time.

"Ideal" lung donor acceptance criteria
Age <55 years
ABO compatibility
Clear chest radiograph
PaO_2 >300 mmHg on FiO_2 = 1.0, PEEP 5 cm H_2O
Tobacco history <20 pack-years
Absence of chest trauma
No evidence of aspiration/sepsis
No prior cardiopulmonary surgery
Sputum gram stain – absence of organisms
Absence of purulent secretions at bronchoscopy

Table 1-1 The "ideal" donor lung acceptance criteria as established by ISHLT.

Any organ donors who fit these criteria would have their lungs taken for transplant, if they do not fit this criteria, they would be deemed unsuitable for transplant by ISHLT. (Adapted from Orens et al., 2003)

1.1.2 Primary graft dysfunction

PGD is major cause of early morbidity and mortality faced in the field of LTx; characterised by acute lung injury that occurs within 72 hours post-transplantation. The reported incidence rate of PGD has been conflicting but one multicentre study found 16.8% of patients developed PGD post-lung transplantation (Diamond et al., 2017). ISHLT published their standardised criteria to define and grade PGD in 2005, which was later updated in 2016 to provide expansion to the severity grading and clarity for clinical trials which use PGD as a trial outcome (Snell et al., 2017). PGD grade is based on three criteria; the ratio of PaO_2 to the fraction of inspired oxygen (FiO_2), the presence of diffuse alveolar infiltrates or pulmonary oedema on a chest radiograph and finally no other secondary cause of PGD identified (Table 1-2). These criteria are assessed at 24, 48 and 72 hours post-transplant (Christie et al., 2010; Snell et al., 2017). A more severe grade of PGD is associated with an increased mortality rate, increased complications, longer intensive care and overall hospital stays. Those with grade 3 PGD diagnosed at 48 hours were found to have poorer short-term and long-term survival rates compared to those who had grade 0-2 PGD (Whitson et al., 2007). Daud *et al,* reported that any grade of PGD was associated with a higher 90-day mortality compared to those with no PGD (Daud et al., 2007). This is supported by Christie *et al,* who demonstrated that grade 3 PGD was associated with a significantly increased mortality risk at 30 days post-transplant and this increased mortality risk continued to 1-year survival (Christie et al., 2010). Whitson *et al,* reported that grade 3 PGD patients had a 10-year survival rate of less than 25%. Therefore, PGD has a significant impact on both short and longer-term outcomes for transplant patients (Whitson et al., 2007).

The pathogenesis of PGD is multifactorial, with several points along the lung transplantation pathway from donor to recipient where potential risk factors for developing PGD can arise.

PGD grade	Pulmonary oedema on chest radiograph	PaO$_2$/FiO$_2$ ratio
Grade 0	No	Any
Grade 1	Yes	>300 mmHg (>40 kPa)
Grade 2	Yes	200 to 300 mmHg (27 to 40 kPa)
Grade 3	Yes	<200 mmHg (<27 kPa)

Table 1-2 PGD grade severity rating according to the revised 2016 ISHLT guidelines.

Presence of pulmonary oedema and a worsening of the PaO$_2$/FiO$_2$ ratio reflects the severity of the PGD grade. PGD grade plays a direct role in patient survival post-transplant. (Adapted from Snell et al., 2017)

1.1.2.1 Donor variables

Donor variables can be classified as inherent or acquired. Inherent donor characteristics include age, smoking history, race and gender (De Perrot et al., 2005). Christie *et al,* reported that incidence of PGD dramatically rose with donors aged above 45, suggesting a greater donor age is associated with an increased risk of PGD (Christie et al., 2003). A study evaluating 1,295 lung transplant procedures during 1999-2010, found patients who received lungs from donors with a known smoking history had worsened survival outcomes, longer hospital stays, and time spent in intensive care (20). Acquired donor risks include brain or circulatory death, prolonged ventilation, pneumonia, blood transfusions or haemodynamic instability before retrieval. Brain death can induce homeostatic dysregulation, disturb the endocrine system and result in a storm of pro-inflammatory cytokines, such as CXC ligand 8 (CXCL8) or interleukin (IL)-8, IL-12, IL-18, tumour necrosis factor-alpha (TNFα) and interferon-gamma (IFNγ), which all have deleterious effects on the lungs (De Perrot et al., 2005; Morrison et al., 2017). Increasingly, DCD donors are being used for lung transplantation, therefore Krutsinger *et al,* carried out a meta-analysis to determine their risk of PGD compared to DBD donors. They reported no significant difference in incidence rates of PGD between cohorts (Krutsinger et al., 2015). Use of extended criteria donors in lung transplantation also appears to increase the risk of PGD with Botha *et al,* reporting a higher incidence rate of grade 3 PGD of 43.9% with recipients who received extended criteria lungs compared to 27.4% of recipients who received standard donor lungs. They also reported a higher incidence of 90-day organ-specific mortality with recipients who received extended criteria donor lungs (Botha et al., 2006).

1.1.2.2 Recipient variables

Recipient variables can include gender, race, age, primary diagnosis resulting in the need for a lung transplant, co-morbidities and obesity. However, ISHLT have reported no association of recipient gender, race or age with the incidence rate of PGD (Diamond et al., 2017). Whitson *et al,* found out of 402 lung transplant recipients, a co-morbidity such as increased pulmonary arterial pressure (PAP) and the patient's primary diagnosis had significantly increased PGD incidence rates (Whitson et al., 2006). A systematic review of 10 studies into primary diagnosis, showed a PGD incidence of 11.8% in recipients with COPD, 12.4% with cystic fibrosis, 18.0% with IPF and 50% with sarcoidosis (Liu et al., 2014). Lederer *et al,* demonstrated through a cohort study of 512 lung transplant recipients, that those with obesity were associated with a two-fold increased risk of grade 3 PGD at 72 hours compared to those with a normal body mass index (BMI) (Lederer et al., 2011).

1.1.2.3 Operative variables

Finally, operative variables associated with PGD include the type of lung transplant (single or double), prolonged cold ischemic time, the need for cardiopulmonary bypass (CPB) or red blood cell transfusions (Diamond et al., 2017). Patients that underwent CPB after their lung transplant had a considerably lower graft survival, with only 80% surviving after one month compared to 93.3% of patients who didn't receive CPB (Aeba et al., 1994). Furthermore, intraoperative red blood cell transfusions are associated with increased mortality rates, longer hospital stays and an increased incidence rate of PGD of 39.3% compared to 5.9% of patients who underwent a plasma transfusion (Weber et al., 2013).

1.1.3 Ischemia Reperfusion Injury

Ischemia reperfusion injury (IRI) is believed to be the main mechanism initiating PGD, with higher mortality rates, prolonged ventilation, longer time spent in the intensive care unit and overall longer hospital stays with patients reported to have IRI (de Perrot et al., 2003; King et al., 2000). IRI is resultant from the cessation of normal blood flow through the lungs for a prolonged period of time, followed by the return of blood flow upon transplant. IRI triggers a series of events (Figure 1-3) involving the

7

formation of reactive oxygen species (ROS), endothelial cell activation, increased vascular permeability, the activation of neutrophils, macrophages, platelets and the complement system, all leading to surge in cytokine production (Table 1-3). This ultimately leads to pulmonary oedema, reduced gas transfer and lung functioning (Diamond & Christie, 2010; Ferrari & Andrade, 2015).

Cytokine/Chemokine	Main cell source	Function
TNFα	Macrophage, lymphocytes	Activates inflammatory pathways
IFNγ	Lymphocytes	Inflammation
MCP-1 (CCL2)	Monocytes, macrophages and epithelial cells	Macrophage chemotaxis
IL-1β	Macrophages, fibroblasts	Inflammation
IL-6	Macrophages, endothelial and epithelial cells	Inflammation
CXCL8 (IL-8)	Macrophages and epithelial cells	Neutrophil chemotaxis
IL-10	Macrophages, lymphocytes	Anti-inflammatory
IL-12	Macrophages	T cell activation
IL-18	Macrophages	T cell activation

Table 1-3 Cytokines and chemokines potentially involved in ischemia reperfusion injury (IRI) during lung transplantation.

IRI involves a storm of cytokines being produced leading to inflammation, macrophage polarisation and neutrophil activation and chemotaxis. (Adapted from de Perrot et al., 2003)

Lungs retrieved for transplantation are flushed with a cold preservation solution and hypothermically preserved whilst transported through static cold storage (SCS) to decrease the metabolic rate and energy requirement necessary for organ preservation until the lungs are transplanted into the recipient. During lung retrieval, the lungs are inflated and sealed, maintaining air within the alveolar sacs during transportation. This period of ischemic cold storage is usually kept between 4 to 8 hours (de Perrot et al., 2003). Although this ischemic period is needed and does not affect the lungs quite as significantly as other organs due to the presence of oxygen, it still leads to immune pathway activation and ROS production. The production of ROS, such as the hydroxyl radical, are highly unstable and can react with the lipid component of cell membranes leading to increased permeability and cell apoptosis. ROS can be produced by airway epithelial and endothelial cells in addition to alveolar macrophages. Ischemia also leads to a deficit in adenosine triphosphate (ATP) which

affects the transport of ions across the cell membrane leading to an accumulation of sodium. This results in water diffusing inside the cell, ultimately leading to pulmonary oedema formation. Reperfusion injury is then triggered by the production of the ROS and donor cell activation that resulted during ischemia, which in turn leads to the activation of recipient's immune system (de Perrot et al., 2003; Ferrari & Andrade, 2015).

It is believed that IRI occurs in a biphasic pattern with the early phase depending primarily on donor characteristics then the later phase depending on the recipient characteristics (Geudens et al., 2007). The initial ischemic phase involves activated alveolar macrophages and the production of cytokines such as TNFα, IFNγ and monocyte chemoattractant protein-1 (MCP-1) (Table 1-3). On the other hand, the later reperfusion phase involves the activation and migration of neutrophils (Ng et al., 2006). However, it should be remembered that PGD is a complex multi-factorial, interconnecting cellular response that ultimately leads to acute injury, of which IRI only plays one part.

1.1.3.1 Role of macrophages

Macrophages play an important role in the early phase of IRI. Fiser *et al,* demonstrated that macrophage inhibition through gadolinium chloride injected into donor lungs before the ischemic period functioned significantly better post transplantation (Fiser et al., 2001). In addition to producing ROS, alveolar macrophages produce large amounts of cytokines and procoagulant factors in response to oxidative stress (de Perrot et al., 2003). TNFα is predominately produced by macrophages and has been indicated to be a key initiating factor for IRI causing a complex inflammatory cascade as well as activating the endothelium, leading to the upregulation of chemotactic agents and adhesion molecules, which leads to the influx of neutrophils into the lungs. This can result in endothelium permeability leading to pulmonary oedema (Maxey et al., 2004). Innate immune receptors such as toll-like receptor-4 (TLR-4) expression on macrophages have also been implicated as an initiating step of IRI by signalling the activation of downstream inflammatory pathways (Merry et al., 2015). Pro-inflammatory M1 or "classically activated" macrophages appear to be the drivers behind this early phase of reperfusion injury (Lin et al., 2016; Lee et al., 2011). Increased expression of anti-

inflammatory M2 or "alternatively activated" macrophages, for example through the addition of dexamethasone, can show improved lung injury in rat lungs with IRI (Xiao et al., 2020).

1.1.3.2 Role of the endothelium

The endothelium plays a significant role in the production of ROS as endothelial cells are highly sensitive to the cessation of blood flow. The absence of blood flow stimulates the endothelium to activate NADPH oxidase, nuclear factor-κB (NF-κB) pathway and upregulates the expression of adhesion molecules, such as intracellular adhesion molecule-1 (ICAM-1) (de Perrot et al., 2003). NADPH oxidase is also activated on neutrophils, this over-stimulation of NADPH oxidase and ROS leads to oxidative stress and further drives inflammation (Chen & Date, 2015). Endothelial cell dysfunction caused by IRI appears to be associated with more severe grades of PGD, with Krenn *et al.,* demonstrating that recipients with grade 2 or 3 PGD had significantly higher serum concentrations of vascular endothelial growth factor (VEGF), a major regulator in vascular permeability, pre-transplant compared to those with less severe PGD (Krenn et al., 2007).

1.1.3.3 Role of neutrophils

Neutrophils also have a critical role in IRI and increasingly infiltrate the lungs during the first 24 hours post-transplant (de Perrot et al., 2003). Neutrophil infiltration into the lungs has been associated with lower PaO_2, higher PAP and microvascular permeability (Ng et al., 2006). Fiser *et al,* demonstrated that leukocyte filtration significantly attenuated the later phase of reperfusion injury (Fiser et al., 2001). The upregulation of surface markers on the endothelium leads to the adhesion of rolling neutrophils and their subsequent trans-migration across the endothelium (Schmidt et al., 2011). Neutrophils then catalyse the production of hypochlorous acid through the action of the myeloperoxidase enzyme, both of which damage the vascular endothelium. Eppinger *et al,* observed a gradual increase in microvascular permeability and progressive infiltration of neutrophils through myeloperoxidase activity after the first hour of reperfusion (Eppinger et al., 1995). Levels of CXCL8, a potent neutrophil chemotactic chemokine produced by alveolar macrophages, also appears to correlate with lung function. De Perrot *et al,* demonstrated CXCL8 levels 2 hours after reperfusion negatively correlated with lung function (De Perrot et al.,

2002). Furthermore, Fisher *et al,* found high levels of CXCL8 in lung tissue and bronchoalveolar lavage, measured in the donor lungs prior to transplant, were associated with the development of a more severe grade of PGD and early recipient mortality post-transplant (Fisher et al., 2001). This demonstrates that lung injury can also exist prior to IRI, highlighting the multifactorial and complex process during the donation pathway which can lead ultimately to PGD.
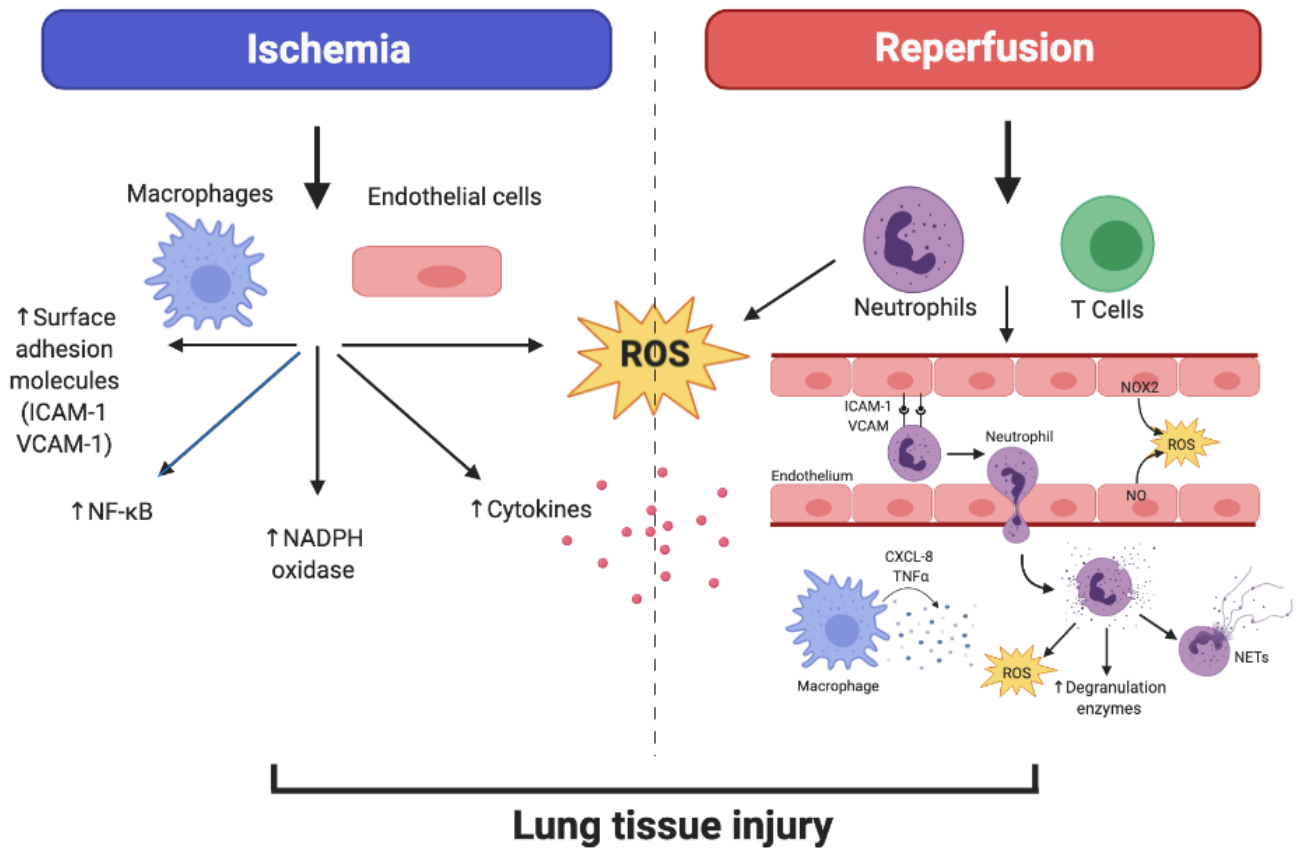
Figure 1-3 Summary of ischemia reperfusion injury events leading to lung tissue injury

Ischemia leads to the activation of alveolar macrophages and endothelial cells which results in a cascade of events including the production of reactive oxygen species (ROS), the upregulation of surface adhesion markers (ICAM-1 and VCAM-1) on the endothelium, cytokine production, the activation of the NK-κB pathway and NADPH oxidase. Upon reperfusion of the blood flow, there is an infiltration of recipient neutrophils and later T cells into the lungs. Due to the activation of endothelial cells, neutrophils trans-migrate through the endothelium releasing digestive enzymes leading to damage of the vasculature. The influx of neutrophils, the inflammatory environment and oxidative stress ultimately leads to lung injury resulting in pulmonary oedema.

1.2 *Ex vivo* lung perfusion

Ex vivo lung perfusion (EVLP) was first developed by Steen and colleagues in Lund, Sweden, as a clinical technique originally purposed for the assessment of lungs from DCD donors (Steen et al., 2001). In addition to the circuit, they developed Steen Solution™, a buffered salt solution with human serum albumin to provide optimal osmotic pressure and dextran 40 to protect the endothelium, preventing the formation of pulmonary oedema. Lungs are placed in an evaluation box and connected to the EVLP circuit. A pump drives the flow of the perfusate solution through an oxygenator, provided with a mixture of gases, and attached to a heater-cooler unit to maintain temperature; then passes through a leukocyte filter and finally into the pulmonary artery of the lungs (Figure 1-4). Pulmonary venous return from the left atrium (LA) is drained into a reservoir which then passes through to the pump again and around the circuit continuously throughout perfusion. The LA can either be left uncannulated as part of an open circuit and drain freely into the reservoir or be cannulated with tubing then connected to the reservoir in a closed circuit. A ventilator is attached to the lungs through the trachea to drive gas exchange. This is typically only started once the lungs have rewarmed to 32°C to avoid mechanical damage. Lungs are maintained at 37°C throughout perfusion (Wierup et al., 2006).
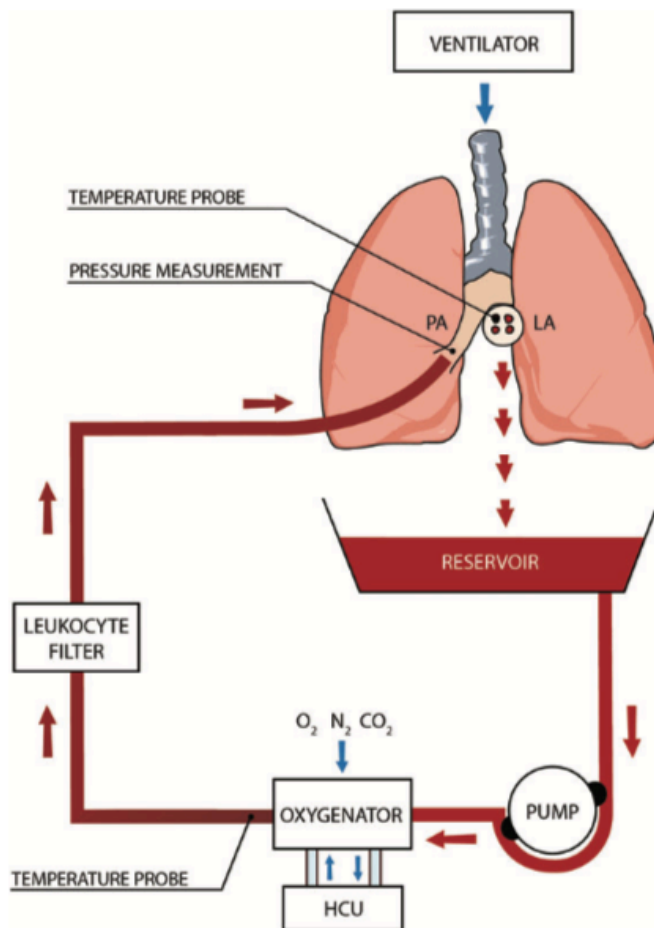
Figure 1-4 Schematic of the EVLP circuit.

Perfusate is pumped through the circuit passing through an oxygenator, heater cooler-unit (HCU) and leukocyte filter then entering into the lungs through the pulmonary artery (PA) and exiting through the left atrium (LA), then collecting in the reservoir before being pumped once again through the circuit. A ventilator is connected to the lungs through the trachea (Andreasson et al., 2014).

1.2.1 A platform for assessment and reconditioning

EVLP provides an opportunity to address the two clinical problems facing the field of LTx by offering a platform to assess, evaluate and recondition extended criteria donor lungs outside the body prior to transplant. This window of opportunity allows clinicians to assess extended criteria donor lungs in a normothermic isolated environment, providing an opportunity to carry out both visual and lung function assessments, thus allowing for more informed decision making. Cypel *et al,* reported a 20% rise in lung activity due to the use of EVLP at their transplant centre. They found out of 50 lungs that underwent EVLP prior to being transplanted showed no significant difference in PGD incidence post-transplant compared to the standard SCS transplant route. Fewer patients required extra corporeal membrane oxygenation (ECMO) in the EVLP group and the intensive care and overall hospital

stays were much the same between the groups (Cypel et al., 2012). Boffini *et al*, reported similar results after performing EVLP on 23 out of 75 lungs rejected for transplant, 7 of these were subsequently transplanted after meeting acceptance criteria during EVLP which increased their centre's activity by 30% (Boffini et al., 2013). Koch *et al*, carried out EVLP on 11 lungs initially deemed 'untransplantable', 9 of these lungs showed improved gas exchange during EVLP so were considered suitable and then successfully transplanted with no significant differences in hospital stay or outcomes compared to the standard donor lungs (Koch et al., 2018). Patients who have received EVLP lungs compared to standard donor lung recipients have similar survival rates up to 10-years with both groups reporting an improved quality of life (Ghaidan et al., 2019; Tikkanen et al., 2015). These studies highlight the potential for EVLP to assess the performance of extended criteria donor lungs that would otherwise be rejected and so could potentially increase the number of lungs suitable for transplantation. This could go some way to address the current clinical lung shortage being seen.

EVLP also has the potential to recondition extended criteria donor lungs, which could further expand the donor pool. Canine DCD lungs that underwent EVLP for 3.5 hours showed significantly improved lung oxygenation, less microthrombi, higher ATP levels compared to the SCS control. The EVLP lungs showed better post-transplant lung oxygenation compared to the SCS control (Nakajima et al., 2012). Mehaffey *et al,* showed that porcine lungs stimulated with LPS to induce sepsis that underwent EVLP showed improved oxygenation and compliance during EVLP and a significant reduction in oedema formation at the end compared to the *in vivo* control. Furthermore, they found a decrease in the production of IL-6 and vascular cell adhesion protein-1 (VCAM-1) expression in the lungs that underwent EVLP (Mehaffey et al., 2017). Andreasson *et al,* reported that 16 donor lungs that improved during EVLP and were transplanted with good outcomes showed a significantly lowered expression of tissue injury markers; high mobility group protein B1 (HMGB1) and syndecan-1,a glycocalyx component, both involved in immune cell influx into the lungs. Furthermore, they found anti-inflammatory IL-10 expression was upregulated (Andreasson et al., 2017). These studies suggest that EVLP can potentially recondition lung injury that occurs during IRI. Furthermore, EVLP also offers a platform to deliver therapeutics, which can be used to target established and prevent lung injury, to further the reconditioning of lungs prior to transplant.

1.2.2 Protocols

Since the initial platform was developed by the Lund group, differing philosophies of EVLP procedure have emerged from the Toronto and Hannover/Madrid groups (Table 1-4). These protocols differ in their perfusates, flow rate, arterial pressure and ventilatory settings. The Lund protocol involves the use of a red blood cell (RBC) supplemented perfusate with an open LA which drains into the reservoir. Furthermore, the Lund protocol involves perfusing at 100% cardiac output, with the aim to assess marginal lungs (Wierup et al., 2006; Steen et al., 2007). The Toronto group have an aim to prolong the perfusion time in order to potentially recondition injured lungs prior to transplant. Therefore, they modified their protocol to use an acellular perfusate to avoid haemolysis, a closed circuit with the LA cannulated to create positive LA pressure and a low flow of 40% of cardiac output to reduce vascular sheer stress (Cypel et al., 2011; Andreasson et al., 2014). Whilst the Lund and Toronto group protocols involve performing EVLP on lungs transported by SCS prior to transplant, the Hannover/Madrid protocol involves perfusing whilst the organ is in transit after being flushed at lung retrieval. The Hannover/Madrid group have developed the portable Organ Care System™ (OCS™) to assess and recondition lungs whilst in transit in order to reduce the cold ischemic time and allow for continuous organ monitoring and assessment from the donor to the recipient. The OCS™ protocol uses a RBC supplemented perfusate similarly to the Lund group protocol but also uses a low flow rate like the Toronto group protocol (Warnecke et al., 2012). There are now four commercial systems based off these three protocols: OCS™ (Transmedics, Andover, USA), Lung Assist™ (Organ Assist, Groningen, The Netherlands), LS™ (Vivoline Medical AB, Lund, Sweden) and XPS™ (XVIVO, Göteborg, Sweden) (Figure 1-5) (Possoz et al., 2019).

Parameter	Lund	Toronto	Hannover/Madrid (OCS™)
Perfusion			
Target flow	100% cardiac output	40% cardiac output	2.0-2.5 L/min
Pulmonary arterial pressure (mmHg)	≤20	≤15	≤20
Left atrial pressure (mmHg)	0 (open LA)	3-5	0 (open LA)
Pump	Roller	Centrifugal	Piston
Perfusate	2 L Steen Solution™ + RBC	2 L Steen Solution™	1.5 L 'OCS™ Lung Solution' + RBC
Ventilation			
Tidal volume (ml/kg)	6-8	7	6
Frequency	10-15	7	10
Peak end-expiratory pressure (cm H_2O)	5	5	5
Fraction of inspired oxygen (%)	50	21	21
Temperature			
Start of perfusion	15	25	32
Start of ventilation	32	32	32

Table 1-4 The current EVLP protocols for clinical lung transplantation.

The three EVLP protocols by the Lund, Toronto and Hannover/Madrid (OCS™) groups and how they differ to each other (Adapted from Andreasson, Dark and Fisher, 2014).
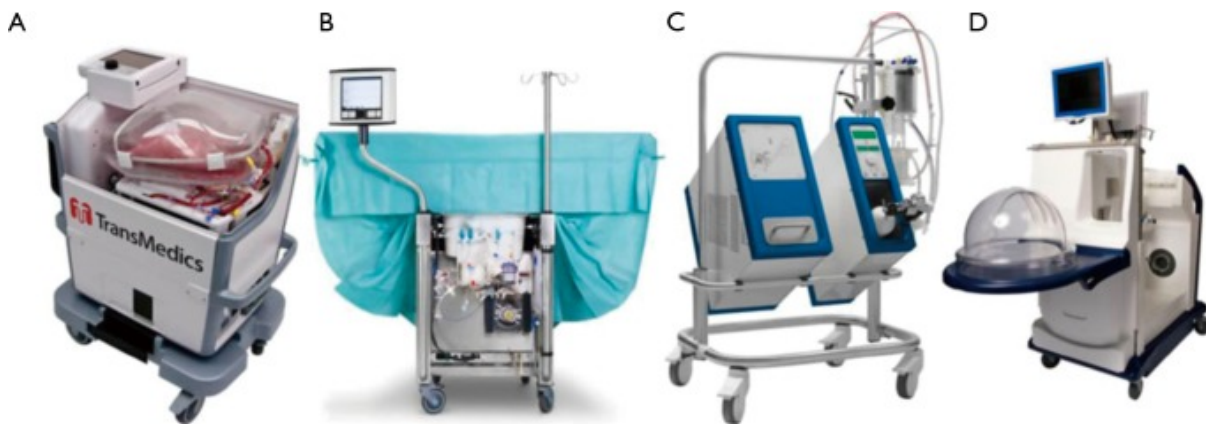
Figure 1-5 Current commercial EVLP systems.

(A) OCS™ (Transmedics). (B) LS™ (Vivoline®). (C) Lung Assist™ (Organ Assist). (D) XPS™ (XVIVO) (Possoz et al., 2019).

1.2.3 Clinical trials

There are multiple ongoing and completed clinical trials that are evaluating the efficacy of EVLP to recondition and assess extended criteria donors in order to expand transplant activity (Table 1-5). The INSPIRE, DEVELOP-UK and EXPAND trial have all been completed so far. The INSPIRE trial met their primary endpoint with 79.4% of patients in the OCS™ group compared to 70.3% in the control group surviving at 3 years. 17.7% of patients in the OCS™ group were reported to have grade 3 PGD within 72 hours post-transplant compared to 29.7% of patients in the control group (Warnecke et al., 2018). The EXPAND trial followed on from INSPIRE using the OCS™ platform and also meeting their primary outcome of 99% of patients surviving 30-days, with a 91% 1-year survival rate. There was also a utilization rate of 87% of lungs (Loor et al., 2018). The DEVELOP-UK trial reported an increase utilization of extended criteria donor lungs through use of EVLP for transplant with no significant difference between survival being seen between the EVLP and control groups. However, they did report an increased rate of early grade 3 PGD formation in the EVLP arm but rates of PGD showed no significant differences between the two groups at 72 hours (Fisher et al., 2016). These clinical trials are demonstrating the ability for EVLP to expand the donor pool by using marginal donor lungs safely. Focus is now moving to the use of advanced therapeutic interventions in order to recondition lungs during EVLP that might otherwise be discarded.

Trial	Start date	Aim	Location	Protocol	EVLP system	Primary Outcome	Completed
NOVEL	2011	Use static EVLP to assess marginal donor lungs	Multicentre - US	Toronto	XPS™	3-year survival	No
INSPIRE	2011	Assess outcome of OCS system during lung transit compared to SCS	Multicentre – multiple countries	OCS™	OCS™	3-year survival	Yes
DEVELOP-UK	2012	Determine clinical and cost-effectiveness of EVLP to increase lung activity	Multicentre – UK	Lund/ Hybrid	Vivoline (LS™)	12-month survival	Yes
EVLP-CHUM	2014	Evaluate effectiveness of EVLP to increase lung transplant activity and investigate biomarkers	Montréal, Canada	Lund	Not reported	12-month survival	No
EXPAND	2014	Assess OCS for preservation and reconditioning of marginal donor lungs	Multicentre - US	OCS™	OCS™	30 day survival, utilization of marginal lungs	Yes
Toronto	2015	Use EVLP to extend preservation time prior to transplant	Maryland, US	Toronto	XPS™	30-day survival, PGD grade 3	No
NPV-EVLP	2018	Determine effect of negative ventilation on lungs during EVLP	University of Alberta, US	Own protocol	NPV device	30-day survival, PGD grade 3	No
CLES	2019	Evaluate effectiveness of centralised lung evaluation system on marginal lungs	Multicentre - US	Toronto	XPS™	6-month survival	No

Table 1-5 Clinical trials involving the use of EVLP.

(Adapted from Gilmour et al., 2020)

1.3 Therapeutics in EVLP

The EVLP platform allows therapeutics to be directly administered to the lungs without the need to worry about deleterious "off-target" effects typically considered when treating patients and could have the potential to recondition or even repair acute damage seen in extended criteria donor lungs. This has the potential to expand the donor pool by being able to safely use these extended criteria lungs that would previously be deemed unusable, whilst also potentially improving post-transplant outcomes.

1.3.1 Traditional pharmaceuticals

There are multiple studies evaluating the use of established pharmaceuticals in EVLP which would traditionally be given to the patient to treat a certain disease. These pharmaceuticals are already clinically available however administering them during EVLP means they can be used at higher doses without risk to other organs. Cosgun *et al,* evaluated the use of trimetazidine, an anti-ischemic fatty acid oxidation inhibitor used to improve cardiac function, to limit IRI occurring post-transplantation. Porcine lungs underwent EVLP for 4 hours with trimetazidine leading to better oxygenation and increased ATP levels. Furthermore, a reduction in immune cell infiltration into the lungs was seen and an inhibition of neutrophil activation, suggesting this drug could potentially limit IRI (Cosgun et al., 2017). Lin *et al,* evaluated the use of alpha-1-antitrypsin (A1AT), which is used clinically to treat emphysema, related to A1AT deficiency. This was shown to increase oxygenation, reduce oedema formation and downregulate the release of IL-1α and CXCL8 after 12 hours of EVLP in porcine lungs (Lin et al., 2018). Haam *et al,* investigated the role of Cyclosporine A, an immunosuppressant, on preserving mitochondrial function to limit IRI using rat lungs that underwent EVLP for 4 hours. They observed improved physiological lung functioning and mitigated mitochondrial dysfunction in lungs treated with Cyclosporine A during EVLP (Haam et al., 2020). These studies show the potential of adding already established pharmaceuticals to the EVLP platform to potentially reduce IRI.

1.3.2 Antimicrobials

Donor to recipient transmission of lung infections poses a significant risk in immunocompromised patients post-transplant, EVLP offers an ideal opportunity to administer high dose antibiotics with a low risk of systemic side effects. Andreasson *et al,* found 13 out of 18 human lungs that underwent EVLP were found to contain aerobic and anaerobic species of bacteria and yeast. Use of high dose antimicrobial agents (meropenem and amphotericin) during EVLP led to a significant reduction in microbial burden in the lungs (Andreasson et al., 2014). Nakajima *et al,* found the use of a high dose broad spectrum antibiotic cocktail during EVLP reduced the bacterial burden in human donor lungs and also improved oxygenation and the compliance of the lungs (Nakajima et al., 2016). Porcine lungs with *Pseudomonas aeruginosa* related pneumonia that underwent EVLP with high dose antibiotics (colistin and amoxicillin) before being transplanted, showed prolonged survival rates compared to the lungs that weren't treated with antibiotics (Zinne et al., 2018). Use of antimicrobials during EVLP could allow for the use of lungs that would have otherwise been turned down for transplant if they showed any bronchoscopic and radiographic signs of infection, thereby having the potential to expand the donor pool of lungs available for transplant (Andreasson et al., 2014).

1.3.3 Receptor agonists/antagonists

Targeting specific cell surface receptors, such as for adenosine or sphingosine-1-phosphate (S1P), could potentially attenuate IRI in extended criteria donor lungs. Adenosine has four G-coupled protein receptors, which have roles in both pro-inflammatory, for example the A_{2B} receptor, and anti-inflammatory pathways, for example the A_{2A} receptor. Use of an A_{2B} antagonist to block the receptor during EVLP shows a decrease in vascular permeability, neutrophil infiltration into the lungs and a downregulation in pro-inflammatory cytokine release, such as IL-12 (Huerter et al., 2016; Charles et al., 2017). On the other hand, use of an A_{2A} receptor agonist, to stimulate this receptor during porcine EVLP demonstrated less oedema formation and downregulated production of pro-inflammatory cytokines, such as IFNγ, IL-1β, IL-6 and CXCL8 (Emaminia et al., 2011). S1P binds to 5 G-coupled protein receptors to play a key role in endothelium integrity. Mehaffey *et al,* administered circulating SIP and a sphingosine kinase 2 (SphK2) inhibitor, which blocks S1P clearance, to murine lungs undergoing EVLP for 1 hour. They found the combination of S1P and the

SphK2 inhibitor resulted in a significant improvement in lung compliance and a significant reduction in vascular permeability (Mehaffey et al., 2018). These studies demonstrate that targeting cell surface receptors through the addition of therapeutics to the EVLP platform can attenuate acute lung injury and reduce vascular permeability.

1.3.4 Gene therapies

EVLP offers an attractive platform for administering gene therapies as they provide the 6-12 hours needed for gene expression through adenoviral vector administration to take place. Furthermore, currently the use of adenoviral vectors can lead to an innate immune response in a patient, therefore EVLP provides an opportunity to minimise this vector-related inflammation due to fewer circulating immune cells (Yeung et al., 2012). Porcine lungs were treated with adenoviral interleukin-10 (AdhIL-10) during EVLP for 12 hours before being auto-transplanted. Lungs transduced with AdhIL-10 showed significantly better gas exchange compared to their untreated counterpart 7 days after transplantation. Furthermore, there was a significant reduction in IL-1β expression in the lungs and IL-6 expression systemically (Machuca et al., 2017). This suggests gene therapies could potentially improve lung functioning and potentially reduce the formation of PGD.

1.3.5 Gases

Certain gases can be administered during ventilation in EVLP to provide a therapeutic benefit by aiding in lung functioning and limiting IRI. One such gas is hydrogen gas, due to hydrogen being shown to have antioxidant and anti-inflammatory effects. Porcine lungs that underwent EVLP for 4 hours whilst being ventilated with 2% hydrogen gas showed improved oxygenation, lowered vascular resistance and significantly lower expression of IL-1β, CXCL8, IL-6 and TNFα (Haam et al., 2015). This improved lung functioning was also observed post-transplant. Furthermore, higher expression of IL-10 was observed in the hydrogen gas treated lung tissue (Haam et al., 2018). Alternatively, Dong *et al,* explored the therapeutic benefit of nitric oxide on rat lungs during the warm ischemic time, EVLP and perioperatively and found a significant reduction in oedema formation and expression of TNFα (Dong et al., 2009). The same group went on to evaluate the use of carbon

monoxide during the warm ischemic time, EVLP and perioperatively and found a reduction in oedema formation, improving oxygenation and decreased expression of IL-6 and IL-1β (Dong et al., 2013). These studies demonstrate that the addition of gases during ventilation could provide a beneficial effect in lung functioning and could aid in limiting IRI. Use of these therapeutic gases could also be used in conjunction to the administration of other therapeutics to the EVLP platform.

1.3.6 Cell-based therapies

Mesenchymal stem cells (MSCs) have been attracting recent attention as an alternative therapy to administer during EVLP due to their ability to target multiple areas by being able to interact with host cells, release immune modulating paracrine factors and even regulate endothelium permeability (Nakajima et al., 2019). A further attractive feature is their lack of immunogenicity due to a low expression of major histocompatibility complex (MHC) class I and II and co-stimulatory molecules (Gennai et al., 2015). Mordant *et al,* evaluated the use of umbilical cord derived MSCs in porcine lungs that underwent EVLP for 12 hours and found a decrease in CXCL8 production but no change in the physiology (Mordant et al., 2016). A follow up study from the same group administered umbilical cord derived MSCs to porcine lungs that had undergone 24 hours of cold storage before undergoing 12 hours of EVLP. They found a reduction in production of IL-18, IFNγ and an increased production of anti-inflammatory IL-4. Tissue expression of TNFα was also significantly lowered. The acute lung injury score was significantly lowered in the MSC treated group. Furthermore, there was a significant decrease in oedema formation observed with lungs treated with the MSCs (Nakajima et al., 2019). McAuley *et al,* evaluated the use of bone marrow derived MSCs on alveolar fluid clearance and found they were effective, despite a prolonged cold ischemic time, after 4 hours of EVLP (McAuley et al., 2014). Martens *et al,* evaluated the use of multipotent adult progenitor cells (MAPCs) in porcine lungs that underwent EVLP. MAPCs have similar characteristics to MSCs but adopt a different phenotype offering a larger proliferative capacity and so can be rapidly expanded from one ideal donor. They found administering MAPCs led to a significant decrease in TNFα, IL-1β and IFNγ production, in addition to a reduction in the number of neutrophils found in the lungs (Martens et al., 2017).

More recently, studies have been looking into MSC-derived extracellular vesicles (EVs) as they also possess the same immunomodulatory and regenerative capacities, but reduce the risks associated with MSC administration such as long-term potential adverse effects in immunosuppressed patients. EVs contain proteins, mRNAs and microRNAs (miRNAs) secreted by the MSCs (Lonati et al., 2019). Due to the increase in the number of studies exploring the use of EVs as a therapeutic, the International Society For Extracellular Vesicles (ISEV) has introduced a number of guidelines including suggested protocols for isolation, biophysical, biochemical and functional assays (Lötvall et al., 2014; Théry et al., 2018). Stone *et al,* found that lungs treated with umbilical cord derived MSC-EVs during EVLP decreased neutrophil infiltration into the lungs and lowered myeloperoxidase production (Stone et al., 2017). Another study using bone marrow derived MSC-EVs in EVLP for 6 hours led to increased fluid clearance by the lungs and improved lung functioning. However, they found there was minimal change in cytokine production (Gennai et al., 2015). These studies highlight the capability of stem cells and their derived EVs to potentially limit IRI in lungs.

1.4 Human amniotic epithelial cells

Human amniotic epithelial cells (hAECs) are a promising cell-based therapy due to their immunomodulatory and stem cell-like characteristics and their lack of ethical issues and tumorigenicity (Miki, 2018). Furthermore, hAECs can be isolated to current good manufacturing practices (cGMP) for clinical use, achieving large yields of over 100 million cells per placental isolation, meaning unlike MSCs there is little need for rapid expansion of these cells (Gramignoli et al., 2016).

hAECs are derived from the amnion membrane of the placenta. The placenta is a discoidal organ and plays a vital role during pregnancy by continually supplying nutrients for foetal development, waste removal, exchanging gases and also playing an important role in immune tolerance towards the foetus (Huppertz, 2008; Taniguchi et al., 2018). Elective caesarean-sections (c-sections) can be performed to deliver the baby and placenta. The placenta can be safely delivered through two c-section methods; spontaneous delivery of the placenta, which is more commonly used due to a decreased risk of blood loss, or through manual removal (Morales et al., 2004).

1.4.1 Amnion membrane

The placenta is surrounded by two foetal membranes; the chorion membrane, which is an outer layer in contact with the maternal cells and the amnion membrane (AM) which surrounds the embryo in the amniotic cavity which is filled with amniotic fluid (Mamede et al., 2012). Upon implantation of the blastocyst into the endometrium, which forms the embryo, shown in Figure 1-6, the trophoblastic cells that form the wall of the blastocyst form the chorion membrane. The innermost epiblast cells form the AM, which becomes visible by day 10 after conception. Over time, the amniotic cavity fills with fluid then adheres to the surface of the chorion, but the two membranes do not fuse together and remain separate (Baradaran-Rafii et al., 2007; Mamede et al., 2012). The amnion membrane is composed of an epithelium layer (hAECs) and a mesenchymal stromal layer. The AM has been found to possess anti-inflammatory and anti-microbial properties alongside being a stimulator of epithelialisation, is non-tumorigenic and has few ethical concerns due to its source. This has made the AM ideal for potential regenerative medicine applications (Huppertz, 2008). The first reported use of the AM for skin transplantation was as early as 1910 (Davis, 1910). Now, the AM can be successfully transplanted into

patients with epithelial defects, corneal ulcers and ocular burns. Wound healing occurs in patients through epithelisation of the cornea occurring below the transplanted AM (Nubile et al., 2008). Liu *et al,* showed through a meta-analysis that AM transplantation is an effective treatment for corneal ulcers and can to an extent improve patients vision (Liu et al., 2019). Dehydrated amniotic-derived allografts have also been shown to have wound healing properties by facilitating skin repair for diabetic foot ulcers. In a prospective case study of 14 patients, the grafts were shown to successfully aid in closing these ulcers, even if the ulcer was greater than 10 cm^2 (Abdo, 2016). hAECs make up the epithelial layer of the AM and therefore possess many of the same regenerative properties making them ideal as a cellular therapy.
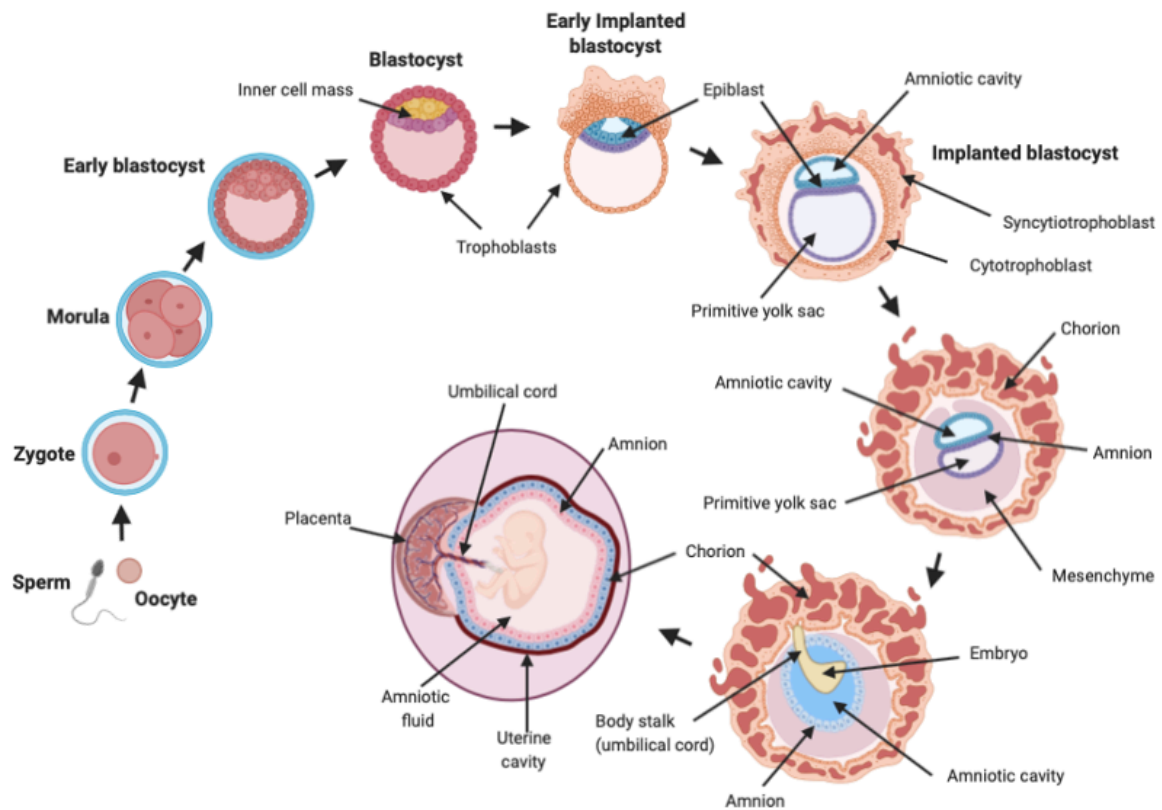
Figure 1-6 The formation of the amnion membrane from conception to full term pregnancy.

Upon conception, the zygote rapidly expands into a morula then an early blastocyst. Upon early implantation of the blastocyst, the epiblast forms from the inner mass of cells. The implanted blastocyst starts forming the amniotic cavity and primitive yolk sac, surrounded by the amnion membrane, from the epiblast. The trophoblast cells form the outer syncytiotrophoblast and inner cytotrophoblast layers, which ultimately form the chorion membrane and the foetal part of the placenta. Over weeks, the embryo forms inside the amniotic cavity surrounded by the amnion membrane, slowly expanding. Finally, the foetus is in amniotic fluid within the cavity and surrounded by the amnion membrane and the chorion membrane, although these membranes are not fused. The fully formed placenta is connected to the foetus by umbilical cord and attached to the uterine wall.

1.4.2 Endogenous properties

As described earlier, the hAECs are formed from the epiblast and so retain many of the pluripotent stem cell characteristics, making them attractive to regenerative medicine (Izumi et al., 2009). hAECs have been shown to express stem cell markers, such as SSEA-4, TRA-1-60, TRA-1-81, Oct4 and Nanog. However, hAECs are a heterogenous cell population due to the expression of these stem cell markers differing based on cell location on the AM (Izumi et al., 2009; Centurione et al., 2018). The pluripotent nature of hAECs means under the right culture conditions, they exhibit the capability of differentiating into all three germ layers; the ectoderm, endoderm and mesoderm. These lineages can include neurons, skin cells, lung epithelium, cardiomyocytes, hepatocytes, adipocytes and osteocytes (Murphy et al., 2010).

27

A further reason why these cells have attracted attention in the field of regenerative medicine is due to hAECs being immune privileged. hAECs lack expression of MHC Class II Human Leukocyte Antigens (HLA)-DR, DP and DQ and co-stimulatory molecules CD40 and CD80. hAECs do appear to express low to moderate levels of MHC Class I HLA-A, B and C (Pratama et al., 2011; Hammer et al., 1997). Expression of HLA-G, which is a non-classical Class I antigen with immunomodulatory properties, has been found on the surface of hAECs (Strom & Gramignoli, 2016). HLA-G is believed to have a role in protecting the foetus from the maternal immune system through modulation of natural killer (NK) and T cells by triggering apoptosis in T cells, impairing NK migration through the endothelium and by modulating cytokine release. Therefore, HLA-G could in part play a role in the reported immune tolerance of transplanted hAECs (Lefebvre et al., 2000). hAECs also express CD59 which is an important complement regulatory molecule and inhibitor (Rooney & Morgan, 1992). Both Fas and Fas Ligand (FasL) have also been found on hAECs. Fas/Fas L likely aids foetal maternal tolerance by mediating apoptosis of lymphocytes and later at full term gestation likely has a secondary role in inducing apoptosis of the amniotic epithelium at term (Harirah et al., 2002; Runic et al., 1998). hAECs also express a number of toll-like receptors (TLRs) including TLR5, TLR6/2 and TLR4. Pathogens activate TLR5 and TLR6/2 on hAECs to produce IL-6 and CXCL8 which result in neutrophil recruitment, matrix metalloproteinase-9 (MMP9) induction and NF-κB activation. hAECs also express TLR4 which has a role in inducing apoptosis. TLR expression of hAECs is the first line of defence against intra-amniotic bacteria during chorioamnionitis infection and so explains why hAECs can also adopt a pro-inflammatory phenotype. This suggests hAECs are able to switch roles depending on the microenvironment they are currently in (Gillaux et al., 2011).

1.4.3 Exogenous properties

In addition to hAECs having stem cell like characteristics and being immune privileged, the immunomodulatory ability of hAECs and their subsequent conditioned media (CM) also offers a therapeutic potential for treating inflammatory disease. hAECs, their CM and subsequently derived EVs have been used to treat pre-clinical disease models such as lung fibrosis, liver fibrosis, wound healing, arthritis, multiple sclerosis and brain injury (Magatti et al., 2018).

1.4.3.1 Whole cells

hAECs appear to modulate the immune system by dampening pro-inflammatory cytokine release, cell signalling and cell infiltration into the tissue, in addition to enhancing anti-inflammatory cytokines and cells, such as regulatory T Cells (Tregs) and M2 macrophages to encourage tissue repair (Magatti et al., 2018). When cultured with mouse macrophages and neutrophils, hAECs significantly reduced the chemotaxis of these cells towards the macrophage inflammatory protein-2 (MIP-2). This lack of chemotaxis was shown not to be due to the macrophages or neutrophils suffering any toxicity and undergoing apoptosis but due to the hAECs expressing macrophage migration-inhibitory factor (MIF) in the supernatant. (Li et al., 2005). Furthermore, Alipour *et al,* showed that hAECs co-cultured with human blood neutrophils enhances their phagocytic capability whilst also decreasing their oxidative burst capacity which allows hAECs to protect the foetus from microbial attacks whilst limiting oxidative stress (Alipour et al., 2020). Tan *et al,* demonstrated through the bleomycin challenge in mice which results in lung injury, that there was reduced macrophage infiltration into the lungs of mice treated with hAECs and increased polarisation of predominately M1 alveolar macrophages into predominately M2 macrophages. This reduced the chemotactic ability of the macrophages whilst increasing their phagocytic ability which could contribute to lung repair by clearing apoptotic neutrophils (Tan et al., 2014). This is supported by Murphy *et al,* who demonstrated that mice with impaired macrophage function that underwent the bleomycin challenge did not have a reduction in macrophage infiltration, furthermore there was no decrease in inflammation or improvement in lung function after hAEC administration. This suggests that hAECs require normal macrophage functioning in order to exert their immunomodulatory effects (Murphy et al., 2012). hAECs also appear to promote endothelial cell migration into scratch wound areas by expressing angiogenic properties, which may also aid in tissue repair (Wu et al., 2017).

hAECs appear to mediate lung repair shown through a variety of neonatal and adult lung disease models. Vosdoganes *et al,* demonstrated that hAECs used to treat hypoxia-induced neonatal injury modestly improved lung functioning and significantly decreased hypoxia-related inflammatory cytokines; IL-1α, IL-6, transforming growth factor-beta (TGF-β) and platelet derived growth factor-β (Vosdoganes et al., 2013).

Zhu *et al,* demonstrated that hAECs administered to a model of bronchopulmonary dysplasia (BPD) mitigated the decrease in tissue-to-air-space ratio seen in the BPD model. Early administration of hAECs lead to reduced numbers of macrophages, dendritic cells and NK cells. Furthermore, hAECs decreased the levels of TNFα and IL-1β compared to the untreated control. Interestingly they observed low engraftment of hAECs into the lungs which may be associated with an activation of the endogenous bronchioalveolar stem cells (BASCs). They found the average numbers of BASCs were greater in the mice that received hAEC treatment, which may contribute to the lung repair observed (Zhu et al., 2017). hAEC treatment of fibrotic lungs in a mouse model also appears to lead to a reduction in MCP-1, TNFα, IL-1, IL-6 and TGFβ and an increase in production of IL-10. Furthermore, they saw bleomycin-induced pneumonitis was significantly reduced by hAEC treatment (Moodley et al., 2010). In a model of inflammation caused in response to mechanical ventilation in pre-term lambs showed that the administration of hAECs found a reduction in CXCL8 production, an increase in IL-10 production and recruitment of Tregs into the lungs. BAL samples from the lungs showed decreased expression of M1 macrophages, suggesting hAECs were modulating the airway inflammation in these ventilated lambs (Melville et al., 2017). Finally, a COPD model in rats received hAEC treatment which led to a reduction in inflammatory cell infiltration and alleviated emphysema. Neutrophil infiltration into the lungs was reduced with hAEC treatment however macrophage and lymphocyte proportions were increased upon hAEC treatment, although this is likely due to an influx in M2 macrophages and Tregs into the lungs. Furthermore, CXCL8 levels were significantly decreased in the lungs (Geng et al., 2016).

hAECs are also being used in the field of transplantation. Islet transplantation is an established therapy for type 1 diabetes however during transplantation there is considerable islet loss due to inflammation at the site of implantation and ischemic stress. Therefore, incorporation of hAECs into islet organoids is being investigated to examine whether hAECs are able to provide cryoprotection to help maintain the functional capacity of islet cells during this time. Lebreton *et al,* demonstrated that hAECs were able to accelerate the revascularisation through an angiogenic effect on the islet cells whilst also significantly improving the secretory function and viability of islet cells upon engraftment (Lebreton et al., 2019).

1.4.3.2 Extracellular vesicles

More recently attention has been turning to the extracellular vesicles secreted by hAECs. Isolated hAECs-extracellular vesicles (hAEC-EVs) fall within the exosome size range of 30-150nm (Tan et al., 2018; Zhao et al., 2017). Proteins in the hAEC-EV cargo are associated with apoptosis, developmental growth, MAP kinase, fibrotic and inflammatory mediated pathways. They also appear to contain miRNAs associated with key fibrotic, cancer, stem cell pluripotency and apoptosis pathways (Tan et al., 2018; Zhang et al., 2019). Zhao *et al*, demonstrated that the administration of hAEC-EVs to a wound healing model in rats led to a significant increase in wound closure and reduced scar formation compared to the PBS control (Zhao et al., 2017). The administration of hAEC-EVs to mouse neutrophils lead to significantly lower myeloperoxidase activity and appeared to induce neutrophil cell death. Furthermore, hAEC-EVs doubled the phagocytic ability of macrophages and also polarised M1 macrophages to the M2 phenotype. In a bleomycin lung injury model, hAEC-EVs showed increased polarization and phagocytosis of macrophages whilst reducing neutrophil and T cell infiltration into the lungs. Furthermore, the administration of hAEC-EVs showed an increase in the proliferation of BASCs in the lungs. Administration of hAEC-EVs at day 7 post-bleomycin injury showed tissue-to-airspace ratio was improved and there was reduced fibrosis observed (Tan et al., 2018). This shows promise that hAEC-EVs still possess immunomodulatory properties and can also mediate lung repair without the need for their cell counterpart.

1.4.4 Clinical trials

Clinical trials testing the safety and tolerability of hAECs are now being explored in several areas of disease including BPD, hepatic fibrosis and ischemic stroke. In 2018, Lim *et al*, reported the first-in-human systemically delivery of hAECs. hAECs were administered to six infants with BPD at a dose of 1 million cells/kg of bodyweight. The first infant received a manual intravenous infusion of hAECs of 2 million/mL in saline, which lead to a cardiorespiratory instability believed to be caused by a cell-related micro-embolism. Following this event, cell delivery method was changed to a 30-minute infusion with a syringe-driver on a rocking platform and a lowered concentration of 0.25 million hAECs/mL in saline. From this point onwards hAEC administration appeared to be feasible, tolerated and safe. The first infant did

not experience any long-term consequences (Lim et al., 2018). Following on from this feasibility study, a phase I dose escalation study has been set up using 24 infants at day 14 of life. The escalation starts with a dose of 2 million cells/kg in a single infusion, then an incremental increase finishing at 30 million cells/kg over three divided doses (Baker et al., 2019). This clinical trial is currently ongoing.

A phase I safety clinical trial in treatment of liver cirrhosis is also currently ongoing. Tolerability and safety will be determined using 12 patients that will undergo intravenous (IV) administration of hAECs, first at a dose of 0.5 million cells/kg then 1 million cells/kg and monitored for 5 days for any serious adverse events (Lim et al., 2017). Finally, a further phase I stage-wise dose escalation, starting at 2 million cells/kg increasing up to 32 million cells/kg, for hAEC therapy in ischemic stroke is currently ongoing. MR imaging of efficacy and effect on immunosuppression are also being monitored which could yield some very interesting results (Phan et al., 2018).

1.5 Hypothesis

The hypothesis of this study is that hAECs or their derivatives added to the vascular compartment of a donor lung undergoing EVLP will reduce pulmonary vascular endothelial activation and limit leukocyte-endothelial interactions after organ reperfusion by their immunomodulatory actions and thus assist in the reconditioning of donor lungs initially declined for transplantation during EVLP assessment.
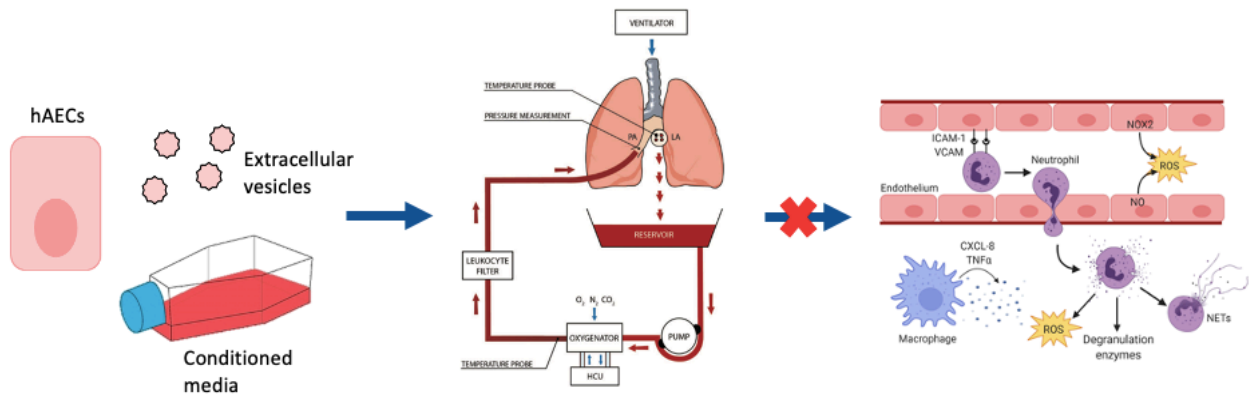
Figure 1-7 Visual representation of the hypothesis of this project.

hAECs or their derivatives of conditioned media or extracellular vesicles will be administered during EVLP to reduce endothelial cell activation, neutrophil migration and pro-inflammatory macrophage activation by providing an immunomodulatory effect.

1.6   Aims and objectives

The aim of my thesis is to characterise hAECs and their derivatives, determine their immunomodulatory functions *in vitro*, then administer the hAECs *ex vivo* to investigate if any biological and physiological changes that take place during EVLP. Three main objectives were established to investigate this aim, which have formed the chapters of my thesis:

1. Establish a robust hAEC isolation technique and characterise the isolated cells and subsequently isolated extracellular vesicles using a variety of purity markers based on the literature.

2. Explore the immunomodulatory properties that hAECs and their derivatives may have on leukocyte-endothelium interactions, endothelium activation and macrophage polarisation.

3. Investigate any physiological effects that may occur by administering hAECs or their derivatives to the lungs during EVLP and determine any biological changes that occur using a panel of key pro-inflammatory and endothelium activation markers.

2   Materials and Methods

2.1   Tissue acquisition

Ethical consent for placental tissue used in this study was gained through the Uteroplacental Biobank located at Newcastle University (REC:10/H0906/71). Placenta was acquired from healthy women undergoing elective c-sections at the Royal Victoria Infirmary, Newcastle Upon Tyne Hospitals Trust Foundation. Ethical approval for lung tissue was approved as part of NHSBT Study 66 entitled 'Further Evaluation of Ex Vivo Lung Perfusion to Improve Transplantation Outcomes' (REC:16/NE/0230). Samples taken during EVLP were then stored in The Newcastle Institute of Transplantation Tissue Biobank (REC: 17/NE/0022).

2.2   Tissue culture

All tissue culture work was carried out inside a Class II Microbiological safety cabinet and using aseptic technique. All safety procedures were performed in accordance with Newcastle University's Safety Policy and proper protective equipment was worn. The relevant BIOCOSHH and COSHH forms were read and signed prior to any use of chemicals or biological reagents. Cells were cultured in 37°C in a humidified atmosphere containing 5% CO_2 throughout. Cells were cultured in either polystyrene 175 cm^3 or 75cm^3 tissue culture flasks with ventilated caps or in polystyrene tissue culture treated plates with 6, 12 and 24 wells (Both Greiner, Austria).

2.2.1   THP-1 cell line

The THP-1 cell line (ATCC® TIB-202™) is a human monocytic cell line derived from an acute monocytic leukaemia patient. The cell line is cultured in RPMI-1640 (Sigma Aldrich, USA) supplemented with 10% fetal bovine serum (FBS) (Lonza, Switzerland), 1% 2 mM L-glutamine, 100 μg/mL penicillin, 0.1 mg/mL streptomycin (All Sigma Aldrich).

2.2.2   HMEC-1 cell line

Human Microvascular Endothelial Cells-1 (HMEC-1) (ATCC® CRL-3243™) are derived from dermal microvascular endothelium from a newborn male, then transfected with SV40 viral DNA sequences in order to turn them into a cell line. The HMEC-1 cell line is cultured in MCDB media (ThermoFisher scientific, UK)

supplemented with 10% FBS (Lonza), 1% 2 mM L-glutamine, 100 µg/mL penicillin, 0.1 mg/mL streptomycin, 10 ng/mL epidermal growth factor and 1 µg/mL hydrocortisone (All Sigma Aldrich).

2.2.3 HTR-8/SVneo cell line

The HTR-8 (ATCC® CRL-3271™) cell line are trophoblasts isolated from the placenta at 6-12 weeks gestation, then transfected with SV40 viral DNA sequences in order to turn them into a cell line. The HTR-8 cell line is cultured in RPMI-1640 (Sigma Aldrich) supplemented with 10% FBS (Lonza), 1% 2 mM L-glutamine, 100 µg/mL penicillin, 0.1 mg/mL streptomycin (Both Sigma Aldrich,).

2.2.4 Cell counting

Cell counts were performed when setting up experiments using a Neubauer haemocytometer. A 10 µL volume of cell suspension was diluted with 10 µL trypan blue (ThermoFisher) and mixed thoroughly before 10 µL was then added to one chamber of the haemocytometer. Cells were counted in each of the four squares on the grid, including those touching to the left and right hand lines. The cell count was calculated by dividing the number of cells by 4 to create an average, then multiplied by 2 to account for the 1:2 dilution with trypan blue. To measure total cell number, this result was then multiplied with the volume of the original cell suspension. The trypan blue dye stains any dead cells blue, allowing for viability to also be calculated by dividing number of viable cells by total number of cells, then multiplying by 100 to get percentage viability.

2.2.5 Cryopreservation

All cell lines and primary cells were resurrected from liquid nitrogen. Cryovials were rapidly thawed at 37°C in a waterbath, then diluted in 10 mL pre-warmed media. Cells were then spun at 300 g for 5 minutes. Cells were then resuspended in media prior to being transferred to a T75 flask.

When freezing down stocks of cell lines and primary cells, an appropriate number of cells in 1 mL of media were resuspended in 1 mL ice cold cryopreservation media containing 20% DMSO (Sigma Aldrich) in FBS, then transferred to a cryovial. The

cryovials were then stored at -80°C in a BioCision CoolCell (Sigma Aldrich) which freezes cells at a controlled rate of -1°C/minute. After 24 hours, the cryovials were moved to liquid nitrogen for long term storage.

2.2.6 Subculture

2.2.6.1 Adherent cells

Subculture for adherent cells was performed when cells were at approximately 80% confluency. Media was discarded from the flask and the cells washed with phosphate-buffered saline (PBS). The PBS was discarded and replaced with 5 mL of 0.25% trypsin-Ethylenediaminetetraacetic acid (EDTA) (Sigma Aldrich) solution for 5-10 minutes at 37°C. The flask was tapped sharply to dissociate the cells, then cells were placed into a falcon tube. 5 mL of media was used to wash the flask then also placed into the falcon to neutralise the trypsin-EDTA solution. Cells were spun at 300 g for 5 minutes before resuspension with media and then divided between 3 flasks alongside 10 mL of media.

2.2.6.2 Suspension cells

Subculture for the THP-1 cell line was performed twice a week (Monday and Thursday or Tuesday and Friday). The cells were split by removing 10 mL of cell suspension from the flask and replaced with 10 mL of fresh media. Every two weeks or when cells were required for experiments, the cell suspension was placed into a falcon tube and spun at 300 g for 5 minutes, then resuspended in 10 mL of media. The cells were then split 1:5 into a new T75 flask with 20 mL of media or used in experiments.

2.3   Histology and cytology

Staining can be performed on tissue and cells grown from culture in order to visualise protein and surface marker expression through immunohistochemistry and immunofluorescence, and morphology through Haemotoxylin and Eosin (H&E) staining.

2.3.1   *Immunohistochemistry*

Immunohistochemistry (IHC) involves using antibodies against specific antigens to detect their expression within fixed or frozen tissue or cells. In this study IHC was performed using the Vector ImmPRESS® HRP peroxidase reagent kit (anti-mouse/rabbit IgG) (Vector Laboratories, USA), which works by using a secondary antibody conjugated to horseradish peroxidase, which binds to the primary antibody, then catalyses the breakdown of a chromogen, 3,3'-diaminobenzidine (DAB), to form a brown precipitate at the location of the antibody which can be visualised using a brightfield microscope. All IHC staining was imaged using the Olympus upright Microscope using CellSense software (Olympus, Japan).

Target protein	Dilution	Description	Source	Antigen retrieval method
EpCAM	1:100	Monoclonal mouse anti-human	ProGen	Trypsin
Vimentin	1:100	Monoclonal mouse anti-human	NovoCastra (now part of Leica biosystems)	Trypsin
CK19	1:100	Monoclonal rabbit anti-human	Abcam	Citric acid
HLA-G	1:100	Monoclonal mouse anti-human	Bio-rad	Citric acid
HLA-DR	1:500	Monoclonal mouse anti-human	Dako	Trypsin
CD31	1:200	Monoclonal mouse anti-human	Dako	Citric acid
CD14	1:20	Monoclonal mouse anti-human	Millipore	Citric acid
CD45	1:100	Monoclonal mouse anti-human	Dako	Citric acid
CXCL8	1:50	Polyclonal rabbit anti-human	Life technologies	Citric acid
3-NT	1:50	Monoclonal mouse anti-human	Hycult Biotech	Citric acid

Table 2-1 Primary antibodies used in immunohistochemistry and immunofluorescence staining.

Primary antibodies were diluted in TBS for immunohistochemistry (IHC) or PBS for immunofluorescence (IF).

2.3.1.1 Tissue

Paraffin embedded amnion tissue was cut onto 3-Aminopropyltriethoxysilane (APES) coated slides (Cellpath, Wales) at a thickness of 4 μm. These slides were dewaxed in xylene for 5 minutes, rehydrated through graded alcohols (99%-70%) prior to blocking with 3% hydrogen peroxide for 10 minutes to block endogenous peroxidase activity. After rinsing with water antigen retrieval was then carried out with the type of antigen retrieval performed varying depending on the antibody to ensure the best outcome (Table 2-1). The two antigen retrieval processes either involved pressure cooking citric acid buffer (10 mM citric acid, 0.05% Tween20, pH 6) for 3 minutes or by placing the slides a trypsin enzyme digest (Trypsin with calcium chloride, pH 7.8) and incubating at 38°C for 10 minutes in a waterbath. Sections were then washed with Tris Buffered Saline (TBS pH 7.6) for 5 minutes then blocked using normal horse serum provided by the Vector ImmPRESS® kit for 10 minutes. Block was replaced with antibody (Table 2-1), except for the negative no primary antibody control, and left to stain for 60 minutes. Sections were washed again with TBS then secondary antibody supplied by the Vector ImmPRESS® kit was added for 30 minutes. Cells underwent a final wash step before being developed using the DAB peroxidase substrate kit (Vector Laboratories) following manufacturer's instructions. The slides were then washed well with running tap water then counterstained with Mayers Haematoxylin (Sigma Aldrich) for 30 seconds. Finally, sections were dehydrated through graded alcohols (70%-99%), cleared with xylene and then mounted using DPX. Placental bed tissue was consistently used as a positive control.

2.3.1.2 Cell chambers

A 15 μL sample of hAECs after isolation was seeded into a chamber slide with 200 μL media. Cells were incubated for 72 hours at 37°C and 5% CO_2. Media was discarded and replaced with 99% ice cold methanol (Fisher Chemicals, UK) and left to fix for 10 minutes. The methanol was discarded and the cell chamber was stored at -20°C until ready to stain. Staining was performed using the same Vector ImmPRESS® kit for tissue however no antigen retrieval was performed. The chamber slide was brought to temperature and washed in TBS then blocked with normal horse serum for 15 minutes. Normal horse serum was replaced with primary antibody and stained for 30 minutes. The chamber slides were then washed in TBS before developing with DAB and counterstaining with Mayers Haemotoxylin following

the same protocol as above (chapter 2.3.1.1). Frozen placental bed tissue was consistently used as a positive control.

2.3.2 Immunofluorescence

Immunofluorescence (IF) staining was carried out in collaboration with Mr Chong Yun Pang and performed on lung tissue collected pre and post EVLP. Paraffin embedded lung tissue was cut onto Superfrost Plus™ (Thermofisher) slides at a thickness of 4 µm. The slides were de-waxed and hydrated through graded alcohols (99% -70%), then washed in deionised (DI) water. Antigen retrieval was then performed with citric acid buffer and pressure cooked for 3 minutes. The slides were then washed briefly with PBS and then blocked with 10% goat serum in PBS for 30 minutes at room temperature. The block was removed and replaced with the CXCL8 and 3-NT (Table 2-1) antibodies and incubated overnight at 4°C. The slides were then washed 3 times with PBS with 0.05% Tween20 for 5 minutes, with gentle agitation. The secondary antibodies, AlexaFlour488 (Goat anti-rabbit, Abcam, USA) and Dylight650 (Goat anti-mouse, ImmunoReagents Inc, USA), were added to the slides and incubated for 1 hour in the dark, at room temperature. The slides were washed twice with PBS with 0.05% Tween20 for 5 minutes, with gentle agitation then mounted with Vectashield® with DAPI (Vector laboratories) and the edges sealed, then stored at 4°C until imaging with the Zeiss AxioImager (Zeiss, Germany).

2.3.3 Haematoxylin and Eosin staining

H&E staining was performed on tissue, cell smears, and cytospins. Smears were prepared using 50 µL of cell solution and pipetted onto a slide. Cytospins were carried out using the Cytospin 3 (Shandon, UK) then fixed in acetone for 10 minutes. Samples were then frozen at -20°C until further use. Amnion or lung tissue was dewaxed in xylene before being rehydrated in graded alcohols. All slides, frozen and paraffin, were then stained with Mayers Haemotoxylin (Sigma Aldrich) for 1 minute, 10 seconds before being thoroughly washed in running DI water. Samples were then allowed to "blue" in Scotts tap water substitute. The slides were then thoroughly washed again prior to staining with alcoholic eosin (Sigma Aldrich) for 30 seconds. The slides were then washed briefly before dehydrated with graded alcohols, then

mounted with DPX (Sigma Aldrich). The slides were imaged using the Olympus upright Microscope using CellSense software.

2.3.4 Diff Quik staining

Diff quik staining was performed as simple and rapid method for determining homogenous populations. Diff quik (Baxter diagnostics, UK) was performed as per manufacturer's instructions by staining with solution II for 30 seconds then counterstaining with solution I for a further 30 seconds. The slides were rinsed rapidly in DI water to remove excess stain then dehydrated through graded alcohols before being mounted with DPX, then imaged using the Olympus upright Microscope using CellSense software.

2.4 Quantitation of gene expression

2.4.1 RNA isolation

Following treatments, THP-1 and HMEC-1s seeded in 12 and 6 well plates respectively would be processed for RNA isolation, which was performed using the RNeasy® Mini kit (Qiagen, USA). Cells would be lysed using RLT buffer provided by the kit supplemented 1:10 with 1% β-mercaptoethanol. 350 μL of the lysis buffer was added to each well and then frozen at -20°C until further processing.

Upon thawing, the wells were scraped before being transferred to Qiashredders (Qiagen), then centrifuged at full speed (17,000 g) for 2 minutes. A 1:1 volume of 70% ethanol was added to the lysate and mixed before up to 700 μL being transferred to a RNeasy mini spin column placed in a 2 mL collection tube, supplied by the RNeasy Mini kit. This was centrifuged for 15 seconds at 8000 g, flow through into the collection tube was discarded. 700 μL of RW1 buffer was added to the spin column before a further centrifuge at 8000 g for 15 seconds, flow through was discarded. To remove salt contamination, 500 μL of RPE buffer was added to the spin column and spun at 8000 g for 15 seconds, flow through was discarded. A further 500 μL of RPE buffer was added to the column and centrifuged at 8000 g for 2 minutes. The RNeasy spin column was placed in a fresh 2 mL collection tube and centrifuged at full speed for 1 minute to dry the membrane. Finally, the RNeasy spin column was placed into a 1.5 mL collection tube, supplied by the kit. 30 μL of RNase-free water was added directly onto the membrane inside the spin column, before being centrifuged at 8000 g for 1 minute, to elute the RNA.

The lung tissue biopsies collected during EVLP were stored in RNAlater™ Stabilization Solution (Thermofisher Scientific) at -80°C prior to RNA isolation. The biopsies were thawed, 20 mg of tissue was weighed out then 350 μL of QIAzol and one 5 mm stainless steel bead was added (both Qiagen). The lung tissue was placed into the ice cold TissueLyser II (Qiagen) and homogenised at 20 Hz for 2 minutes each side. Then 140 μL of chloroform (Sigma Aldirch) was added and the tube shaken vigorously for 15 seconds. The tube was incubated at room temperature for 2-3 minutes then centrifuged at 12,000 g for 15 minutes at 4°C. The upper aqueous phase was transfer to a Qiashredder then centrifuged at 17,000 g for 2 minutes. 250 μL of 70% ethanol was added to the lysate then transferred to an RNeasy mini spin column. The sample was centrifuged for 15 seconds at 8000 g, then 350 μL of RW1

buffer was added before a further centrifuge at 8000 g for 15 seconds. The flow through was discarded. 10 μL of DNase I stock solution (Qiagen) was added to 70 μL RDD buffer for DNase digestion. This was then added to the RNeasy spin column and left to incubate for 15 minutes at room temperature. A further 350 μL of RW1 buffer was added and the spin column was centrifuged at 8000 g for 15 seconds. Salt contamination wash steps with the RPE buffer and subsequent RNA elution was carried out as described above for the cell-based RNA extractions.

The RNA was stored on ice whilst measuring RNA quantity and quality on the Nanodrop One (Thermofisher Scientific) by using 1 μL of RNase free water to blank the machine, then 1 μL of the RNA. The RNA would then either be further processed to cDNA or stored at -80°C until further use.

2.4.2 cDNA synthesis

Complementary DNA (cDNA) synthesis was carried out using the Tetro cDNA synthesis kit (Bioline, UK) from 1000 ng of total isolated RNA. To each sample of RNA, 1 μL 10mM dNTP mix, 1 μL Ribosafe RNase inhibitor, 1 μL Tetro reverse transcriptase, 4 μL RT buffer and 1 μL of either Oligo DT for HMEC RNA or 1 μL of Random hexamers for THP-1 RNA. Volume was adjusted using DEPC treated water to 20 μL and mixed gently. Samples were spun in a picofuge then incubated in a thermocycler (Biorad, USA) depending on whether they contained random hexamers or oligo DT (Figure 2-1). Samples were stored at -20°C until further use.

Random hexamers

25˚C for 10 minutes

↓

45˚C for 30 minutes

↓

85˚C for 5 minutes

Oligo DT

45˚C for 30 minutes

↓

85˚C for 5 minutes
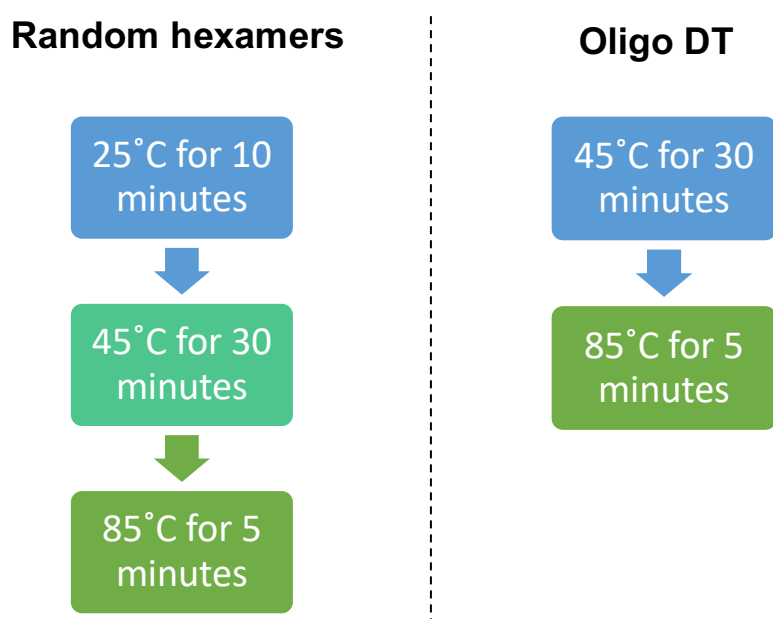
Figure 2-1 cDNA incubation steps in a thermocycler dependent on whether random hexamers or oligo DTs were used to make up the reaction.

Random hexamers were used to bind 18S ribosomal RNA to increase chance of amplification during real time PCR. Oligo DTs were used to bind complementary mRNA for exon spanning primers probes.

2.4.3   Real time PCR

Real time polymerase chain reaction (PCR) was performed using the TaqMan® gene expression assays (Thermofisher Scientific, UK) throughout this study. This involves using a fluorescent dye and quencher attached to the Taqman probe, which is then cleaved by DNA polymerase separating the dye and quencher. With each cycle more fluorescent dye is released to detect the accumulation of a PCR product through an amplification plot (Figure 2-2). The comparative (2-$\Delta\Delta$Ct) Ct method was used to calculate the gene expression between a specific experimental gene and a control housekeeping gene. To allow for three replicates to be performed, 20 μL of TaqMan™ Universal PCR Master Mix (Thermofisher Scientific, UK), 8 μL of cDNA, 2 μL of primer probe (Table 2-2) and 10 μL of RNase free water was used. Samples were mixed thoroughly before 10 μL triplicates were pipetted into a qPCR 96-well plate (STARLAB, UK). The qPCR plate was sealed and centrifuged at 500 g for 1 minute, then placed in StepOnePlus™ real time PCR machine (Applied Biosystems, USA). 18S was used as a housekeeping gene for calculating relative gene expression for the THP-1 cell line and HPRT-1 was used as a housekeeping gene for calculating relative gene expression for the HMEC cell line. RPLP0 was used as a housekeeping gene for calculating relative gene expression in the lung tissue collected during EVLP.
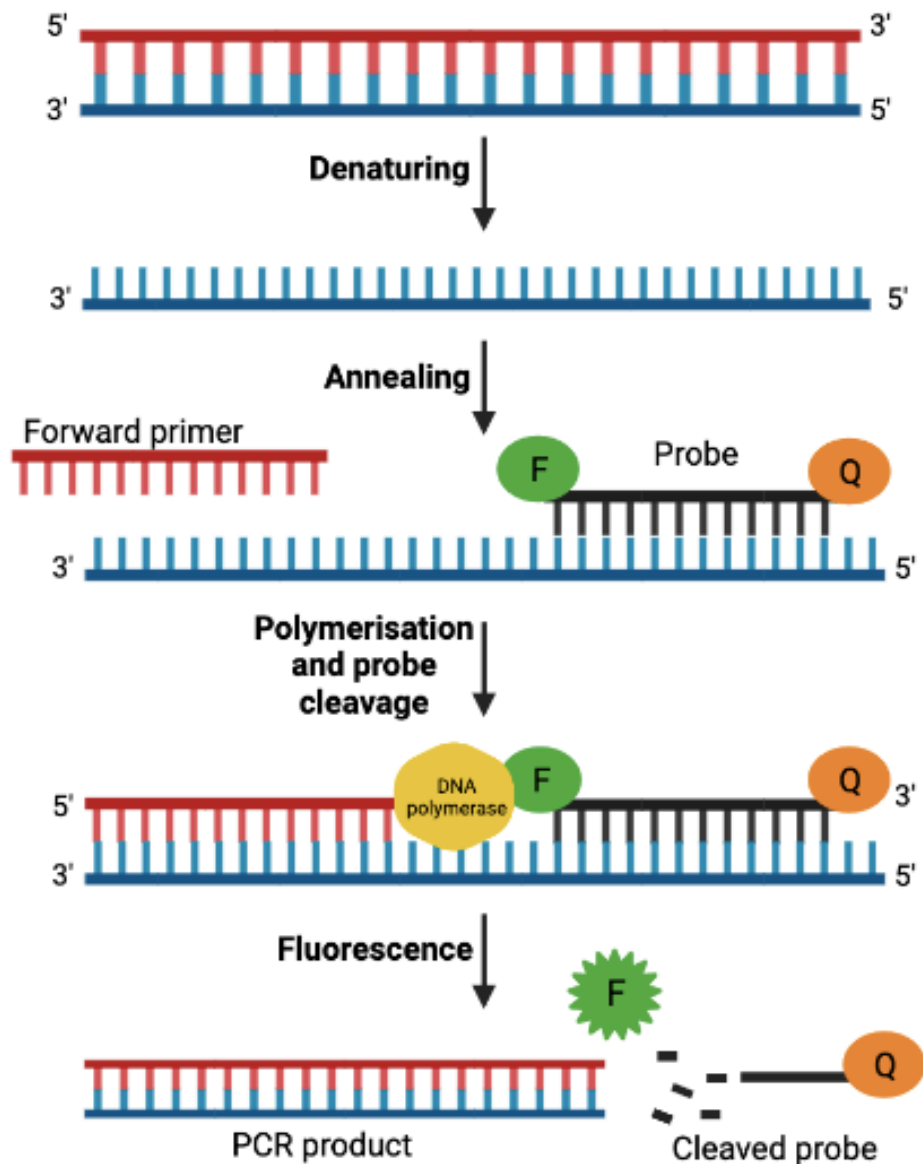
Figure 2-2 Real time PCR with Taqman probes.

DNA is denatured then the probe/primer is annealed to the single-stranded cDNA. The DNA polymerase enzyme extends the strand and upon meeting the probe, cleaves it, resulting in the fluorescent reporter probe moving away from the quencher. Thus, the fluorescent signal can then be detected by the PCR machine. Accumulation of fluorescence is directly proportional to amount of PCR product synthesised.

Target gene	Gene expression assay	Assay design
CXCL8	Taqman Hs00174103_m1	Probe spans exons
TNFα	Taqman Hs00174128_m1	Probe spans exons
IL-6	Taqman Hs00174131_m1	Probe spans exons
IL-10	Taqman Hs00961622_m1	Probe spans exons
MRC1	Taqman Hs00267207_m1	Probe spans exons
ICAM-1	Taqman Hs00164932_m1	Probe spans exons
VCAM-1	Taqman Hs01003372_m1	Probe spans exons
SIPR1	Taqman Hs00173499_m1	Probe spans exons
SIPR3	Taqman Hs01019574_m1	Probe spans exons
18S	Taqman Hs03003631_g1	Non-standard annotation
HPRT-1	Taqman Hs02800695_m1	Probe spans exons
RPLP0	Taqman Hs00420895_gH	Probe spans exons

Table 2-2 Taqman primer probes used for real time PCR.

Primer probes used to determine changes in gene expression between treatments by real time PCR. 18S, HPRT-1 and RPLP0 were used as housekeeping genes.

2.5 Flow cytometry

Flow cytometry was performed to measure the surface markers of hAECs, hAEC-EVs and isolated neutrophils, by incubating them with antibodies conjugated to a fluorescent dye. When run through a flow cytometer, a single fluid stream of cells are excited by a laser whereby they scatter light and emit fluorescence at certain wavelengths which can then be detected and analysed by a computer. Freshly isolated hAECs or neutrophils were aliquoted in fluorescence activated cell sorting (FACS) tubes (Fisher Scientific, USA) then washed with FACS buffer (2% FBS in PBS) and centrifuged at 350 g for 10 minutes for hAECs. Supernatant was discarded and 2.5 µL of FC receptor block (Biolegend, USA) in 100 µL FACS buffer total was added and incubated on ice for 15 minutes. The FC receptor block was washed out before the antibody at the appropriate dilution was added to the samples (Table 2-3), with an IgG isotype control included for each antibody and an unstained control. The samples were incubated for 30 minutes on ice in the dark. After the incubation, 500 µL of FACS buffer was added to the samples and spun at 350 g for 10 minutes. A further wash step with FACS buffer was performed. Supernatant was discarded and the samples were resuspended in 500 µL FACS buffer, ready to run on the FACS Canto II or Fortessa X20 (BD Biosciences, USA). FlowJo software (BD biosciences) was used to gate and analyse the data.

Antibody	Host	Concentration	Isotype	Manufacturer
EpCAM-PE	Mouse	2.5 µL (0.0625 µg)	IgG1, κ PE	eBioscience, Thermofisher, USA
CD45-PE-Cyanine7	Mouse	2.5 µL (0.0625 µg)	IgG1, κ PE-Cy7	eBioscience, Thermofisher, USA
CD105-BV421	Mouse	5 µL (0.125 µg)	IgG1, κ BV421	BD Biosciences, USA
CD90-FITC	Mouse	5 µL (0.125 µg)	IgG1, κ FITC	eBioscience, Thermofisher, USA
CD31-APC	Mouse	1 µL (0.025 µg)	IgG1, κ APC	eBioscience, Thermofisher, USA
CD9-FITC	Mouse	5 µL (0.125 µg)	IgG1, κ FITC	eBioscience, Thermofisher, USA
CD63-PE	Mouse	5 µL (0.125 µg)	IgG1, κ PE	eBioscience, Thermofisher, USA
CD81-APC	Mouse	5 µL (0.125 µg)	IgG1, κ APC	eBioscience, Thermofisher, USA
CD14-PE	Mouse	5 µL (0.125 µg)	IgG1, κ PE	Biolegend, USA
CD193-APC	Mouse	2.5 µL (0.0625 µg)	IgG2b, κ APC	Biolegend, USA
CD15-PE-Cyanine7	Mouse	5 µL (0.125 µg)	IgG1, κ PE-Cy7	Biolegend, USA
CD16-FITC	Mouse	5 µL (0.125 µg)	IgG1, κ FITC	BIolegend, USA

Table 2-3 Monoclonal primary antibodies used for flow cytometry.

Antibodies were diluted in FACS buffer to the relevant concentrations and used to assess the purity of isolated hAECs, hAEC-EVs and isolated neutrophils.

2.6   Enzyme linked-immunosorbent assays

"Sandwich" enzyme linked-immunosorbent assays (ELISAs) were used to quantify protein secretion (Figure 2-3). CXCL8, TNFα, IL-6, IL-10 and sICAM Duoset ELISA kits (R&D systems, USA) were used. The capture antibody was diluted to the working concentration in PBS and used to coat a 96-well microplate and left overnight at room temperature. The capture antibody was removed the next morning and the plate washed with 200 μL wash buffer (Table 2-4) three times, then finally blotting it against a clean paper towel. The plate was then blocked using 250 μL block buffer and left for 1 hour to block at room temperature. A further three washes were performed. Diluted samples or standards made up to the relevant concentration were added to each well in triplicate and incubated for 2 hours. A further three washes were performed. Detection antibody was diluted in reagent diluent to the working concentration (Table 2-5) and left to incubate for a further 2 hours. A further three washes were performed before a working dilution of streptavidin-HRP diluted in reagent diluent was added to the plate for 20 minutes outside of direct light. A final three washes were performed. A 1:1 dilution was performed using colour reagent A and colour reagent B and 50 μL of this dilution was added to each well. The plate was left outside of direct sunlight until sufficient development of colour had occurred in the standards. 50 μL of stop solution added to each well and the plate gently tapped to ensure thorough mixing to completely stop the reaction. The plate was then read at 450 nm immediately using the Synergy™ HT Multi-Detection Microplate (Biotek, USA).
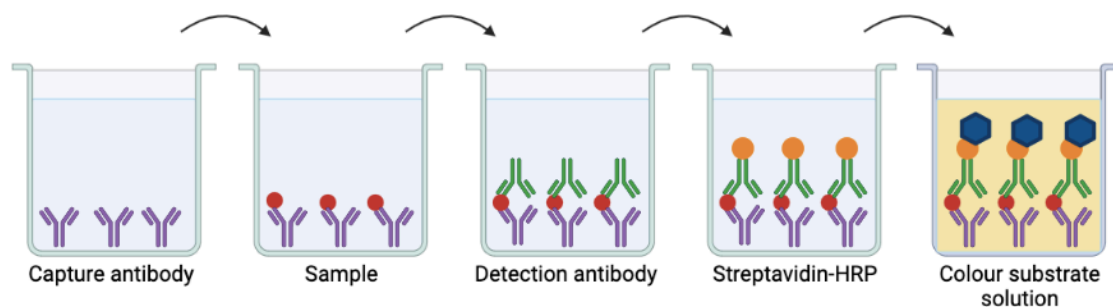
Figure 2-3 The sandwich enzyme-linked immunosorbent assay (ELISA) methodology.

A 96-well plate is coated with a capture antibody which entraps the protein of interest. A detection antibody specific for the capture antibody then binds, followed by streptavidin-HRP. A colour substrate solution then binds to determine level of protein expression and the reaction is finally stopped with the addition of 2 N H_2SO_4.

	CXCL8	TNFα, sICAM, IL-6, IL-10
Wash buffer	0.05% Tween20 in PBS	0.05% Tween20 in PBS
Reagent diluent	1% BSA in Tween20 in PBS	1% BSA in PBS
Substrate solution	1:1 dilution of colour reagent A (H_2O_2) to colour reagent B (Tetramethylbenzidine)	1:1 dilution of colour reagent A (H_2O_2) to colour reagent B (Tetramethylbenzidine)
Stop solution	2 N H_2SO_4	2 N H_2SO_4
Block buffer	5% BSA in Tween20 in PBS	See reagent diluent

Table 2-4 List of solutions required and made up for each of the different ELISA protocols.

Buffers were made up according to manufacturer's instructions for each different ELISA kit.
PBS – phosphate buffered saline, BSA – bovine serum albumin

	CXCL8	TNFα	sICAM	IL-6	IL-10
Capture antibody	4.0 µg/mL	4.0 µg/mL	4.0 µg/mL	4.0 µg/mL	4.0 µg/mL
Detection antibody	20.0 ng/mL	50.0 ng/mL	100 ng/mL		
Streptavidin-HRP	40 fold dilution	40 fold dilution	40 fold dilution	40 fold dilution	40 fold dilution
Standards	31.3 - 2000 pg/mL	15.6 - 1000 pg/mL	31.3 - 2000 pg/mL		31.3 - 2000 pg/mL

Table 2-5 Working concentrations of reagents used as per manufacturers recommendation.

Capture antibody was diluted in PBS to the working concentration, detection antibody, standards and streptavidin-HRP were diluted in the relevant reagent diluent.

2.7 Statistical analysis

All statistical analysis was performed using Graphpad Prism 8 software (Graphpad Software Inc., La Jolla, CA). Error bars included on graphs and statistical tests used are described for each experiment individually. Statistical significance is indicated by the following:

$*$ $p = <0.05$

$**$ $p = <0.01$

$***$ $p = <0.001$

$****$ $p = <0.0001$

3   Isolation and characterisation of isolated hAECs and derivatives

3.1   Introduction

EVLP offers a unique opportunity to administer novel therapeutics directly to the lungs with minimal potential for "off-target" effects that can occur when systemically administered to patients, to recondition extended criteria donor lungs. This gives the potential to expand the donor pool available for transplant. Stem cell therapies, such as MSCs, have attracted attention as a therapy that can be administered to the EVLP platform over the past few years due to their more encompassing effect compared to traditional therapeutics through host cell interactions and immunomodulation via a variety of pathways (Griffiths et al., 2020). EVs derived from stem cells offer an alternative cell-free therapeutic which could rehabilitate extended criteria donor lungs through their influence in modulating the microenvironment by the transfer of bioactive molecules and genetic material, which can lead to immunomodulation and tissue regeneration after injury. EVs could offer a potential advantage over cell therapies due to their small size, which could prevent entrapment in lungs and being more biostable through their encapsulated cargo (Valadi et al., 2007; Xie et al., 2020; Grange et al., 2020).

hAECs offer an alternative promising cell-based therapy to MSCs as they possess immunomodulatory and stem cell like characteristics. They also present minimal risk of tumorigenicity and have low expression of MHC class II HLA and co-stimulatory molecules (Miki, 2018; Pratama et al., 2011). hAECs are derived from the amnion membrane of the placenta and formed from the epiblast during the formation of the foetus (Izumi et al., 2009). The placenta can be collected for the isolation of hAECs from patients undergoing elective c-sections and so face few ethical concerns compared with most cell therapies. Isolation of hAECs can also achieve over 100 million cells per isolation, so unlike MSCs there is little need for rapid expansion. Furthermore, hAECs can now be isolated to cGMP standards to allow for clinical use (Gramignoli et al., 2016).

As discussed in chapter 1.4.4., the immunomodulatory functions of hAECs have been extensively evaluated in acute and chronic pre-clinical lung injury models (Zhu et al., 2017; Moodley, Ilancheran, Samuel, Vaghjiani, Atienza, Elizabeth D. Williams, et al., 2010; Vosdoganes et al., 2013; Melville et al., 2017; Geng et al., 2016). In addition to the whole cells showing immunomodulatory functions, the subsequently

derived conditioned media and EVs have also been demonstrated to have immunomodulatory functions in pre-clinical lung models (Tan et al., 2018). Therefore, hAECs, their conditioned media and hAEC-EVs, if isolated, could offer a potential therapeutic benefit to extended criteria donor lungs if administered via the EVLP platform.

3.1.1 Specific aims

This chapter will focus on developing a reliable and reputable method to isolate hAECs and hAEC-EVs by:

- Developing a method to isolate hAECs through serum-free methodology to achieve high yields and viability
- Demonstrate suitable purity can be achieved through hAEC isolation technique
- Generate hAEC-CM and isolate subsequent extracellular vesicles using differential ultracentrifugation to a suitable purity.

3.2 Materials and methods

3.2.1 Isolation of hAECs

Full term placenta was acquired from healthy women undergoing elective c-sections at the Royal Victoria Infirmary (RVI), Newcastle upon Tyne Hospitals Trust Foundation. Initially, the isolation process for the hAECs involved using serum containing reagents, described in 3.2.1.1. In order to move towards a good manufacturing process (GMP) standard isolation process, we developed an isolation process that involved serum-free reagents instead, described in 3.2.1.2. Figure 3-1 provides an overview of the isolation process.

3.2.1.1 Serum containing isolations

After the placenta was collected and brought up to the lab, the amnion membrane was peeled from the chorion membrane and cut at the base of the umbilical cord (Figure 3-2A). The amnion membrane was washed using Hanks' Balanced Salt Solution (HBSS) (ThermoFisher Scientific) to remove red blood cells. Any blood clots that remained were manually removed by cutting them from the amnion membrane. A section of the amnion membrane was placed in formalin at this point to later be processed by the Cellular Pathology Node in the RVI for histology. The remaining membrane was then cut into approximately 4x4 cm pieces and placed equally into 4 falcon tubes containing 0.05% Trypsin-EDTA (ThermoFisher Scientific) for 15 minutes at 37°C whilst rotating on a MACSmix™ Tube Rotator (Miltenyi Biotec, UK). Afterwards, the membrane was placed into another 4 falcon tubes containing fresh 0.05% Trypsin-EDTA, then further incubated for 1 hour at 37°C whilst rotating on a MACSmix™ Tube Rotator (Figure 3-2B). After this digest, the membrane was gently scraped against the container wall, mechanically removing any remaining cells left on the membrane into the digest solution (Figure 3-2C). Once all the pieces were scraped, 5 mL of FBS was added to the digest solution to prevent any further digestion. This solution was then filtered through a 100 μm sterile filter (VWR, USA). The solution was then spun at 350g for 10 minutes at 4°C. The cell pellet was then resuspended in 5 mL DMEM-F12 media (ThermoFisher Scientific) supplemented with 10% FBS (Lonza), 1% 2 mM L-glutamine, 100 μg/mL penicillin, 0.1 mg/mL streptomycin (All Sigma Aldrich). This was then filtered using a 70 μm sterile filter (VWR) and then the cells were brought to a convenient volume for cell counts

(usually between 20-35 mL). A cell count was then performed using trypan blue and a haemocytometer.

The hAECs were then ready for further processing and purity checking through flow cytometry. To freeze the cells, 5 million freshly isolated hAECs were added to FBS with 10% DMSO in a 1:1 dilution, then placed in a CoolCell® Cell Freezing Container (BioCision, USA) in a -80°C freezer for 24 hours. The hAECs were then moved to liquid nitrogen for more permanent storage.

3.2.1.2 Serum-free isolations

The placenta was collected, the amnion membrane peeled and washed using HBSS as described above in 3.2.1.1. The membrane was digested for 15 minutes with 0.05% Trypsin-EDTA or 15 minutes at 37°C whilst rotating on a MACSmix™ Tube Rotator. The membrane was then added to fresh 0.05% Trypsin-EDTA then further incubated for 1 hour at 37°C on a MACSmix™ Tube Rotator. The cells were then mechanically removed as described above in 3.2.1.1 through scraping. A trypsin inhibitor from *Glycine max* (Sigma Aldrich) was used to stop any further digestion at a concentration of 1 mg/mL. The solution was then filtered through a 100 μm sterile filter, spun at 350g for 10 minutes at 4°C. The cell pellet was then resuspended in 5 mL UltraCULTURE™ media (Lonza) supplemented with 1% 2 mM L-glutamine, 100 µg/mL penicillin, 0.1 mg/mL streptomycin. This was then filtered using a 70 μm sterile filter, brought to a convenient volume and a cell count was performed using trypan blue and a haemocytometer.

The freshly isolated hAECs were then purity checked through flow cytometry or frozen down. To freeze the hAECs, 5 million cells were resuspended in Synth-a-Freeze medium (ThermoFisher Scientific) then placed in a CoolCell® Cell Freezing Container in a -80°C freezer for 24 hours before being moved to liquid nitrogen for more permanent storage.
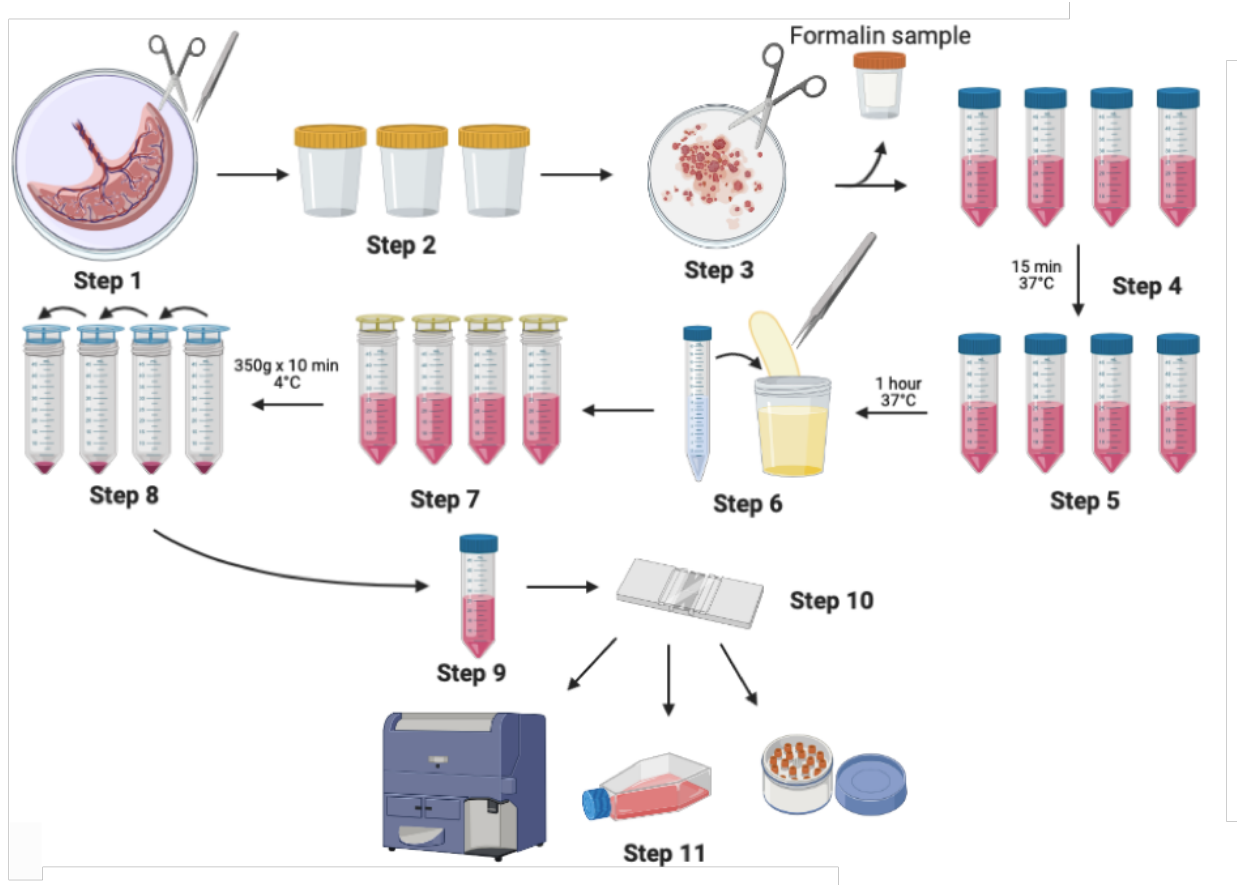
Figure 3-1 Isolation process for hAECs.

An overview of the hAEC isolation process from fresh placenta. Step 1: The amnion is peeled from the placenta. Step 2: The amnion membrane is washed in HBSS at least three times. Step 3: Any remaining blood is cut away and a sample of the membrane is placed in formalin. Step 4: The membrane is cut up and placed in 0.05% trypsin-EDTA for 15 minutes at 37°C. Step 5: The membrane is placed in fresh 0.05% trypsin-EDTA for an hour at 37°C. Step 6: The membranes are manually scraped for any remaining cells and 5 mL of trypsin inhibitor added. Step 7: The trypsin mix is filtered through a 100 μm filter and spun at 350g for 10 minutes. Step 8: The supernatant was discarded, 5 mL of media was added to the cells and filtered in 70 μm, resuspending the cell pellets each time. Step 9: The pooled cells were then topped up to a suitable volume. Step 10: the cells were counted with trypan blue. Step 11: The cells are then purity checked using the FACs Canto II and either frozen or cultured for conditioned media. (Figure adapted from Rebecca Charlton's MRes Thesis, 2020).

Figure 3-2 Isolation of hAECs.

Images were taken during the serum free isolation process using fresh term placentae. (A) Amnion membrane is peeled inside a Class II Microbiological safety cabinet. (B) The membrane is cut up and placed in 0.05% trypsin and rotated in a MACSmix™ Tube Rotator. (C) The digested amnion membrane was scraped against the side of the tube to ensure all hAECs were being removed from the membrane.

3.2.2 Production of conditioned media

To produce the conditioned media used for *in vitro* assays, 60,000 cells/cm^2 were added to a T75 culture flask (Greiner Bio-One, UK) and topped up with UltraCULTURE™ media supplemented with 1% 2 mM L-glutamine, 100 µg/mL penicillin, 0.1 mg/mL streptomycin. The flasks were then incubated for 4 days in 37°C, 5% CO_2. The media was then harvested and spun at 350g for 10 minutes at 4°C to pellet the cells. 1 mL aliquots of the media were stored in the -80°C freezer.

In order to produce the conditioned media used to isolate EVs, 60,000 cells/cm^2 were seeded into a T175 culture flask (Greiner Bio-One) and topped up with complete UltraCULTURE™ media to 25 mL, then left to incubate for 4 days in 37°C, 5% CO_2. The media harvested into a 50 mL falcon then spun at 350 g for 10 minutes at 4°C to pellet the cells. The supernatant was then transferred into a fresh 50 mL falcon and spun at 2,000g for 10 minutes at 4°C to pellet any dead cells or debris. The supernatant was then pooled together and stored at -80°C until further processing into EVs.

3.2.3 Isolation of extracellular vesicles through differential ultracentrifugation

Conditioned media produced as described in 3.2.2. was thawed overnight at 4°C in order to isolate the EVs. The conditioned media was then transferred to high-speed spin tubes and balanced within 1 g of each other, topping up with PBS (ThermoFisher Scientific) as necessary. The tubes were placed into the JA25.50 rotor in the Avanti J-E high speed centrifuge (Beckman Coulter, USA) and spun at 10,000 g for 30 minutes at 4°C. The conditioned media was transferred back to 50 mL falcons carefully as to not disturb the pellet. The conditioned media was then transferred to 38 mL UltraClear Ultracentrifuge tubes (Beckman Coulter), placed into the metal casings then balanced with 1 mg of each other, topping up with PBS as necessary. The casings were then hung on the SW28 rotor. The rotor was loaded into the Optima XE-90 Ultracentrifuge (Beckman Coulter) and the conditioned media was spun for 25,000 rpm (100,000 g) for 2 hours at 4°C. The exosome depleted media was carefully removed into a collection pot, leaving only a few mL behind. The EVs were resuspended and stored at 4°C. The exosome depleted media was then re-spun at 25,000 rpm for 2 hours at 4°C. Exosome pellets collected from the first run

were then pooled with the second run then topped up with PBS. Finally, the EVs were spun at 25,000 rpm for 1 hour and 10 minutes at 4°C. The supernatant was carefully removed as to not disturb the exosome pellet. The pellet was then resuspended in 300-800 μL PBS, aliquoted for further use, then stored at -80°C.

3.2.4 Histology

The amnion membrane collected during the isolation process was paraffin embedded by the Cellular Pathology Node then cut on to APES coated slides at a thickness of 4 μm. An H&E stain and immunohistochemistry was performed on the membrane. The H&E was performed as described in chapter 2.3.2. Immunohistochemsitry was carried out on the tissue as described in chapter 2.3.1.1 using the Vector ImmPRESS® kit, using epithelial markers EpCAM and CK19, mesenchymal marker vimentin, endothelial cell marker CD31, immune cell markers CD45 and CD14, human leukocyte antigens G and DR (HLA-G and HLA-DR). Paraffin embedded placental bed tissue was used as a positive control for this staining.

3.2.5 Cytology

After isolation,15 μL of freshly isolated cells were seeded onto a chamber slide with 200 μL UltraCULTURE™ media and incubated for 72 hours at 37°C and 5% CO_2. The cells were then fixed with 99% methanol for 10 minutes then stored at -20°C until staining. The staining was performed as described in 2.3.1.2, using the same markers CK19, EpCAM, Vimentin, CD31, CD45, CD14, HLA-G and HLA-DR. In addition to this, a smear prepared using 50 μL of freshly isolated hAECs were pipetted onto a slide, left to dry and then fixed with acetone for 10 minutes. A cytospin of 0.5 x 10^6 freshly isolated hAECs were spun using the Cytospin 3 (Shandon), then fixed in acetone for 10 minutes. Both smears and cytospin slides were stored at -20°C prior to staining with H&E and Diff Quik as described in chapter 2.3.2 and 2.3.3. respectively.

3.2.6 Flow cytometry on hAECs

Flow cytometry analysis was used to purity check the hAECs and subsequently derived hAEC-EVs. The antibodies EpCAM, CD45, CD90, CD105 and CD31 were used to purity check the hAECs and were titrated prior to use. This was carried out

by aliquoting 0.5 x 10⁶ freshly isolated hAECs into FACS tubes, then spun at 350 g for 10 minutes at room temperature. The cells were washed with FACS buffer (2% FBS in PBS) then spun again at 350 g for 7 minutes. The pellet was then resuspended with a single antibody in the following dilutions; 5 μL, 2.5 μL, 1 μL and 0.5 μL to make up a total of 100 μL FACS buffer. An unstained control was also included. The cells were incubated for 30 minutes, on ice in the dark, then 1 mL of FACS buffer was added to each tube and spun at 350 g for 10 minutes. The cells were washed again with FACs buffer, then finally resuspended in 500 μL FACS buffer and run on the FACS Canto II. The stain index calculation was then used to determine the optimal concentration of antibody:

$$Stain\ index = \frac{(Median\ of\ positive - Median\ of\ negative)}{(SD\ of\ negative\ \times 2)}$$

Where there were no clear positive or negative populations, the coefficient of variance (CV) was calculated to determine optimal concentration of antibody:

$$CV = \frac{SD}{Median\ fluorescence\ of\ population}$$

Once the optimal concentration of the antibodies was achieved, flow cytometry was performed after every placental isolation to ensure the hAECs derived were of sufficient purity, as described in chapter 2.5. Briefly, 0.5 x 10⁶ freshly isolated hAECs were spun at 350 g for 10 minutes, resuspended in 95 μL FACS buffer and 5 μL of FC receptor block and incubated for 15 minutes. The cells were washed then resuspended in 2.5 μL of EpCAM-PE, 2.5 μL CD45-PeCy7, 5 μL CD105-BV421, 5 μL CD90-FITC and 1 μL CD31-APC with 84 μL of FACS buffer then incubated for 30 minutes on ice in the dark. An IgG isotype control was included for each antibody and an unstained control. 500 μL was then added to each FACS tube, spun at 350 g for 10 minutes. An additional wash step was carried out. Finally, the cells were resuspended in 500 μL FACS buffer and run on the FACS Canto II. To compensate, each antibody was diluted at the appropriate concentration in FACS buffer in a separate FACS tube then a drop of OneComp eBeads™ compensation beads (ThermoFisher Scientific) was added, the tube was vortexed then run on the FACS Canto II. FlowJo software was used to gate and analyse the data.

3.2.7 Flow cytometry on hAEC-EVs

The flow cytometry protocol carried out to characterise the hAEC-EVs was based of the protocol published by (Théry et al., 2006). 20 μg of purified EVs were incubated with 5 μL 4 μM aldehyde/sulphate latex beads (ThermoFisher Scientific) at room temperature for 15 minutes in a 1.5 mL eppendorf, to allow for detection on the flow cytometer. PBS was then added to a final volume of 500 μL and incubated for 2 hours at room temperature on a tube revolver rotator. The eppendorf was then topped up to 1 mL with PBS, then 110 μL 1 M glycine was added, mixed gently and the eppendorf was left to stand on the bench at room temperature for 30 minutes. The EVs-bead mix was then washed by spinning at 4000 rpm for 3 minutes. The supernatant was removed carefully and the pellet resuspended in 1 mL PBS with 0.05% BSA. This wash step was then repeated again. The EV-bead mix was then incubated with 2.5 μL CD81-APC, 2.5 μL CD63-PE and 2.5 μL CD9-FITC in a total of 50 μL PBS with 0.05% BSA, at 4°C overnight. An IgG isotype control was included for each antibody and an unstained control. The pellet was then washed twice with PBS with 0.05% BSA as described above before resuspending in 200 μL of PBS with 0.05% BSA, transferred to FACS tubes then run on the FACS Canto II. Both single and doublet beads were gated and analysed by comparing to the relevant isotype control using the FlowJo software.

3.2.8 Electron microscopy

Transmission electron microscopy (TEM) was performed on the hAEC-EV samples by Tracey Davey from the Electron Microscopy Research Services unit, Newcastle University. 20 μL of each sample of purified EVs were provided for TEM. Negative staining was carried out involving applying the EVs onto a coated grid, then a drop of heavy metal salt is applied to surround the sample, then when the electron beam passes through the sample the EVs will appear light on a dark background to reveal their structural details. The EVs were imaged by the Hitachi HT7800 120kV TEM microscope.

3.2.9 BCA assay

To quantify the hAEC-EV protein concentrations after isolations, a Bicinchoninic acid (BCA) assay was carried out, the principle behind this assay is the proteins will

reduce Copper $(Cu)^{2+}$ to Cu^+ in a highly alkaline solution, this results in a purple colour forming by bicinchoninic acid. The amount of Cu^{2+} reduced is proportional to the amount of protein. Using the Pierce™ BCA Protein Assay Kit (Thermofisher Scientifc), a standard was made up through serial dilution of BSA in PBS, for a working range of 125–2000 μg/mL. A BCA working reagent was prepared by mixing 50 parts of BCA reagent A with 1 part Reagent B, provided by the kit. 10 μL of each standard and EV prep was added to a 96-well plate in triplicate. 200 μL of the working reagent was added to each well, the plate was then rotated for 30 seconds before being covered and incubated at 37°C for 30 minutes. The plate was cooled before being read at 562 nm on the Synergy™ HT Multi-Detection Microplate (Biotek).

3.3 Results

3.3.1 Donor information, cell counts and viabilities of the isolations

The total number of isolations carried out during this project was 36. 25 of the placentae were used for experiments as described in Table 3-1, 6 were not used either due to the isolation being halted or ideal purity not being achieved, the rest have been stored for future use. All placentas collected were from donors at 39-40 weeks pregnancy before undergoing C-section. Notably, the largest impact observed to lower cell counts or viability appeared to be whether the placenta was observed to be cold or warm upon arrival to the lab. Secondly, the other factor that appeared to influence cell counts was if the placenta was noticeably bloodier or containing a large number of blood clots, resulting in more of the membrane having to be cut away. Medications taken by the donor mother did not appear to have an effect on cell counts or viability. Initially a serum-containing isolation process was used, but after changing to a serum-free isolation process (from HP009) there was no decrease in cell count or viability observed (Figure 3-3).

Placenta ID:	Assay used:	Age:	BMI:	Medications:	Isolation comments:	Cell count:	Viability:
HP001	H&E and IHC	37	32.6			132.5 x10^6	91%
HP002		n/a	23		Delay in receiving placenta	107 x 10^6	89%
HP003		35	20		Placenta was surgically damaged, Plaques	96.41 x 10^6	91.20%
HP004		30	30	Symbicort, terbutaline, pulmicort (Asthma)	Bloody, cold	69.92x10^6	94.40%
HP005		28	28		Small placenta, cold	81.53 x 10^6	95.70%
HP009*	Conditioned	33	37	Metformin (Gestational diabetes)	First serum free isolation	132.60x10^6	92%
HP010	media	33	24		Cold	86.94x10^6	97.90%
HP011	experiments	31	26.5		Placenta was surgically damaged, blood clots	78.33X10^6	96.10%
HP012**		32	29	Adalimumab and lansaprazole	Many blood clots	61.9 X10^6	94.40%
HP013		41	29	Aspirin	Thin membrane, tore easily	135.47 X10^6	97.10%
HP015		26	20.5		Plaques	114.22 x10^6	94.50%
HP016		n/a	30		Cold	76.74 x 10^6	93.20%
HP017		32	23		Cold	89.9 x 10^6	95.40%
HP020	EV isolation	38	25	Multivitamins		173.38 x10^6	95.20%
HP021		29	21.1	Ferrous sulphate		164.42 x10^6	95.50%
HP024		27	24.8	Infliximab and azathioprine (Crohn's disease)		114.5 x10^6	92.70%
HP025		24	n/a		Very bloody	84.8 x10^6	93.60%
HP026		43	n/a			236.7 x 10^6	94.20%
HP028		31	22.6			203.2 x 10^6	90.40%
HP029	EVLP	31	26		Very bloody, large proportion cut away	89.2 x20^6	90.40%
HP030		33	34.2	Symbicort (asthma)		118.1 x 10^6	93.80%
HP031		32	26			241.3 x 10^6	95.95%
HP033		32	26.4	Omeprazole		76.95 x 10^6	93.50%
HP034		30	28.3			143.8 X 10^6	93.50%
HP036		33	27.9	Omeprazole and folic acid		261.73 x 10^6	95.80%

Table 3-1 Donor information, cell counts and viabilities of hAEC isolations and what each were subsequently used for in assays.

The table features any medication, any information observed during the hAEC isolations and ultimately what cell count and viability was achieved. The isolations are categorised into what assays they were then used for; staining, conditioned media assays, EV isolation preparations or for use in EVLP. * = HP009 is the point at which the isolations were carried out using serum free reagents. ** = HP012 was subsequently tested in the conditioned media assays and found to elicit a pro-inflammatory response, this could be due to the combination of anti-inflammatory medications used by this donor.
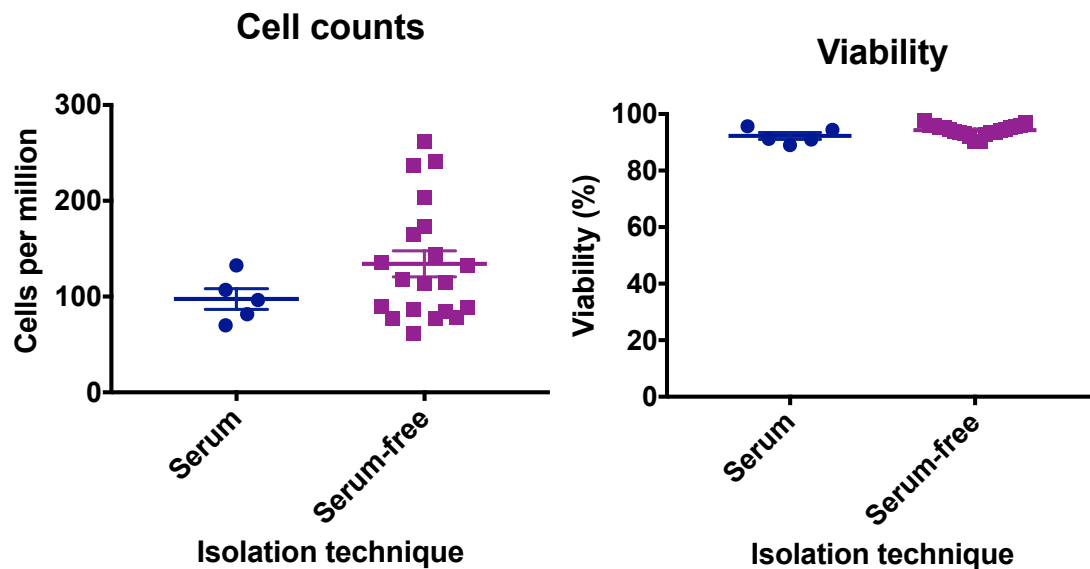
Figure 3-3 Cell counts and viabilities for hAEC isolations that contain serum or serum free.

The cell counts for the serum-free isolation process do not drop much lower than serum containing process, in fact higher cell counts were observed during the serum-free isolation process. The viability was not affected by the change to a serum-free isolation process with viabilities consistently over 90%.

3.3.2 Purity of hAEC isolations

Flow cytometry was used to assess purity for every isolation using freshly isolated hAECs. Five antibodies were chosen to test purity including EpCAM, an epithelial cell marker, CD45, a leukocyte marker, CD31, an endothelial cell marker, CD90, MSC marker and CD105, a stem cell marker. The choice of markers were based on the work done by Murphy *et al* to characterise the hAECs (Murphy et al., 2010).

3.3.2.1 Titration of purity antibodies for flow cytometry

The purity antibodies were titrated in order to have an optimally functioning and cost-effective purity test. Four concentrations were used: 0.5 μL, 1 μL, 2.5 μL and 5 μL. In order to determine the best concentration of the EpCAM antibody, where there was clear positive and negative populations, the stain index was calculated (Figure 3-4A). There was a levelling out in stain index after 2.5, μL, indicating a peak saturation of antibody and optimal concentration had been achieved (Figure 3-5A). For the markers CD90, CD105, CD31 and CD45 where there were no clear positive and negative populations (Figure 3-4), the CV was calculated and plotted instead of the stain index, where a decrease in CV would indicate optimal concentration (Figure 3-5). A decrease was observed at 2.5 μL of CD45 and 1 μL of CD31, indicating that

these are the optimal concentrations of antibody. For CD105 and CD90 there was no continual decrease in CV, therefore these antibodies required 5 μL.
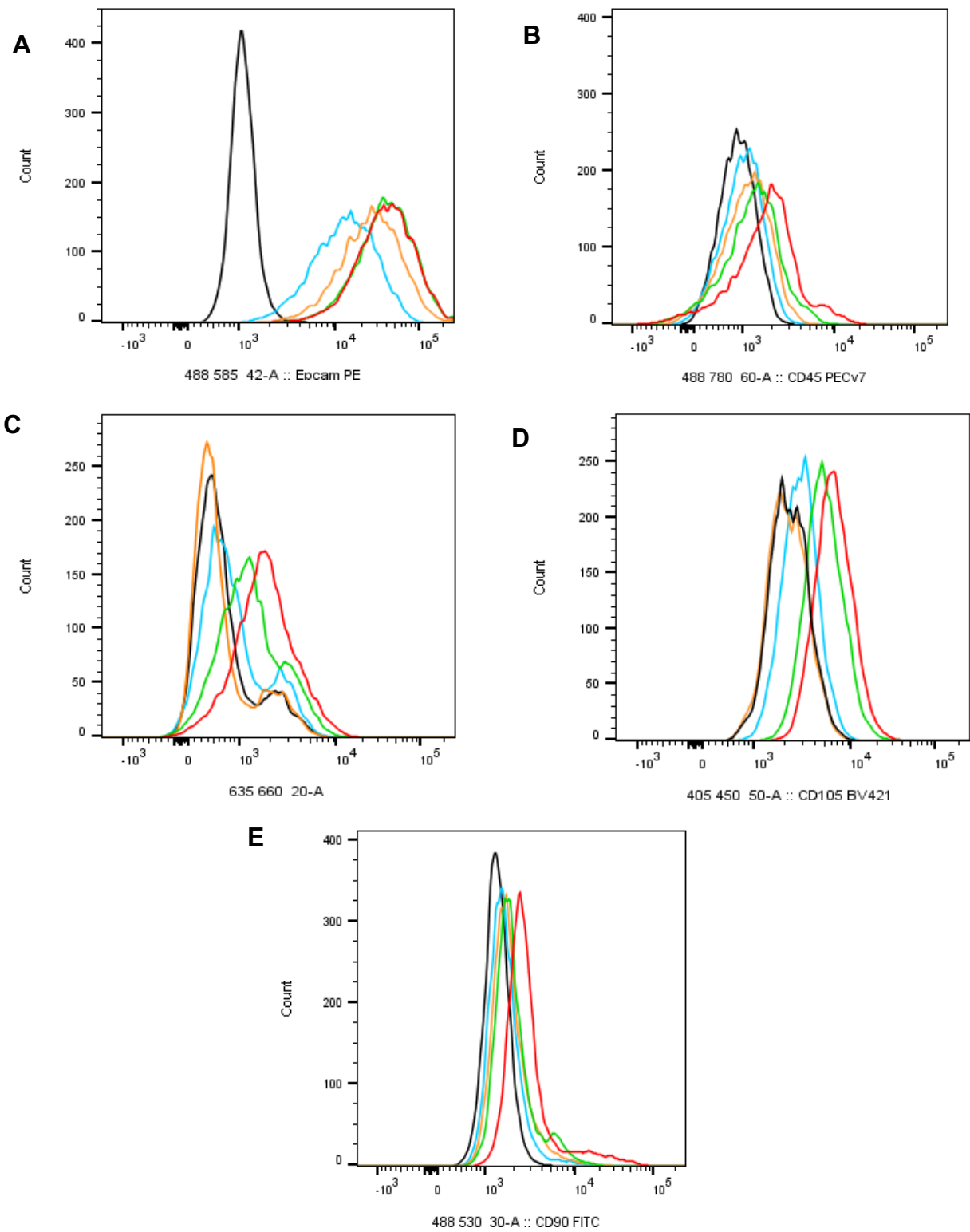
Figure 3-4 Titration of purity antibodies.

A histogram of mean fluorescence intensity (MFI) was plotted for each of the four chosen concentrations; 0.5 μL (blue), 1 μL (orange), 2.5 μL (green) and 5 μL (red), alongside the unstained population (black), for each of the chosen antibodies of; (A) EpCAM (B) CD45 (C) CD31 (D) CD105. (E) CD90. N=1
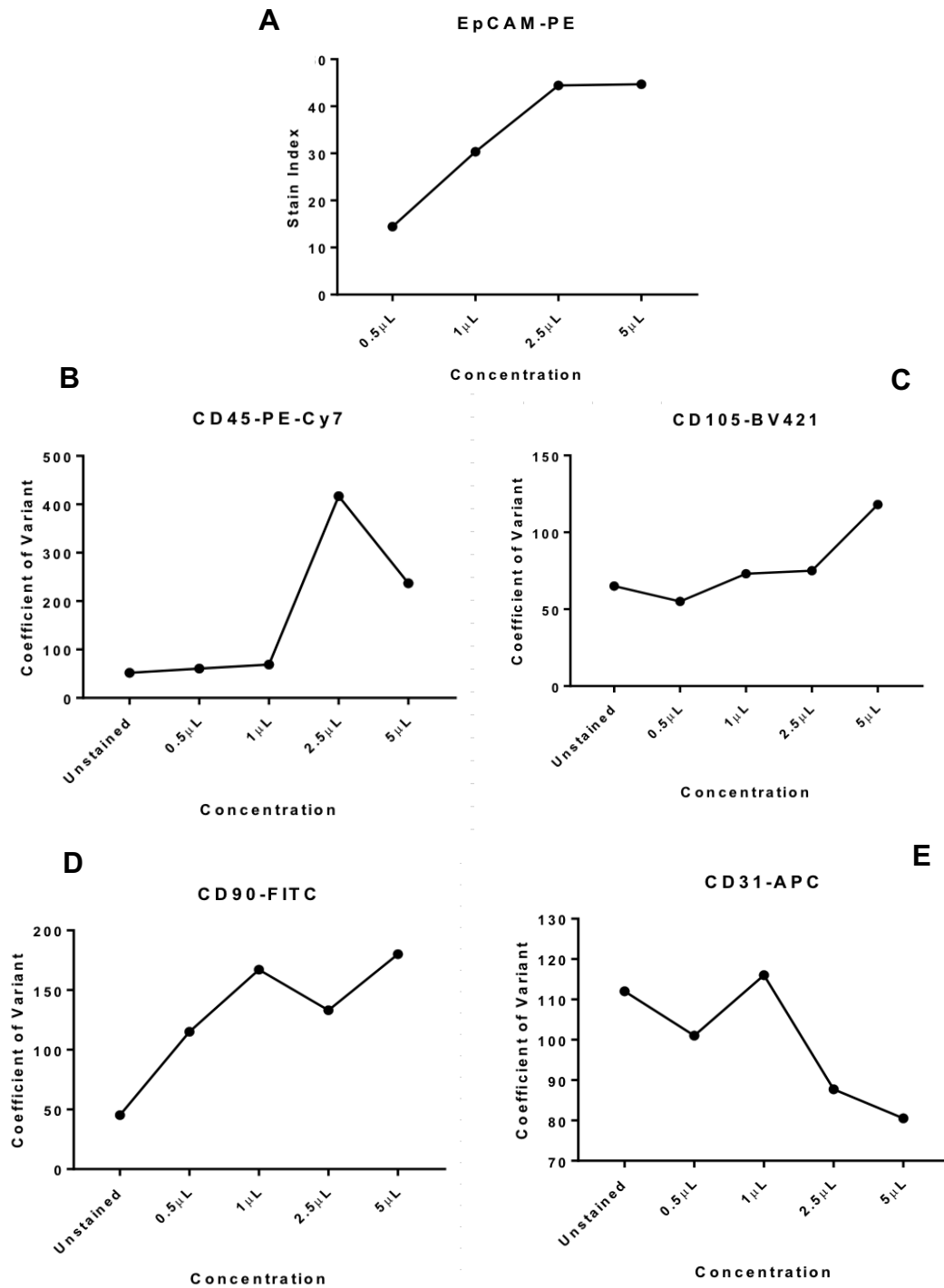
Figure 3-5 Optimisation of hAEC purity antibodies used in flow cytometry.

The stain index was plotted for EpCAM and the coefficient of variance (CV) for CD105, CD90, CD31 and CD45. (A) The stain index plateaued after 2.5 μL for EpCAM-PE. (B) CV decreases after 2.5 μL of CD45-PeCy7. (C) The CV continued to gradually increase as antibody concentration increased. (D) There is no continual decrease in CV observed for CD90-FITC. (E) There was a continual decrease after 1 μL of CD31-APC. N=1

70

3.3.2.2 Flow cytometry purity analysis of hAECs

Following optimisation, flow cytometry was performed after every isolation to ensure suitable purity was achieved. EpCAM expression was consistently high with an average expression of 94%. Only isolations with a purity of over 90% EpCAM expression were used in subsequent functional assays (Figure 3-6). Expression of negative markers CD45, CD105 and CD31 were consistently under 2% average expression. CD90, a stem cell marker, showed some expression, suggesting a heterogenous population with a small population of stem cells isolated.
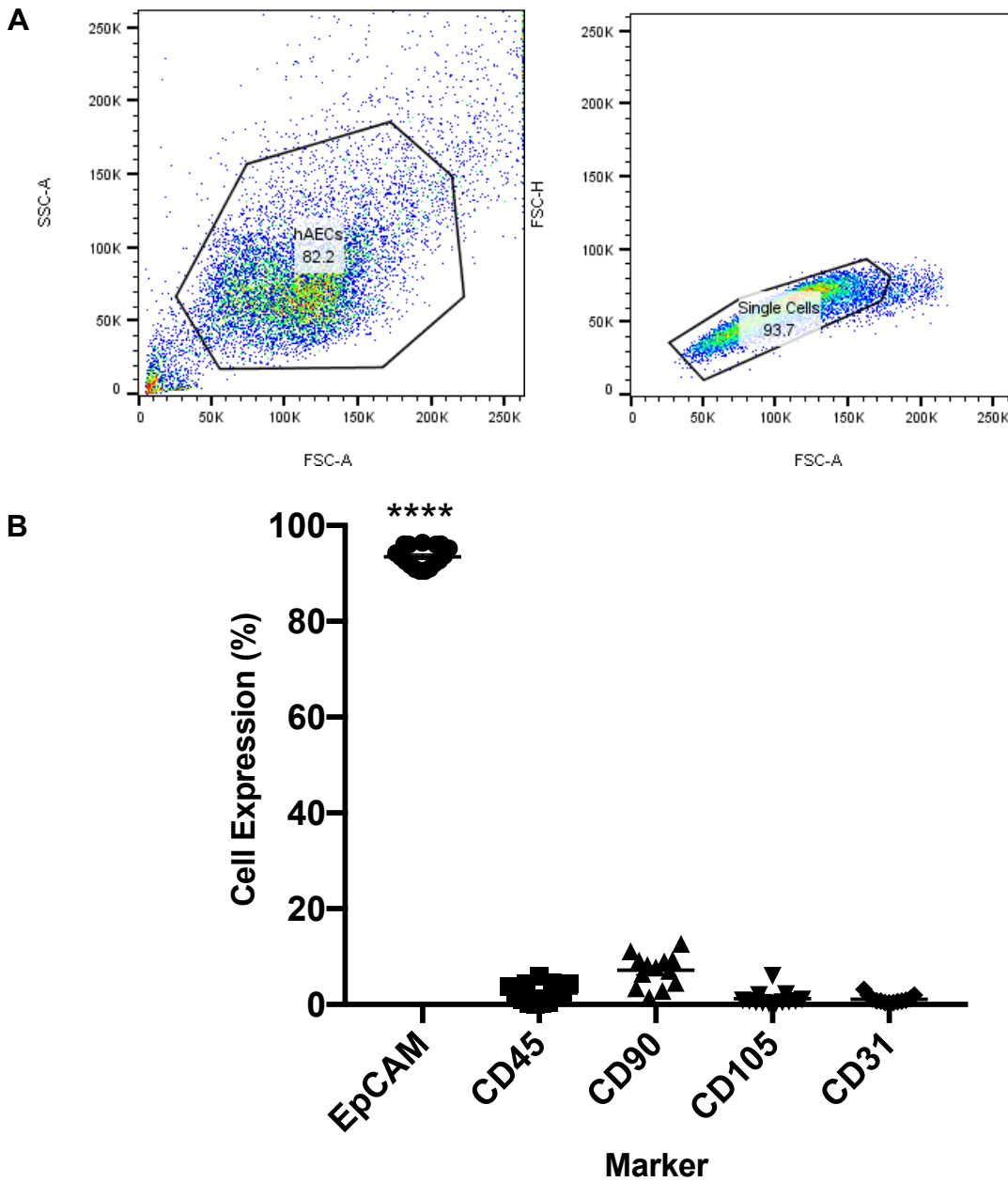
Figure 3-6 Purity of serum-free hAEC isolations.

Flow cytometry was used to perform purity checks on hAEC isolations. (A) The gating strategy used to gate the hAEC population and subsequent single cell population (B) Purity from the serum-free isolations subsequently used in functional assays. N=17. Statistical significance was determined by a one-way ANOVA. **** $p < 0.0001$.

3.3.3 Characterisation of the amnion membrane through immunohistochemistry

We characterised the amnion membrane from three placentae, to further our understanding of which cell populations may reside natively on the membrane and of which cells may be isolated from the membrane with hAECs to aid in our later characterisation of the isolated hAECs once cultured in media (Chapter 3.3.4). Sections of amnion membrane were collected during the isolation process and formalin fixed, processed to paraffin blocks and sectioned. Both H&E and IHC were performed on the amnion membrane to visualise structure and also characterise the expression of markers on the amnion membrane, respectively. H&E staining carried out on the amnion membrane demonstrated the hAECs reside and are attached to the edge of the membrane and have the classic polygonal shaped morphology of epithelial cells (Figure 3-7).

IHC performed on the amnion membrane highlighted the hAECs lining the edge of the amnion membrane, shown by the strong positive staining of epithelial cell marker CK19 (Figure 3-8). Unfortunately, EpCAM staining appeared to be non-specific. There was some positive staining of immune cell makers CD45 and CD14, suggesting the presence of placental macrophages on the amnion membrane. However, HLA-DR staining, which is expressed on antigen presenting cells, appeared to be non-specific. There is some mesenchymal (vimentin) and endothelial (CD31) cell staining visible on the amnion membrane. Placental bed tissue was used as a positive control.
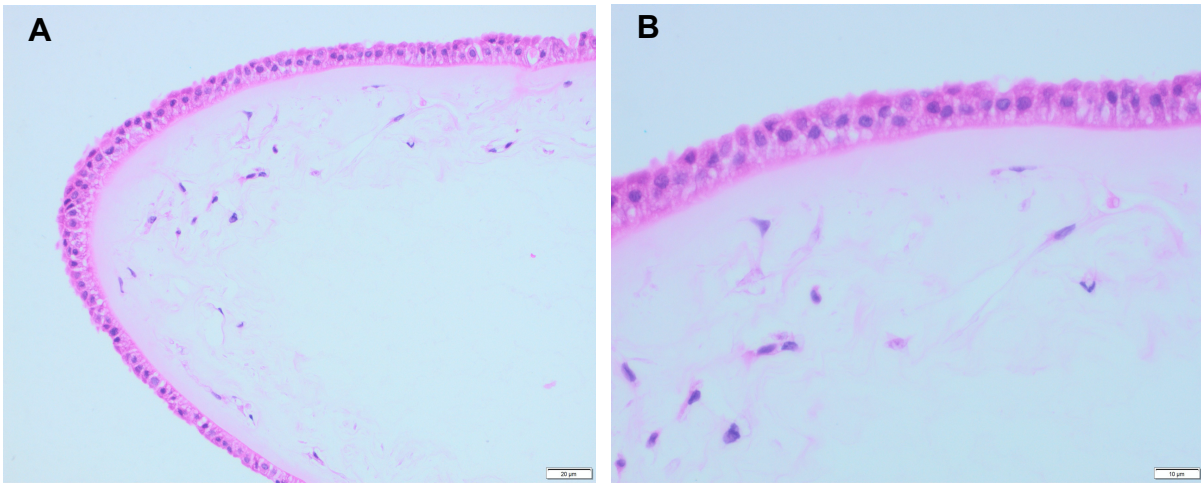
Figure 3-7 H&E staining on the amnion membrane.

H&E staining was performed on formalin fixed amnion membrane harvested after the separation from the chorion membrane during the hAEC isolation process. (A) The epithelial cells can be seen to line the edge of the amnion membrane (x20), scale: 20 μM. (B) hAECs express the classic polygonal morphology typical of epithelial cells (x40), scale: 10 μM. Images are representative of n=5.
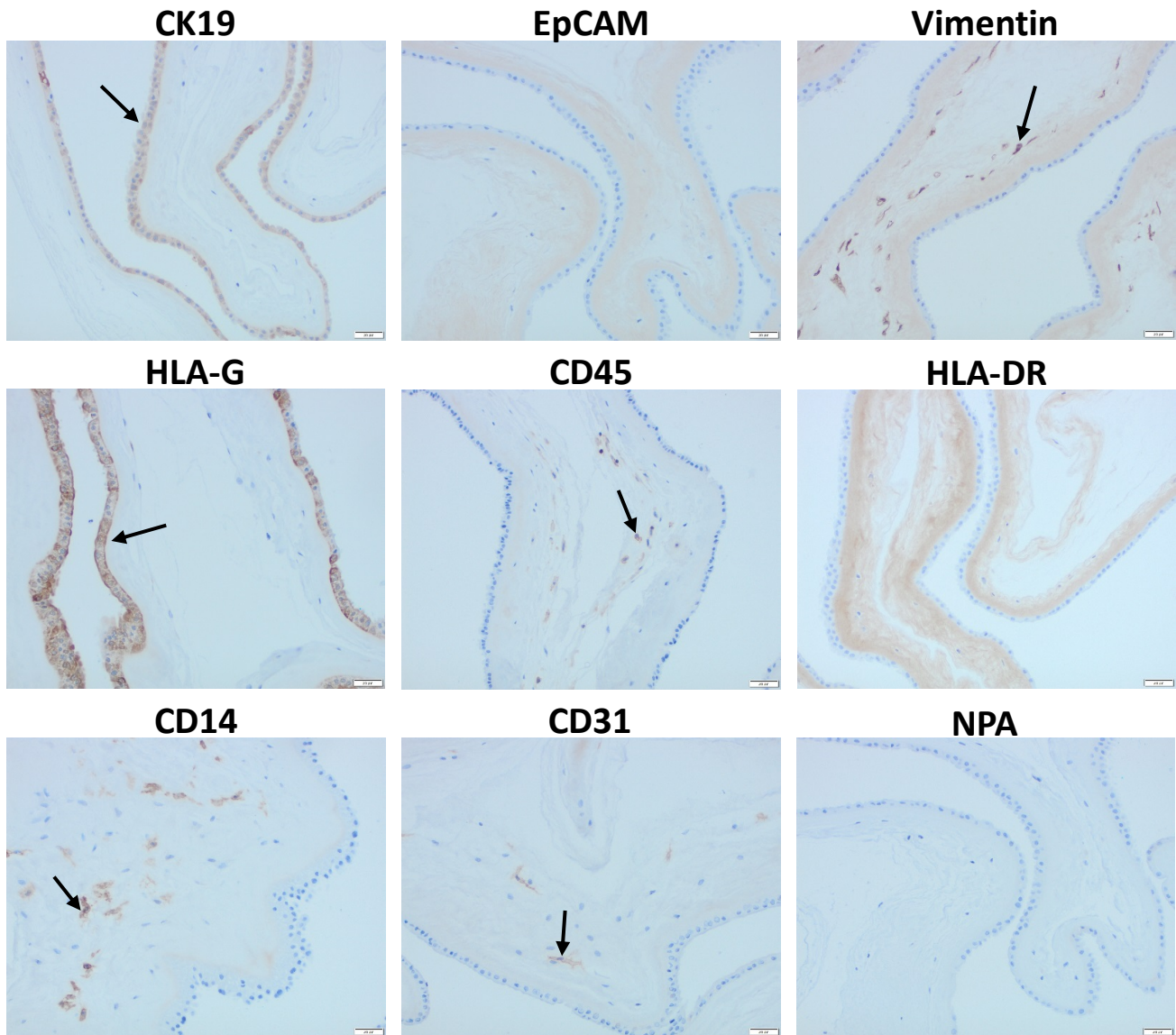
Figure 3-8 Immunohistochemistry (IHC) staining on amnion membrane.

IHC was carried out on formalin fixed paraffin embedded amnion membrane collected during the hAEC isolation process. Epithelial cell markers CK19 and EpCAM, mesenchymal marker Vimentin, leukocyte marker CD45, macrophage marker CD14, endothelial cell marker CD31 and MHC markers HLA-DR and HLA-G were used to characterise cell expression on the amnion membrane. A no primary antibody (NPA) was included. All images are x20 and representative of 3 fields of view per section. Scale: 20 μM. These images are representative of n=3.

3.3.4 Characterisation of hAECs in culture using immunocytochemistry

Prior to culturing the hAECs, H&E and diff quik staining was performed on freshly isolated hAECs through a smear and cytospin respectively, to provide understanding of morphology of the cells. H&E staining on the smear demonstrates the epithelial cell-like morphology (Figure 3-9A), however the diff quik staining on the cytospin provides a clearer idea of the morphology of the cells (Figure 3-9B). The colour of the diff quik staining being the same also highlights mostly epithelial cells are being isolated.

Immunocytochemistry staining was carried out on hAECs cultured for 3 days and the same markers were used as chapter 3.3.3 to provide a comparison to the positive staining observed on the amnion membrane. Positive staining can be observed for epithelial cell markers CK19 and EpCAM and mesenchymal marker vimentin (Figure 3-11). Some positive staining was observable for HLA-G, CD45, HLA-DR, CD14 and CD31 (Figure 3-11), however overall these markers showed minimal expression (Figure 3-10). Counts on the staining were performed by Miss Rebecca Charlton, under my supervision. These counts showed a high percentage expression of CK19, suggesting hAECs are the largest population being isolated. EpCAM staining had weaker expression however this is likely due to a poor antibody (Figure 3-10).
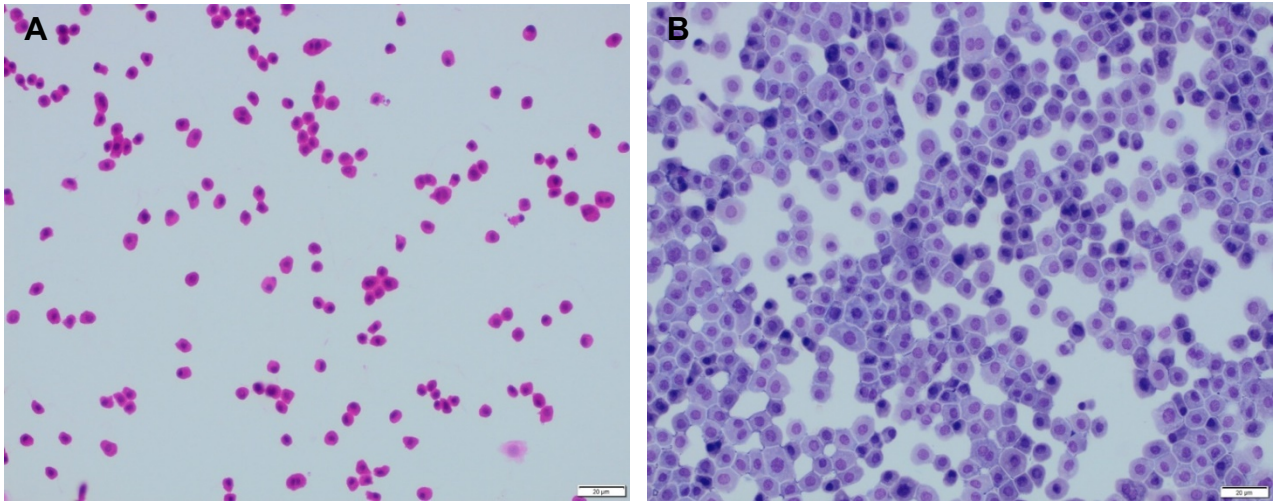
Figure 3-9 H&E and Diff Quik staining on hAECs.

(A) H&E of a smear of isolated cells which show a similar epithelial cell-like morphology. N=5 (B) Diff Quik staining of a cytospin performed on freshly isolated hAECs. Same colour staining and epithelial cell-like morphology can be observed. Scale: 20 μM (x20). N=1
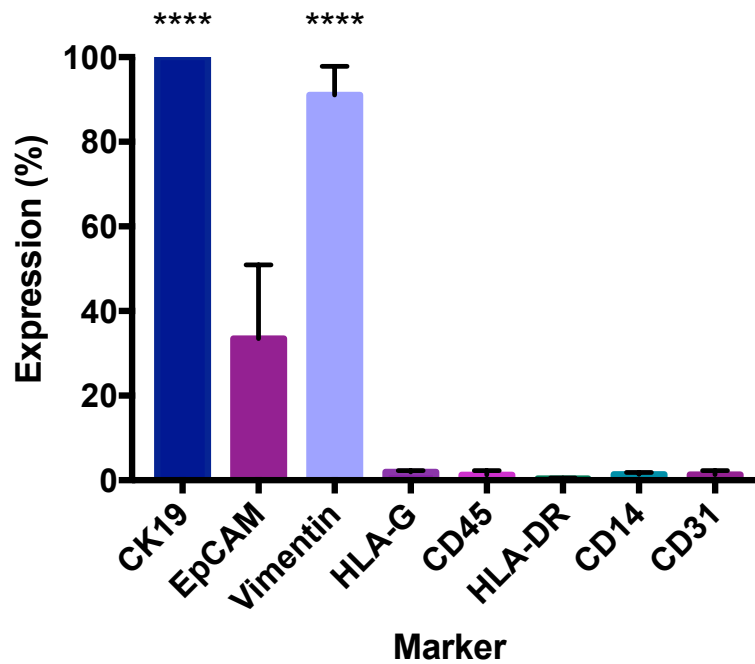
Figure 3-10 Cell counts performed on the immunocytochemistry on hAECs in culture.

Cell counts were carried out for each marker on n=3 hAEC preps to calculate overall expression. Statistical significance was determined by one way ANOVA. **** $p<0.0001$
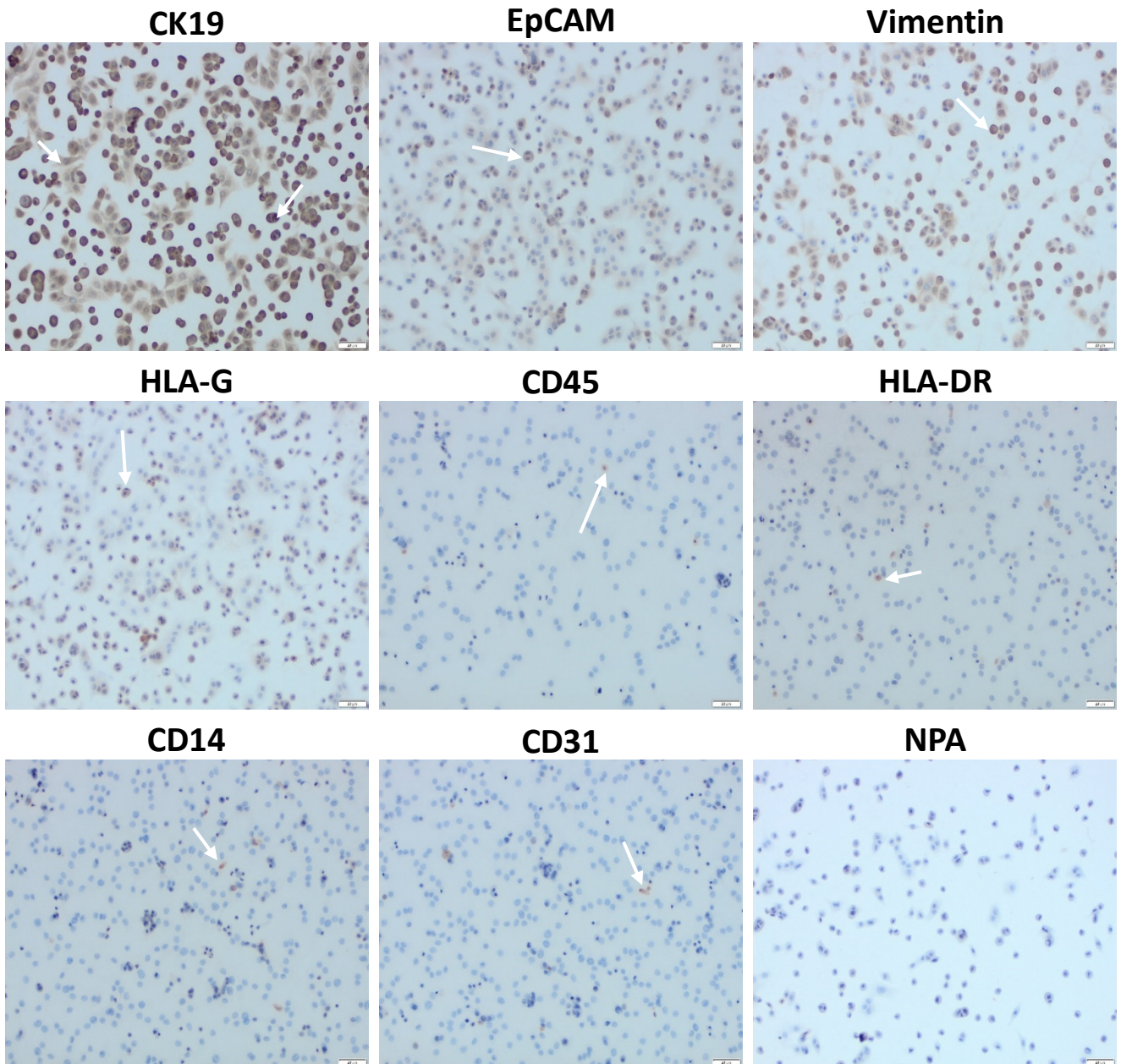
Figure 3-11 Immunocytochemistry staining on hAECs in culture.

Immunocytochemistry was performed on hAECs after 3 days of culture. Epithelial cell markers CK19 and EpCAM, leukocyte marker CD45, macrophage marker CD14, endothelial cell marker CD31 and MHC markers HLA-DR and HLA-G were used to characterise cell expression. A no primary antibody (NPA) control was included. All images are x20 and the white arrows point to positively stained cells. Scale: 20 μM. Representative of 3 fields of view per section. N=3.

3.3.5 Quantifying purified hAEC-EVs

In order to isolate the EVs, hAECs were cultured in serum-free UltraCULTURE™ media for 4 days. This conditioned media then underwent ultracentrifugation to pellet the hAEC-EVs which were then subsequently resuspended in PBS. There is no specific assay that can be used to quantify EV content, therefore a BCA assay was carried out to determine protein content on each prep to provide a guideline for the amount of EVs isolated (Table 3-2). The average hAEC-EVs yield after ultracentrifugation was 240 µg.

Sample	Protein (µg/mL)	Volume in PBS (µL)	Total protein (µg)
HP020	340.92	825	281.26
HP021	344.54	700	241.18
HP024	318.50	720	229.32
HP025	546.29	305	166.62
HP026 (a)	612.10	450	275.44
HP026 (b)	527.49	460	242.65
HP028	462.41	525	242.76

Table 3-2 Total protein content for hAEC-EV isolations.

A BCA assay was used to determine protein content for each hAEC-EV isolation prep. Protein was calculated using known standard protein concentrations. Total protein was then calculated based on the volume of PBS each prep was resuspended in.

3.3.6 Flow cytometry purity analysis of EVs

Due to the small size of the hAEC-EVs, they had to be bound to 4 µM aldehyde/sulphate latex beads in order to be able to be read by the flow cytometer. Tetraspanin markers CD9, CD81 and CD63 are widely used as exosome makers, and these can be detected through flow cytometry. Amount of purified EVs and antibody incubation time was briefly optimised. It was found that a higher concentration of 20 µg of EVs and overnight staining achieved the strongest expression of exosome markers CD9, CD81 and CD63 (Figure 3-12).

Once optimised, 20 µg of hAEC-EVs from each isolation underwent purity analysis using the three markers CD9, CD81 and CD63.Single and double bead populations were gated to ensure all EV expression was included. CD9 expression was highest with over 80% bead expression observed. A high percentage of CD63 and CD81 expression was also observed compared to the isotype controls. The high expression of these markers on the beads, suggests that the EVs bound successfully and also that the EVs express these markers (Figure 3-13).
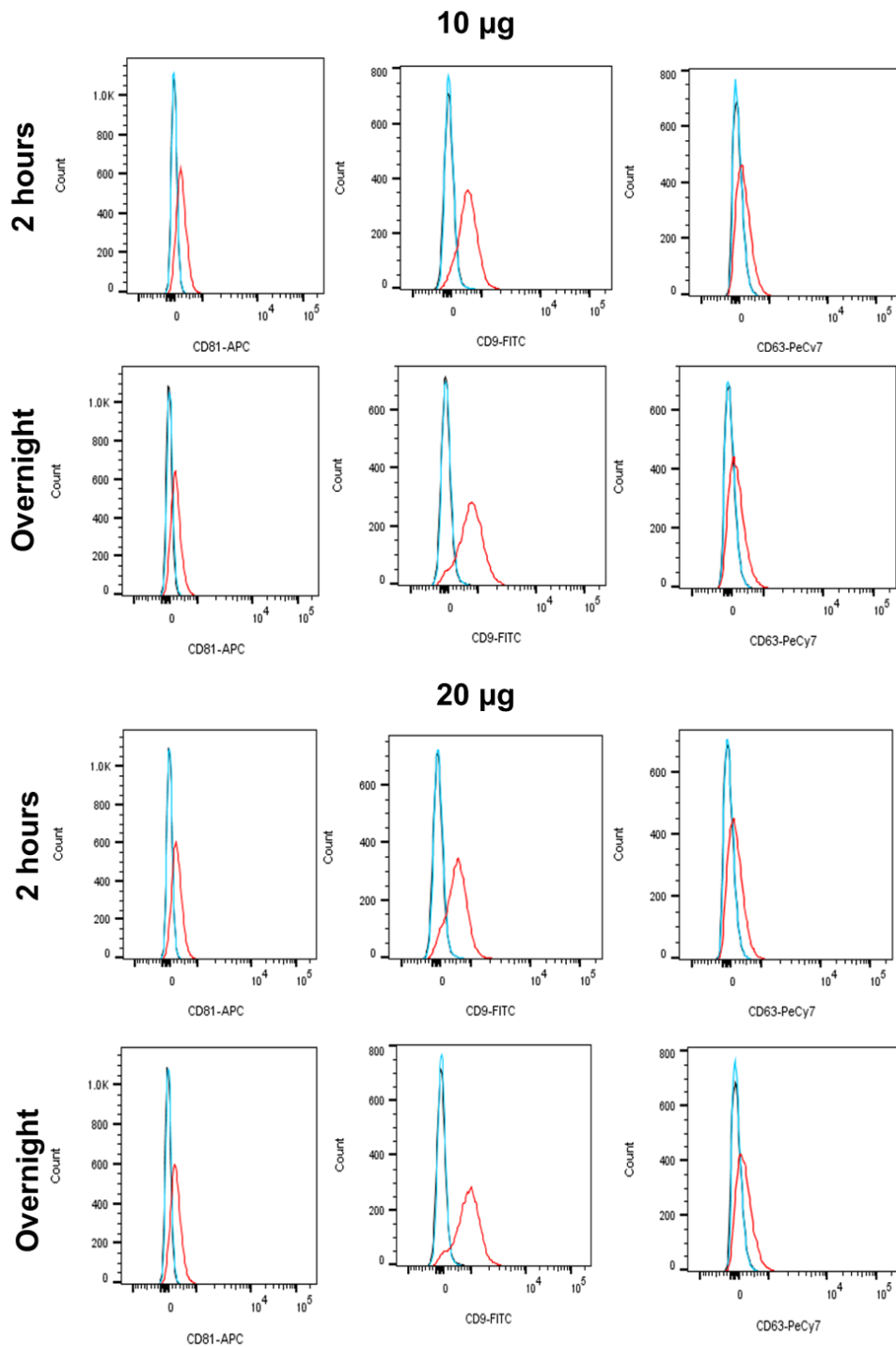
Figure 3-12 Flow cytometry histograms on exosome markers CD9, CD81 and CD63 for 10 µg and 20 µg purified hAEC-EVs.

Amount of purified hAEC-EVs and antibody staining time was optimised on flow cytometry prior to purity analysis of all the preps. Tetraspanin exosome markers CD9, CD63 and CD81 were used. Overnight staining with 20 µg was used going forward.
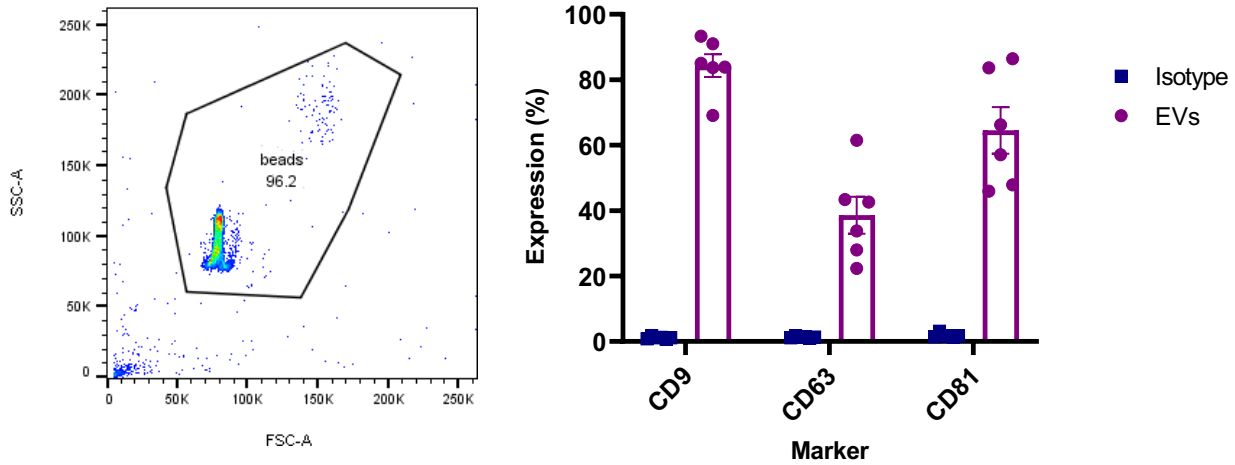
Figure 3-13 Purity analysis of hAEC-EVs through flow cytometry.

Flow cytometry was performed using 4 µm aldehyde/sulphate beads bound to the hAEC-EVs purified through ultracentrifugation. Both single and doublet beads were gated on the SSC area vs. FSC area plot, to ensure expression of all EVs were detected. There was positive expression for all three exosome markers; CD9, CD63 and CD81 compared to the isotype control.

3.3.7 Electron microscopy of EVs

TEM was performed on three of the hAEC-EV preps in order to examine whether the typical characteristics of exosomes could be observed. Electron microscopy carried out on these preps shows characteristic cup-shaped membranes that are the expected morphology for exosomes, as indicated with white arrows (Figure 3-14). The electron microscopy also reveals a smaller number of large apoptotic bodies are also being isolated through the ultracentrifugation, as indicated with the red arrows. Measurements added to the electron microscopy indicate mostly exosomes are purified through ultracentrifugation as they fit within the typical range of 30-150 nm.
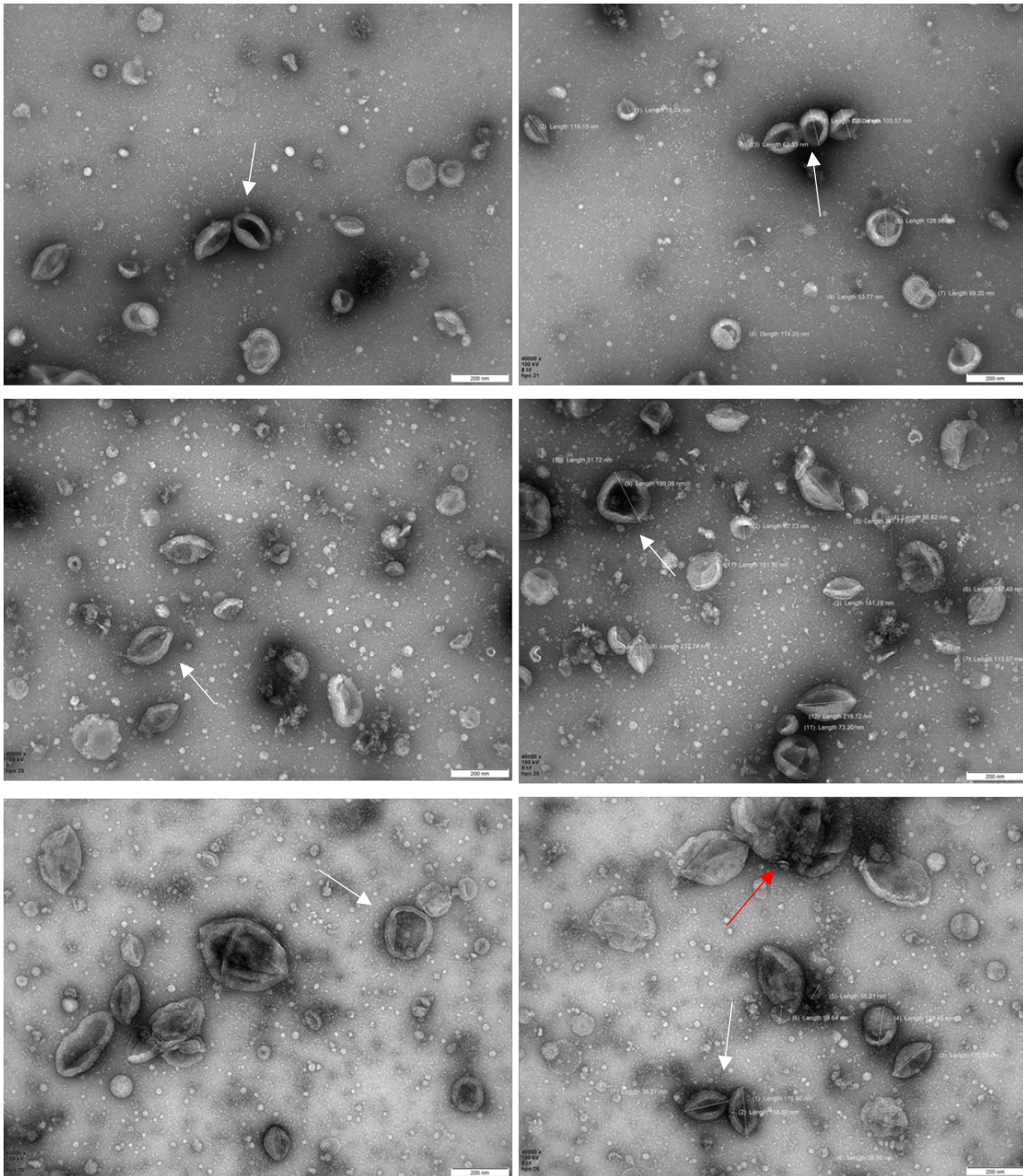
Figure 3-14 Transmission electron microscopy on hAEC-EV isolation.

TEM was carried out on three hAEC-EV isolations, courtesy of the Electron Microscopy Research Services unit, Newcastle University. Each isolation showed the exosomes with the typical cup shaped morphology, indicated with white arrows. Apoptotic bodies were occasionally visible in the EV isolations, indicated with red arrows. Measurements of the exosomes demonstrated they mostly fall within the typical range 30-150 nm. Scale: 200nm. N=3.

3.4 Discussion

The human placenta is surrounded by three membrane layers: amnion, chorion, and decidua. The amnion membrane is derived from the epiblast 8 days after fertilisation of the embryo and is made up of two layers: a surface epithelial layer (hAECs) and a deeper mesodermal layer. This layer of hAECs retain their immunomodulatory properties and pluripotent ability even at full-term pregnancy. Therefore, hAECs can be readily isolated at a relatively low cost from full-term placenta, which is a tissue generally discarded after delivery and so offers a plentiful source free from religious and ethical issues that most stem cell therapies face. Furthermore, they offer minimised risk for tumorigenicity as no expansion in culture is required and due to their low expression of MHC Class I and II antigens and co-stimulatory molecules, they have shown no transplant rejection (Tahan & Tahan, 2014; Motedayyen et al., 2017).

There are several protocols reported in the literature used to isolate hAECs giving cell yields of 12×10^6 to 300×10^6 and viabilities ranging between $83 - 98\%$ (Gramignoli et al., 2016; Murphy et al., 2010, 2014; Tabatabaei et al., 2014; Miki et al., 2010; Gomez, 2008; Gottipamula & Sridhar, 2018; Motedayyen et al., 2017). With our average isolation yielding 134.2×10^6 and viabilities >90%, we can be confident our isolation procedure is effective and is very close to the yields achieved by Murphy *et al.,* upon which our serum free methodology is based on. Their group described yields of $120 \pm 40 \times 10^6$ and viability of $83 \pm 4\%$ (Murphy et al., 2014).

All hAEC isolation protocols are similar in that they use a trypsin digest rather than a collagenase digest. Collagenase is frequently used to isolate MSCs from the amnion membrane as it is better at digesting internal tissues. Since the hAECs have a weak cell-cell adhesion to the membrane, trypsin is able to separate these bonds, therefore use of collagenase in hAEC isolation could lead to MSC contamination from the mesodermal layer (Pelekanos et al., 2016; Motedayyen et al., 2017). Most protocols used 0.05% trypsin for their digest, which our protocol followed. However, Gottipamula and Sridhar and Maymó *et al,* used 0.25% but this showed no benefit in cell counts or viability compared to the protocols using 0.05% (Gottipamula & Sridhar, 2018; Maymó et al., 2018). The main differences in protocol involved the number of trypsin digest steps. Most protocols chose to discard their initial first step to minimise red blood cell contamination and cellular debris, our protocol chose to

also follow this step (Murphy et al., 2014; Motedayyen et al., 2017; Miki et al., 2010; Gramignoli et al., 2016; Tabatabaei et al., 2014). Miki *et al,* Motedayyen *et al* and Maymó *et al* carried out two further shorter trypsin digests, then pooled the cells together. Tabatabaei *et al,* carried out three further 20 minute digestion steps, then pooled the cells together. The Murphy *et al* protocol used two 60 minute digests, however they found viability decreased the longer the digestion time. Our protocol uses a single digest step for an hour, following the Murphy *et al* protocol, however we didn't carry out that second 60 hour digestion step as we already achieved a high yield of cells with good viability (Murphy et al., 2014).

Our initial isolation protocol used serum-containing consumables, however we wanted to move closer to cGMP standards and so altered our protocol to use serum-free consumables. We chose to follow the Murphy *et al* protocol, who demonstrated that changing to a cGMP methodology actually yielded more cells and showed no significant changes in cell viability (Murphy et al., 2014). This reflected our own findings when transitioning to a cGMP methodology.

Our hAEC isolation protocol yielded an average of 94% EpCAM positive staining through flow cytometric analysis. This reflected what has been reported in the literature with Murphy *et al,* reporting they achieved over 92% EpCAM positive staining through flow cytometry and Gramignoli *et al* reported over 85% EpCAM positive staining (Murphy et al., 2010, 2014; Gramignoli et al., 2016). In addition to this, Motedayyen *et al,* and Tabatabaei *et al,* reported over 95% positive and 99% positive staining for cytokeratin, respectively (Motedayyen et al., 2017; Tabatabaei et al., 2014). Finally, Gomez reported 97% CK19 positive staining through flow cytometric analysis (Gomez, 2008). We consistently showed <2% staining for our other purity markers CD105, CD31 and CD45. CD90 expression showed some positive staining, which could suggest a few MSCs are being isolated during the process. Gramignoli *et al,* and Tabatabaei *et al,* also reported MSCs being isolated. On the other hand, Murphy *et al,* and Motedayyen *et al,* demonstrated that their methodology could isolate hAECs without MSC contamination, showing only <1% positive staining of MSC markers CD105 and CD90 (Gramignoli et al., 2016; Tabatabaei et al., 2014; Murphy et al., 2010, 2014; Motedayyen et al., 2017).

Immunohistochemistry on the amnion membrane showed CK19 positive staining along the surface of the membrane, highlighting the hAEC monolayer. This supported the immunocytochemistry performed on the hAECs grown in culture for 72 hours, which showed strong CK19 staining, demonstrating we were indeed isolating the hAEC monolayer on the amnion membrane. EpCAM staining of hAECs in culture showed very low expression, but due to the high CK19 positive staining we concluded this was due to a poor antibody. We also found strong vimentin staining on the hAECs in culture. Vimentin is a mesenchymal marker and as it is co-localising with the CK19 staining, this could suggest the hAECs are dedifferentiating through epithelial to mesenchymal transition. Gomez also reported co-localising positive vimentin and CK19 staining at passage 0 but after passage 6, the expression of CK19 was decreased but the vimentin staining remained positive. They postulated that the co-expression of these two markers of hAECs in culture demonstrated their pluripotent ability to differentiate into other precursor cell types, especially as increased positive expression of CD105 could then be observed at passage 6 (Gomez, 2008).

HLA-G is a non-classical HLA Class Ib antigen, expressed by placental cells and plays a key role in foetal-maternal tolerance. Unlike classical class Ia and II antigens, HLA class Ib antigens aid in graft acceptance rather than rejection. HLA-G has shown to have an important role in modulating T cell and NK cell response (Le Bouteiller et al., 1999; Strom & Gramignoli, 2016). hAECs have been reported in the literature to also express HLA-G (Le Bouteiller et al., 1999; Pratama et al., 2011; Lefebvre et al., 2000; Kolanko et al., 2019). However, we found very low expression of HLA-G when we performed immunocytochemistry on hAECs in culture. This could be explained by the observations of Kolanko *et al,* who showed that HLA-G expression decreased over time in culture and showed very low expression after 64 hours (Kolanko et al., 2019). Lefebvre *et al,* demonstrated that HLA-G expression increased when hAECs were cultured with IFNγ and Kolanko *et al* also showed increased HLA-G expression when cultured with IL-1β and IFNγ, this may suggest that certain stimuli, or a pro-inflammatory environment, are needed for higher HLA-G expression (Lefebvre et al., 2000; Kolanko et al., 2019). Therefore, we may not have observed HLA-G expression during our cultures due to a lack of a pro-inflammatory environment, but we may see higher expression when hAECs are administered to the lungs during EVLP.

EVs have recently gained significant interest for their potential therapeutic applications in both regenerative medicine and cell free cancer immunotherapies. EVs are made up of two subtypes. The larger subtype is microvesicles which range in size from 50-1500 nm, and exosomes, which are smaller and around 30-120 nm in size. Apoptotic bodies can also be found which are 50-2000 nm in size. There are several methods that can be used to isolate EVs, including differential ultracentrifugation, HPLC chromatography and beads with specific exosome markers (Xu et al., 2016; Théry et al., 2006). The isolation method most used to isolate hAEC exosomes is differential ultracentrifugation on the conditioned media (Sheller et al., 2016; Tan et al., 2018; Hadley et al., 2018; Ren et al., 2020). The principle behind this purification technique involves firstly pelleting dead cells and debris by centrifugation at increasing speeds. Finally, the supernatant undergoes an ultracentrifuge spin at 100,000 g which is required to pellet the exosomes. Then a PBS wash step is performed to eliminate any contaminating proteins and spun once again at 100,000 g (Théry et al., 2006). Sheller *et al,* used differential centrifugation as described above and carried out a single ultracentrifuge step of 100,000 g for 2 hours followed by a PBS wash step for 1 hour (Sheller et al., 2016; Hadley et al., 2018). Ren *et al,* differed to this approach by only doing a singular ultracentrifuge step for 70 minutes at 100,000g (Ren et al., 2020). Our protocol reflected more closely that of Tan *et al,* who performed two ultracentrifuge steps of 100,000g for 2 hours followed by a PBS wash step for 1 hour 10 minutes (Tan et al., 2018).

Much of the characterisation for exosomes has been well established through the work by Théry *et al* (Théry et al., 2006)*.* Our protocols for bead-based flow cytometry and TEM were based off their well-respected protocols. TEM is used as a standard way of determining whether the classic cup-shaped morphology and size of exosomes can be observed, Sheller *et al,* Ren *et al* and Tan *et al,* all observed this phenotype, which is also visible within our TEM (Sheller et al., 2016; Ren et al., 2020; Tan et al., 2018). Bead based-flow cytometry or western blot techniques can be carried out to measure expression of tetraspanin exosome markers CD9, CD63, CD81 and EV auxiliary protein marker ALIX. Ren *et al* used western blot to confirm expression of CD63 and ALIX; while Tan *et al* used a combination of western blot and bead-based flow cytometry to observe expression of CD9, CD81 and ALIX (Ren et al., 2020; Tan et al., 2018). However, Sheller *et al,* only found expression of CD9

and CD63 but no ALIX expression (Sheller et al., 2016; Hadley et al., 2018). Therefore, purity results appear to be variable. Our studies showed an average expression of 80% CD9, 60% CD81 and 40% CD63 determined through bead-based flow cytometry. This expression was lower than that reported by Tan *et al,* who found >90% expression for CD81 and >85% expression for CD9 through flow cytometry (Tan et al., 2018). However, Sheller *et al* found only 70% expression for CD9 but 64% CD63 expression through flow cytometry (Sheller et al., 2016). Finally, Nanoparticle tracking analysis (NTA) and dynamic light scattering (DLS) can be used to determine the size and distribution of exosome isolations. Sheller *et al* reported a peak at 39.1±2.97 nm through DLS analysis (Sheller et al., 2016). Tan *et al*, Ren *et al* and Hadley *et al,* all reported peaks around 100 to 150 nm through NTA (Tan et al., 2018; Ren et al., 2020; Hadley et al., 2018). Unfortunately, in this study NTA could not be carried out on the EV isolation preps due to restriction of access by the COVID-19 pandemic health and safety protocols to the facility where the NTA resides, therefore we could not determine the distribution of size of our isolations.

3.4.1 Conclusions

In conclusion, an isolation technique for hAECs can be put in place through a trypsin digest on fresh placentae from donors undergoing c-section to achieve high yields, viabilities, and good purity. Subsequently, conditioned media can be generated in large quantities then EVs can be isolated through differential ultracentrifugation with good yields. Subsequently, isolated EV preps express tetraspanin exosome markers CD9, CD63 and CD81 and have the classic cup-shaped morphology typical of exosomes. The hAECs, generated conditioned media, and subsequently isolated EVs can then be tested within our platforms to determine their immunomodulatory effects.

4 Functional testing of human amniotic epithelial cells

4.1 Introduction

The pathogenesis of PGD is complex with multiple steps along the transplant pathway that can lead to its development. This includes any trauma or injury prior to death, brain death leading to a dysfunction in homeostasis and warm ischemia during retrieval followed by cold ischemia. Any or all of these insults can lead to deterioration in the tissue and an inflammatory cascade (Lee et al., 2010). Donor factors can also increase the risk of PGD, such as age and smoking history and recipient factors, such as obesity and pulmonary hypertension can also increase the risk (De Perrot et al., 2005; Diamond et al., 2017). Central to this, during organ transport, IRI presents a significant clinical problem by compounding injury leading to the development of PGD. PGD is associated with more postoperative complications, longer hospital stays and lower 1 year survival rates (Christie et al., 2018). IRI is a complex pathway of events that causes sterile inflammation, microvascular permeability and endothelial cell breakdown resulting in pulmonary oedema and impaired gas exchange. Innate immune cells, including macrophages and neutrophils are major players in IRI, directly inducing lung tissue injury and augmenting inflammation through the production of pro-inflammatory cytokines and damage-associated molecular patterns (DAMPs) (Laubach & Sharma, 2016; Talaie et al., 2021).

IRI appears to work in a biphasic pattern. Eppinger *et al,* demonstrated with rat lungs that after 90 minutes of ischemia, injury of the lungs peaked at 30 minutes and 4 hours of reperfusion. Furthermore, they observed key macrophage related cytokines: TNFα, IFNγ and MCP-1 were involved in early injury, and only TNFα in the later phase (Eppinger et al., 1997). Supporting this, Fiser *et al,* demonstrated macrophages played a significant role in the first phase and neutrophils in the latter phase (Fiser et al., 2001). TNFα has been indicated to have a prominent role in IRI by being a key initiating factor for the inflammatory cascade, activating the endothelium which ultimately upregulates chemotactic agents and surface adhesion molecules resulting in an influx of recipient neutrophils migrating into the lungs (Maxey et al., 2004). The upregulation of surface markers, such as ICAM-1, leads to the trans-migration of neutrophils through the endothelium resulting in the production of myeloperoxidase thus damaging endothelial integrity (de Perrot et al., 2003;

Schmidt et al., 2011; Eppinger et al., 1995). Endothelial cell dysfunction has been associated with more severe grade of PGD developing post-transplant (Krenn et al., 2007). Neutrophil infiltration into the lungs has also been associated with impaired gas exchange and microvascular permeability (Ng et al., 2006). CXCL8, a potent neutrophil chemoattractant also plays a key role in PGD, with higher levels correlating with poor lung function, more severe grading of PGD and early recipient mortality (De Perrot et al., 2002; Fisher et al., 2001). Therefore, therapeutics that could be administered pre- or post-transplant are being explored to ameliorate the impact of IRI and other lung injury, to limit the formation of PGD post-transplantation and improve both short term and ultimately long-term graft survival.

The immunomodulatory functions of hAECs and subsequent derivatives have promise as a therapeutic to target these key players in IRI and potentially attenuate injury and improve PGD outcomes. hAECs modulating neutrophil functioning has been demonstrated in the literature with a reduction in neutrophil infiltration into injured lungs being observed, enhanced phagocytic capability, decreased oxidative burst capacity and chemotaxis towards MIP-2 (Li et al., 2005; Alipour et al., 2020; Geng et al., 2016). hAEC treatment has also demonstrated a reduction in macrophage infiltration, increased polarisation of M1 pro-inflammatory macrophages to M2 anti-inflammatory macrophages and increased macrophage phagocytosis (Li et al., 2005; Tan et al., 2014). Lung injury models have also observed improved lung function, mediation of lung repair, a reduction in pro-inflammatory cytokine production, including TNFα and CXCL8, and increased production of IL-10 upon hAEC treatment (Vosdoganes et al., 2013; Zhu et al., 2017; Melville et al., 2017; Moodley, Ilancheran, Samuel, Vaghjiani, Atienza, Elizabeth D Williams, et al., 2010).

Extracellular vesicles derived from hAECs, have been observed to have similar immunomodulatory effects compared to their whole cell counterpart. Tan *et al,* demonstrated that hAEC-EVs reduced murine neutrophil myeloperoxidase activity and induced neutrophil cell death. They also observed increased phagocytic capability of macrophages and polarisation to the M2 phenotype. A murine lung injury model treated with hAEC-EVs showed a reduction in neutrophil infiltration into the lungs whilst an increased polarisation and phagocytic ability in macrophages, and ultimately observed lung repair 7 days post-administration, without the need for their cell counterpart (Tan et al., 2018).

4.1.1 Aims and objectives

This chapter aims to functionally test hAECs in the context of macrophage activation, endothelial activation, and neutrophil migration to determine their effect on mitigating some of the key biological events that characterise ischemia reperfusion related injury by:

- Investigating the effect of hAECs, their conditioned media and EVs on the production of key pro-inflammatory cytokines; TNFα and CXCL8, and phagocytic capability of THP-1 cell line derived macrophages
- Determining the effect of hAECs, conditioned media and EVs on endothelial cell activation and production of key pro-inflammatory cytokines using the HMEC-1 cell line
- Investigating any changes in endothelial integrity upon treatment with hAECs, their conditioned media or EVs
- Determine the effect of hAECs, conditioned media and EVs on trans-endothelial migration by neutrophils.

4.2 Materials and Methods

4.2.1 *Differentiation of the THP-1 cell line*

It has been well established in the literature that the THP-1 monocyte cell line, can be differentiated into macrophages through treatment with Phorbol 12-Myristate 13-Acetate (PMA) (Park et al., 2007). To determine the optimal dose of PMA for the seeding density of THP-1 cells used, a dose response was performed. 500,000 THP-1 cells were seeded per well in 12 well plate and treated with 1, 2.5, 5 and 10 ng/mL of PMA for 24 hours at 37°C, 5% CO_2. A DMSO vehicle control for the PMA was included. After the 24-hour incubation, supernatants were harvested and CXCL8 concentration was evaluated as an output as determined through an ELISA (as described in chapter 2.6). All doses of PMA resulted in THP-1 cell adherence to the well plate, but 5 ng/mL was determined to be the best dose as CXCL8 concentration plateaued from this point (Figure 4-1). This is supported by the dose optimisation performed by Park *et al.,* who also found 5 ng/mL to be a sufficient dose of PMA needed to differentiate THP-1 cells into macrophages (Park et al., 2007).
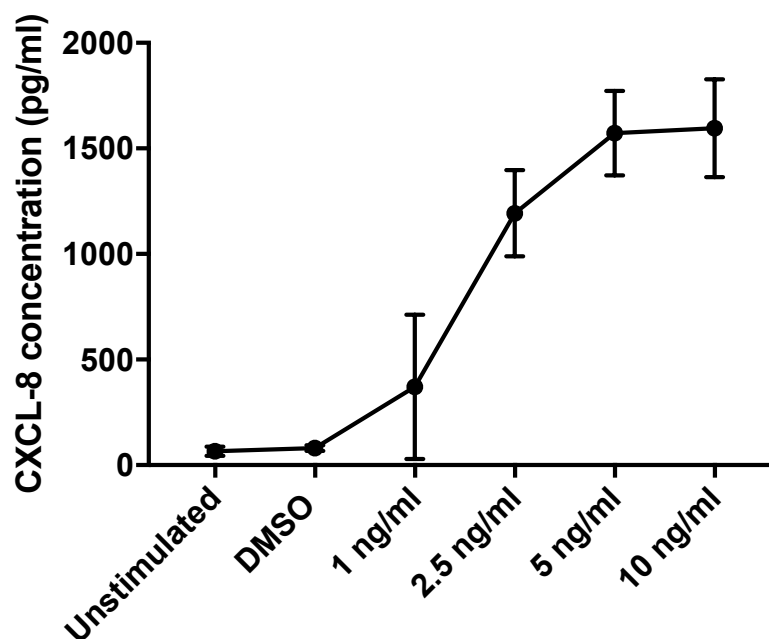
Figure 4-1 The Phorbol 12-Myristate 13-Acetate (PMA) dose response curve of the THP-1 cell line.

CXCL8 concentration increases upon treatment with PMA after 24 hours and plateaus after 5 ng/mL, making this the optimal dose for THP-1 stimulation. N=3.

4.2.1.1 Polarisation to M1 and M2 macrophages

After differentiation into resting (M0) macrophages, THP-1 cells can be further
polarised into M1 (pro-inflammatory) or M2 (anti-inflammatory) macrophages using
certain stimuli. 500,000 THP-1 cells were seeded per well in a 12 well plate and
treated with 5 ng/mL of PMA for 24 hours. Treatment was then removed, the cells
washed with PBS then replaced with fresh media with no stimulus overnight to rest.
After another wash with PBS, cells were treated with either 20 ng/mL IFNγ and 10
ng/mL LPS to achieve a M1 phenotype or 20 ng/mL IL-4 and 20 ng/mL IL-13 to
achieve an M2 phenotype, for 24 hours at 37°C, 5% CO_2. Supernatant was
harvested and CXCL8 ELISA (as described in chapter 2.6) performed to confirm that
treatment with 10 ng/mL LPS and 20 ng/mL IFNγ was sufficient to cause a pro-
inflammatory M1 phenotype (Figure 4-2).
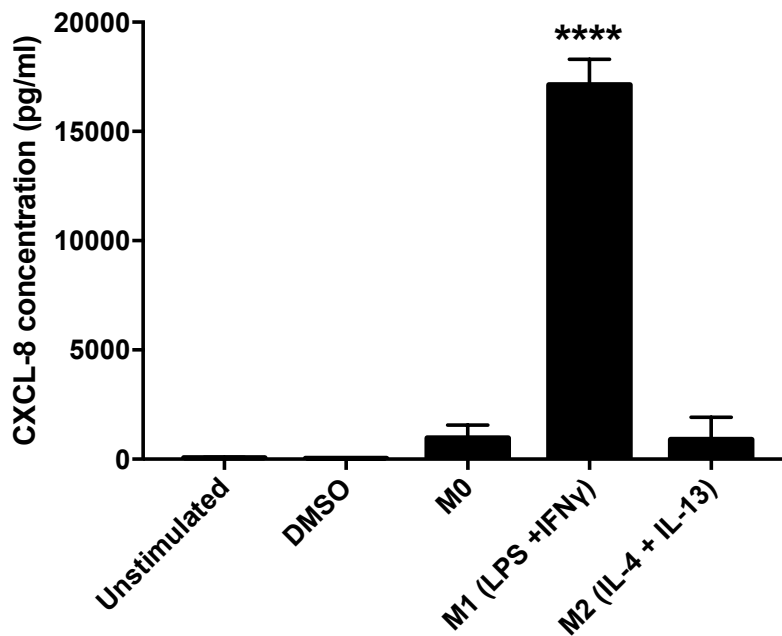
Figure 4-2 CXCL8 concentration of polarised THP-1 derived macrophages.

THP-1 monocytic cells were treated with 5 ng/mL of PMA for 24 hours to get a resting (M0)
phenotype, then subsequently treated with 10 ng/mL LPS and 20 ng/mL IFNγ to achieve a pro-
inflammatory (M1) phenotype or 20 ng/mL IL-4 and 20 ng/mL IL-13 to achieve an anti-
inflammatory (M2) phenotype. CXCL8 secretion was determined through ELISA. N=3. Statistical
significance determined by a one-way ANOVA. ∗∗∗∗ $p < 0.0001$

4.2.2 THP-1 treatments

In a 12 well plate, 500,000 cells/well were seeded and treated with 5 ng/mL PMA for 24 hours. Media was then removed, cells washed with PBS and rested overnight. Cells were then treated with 20 ng/mL IFNγ and 10 ng/mL LPS for 24 hours in starved RPMI containing only 0.5% FBS, to induce a pro-inflammatory phenotype. The cells were then treated with hAECs, conditioned media or EVs and their relevant controls required shown in table 4-1 and as described below:

For the experiments using hAECs; cryovials of frozen hAECs and the HTR-1 cell line were rapidly thawed at 37°C then resuspended in PBS before being spun at 350g for 10 minutes. The cells were then resuspended in starved RPMI and counted with trypan blue. 0.1×10^6, 0.2×10^6 and 0.5×10^6 hAECs were added to 3 μM pore Transwell® inserts (Corning, USA) in each well in addition to a further 10 ng/mL LPS. HTR-1 cells with 10 ng/mL LPS were used as a cell control, a positive control of just 10 ng/mL LPS and unstimulated controls were also used. The THP-1s were treated for 6 hours at 37°C, 5% CO_2, then supernatants were collected, and the THP-1 cells were lysed with RLT buffer for downstream qPCR.

For hAEC conditioned media (hAEC-CM) treatments; THP-1 cells were treated with a 1:1 dilution of hAEC conditioned media (cultured as described in Chapter 3.2.2) or UltraCULTURE™ media to starved RPMI media, for 6 hours at 37°C, 5% CO_2. Supernatants were then harvested, and the cells lysed with RLT buffer for RNA extraction.

For the hAEC-EV treatments; EVs were thawed and 5 μg, 10 μg and 20 μg was used to treat per well with 10 ng/mL LPS. An EV-depleted conditioned media with 10 ng/mL LPS stimulus control was included to evaluate if immunomodulatory effects were detectable in the absence of EVs. Unstimulated and positive (10 ng/mL LPS) controls were also included. Treatment lasted 6 hours at 37°C, 5% CO_2, then supernatants were harvested, and cells lysed with RLT buffer for RNA extraction.

4.2.3 HMEC treatments

Prior to the activated HMEC-1 cells undergoing treatment with the hAECs, hAEC-CM and hAEC-EVs, IL-1β concentration to activate the endothelial cells was optimised. In a 6 well plate, 200,000 HMEC-1 cells were seeded and incubated for 24 hours at 37°C, 5% CO_2. The cells were then stimulated with IL-1β at the concentrations of 0.1, 0.5, 1, 5 and 10 ng/mL for 6 hours. The cells were then harvested using 500 μL of accutase, stained for the markers E-selectin, VCAM-1 and ICAM-1 as described in chapter 2.5 for flow cytometry and run on the FACS Canto II (Figure 4-3). Expression at 0.5 ng/mL of IL-1β appeared to be sufficient to stimulate ICAM-1 and VCAM-1 marker expression on HMEC-1 compared to the untreated control (p=<0.0001) and was not significantly different to the higher concentrations of 1, 5 and 10 ng/mL. E-selectin showed very little expression on HMEC-1 with no overall significant change through IL-1β stimulation and so was not pursued any forward as a marker.
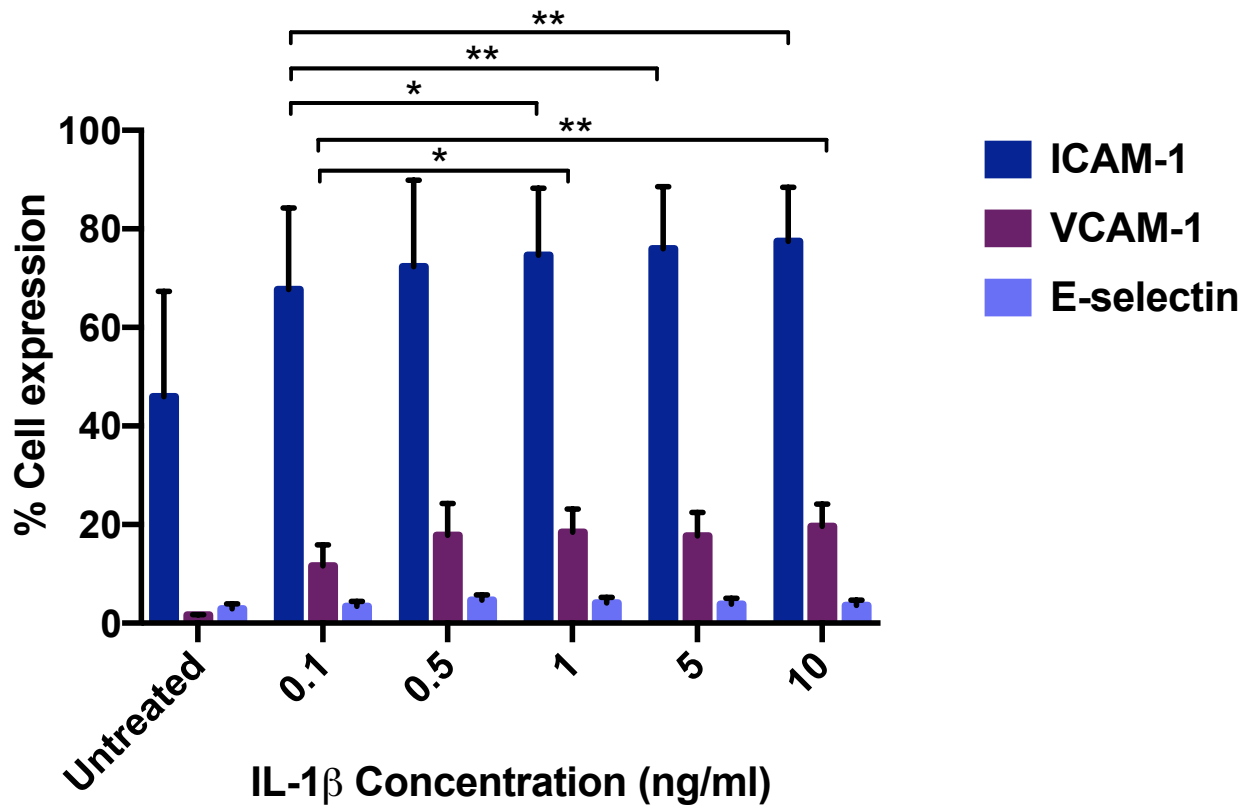
Figure 4-3 Optimisation of IL-1β concentration using the HMEC-1 cell line.

HMEC-1 were treated with 0.1, 0.5, 1, 5 and 10 ng/mL of IL-1β for 6 hours, then cell expression for markers ICAM-1, VCAM-1 and E-selectin were determined through flow cytometry. N=1 with three technical repeats. Statistical significance was determined by two-way ANOVA. *p<0.05, **p<0.01.

For HMEC-based treatments, 200,000 cells were seeded in a 6 well plate and left to adhere for 24 hours at 37°C, 5% CO_2. The cells were then washed with PBS prior to treatment with either hAECs, conditioned media or EVs and their relevant controls (Table 4-1).

For the experiments using hAECs, these were resurrected in the same manner as described above in Chapter 4.2.2, 0.1×10^6, 0.2×10^6 and 0.5×10^6 hAECs were added to 3 μM pore Transwell® inserts in each well with 0.5 ng/mL IL-1β to stimulate the HMECs. HTR-1 cells treated with 0.5 ng/mL IL-1β were used as cell controls. HMECs were stimulated with 0.5 ng/mL IL-1β as a positive control and an unstimulated control was also included. The cells were left to incubate for 6 hours at 37°C, 5% CO_2. Supernatants were then collected, and the HMEC-1 cells lysed with RLT buffer for RNA isolation.

For hAEC-CM treatments; HMEC cells were treated with a 1:1 dilution of hAEC conditioned media or UltraCULTURE™ media to starved MCDB media + 0.5 ng/mL IL-1β for 6 hours at 37°C, 5% CO_2. A positive control of 0.5 ng/mL IL-1β stimulated HMECs and an unstimulated control was also included. Supernatants were then harvested, and the cells lysed with RLT buffer for RNA extraction.

 For the hAEC-EV treatments; EVs were thawed and 5 μg, 10 μg and 20 μg was used to treat per well + 0.5 ng/mL IL-1β. An EV-depleted conditioned media + 0.5 ng/mL IL-1β control was included. Unstimulated HMEC-1 and a positive control of 0.5 ng/mL IL-1β stimulated HMECs were also included, then incubated for 6 hours at 37°C, 5% CO_2. Supernatants were harvested and cells lysed with RLT buffer for RNA extraction.

hAEC treatment	hAEC or derivatives dosage	Specific controls	Standard controls
Cells	• 0.1×10^6 • 0.2×10^6 • 0.5×10^6	• HTR-1 Cell line • hAEC cell dose equivalent to conditioned media generation	• Untreated • Positive control (LPS/IL-1β)
Conditioned media	1:1 dilution: Conditioned media: RPMI/MCDB	1:1 dilution: • HTR conditioned media: RPMI (phagocytosis and chemotaxis assays only) • UltraCULTURE™ media: RPMI	• Untreated • Positive control (LPS/IL-1β)
EVs	• 5 μg • 10 μg • 20 μg	• EV-free conditioned media	• Untreated • Positive control (LPS/IL-1β)

Table 4-1 An outline of dosages and controls used for the hAECs, Conditioned media and EV treatments.

Each dose, specific controls for that experiment and standard experimental controls are outlined for each of the three treatments; hAECs, conditioned media and EVs. Each dose and specific control were also stimulated with 10 ng/mL LPS for THP-1 based treatments or 0.5 ng/mL IL-1β for HMEC based treatments. Positive controls were also stimulated with either 10 ng/mL LPS or 0.5 ng/mL IL-1β for their respective assays. All treatments were incubated for 6 hours at 37°C and 5% CO_2 before being harvested.

4.2.4 Real time PCR

After treatments, as described in chapter 4.2.2 and 4.2.3, HMEC-1 or THP-1 cells were washed with PBS, lysed with RLT buffer supplemented with 1% β-mercaptoethanol then frozen at -20°C until RNA isolation. RNA was isolated as described in chapter 2.4.1 using the RNeasy® Mini kit (Qiagen, USA). 1000 ng of isolated RNA was then used to synthesise cDNA as described in chapter 2.4.2. Real time PCR was then carried out as described in chapter 2.4.3 using TaqMan® gene expression assays. ICAM-1, VCAM-1, SIPR1, SIPR3 and CXCL8 primers were used to determine changes in gene expression for the HMEC based treatments, with HPRT-1 used as a housekeeping gene. CXCL8, MRC1 and TNFα primers were used to determine any changes in gene expression for the THP-1 based treatments, with 18S used as a housekeeping gene.

4.2.5 ELISA

Supernatants collected from the treatments described in chapter 4.2.2 and 4.2.3 were stored at -80°C until an ELISA could be performed to quantify protein secretion. Supernatants were thawed slowly and an Duoset ELISA kit (R&D systems) was used as described in chapter 2.6. Supernatants collected from the THP-1 based assays were used to determine CXCL8 (samples diluted 1:20), TNFα and sICAM (samples diluted 1:10) concentrations. Supernatants harvested from the HMEC-1 based assays were used to determine CXCL8 (samples diluted 1:2) and sICAM concentrations.

4.2.6 Phagocytosis assay

Macrophage phagocytosis was determined using pHrodo™ Red *Escherichia coli* BioParticles™ (Thermofisher Scientific, UK) which works through detecting phagocytosis by detecting changes in pH. The BioParticles™ are non-fluorescent outside the cell but upon phagocytosis, the increase in acidity causes the particles to fluoresce, this can then be measured using the FACS Canto II. Prior to beginning the assay, a vial of the particles was reconstituted with 2 mL PBS, vortexed and then sonicated for 5 minutes. THP-1 cells were seeded and differentiated into macrophages as described in chapter 4.2.1 using PMA. Cells were then washed and replaced with uptake buffer (PBS supplemented with 500nM EDTA + 1% FBS). No

further stimulation to M1 pro-inflammatory macrophages was necessary for this protocol. The THP-1 cells were then treated with hAECs, conditioned media or EVs as described in chapter 4.2.2 but without the additional stimulation with LPS step included. This diluted the uptake buffer 1:1 with RPMI in the case of hAECs and EV based treatments or conditioned media. 25 μg of pHrodo™ particles were then added to each well. An untreated control, a control well with no pHrodo™ particles and a negative control treated with 10μM of cytochalasin D were included. The cells were left to incubate for 6 or 24 hours at 37°C, 5% CO_2. The plates were then washed with PBS and cells dissociated from the plate using 500 μL accutase, then transferred to FACS tubes and spun at 300g for 5 minutes. They were then resuspended with 200 μL FACS buffer (PBS + 2% FBS) and run on the FACS Canto II. FlowJo software was used to gate and analyse the data.

4.2.7 Neutrophil chemotaxis

4.2.7.1 Neutrophil isolation

Peripheral blood neutrophils were isolated from healthy volunteers by either Mr Jonathan Scott from the Simpson Laboratory at Newcastle University using the percoll gradient method or by myself using the MACSxpress ® whole blood neutrophil isolation kit (Miltenyi Biotec, Germany). To isolate the neutrophils through the MACSxpress ® kit, one vial of whole blood neutrophil isolation bead cocktail was reconstituted in Buffer A, then made into an isolation mix by adding buffer B at a 1:1 ratio with the bead cocktail. This was then added to 4-8 mL of blood in EDTA tubes at a 1:2 ratio of isolation mix to blood. The sample was then inverted gently three times and incubated for 5 minutes on the MACSmix™ Tube Rotator at room temperature. The sample was then placed in the MACSxpress® Separator magnetic field for 15 minutes with the cap off. Labelled neutrophils bound to the wall of the tube and erythrocytes sedimented to the bottom. The labelled cells were carefully collected and centrifuged at 300 g for 10 minutes, with no brake. The pellet was then resuspended in 4 mL 1 x red blood cell lysis buffer (Thermofisher Scientific) and incubated on the MACSmix™ Tube Rotator for 10 minutes or until the solution was opaque. The cells were then centrifuged at 300 g for 10 minutes, with no brake, resuspended in serum-free RPMI media (containing only 0.1% BSA) and counted using a haemocytometer and trypan blue.

To characterise the isolated neutrophils, a cytospin was carried out, then stained with H&E as described in chapter 2.3.2 and flow cytometry was performed using the markers CD14, CD15, CD16 and CD193. This was performed as described in chapter 2.5 using 200,000 freshly isolated neutrophils. FlowJo software was used to gate and analyse the data after running the samples on the FACS Canto II.

4.2.7.2 Neutrophil transendothelium migration assay

HMEC-1 cells were briefly optimised for seeding density on the 3 μM pore Thincert® cell culture inserts (Greiner Bio-one, UK). HMEC-1 cells were seeded at the densities of 150,000, 200,000, 250,000, or 300,000 cells per insert, and incubated for 48 hours at 37°C, 5% CO_2. The filters were then removed and fixed in ice cold methanol and stored at -20°C until further use. The inserts were then stained by H&E as described in chapter 2.3.2. The cell density of 250,000 cells had the best coverage with no missing patches while also not growing beyond a single monolayer (Figure 4-4).

Once optimised, 250,000 HMEC-1 cells were seeded into 3 μM pore Thincert® cell culture inserts and incubated for 48 hours. The HMEC-1 cell inserts were then treated with hAECs, hAEC-CM or hAEC-EVs as described in Table 4-1, with 0.5 ng/mL IL-1β simulation, for 6 hours. The filters were transferred to a 24-well plate blocked previously in 2% BSA in PBS for over an hour. 30 nM CXCL8 in serum-free RPMI was added below the insert, and 200,000 neutrophils were added above the insert. A chemokinesis control was also included by adding 30 nM CXCL8 to both above and below the insert. The neutrophils were left to migrate for 1.5 hours before any in the lower chamber were harvested into FACS tubes using 500 μL accutase. The cells were spun down then resuspended in 200 μL FACS buffer (PBS + 2% FBS), to which 30 μL of CountBright™ Absolute counting beads (Thermofisher Scientific) was added. The samples were then run on the FACS Canto II and data was gated and analysed using Flowjo software (Figure 4-5). To determine the cell concentration as cells/μL the following equation was used:

$$\frac{number\ of\ cell\ events}{number\ of\ bead\ events} \times \frac{number\ of\ beads\ added}{volume\ of\ sample}$$

The chemotactic index was then calculated by normalising the number of neutrophils that migrated through the untreated well to the treated wells.
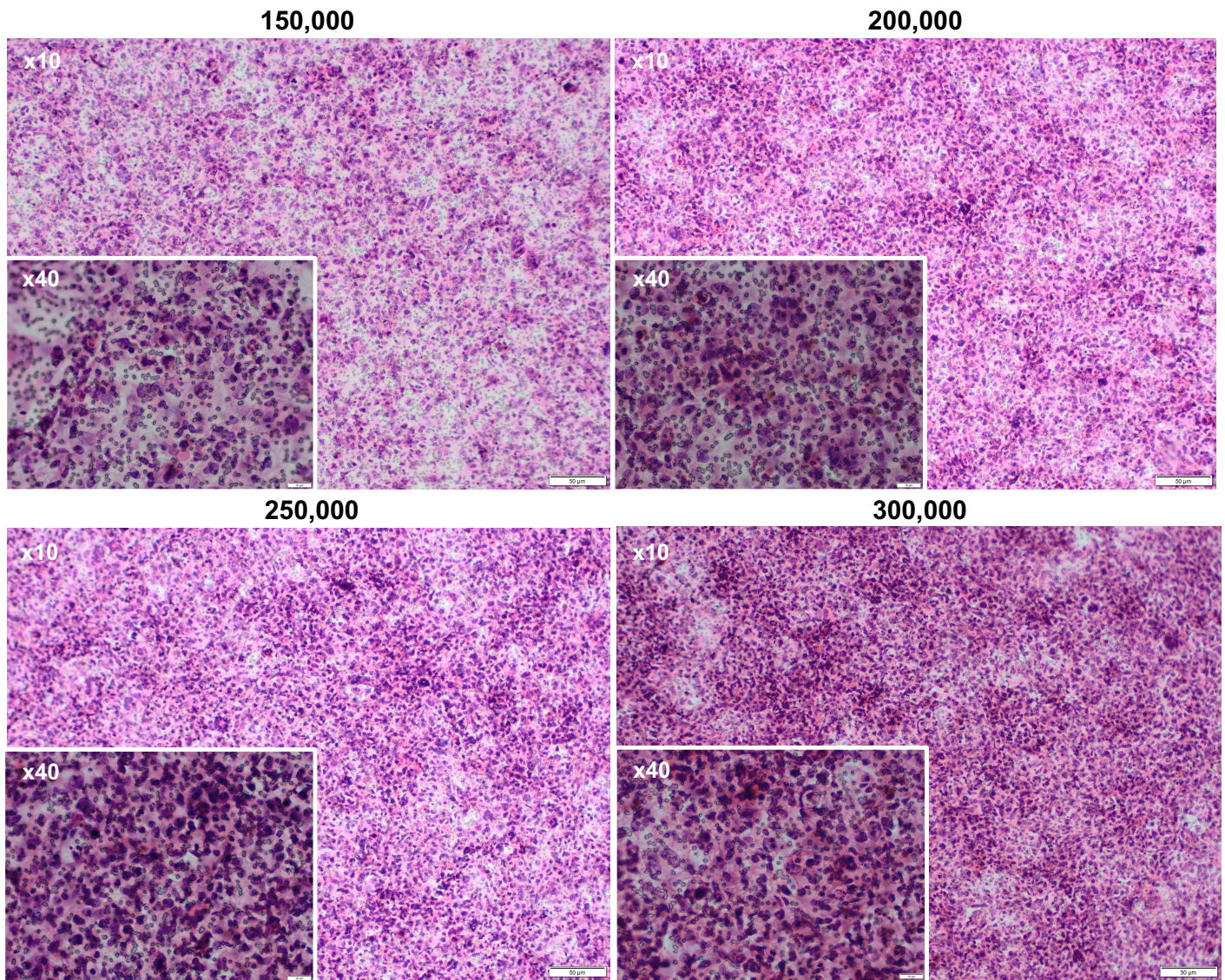
Figure 4-4 Optimising the seeding density of the HMEC-1 cell monolayer on inserts for the transendothelium migration assay.

HMEC-1 cells were seeded at densities of 150,000, 200,000, 250,000 and 300,000 cells per 3 μM pore Thincert® cell culture insert. H&E staining was then carried out on each insert to determine cell monolayer density. Magnification was either x10, Scale: 50 μM or x40, scale: 10 μM. N=3.
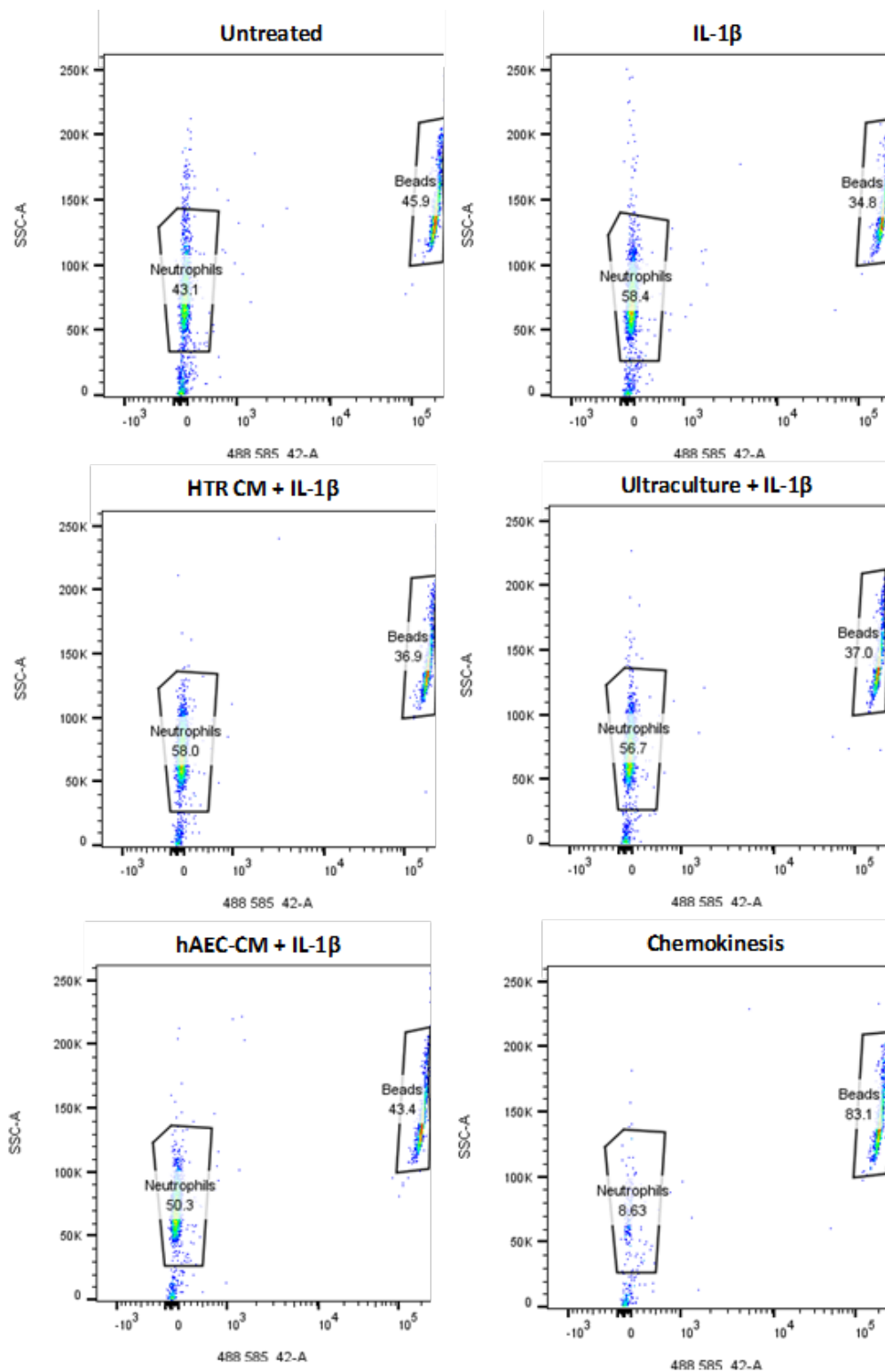
Figure 4-5 An example of the gating method for the transendothelial migration assay, from the hAEC-conditioned media treated IL-1β activated HMEC-1.

Flow cytometry was used to determine the number of neutrophils that migrated through the HMEC-1 monolayer, by calculating the ratio of beads to neutrophils. Each population was gated and a set number of bead events was read by the FACS Canto II. The cell concentration was then determined as described above.

4.3 Results

4.3.1 Effect of hAECs and their derivatives on inflammatory marker expression on macrophages

THP-1 derived macrophages were used to determine any changes in pro-inflammatory CXCL8, sICAM and TNFα expression. Furthermore, Mannose Receptor C-type 1 (MRC1) gene expression was monitored to assess whether hAECs or their derivatives led to a shift from the M1 phenotype to the M2 phenotype.

4.3.1.1 The effect of hAEC treatments

The dose of hAEC treatments was first optimised using THP-1 derived macrophages polarised to an M1 phenotype with IFNγ and LPS for 24 hours prior to being treated with 0.05×10^6, 0.1×10^6, 0.2×10^6, 0.5×10^6 and 1×10^6 hAECs, with an additional LPS stimulation for 6 hours. Gene expression of CXCL8 and TNFα were used to determine the optimal doses. The largest decrease observed in CXCL8 gene expression was for the doses 0.2×10^6 and 0.5×10^6 compared to the M1 positive control (Figure 4-6). TNFα expression showed a decrease in gene expression for all the hAEC cell doses.

The chosen doses of 0.1×10^6, 0.2×10^6 and 0.5×10^6 of hAECs were used for further treatments and the HTR cell line was then used as a cell control. Gene expression of CXCL8, TNFα and MRC1 were determined through real time PCR and protein expression of CXCL8, TNFα and sICAM were determined through ELISA. For CXCL8, both gene expression and concentration in the supernatant was decreased upon hAEC treatment (Figure 4-7A). The largest decreases observed were with the 0.2×10^6 (p=0.0290) and 0.5×10^6 (p=0.0290) cell treatments for gene expression, with these being significantly decreased compared to the HTR cell positive control. The hAEC treatment of 0.2×10^6 led to a significant decrease (p= 0.0465) and 0.5×10^6 led to a decrease (p= 0.1344) in CXCL8 production in the supernatants compared to the LPS positive control. Both treatments also showed significance with the HTR cell positive control (p=<0.0001 and p=0.0002 respectively) in CXCL8 production in the supernatants. Similarly, TNFα gene expression with the 0.2×10^6 and 0.5×10^6 hAEC treatments led to a significant decrease (p=0.0158 and p=0.0130 respectively) compared to the HTR cell positive control and also decreased

compared to the LPS positive control, although not significantly so (Figure 4-7B). This was reflected with the TNFα protein concentration, which decreased with all hAEC treatments, but showed the most significant decrease with the 0.5×10^6 hAEC treatment compared to the LPS positive control (p=0.0036). Furthermore, sICAM protein concentration in the supernatant showed the same pattern with the 0.5×10^6 hAEC treatment significantly decreasing sICAM production compared to the HTR cell positive control (p=0.0190) (Figure 4-7D). On the other hand, for MRC1, all treatments that received LPS stimulation led to a decrease in gene expression. Although not significant, an increase in MRC1 expression was observed at 0.1×10^6 and the conditioned media control hAEC treatment (0.225×10^6), suggesting hAEC treatment is showing a trend of polarising macrophages towards a M2 anti-inflammatory macrophage phenotype (Figure 4-7C).
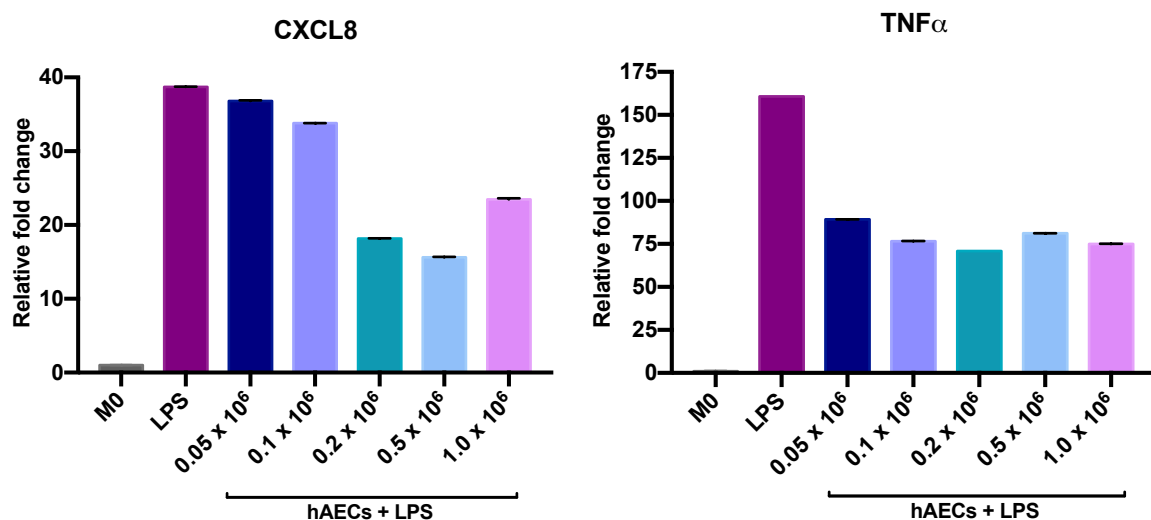
Figure 4-6 Optimising the dose of hAECs to treat macrophages.

THP-1 derived M1 macrophages were treated with 0.05×10^6, 0.1×10^6, 0.2×10^6, 0.5×10^6 and 1×10^6 of hAECs and/or 10 ng/mL LPS for 6 hours. CXCL8 and TNFα concentration in the supernatants were determined through ELISA. N=1.

Figure 4-7 The effect of hAECs on macrophage inflammatory marker expression.

THP-1 derived macrophages were treated with hAECs or HTR cells and 10 ng/mL LPS for 6 hours. (A) Real time PCR and ELISA were carried out on the cells and supernatants for CXCL8 expression. HTR concentration was significantly (B) Real time PCR and ELISA were carried out on the cells and supernatants for TNFα expression. (C) Mannose Receptor C-Type-1 (MRC-1) gene expression was determined by real time PCR. (D) Soluble ICAM (sICAM) concentration in the supernatants were determined by ELISA. N=3. Statistical significance was determined by a one-way ANOVA with Tukey's multiple comparisons test.*p<0.05, ** p<0.01, *** p<0.001, **** p<0.0001

4.3.1.2 The effect of hAEC conditioned media

THP-1 derived macrophages polarised to an M1 phenotype with IFNγ and LPS for 24 hours prior to being treated with hAEC conditioned media or UltraCULTURE™ control media in a 1:1 dilution with starved RPMI media, with the additional stimulation of 10 ng/mL LPS for 6 hours. Gene expression of CXCL8, TNFα and MRC1 were measured using real time PCR and protein expression of CXCL8 and TNFα were determined through ELISA. In Figure 4-8A, hAEC conditioned media treatments after 6 hours led to a decrease in both CXCL8 gene expression and protein expression compared to the LPS positive control, although this was only significant with the CXCL8 concentration in the supernatants (p= <0.0001). A significant decrease in TNFα gene expression and protein expression was observed in the presence of hAEC conditioned media treatment (p= 0.0445 and p=0.0027 respectively). Although a decrease in the control UltraCULTURE™ media was observed in TNFα gene expression, at the protein expression level an increased trend was observed (Figure 4-8B). Similarly, to the hAEC treatments, all LPS-based treatments led to a decrease in MRC1 gene expression. However, there was no increase observed upon hAEC-CM treatment (Figure 4-8C).

Whilst measuring the responses of pro-inflammatory macrophages upon conditioned media treatment, one particular donor exhibited the opposite trend to what was observed above (Figure 4-9). For TNFα there was a large increase in concentration and there was no observable decrease in CXCL8 concentration in the supernatants after a 6-hour treatment. This donor, unlike other donors was on two anti-inflammatory medications: adalimumab and lansoprazole. Adalimumab has a role in the TNFα pathway, which could explain the differences observed. The medication the donor is on appears to have an effect on the performance of the hAECs therefore this donor was removed from the pooled data observed in Figure 4-8.
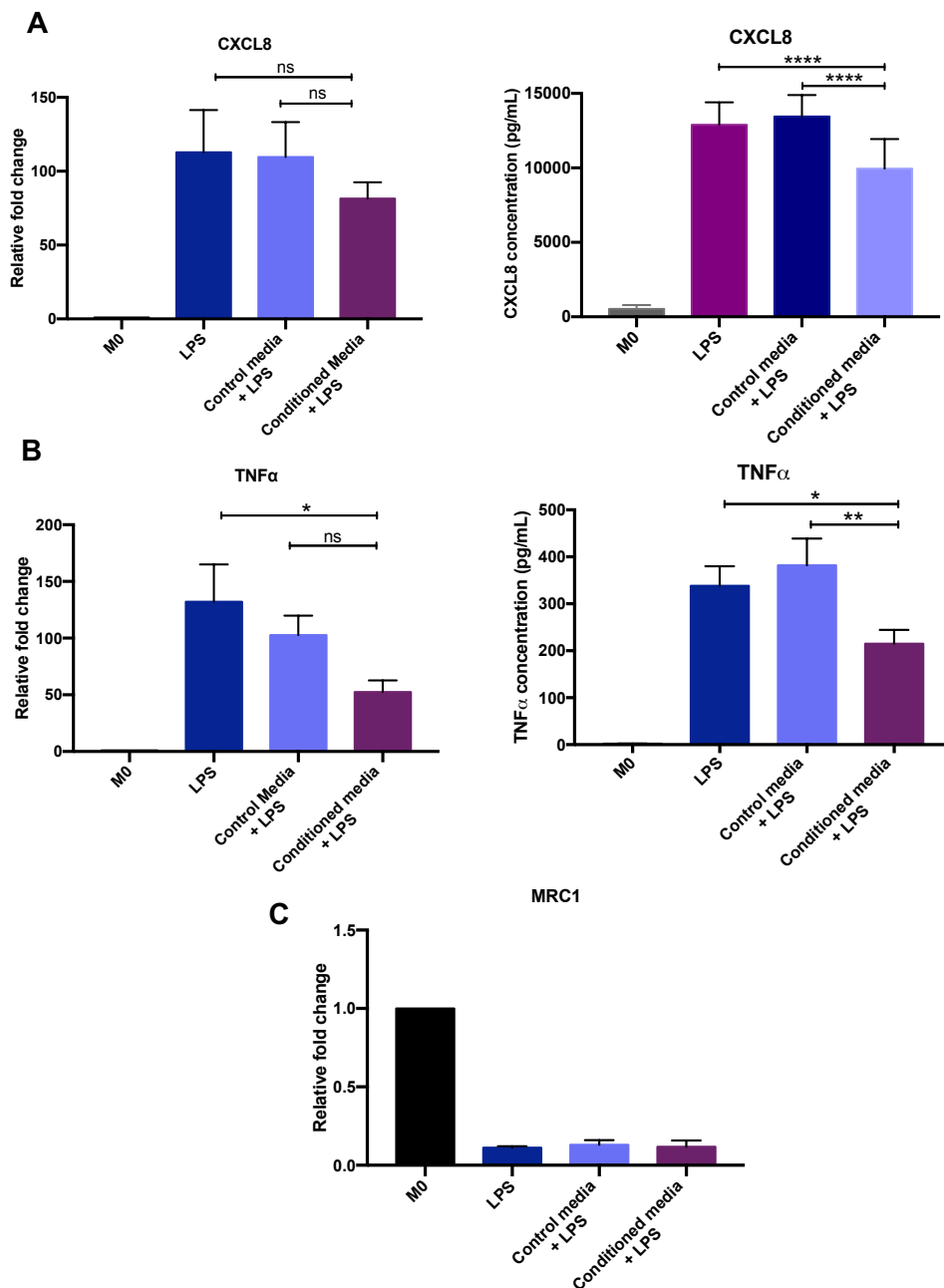
Figure 4-8 The effect of hAEC conditioned media on macrophage inflammatory marker expression.

THP-1 derived macrophages were treated with hAEC derived conditioned or control media for 6 hours with 10 ng/mL LPS stimulation. (A) CXCL8 concentration was determined through real time PCR and ELISA (B) TNFα gene expression was determined through real time PCR and ELISA (C) Mannose Receptor C Type-1 (MRC1) gene expression was determined through real time PCR. N=5 Statistical significance was determined by a one-way ANOVA with Tukey's multiple comparisons test. *p<0.05, ** p<0.01, **** p<0.0001

110
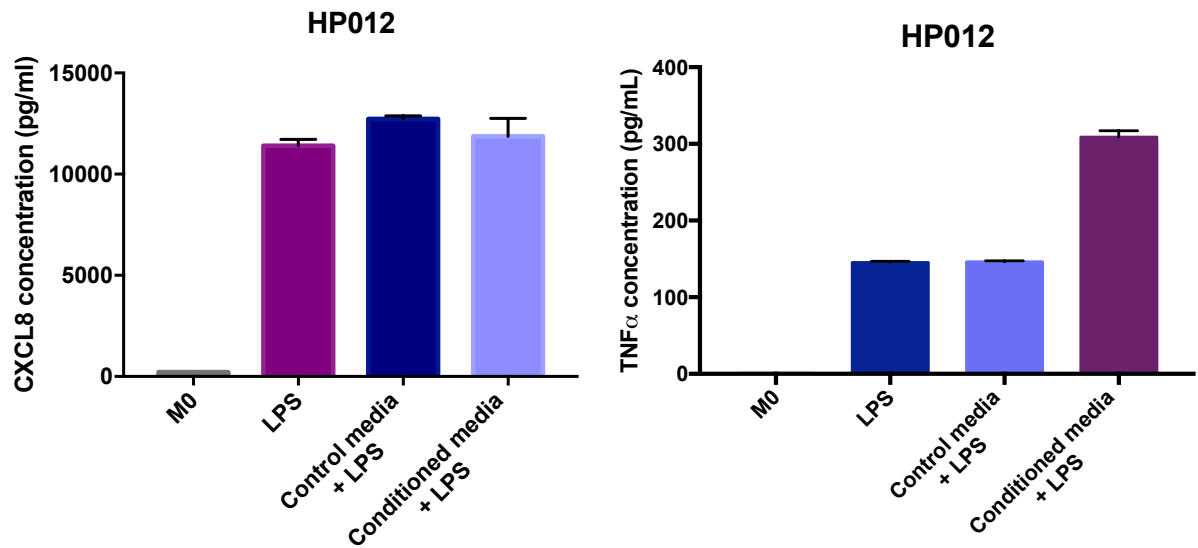
Figure 4-9 hAEC conditioned media treatment that increased CXCL8 and TNFα production of macrophages.

A donor on anti-inflammatory medications (adalimumab and lansoprazole) showed a deviation in response with the THP-1 derived assays with an increase in TNFα and no decrease in CXCL8 production observed. N=1 with three technical repeats.

4.3.1.3 The effect of hAEC-EVs

THP-1 derived macrophages polarised to an inflammatory M1 phenotype were treated with 5, 10 and 20 μg of hAEC-EVs with further LPS stimulation, for 6 hours. An EV-depleted conditioned media control was also used to observe any effects that may still occur once containing only a minimal amount of EVs. CXCL8, TNFα and MRC1 gene expression was determined through qPCR, and ELISA was used to determine the concentration of CXCL8, TNFα and sICAM within the supernatants.

CXCL8 gene expression appeared to increase after hAEC-EV treatment compared to the LPS control, although a trend in decreasing CXCL8 concentration in the supernatants could be observed with 5 μg of EVs (Figure 4-10A). This may suggest that the gene expression changes may be missed at the 6-hour timepoint. No change in TNFα expression was observed at the gene level compared to the LPS control, but a decrease was observed in the supernatants, with the biggest decrease also observed with 5 μg of EV treatment (Figure 4-10B). However, overall the largest decrease in TNFα concentration was the EV depleted conditioned media treatment rather than the EV treatments compared to the LPS control, although not significant. Gene expression of M2 marker, MRC1, was generally very low after the macrophages experienced LPS treatment, however, all three EV treatments led to a slight increase in MRC1 expression (Figure 4-10C). This was also observed with the EV depleted conditioned media. The expression of sICAM did show decreasing concentration in the supernatants as the hAEC-EV treatment concentrations did increase, although not significantly (Figure 4-10D). Like the TNFα concentrations, the largest decrease observed in sICAM expression was with the EV depleted conditioned media.
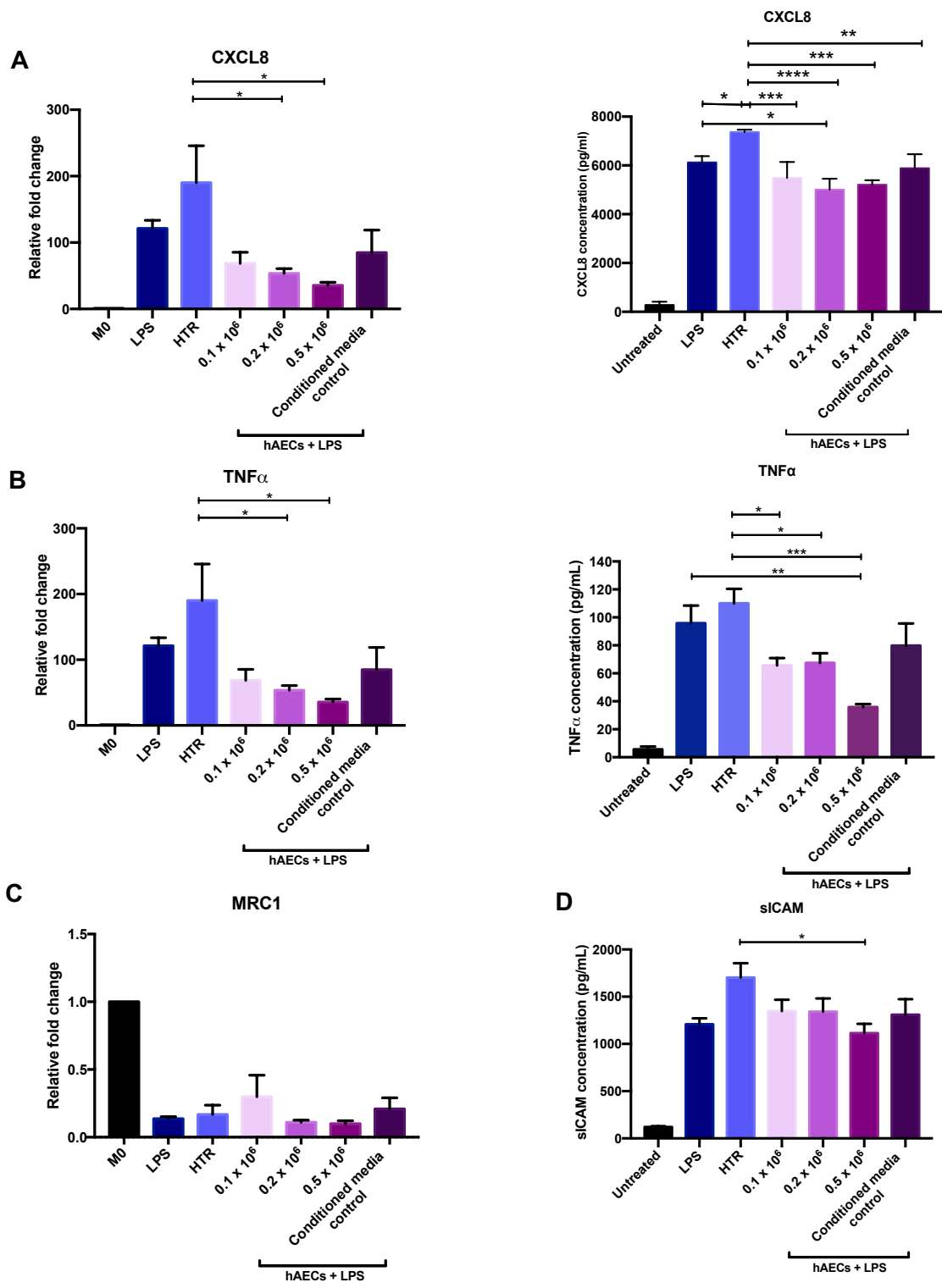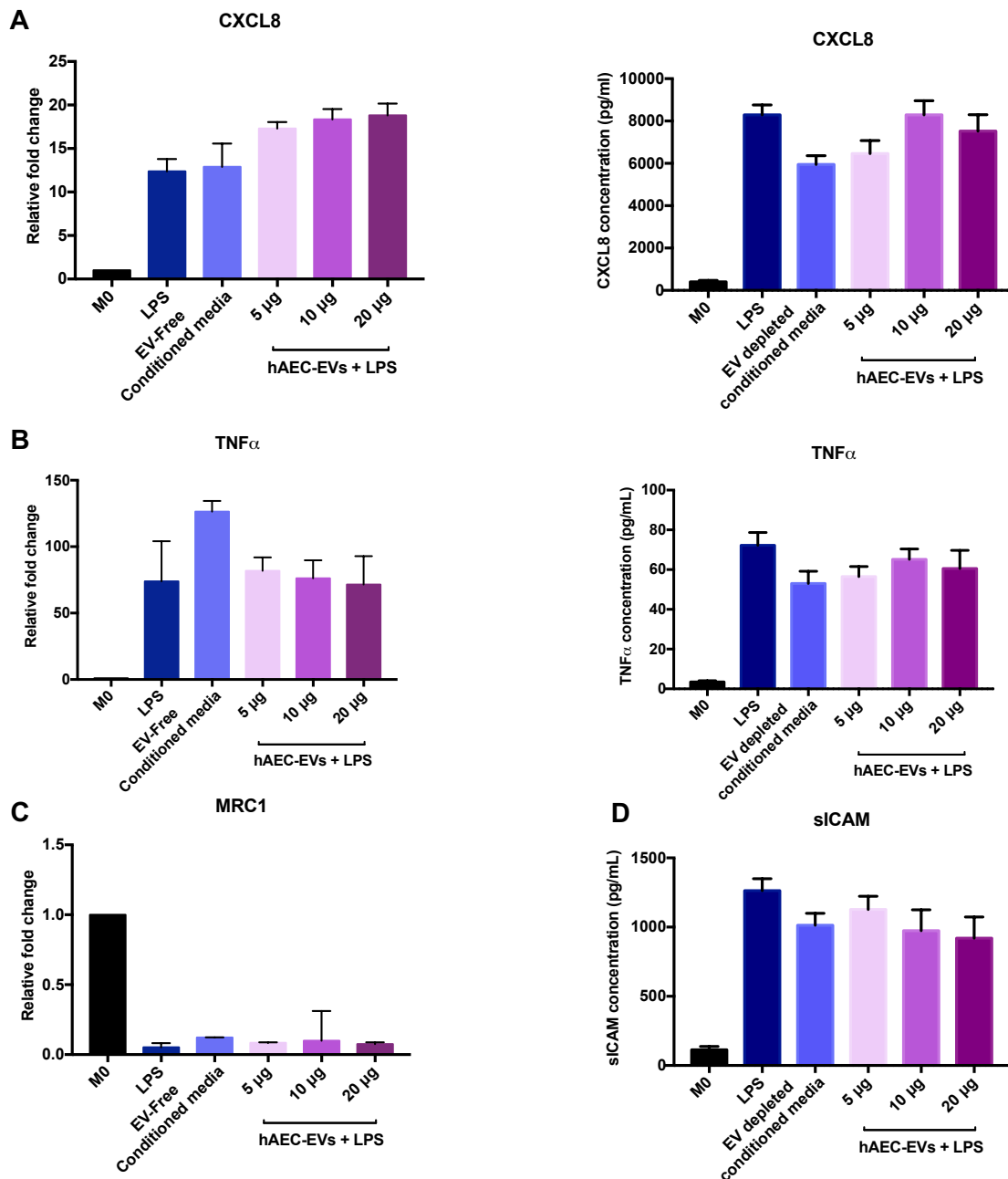
Figure 4-10 The effect of hAEC-EVs on macrophage inflammatory marker expression.

THP-1 derived macrophages were treated with 5, 10 or 20 μg hAEC-EVs or "EV depleted" conditioned media with 10 ng/mL LPS stimulation. (A) CXCL8 gene expression and protein concentration were determined by qPCR and ELISA. (B) TNFα gene expression and protein concentration were determined by qPCR and ELISA. (C) Mannose Receptor C Type-1 (MRC1) gene expression was determined by qPCR (D) Soluble ICAM (sICAM) concentration in the supernatants were determined by ELISA. N=3. Statistical significance was determined by a one-way ANOVA with Tukey's multiple comparisons.

4.3.2 Effect of hAECs and their derivatives on macrophage phagocytosis

4.3.2.1 Optimising the dose and treatment times for the pHrodo™ Red E. coli BioParticles™

Prior to treating the THP-1 cells with hAECs, conditioned media or EVs, the pHrodo™ particle dose and duration of treatment was optimised. After the THP-1 cells were seeded and differentiated to THP-1 derived macrophages, 5 μg, 10 μg or 25 μg of the particles were administered for one hour with or without 10 ng/mL LPS stimulation. The cells were then harvested and flow cytometry was performed using the FACS Canto II. The THP-1 derived macrophages were gated as per the strategy outline in Figure 4-11A. THP-1 derived macrophages treated with 25 μg of the particles showed the most phagocytosis after the hour (Figure 4-11B) therefore this dose was used for future experiments. Interestingly at the 25 μg dose, the LPS treated THP-1 derived macrophages exhibited reduced phagocytosis in comparison to the untreated THP-1 derived macrophages. A reduction in macrophage phagocytosis with LPS stimulation has also been observed in the literature (Feng et al., 2011).

At the chosen dose of 25 μg, a time course was then performed at 6, 12 and 24 hours. A negative control using 10 μM of cytochalasin D, an inhibitor of phagocytosis was included. The THP-1 derived macrophages were gated as per the strategy outlined in Figure 4-11A. Expression of the pHrodo™ particles was higher than that observed previously at 1 hour for all timepoints (Figure 4-12). Phagocytosis increased throughout the time course without plateauing. A sufficient level of phagocytosis was observed at 6 hours, so this was taken forward for future experiments and also more accurately reflected the time period of an EVLP. 24 hours was also taken forward to observe if there was a more noticeable difference observed with hAEC and derivatives at a higher level of phagocytosis.
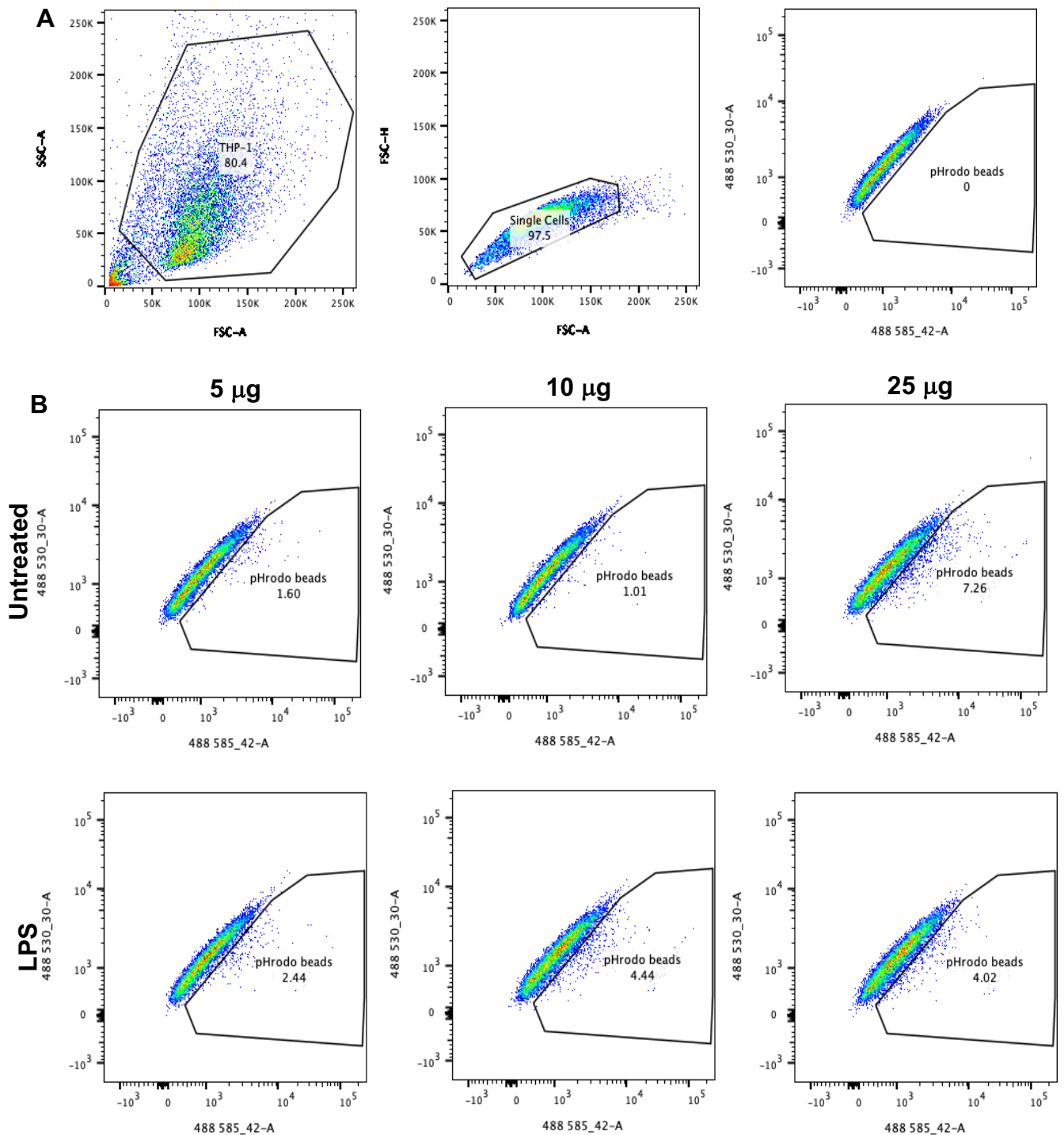
Figure 4-11 Macrophage phagocytosis of pHrodo™ particles at the doses of 5, 10 and 25 µg.

(A) THP-1 derived macrophages were gated, then the single cell population was identified. A gate was then set up to identify pHrodo™ particles using the 488 channels. (B) THP-1 derived macrophages were left untreated or treated with 10 ng/mL LPS and 5, 10 and 25 µg of pHrodo particles were then administered for 1 hour. N=1.
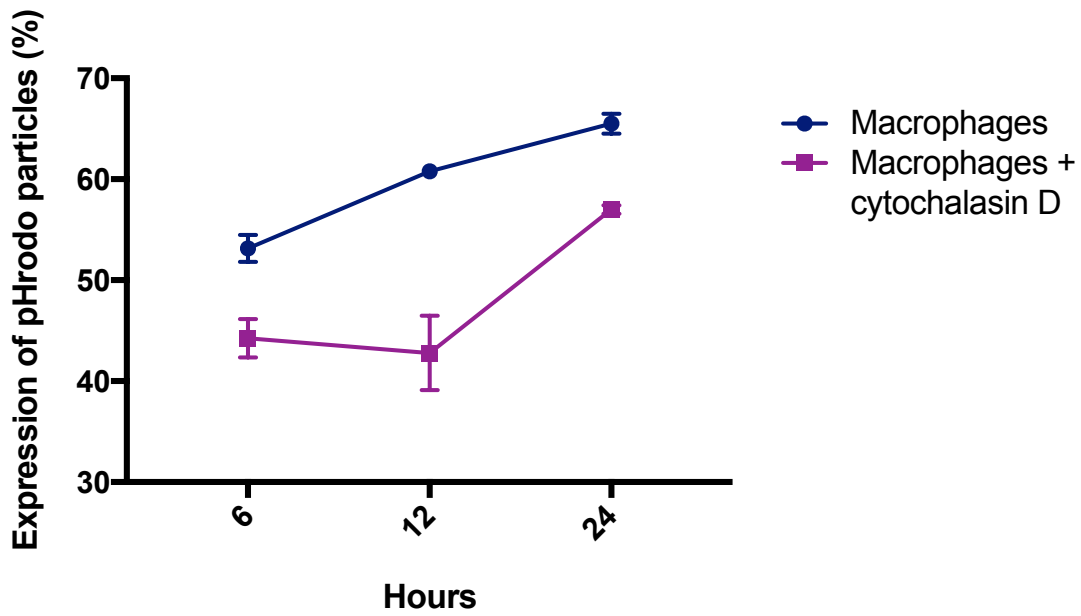
Figure 4-12 A time course for the expression of pHrodo™ particles in macrophages at 6, 12 and 24 hours.

THP-1 derived macrophages were treated with 25 μg pHrodo™ particles and flow cytometric analysis was performed at 6, 12 and 24 hours to measure phagocytosis. Phagocytosis was found to increase over the time course. N=1 with three technical repeats.

4.3.2.2 hAECS and their derivatives increase macrophage phagocytosis

Firstly, THP-1 derived macrophages were treated with 0.1×10^6, 0.2×10^6 and 0.5×10^6 hAECs, a conditioned media cell control (0.225×10^6), HTR cells as a control cell type, cytochalasin D as a negative control or untreated (M0) macrophages as a positive control for 6 and 24 hours. The percentage of phagocytosis was determined by the percentage of THP-1 derived macrophages expressing pHrodo™ particles (Figure 4-13A). At 6 hours, the M0 THP-1 derived macrophages significantly increased phagocytosis compared to the cytochalasin D, HTR cells and 0.5×10^6 dose of hAEC cells (p=<0.0001, p=0.0046 and p=0.0495 respectively). All hAEC treatments led to a visible increase in phagocytosis compared to the HTR cell control, although not significant. The lowest hAEC dose of 0.1×10^6 showed the largest increase in phagocytosis which is shown by the lack of significance compared to the M0 positive control. However, after 24 hours, all the hAEC treatments levelled out in phagocytosis and were at similar levels compared to the M0 positive control. HTR cell treatment still resulted in a lower percentage of phagocytosis compared to the hAEC treated and M0 positive control counterparts.

Following on from this, THP-1 derived macrophages were then treated with hAEC conditioned media, HTR conditioned media or the control UltraCULTURE™ media for 6 and 24 hours (Figure 4-13B). hAEC conditioned media appeared to upregulate phagocytosis compared to the HTR conditioned media, with near significance (p=0.0732), although this did not achieve the same levels as the positive M0 control at 6 hours. After 24 hours, the hAEC conditioned media further increased phagocytosis compared to the HTR control (p=0.0586) and was significantly higher than the control media (0.0008). However, the HTR conditioned media also showed an increase in phagocytosis after this time and was also significant against the control media (p=0.0339).

Finally, THP-1 macrophages were treated with 5, 10 and 20 μg of hAEC-EVs or EV-depleted hAEC conditioned media for 6 and 24 hours (Figure 4-13C). At 6 hours, all the doses of hAEC-EVs visibly increased the phagocytotic capability of the macrophages relative to the M0 control, with 20 μg showing the highest increase, although this was not significant. All treatments were significantly increased compared to the cytochalasin D negative control (p=<0.0001). After 24 hours, all doses of hAEC-EVs showed similar levels of phagocytosis, suggesting the treatment

could have lost effect after this time. Despite being EV-depleted conditioned media, the treatment still upregulated phagocytosis at both 6 and 24 hours, at similar levels to that observed with the hAEC conditioned media treatments seen in Figure 4-13B, suggesting that the EV-depleted conditioned media still has a therapeutic effect.
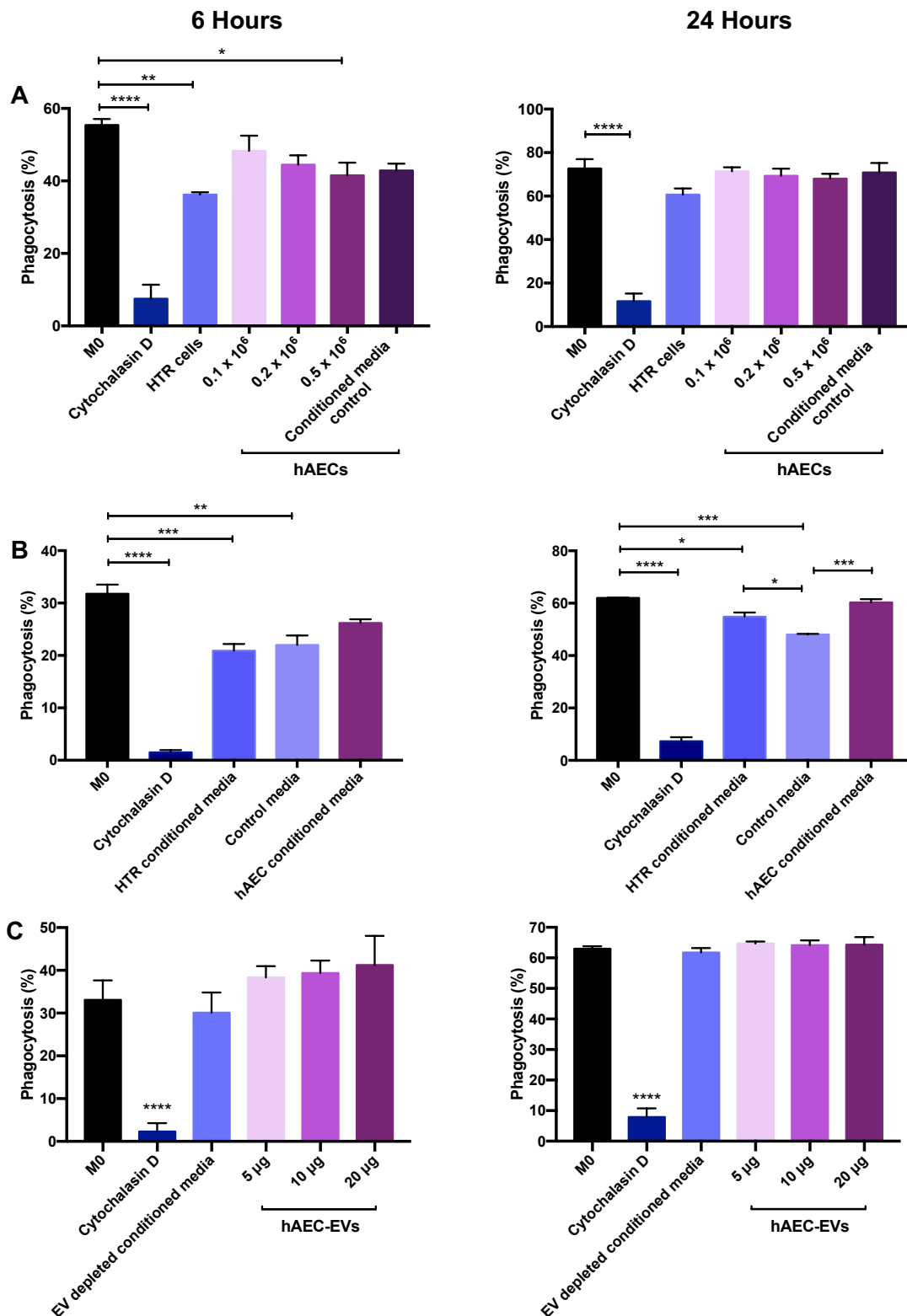
Figure 4-13 Macrophage phagocytosis after treatment with hAECs, Conditioned media or hAEC-EVs.

Macrophage phagocytosis was determined by the percentage of cells that expressed pHrodo™ particles. (A) Macrophage phagocytosis after treatment with 0.1×10^6, 0.2×10^6 and 0.5×10^6 hAECs or HTR cells for 6 and 24 hours. (B) THP-1 derived macrophages were treated with hAEC conditioned media, HTR conditioned media or control media. (C) Macrophage phagocytosis after 5, 10 or 20 μg hAEC-EVs. All N=3. Statistical significance was determined by a one-way ANOVA and Tukey's multiple comparisons. ∗p<0.05, ∗∗ p<0.01, ∗∗∗ p<0.001, ∗∗∗∗ p<0.0001.

119

4.3.3   The effect of hAECs and their derivatives on endothelium activation and inflammation markers

4.3.3.1 The effect of hAECs

HMEC-1 endothelial cells were treated with the same hAEC concentrations as the THP-1 macrophage-based assays; 0.1×10^6, 0.2×10^6 and 0.5×10^6 cells. HMEC-1 were treated with these doses for 6 hours in the presence of 0.5 ng/mL IL-1β. A conditioned media control (0.225×10^6 hAECs) and HTR positive control was also included, both also receiving IL-1β stimulation. To determine the effect of hAECs on endothelial activation, the markers ICAM-1 and VCAM-1 were measured. ICAM-1 gene expression upon hAEC treatment, showed a decrease for all three concentrations compared to the IL-1β and HTR positive controls, although not significant. sICAM concentration also decreased upon hAEC treatment compared to the IL-1β and HTR positive controls (Figure 4-14A) The HTR control was significantly (p=<0.0001) increased compared to all treatments. Although the decrease was not significant compared to the IL-1β positive control, 0.2×10^6 and conditioned media control were also not significant compared to the untreated control. VCAM-1 gene expression was significantly decreased upon 0.2×10^6, 0.5×10^6 and the conditioned media control (p=0.0198, p=0.0326 and p=0.0250 respectively), compared to the IL-1β positive control (Figure 4-14C). In figure 4-14B, CXCL8 gene expression by HMEC-1 upon hAEC treatment was decreased at 0.1×10^6 hAECs compared to the positive controls, furthermore it was the only hAEC treatment that was not significant compared to the untreated. This decrease was also reflected with CXCL8 concentration.
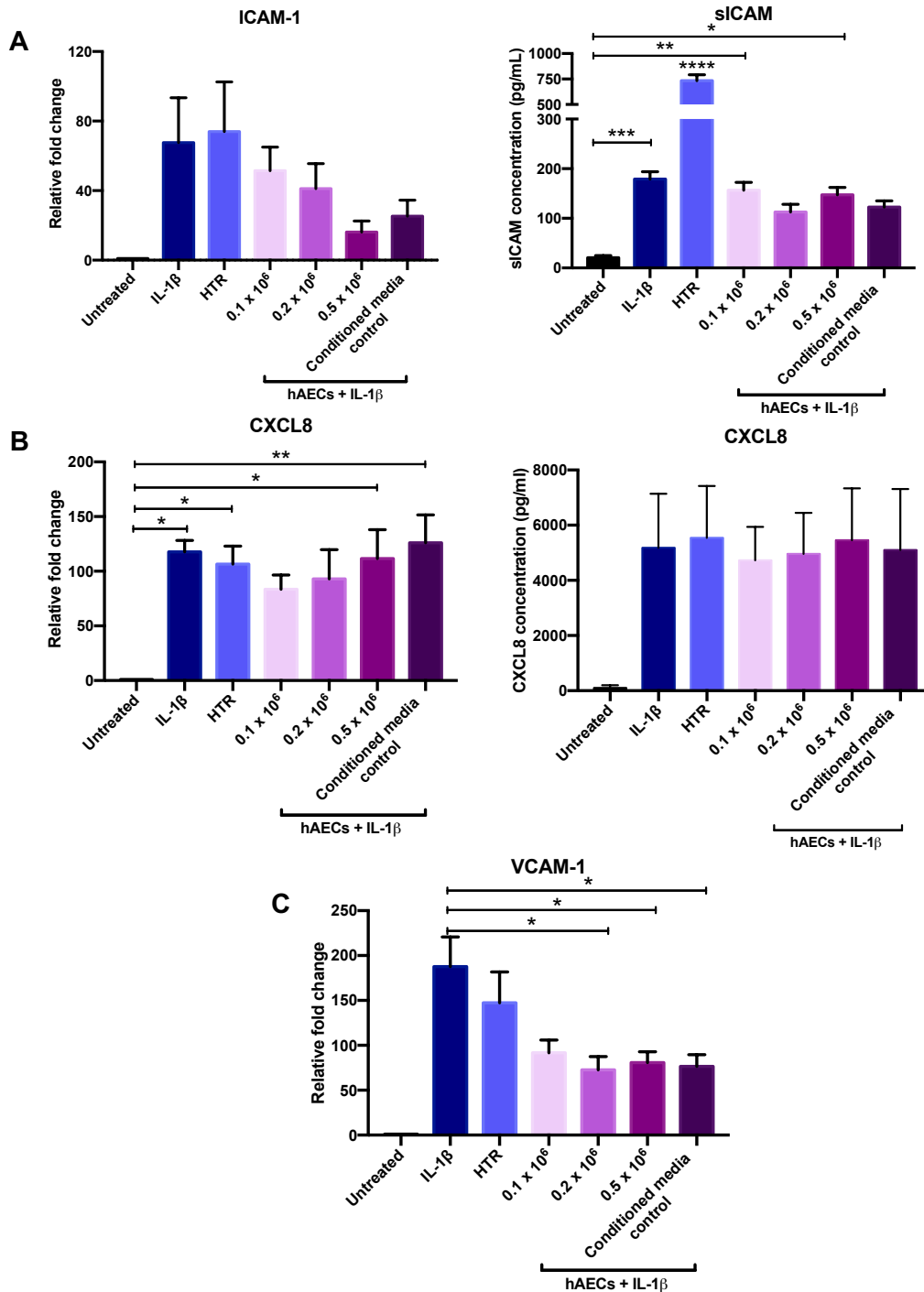
Figure 4-14 The effect of hAECs on endothelial activation and CXCL8 expression.

HMEC-1 were cultured with 0.1×10^6, 0.2×10^6 and 0.5×10^6 hAECs or HTR cells for 6 hours in the presence of 0.5 ng/mL IL-1β stimulation. (A) ICAM-1 gene expression by qPCR and soluble ICAM-1 (sICAM-1) concentration by ELISA. (B) Real time PCR and ELISA were used to determine CXCL8 expression (C) VCAM-1 gene expression was determined through real time PCR. N=3. Statistical significance was determined by a one-way ANOVA. *$p<0.05$, ** $p<0.01$, *** $p<0.001$, **** $p<0.0001$.

4.3.3.2 The effect of hAEC conditioned media

HMEC-1 were treated with hAEC-conditioned media for 6 hours in the presence of IL-1β. The activation markers ICAM-1 and VCAM-1 expression were determined by qPCR and CXCL8 expression by qPCR and ELISA. ICAM-1 gene expression decreased upon hAEC-conditioned media treatment despite the IL-1β stimulation (Figure 4-15A), however this was also observed with the control UltraCULTURE™ media, compared to the IL-1β positive control. A similar trend was observed with VCAM-1 gene expression, however only the hAEC conditioned media treatment was significantly decreased (p=0.0119) compared to the IL-1β positive control (Figure 4-15B). CXCL8 gene expression was significantly reduced upon hAEC conditioned media treatment compared to the IL-1β control and control media (p=0.0051 and p=0.0312) (Figure 4-15C). However, this was not reflected in the CXCL8 concentration in the supernatants, suggesting that conditioned media treatment was required for a longer period to have an effect at a protein level.
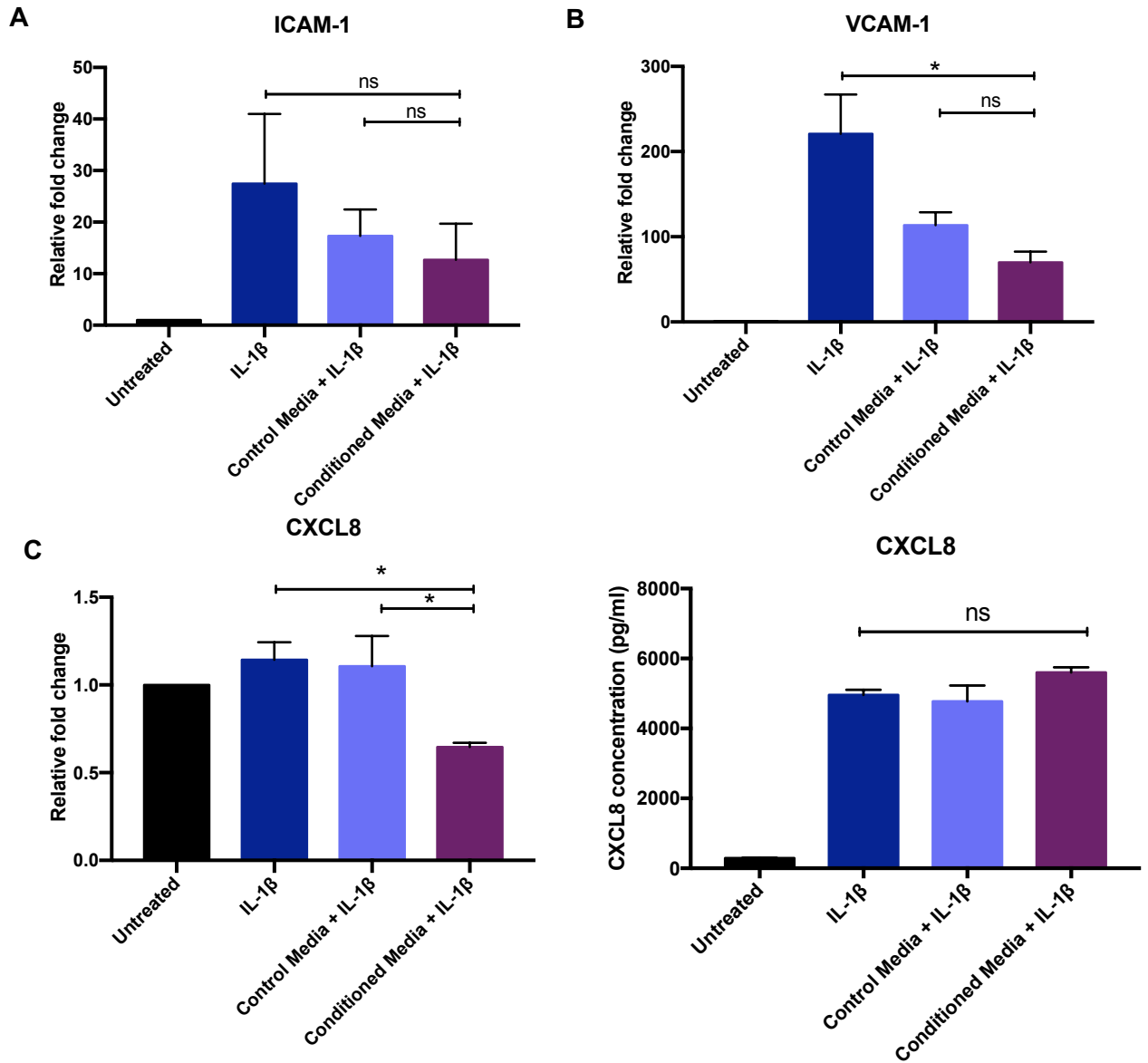
Figure 4-15 The effect of hAEC-conditioned media on the endothelial activation markers (ICAM-1 and VCAM-1) and CXCL8 expression.

HMEC-1 were cultured with hAEC conditioned media or control media for 6 hours in the presence of 0.5 ng/mL IL-1β stimulation. Real time PCR was used to determine the expression for (A) ICAM-1 (B) VCAM-1 (C) CXCL8 and supernatant concentration was determined through ELISA. N=5. Statistical significance was determined by a one-way ANOVA and Tukey's multiple comparisons. $*p<0.05$.

4.3.3.3 The effect of hAEC-EVs

HMEC-1 cells were treated with 5 μg, 10 μg and 20 μg of EVs, generated from the hAEC conditioned media, for 6 hours with 0.5 ng/mL IL-1β. Endothelial activation marker ICAM-1 gene expression was determined by qPCR and sICAM concentration in the supernatant was determined by ELISA. Furthermore, the endothelial activation marker VCAM-1 gene expression was also determined by qPCR.

The treatment of 5 μg of hAEC-EVs led to a decrease in the gene expression of ICAM-1 compared to the IL-1β positive control, which was the only EV treatment to not achieve significance relative to the untreated control (Figure 4-16A). However, this decrease was not observed for sICAM concentration in the supernatants. VCAM-1 gene expression was decreased upon hAEC-EV treatment compared to the IL-1β positive control (Figure 4-16B). Similarly, with ICAM-1, 5 μg was the only EV treatment that didn't significantly increase ICAM-1 gene expression compared to the untreated control, suggesting 5 μg is the best dose for HMEC-1 treatments. On the other hand, both ICAM-1 and VCAM-1 gene expression was most decreased by the EV-depleted conditioned media, this suggests the EV-depleted conditioned media influenced gene expression without the need for the presence of EVs. Inflammatory marker CXCL8 expression upon hAEC-EV treatment was determined by qPCR and ELISA. This revealed that 5 μg of hAEC-EVs led to a decrease in the gene expression of CXCL8 compared to the IL-1β positive control, however this was not significant (Figure 4-16B). A slight decrease with all hAEC-EV treatments was observed for CXCL8 concentration in the supernatants. 10 μg of EVs led to significant decrease in CXCL8 concentration compared to the EV-depleted conditioned media control (p=0.0301), which directly contradicted the gene expression data which observed an increase in CXCL8 expression upon 10 μg, which was significant compared to the EV-depleted conditioned media control (p=0.0216).
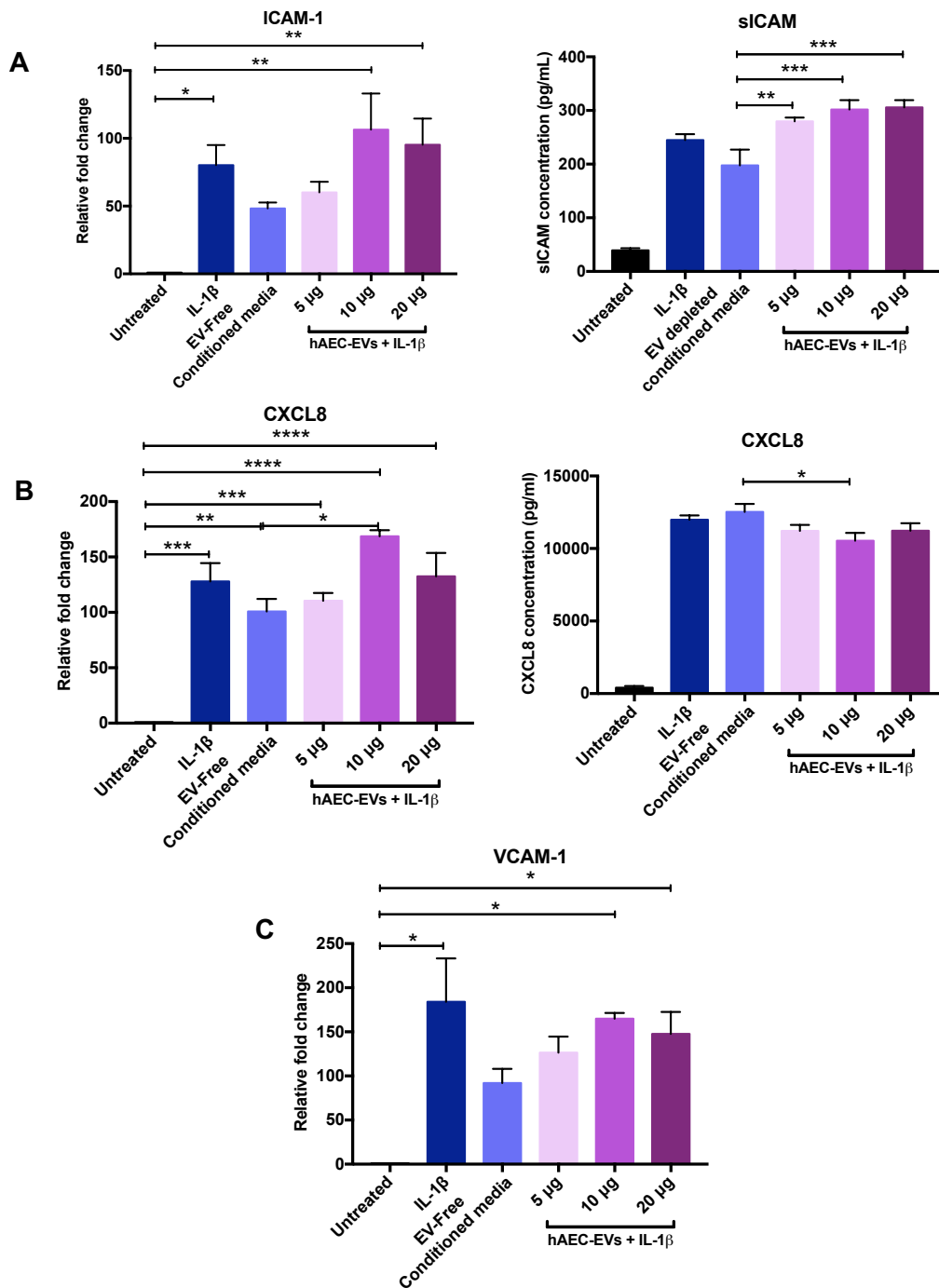
Figure 4-16 The effect of hAEC-EVs on endothelial activation and CXCL8 expression.

HMEC-1 were cultured with 5, 10 and 20 μg hAEC-EVs or "EV depleted" conditioned media and 0.5 ng/mL IL-1β for 6 hours. (A) ICAM-1 and soluble ICAM-1 (sICAM) expression in the cells and supernatants were determined through real time PCR and ELISA respectively. (B) CXCL8 gene expression was determined through real time PCR and CXCL8 concentration in the supernatants through ELISA. (C) VCAM-1 gene expression was determined by real time PCR. N=3. Statistical significance was determined by a one-way ANOVA and Tukey's multiple comparisons. ∗p<0.05, ∗∗ p<0.01, ∗∗∗ p<0.001, ∗∗∗∗ p<0.0001.

4.3.4 The effect of hAECs and their derivatives on endothelium permeability markers

To deepen our understanding of the effect hAEC treatment may have on the endothelium, the expression of sphingosine-1-phosphate receptor 1 (SIPR1) and 3 (SIPR3), which have a role in permeability and neutrophil chemotaxis, was determined to see if hAEC treatment influenced their expression on HMEC-1.

After 6 hours of treatment of IL-1β with either hAECs or HTR cells, an increase in the expression of SIPR1 was observed, although this was variable, compared to the IL-1β and HTR cell positive controls (Figure 4-17A). Complimentary to this, a decrease in SIPR3 expression was observed with hAEC treatment despite the addition of IL-1β, in comparison to the IL-1β and HTR cell positive controls. A similar trend could be observed upon treatment of HMEC-1 with hAEC-conditioned media with an increase in SIPR1 and decrease in SIPR3 expression compared to the IL-1β positive control (Figure 4-17B). However, the control UltraCULTURE™ media appeared to also decrease the expression of SIPR3, although this could be due to the serum-supplementation of the media potentially aiding in endothelial integrity. Conversely, treatment of the HMEC-1 with hAEC-EVs lead to no increase in SIPR1 expression and in the case of 10 μg of EVs, lead to an increase in SIPR3 expression compared to the IL-1β positive control (Figure 4-17C). However, the EV-depleted conditioned media lead to a slight increase in SIPR1 expression and decreased SIPR3 expression, therefore this may suggest the conditioned media still contains as yet undefined biologically functional molecules that may aid in endothelial integrity.
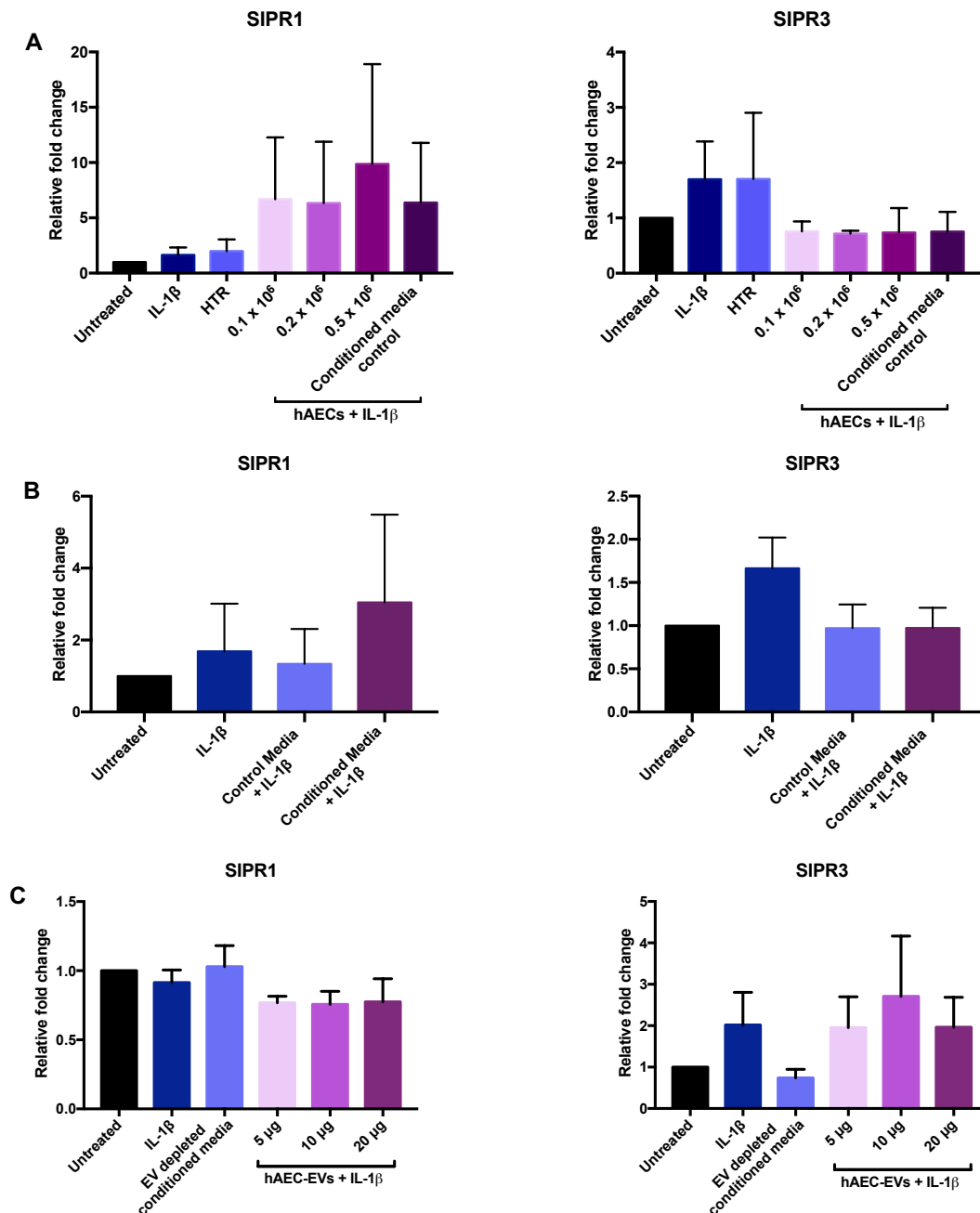
Figure 4-17 The expression of SIPR1 and SIPR3 on HMEC-1 after hAEC, hAEC-conditioned media, and hAEC-EV treatment.

Sphingosine-1-phosphate receptor 1 (SIPR1) and Sphingosine-1-phosphate receptor 3 (SIPR3) gene expression was determined by real time PCR for the following treatments of (A) 0.1×10^6, 0.2×10^6 or 0.5×10^6 hAECs or HTR cells with 0.5 ng/mL IL-1β (B) hAEC conditioned media or control media with 0.5 ng/mL IL-1β (C) 5, 10 and 20 μg hAEC-EVs or "EV depleted" conditioned media with 0.5 ng/mL IL-1β. Statistical significance was determined by a one-way ANOVA. N=3.

127

4.3.5 Effect on neutrophil transendothelium migration

To determine the effect on neutrophil migration through an activated endothelial monolayer after treatment with hAECs, hAEC-CM and hAEC-EVs, human neutrophils were either isolated by Mr Jonathan Scott of the Simpson Laboratory or by magnetic bead separation, using peripheral blood from healthy volunteers.

Neutrophils isolated by the magnetic bead separation technique were tested for purity through flow cytometry for markers CD16, CD14, CD15 and CD193. The neutrophil population was gated, followed by the single cell population (Figure 4-18A). The neutrophil population were positive for markers CD16 and CD15, but negatively expressed CD14, confirming the majority of the isolated population was neutrophils. Due to an increased expression of CD193 (CCR3), this may suggest the presence of a few contaminating eosinophils. However, a cytospin of a sample of the isolated population also confirmed neutrophil morphology could be observed (Figure 4-18B).

An HMEC-1 endothelial monolayer was activated with IL-1β and treated with hAECs, hAEC-CM or hAEC-EVs for 6 hours, with their relevant controls. The treatments were removed and CXCL8 was added as a chemoattractant, then neutrophils were added to the top of the monolayer and left to migrate through the endothelium for 1.5 hours. The number of neutrophils that migrated through was determined using flow cytometry. All hAEC treatments showed a reduction in neutrophil migration compared to the HTR cells and IL-1β positive control (Figure 4-19A). This was significant with the 0.2 x 10^6 hAECs treatment compared to the HTR cell control (p=0.0128), which appeared to increase chemotaxis. Treatment of the HMEC-1 monolayer with hAEC-conditioned media led to a small reduction in neutrophil migration compared to the positive controls, although not significant but demonstrated by the lack of significance to the untreated control, which the IL-1β and HTR conditioned media positive controls were significant to (Figure 4-19B). On the other hand, treatment with the hAEC-EVs derived from the conditioned media showed a reduction in neutrophil migration, with 10 μg showing the most significant decrease (p=0.0079) (Figure 4-19C).
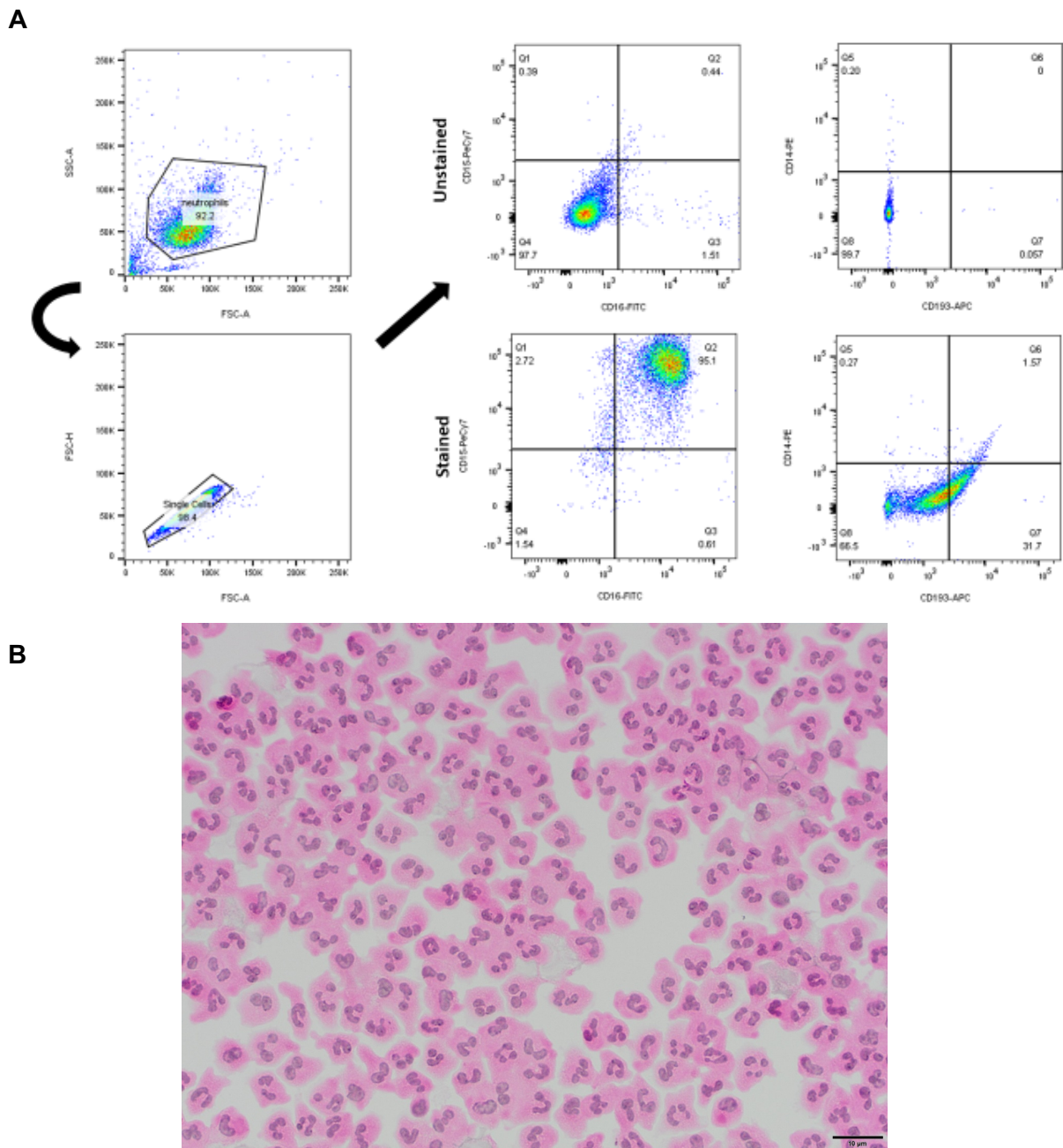
Figure 4-18 Purity from the isolations of neutrophils from peripheral blood.

Neutrophils were isolated from human peripheral blood using the magnetic bead separation technique. (A) Flow cytometric analysis on freshly isolated neutrophils. The neutrophil population was gated, then single cells were gated. The neutrophils were shown to have strong positive expression of CD15 and CD16, and low expression of CD193 and CD14. (B) Freshly isolated neutrophils underwent a cytospin then were stained by H&E, revealing the classic polymorphonuclear morphology. Magnification: x40, Scale: 10 μM. N=3.
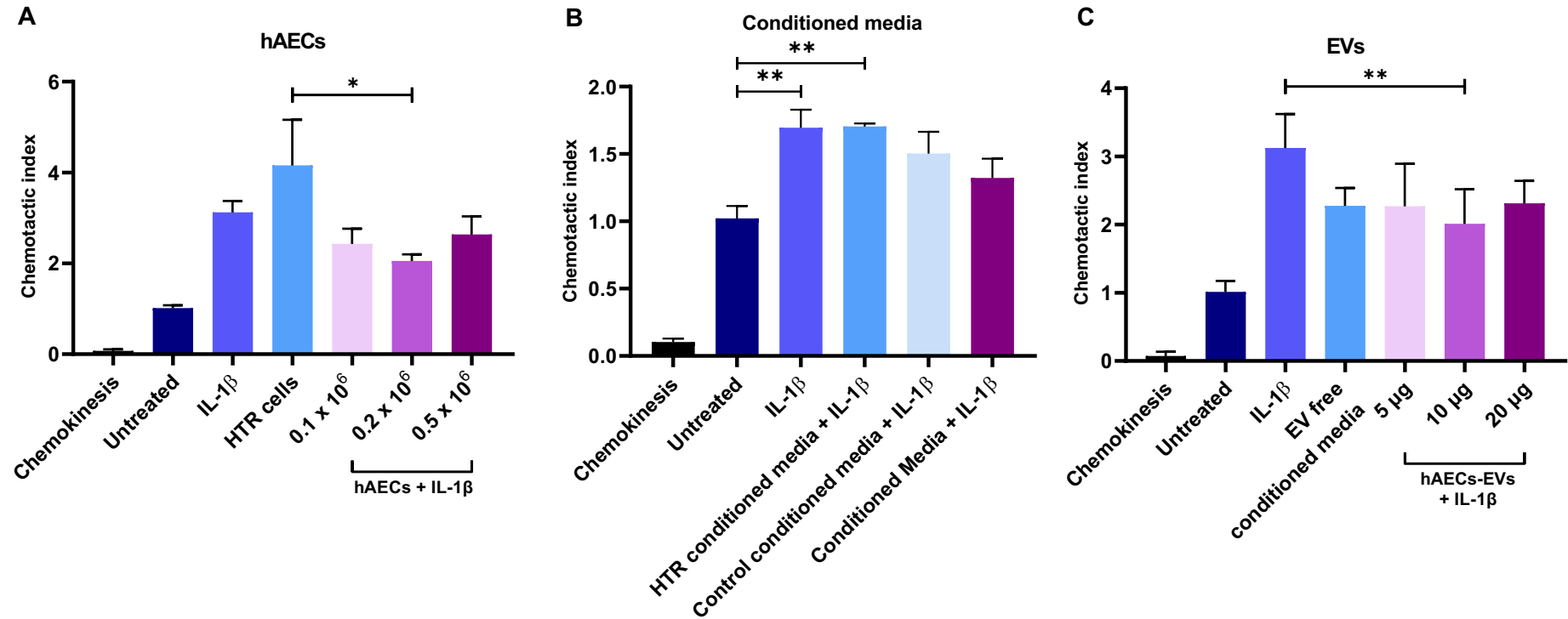
Figure 4-19 Neutrophil migration through IL-1β activated HMEC-1 after hAECs, hAEC-conditioned media and hAEC-EV treatment.

A HMEC-1 monolayer was treated with (A) 0.1×10^6, 0.2×10^6 or 0.5×10^6 hAECs or HTR cells with 0.5 ng/mL IL-1β (B) hAEC conditioned media, HTR conditioned media or control (UltraCULTURE™) media with 0.5 ng/mL IL-1β (C) 5, 10 and 20 μg hAEC-EVs or "EV depleted" conditioned media with 0.5 ng/mL IL-1β. Neutrophils were then left to migrate towards CXCL8 through the monolayer for 1.5 hours. All N=3. Statistical significance determined by a one-way ANOVA with Tukey's multiple comparisons. ∗p<0.05, ∗∗ p<0.01.

4.4 Discussion

Despite progress, lung transplantation has some of the worst clinical outcomes of solid organ transplant as they're particularly susceptible to injury, with PGD being one of the most common early complications and the main cause of morbidity and mortality in patients during the immediate post lung transplant period. PGD is a form of acute lung injury that occurs in the first 72 hours of the postoperative period. The underlying mechanism behind PGD is multifactorial caused by injury to the donor lungs due to the circumstances surrounding the donor's demise and exacerbated by IRI which develops in the cold ischemic time during storage and transport of the organ and upon reperfusion of the blood flow being restored during transplantation. This sterile inflammation triggers a cascade of events which ultimately can lead to pulmonary oedema, impaired gas exchange and lung vascular damage (Jin et al., 2020; Laubach & Sharma, 2016). The shortage of 'ideal' donor lungs available compared to the numbers of patients on the transplant waiting list has led transplant centres to use more lungs from extended criteria donors. Extended criteria donors include those with a more extensive smoking history, aged over 55 or a PaO_2 of >250 mmHg. Although there is more use of these extended criteria donors, this has been reported not to impact overall lung transplant survival (Reyes et al., 2010). However, Diamond *et al.,* reported an increased risk of severe PGD development if the donor had any smoking history, pulmonary arterial hypertension, elevated pulmonary arterial pressures, or an obese recipient. This was associated with an increased risk of 90-day and 1-year mortality (Diamond et al., 2013). Treatment options addressing PGD and the underlying mechanism of IRI are limited, therefore more research into potential therapeutics is required to allow for further expansion of the potential donor pool, allowing for more lungs to be used for transplant. hAECs offer a potential novel therapeutic to target this clinical problem faced in the field of lung transplantation.

In the context of murine and lamb lung injury models in the literature, hAECs have been shown to reduce the production of CXCL8 and $TNF\alpha$ (Zhu et al., 2017; Moodley, Ilancheran, Samuel, Vaghjiani, Atienza, Elizabeth D Williams, et al., 2010; Melville et al., 2017). Our aim was to determine whether pro-inflammatory macrophages and activated endothelium, which have a role in IRI, also showed this reduction in CXCL8 and $TNF\alpha$ levels after treatment with hAECs and their derivatives. In THP-1 derived macrophage model, the use of hAECs led to the most consistent significant reduction in CXCL8 and $TNF\alpha$ gene and protein expression

compared to the hAEC-CM or EVs (Table 4-2). In the case of the hAEC-EVs, no decrease was observed in CXCL8 and TNFα gene expression levels, but a decrease was observed in the concentration within the supernatants. This was also observed with CXCL8 production with the HMEC-1 endothelial model. This suggests that the mechanism in which the hAEC-EVs work is different to that of the cells and conditioned media. EVs are well established in the literature to package cytokines, including CXCL8 and TNFα, which cannot be detected through ELISA. Alternatively, EVs could be binding to specific cytokine receptors, in order to uptake into the cell (Berenguer et al., 2018; Barnes & Somerville, 2020).

CXCL8 gene and protein expression was also reduced in the HMEC-1 endothelial model upon treatment with hAECs, despite the addition of IL-1β, compared to the IL-1β positive control (Table 4-2). Gene expression of CXCL8 was also observed to decrease in HMEC-1 after treatment with hAEC conditioned media, but this was not reflected in the concentration of CXCL8 in the supernatants. This suggests that hAEC conditioned media may take a longer treatment time than 6 hours to show a reduction in CXCL8 concentration by HMEC-1.

As described previously, TNFα is a significant key initiator to the cascade of events caused by IRI leading to endothelial damage. Naidu *et al,* observed that alveolar macrophages secreted TNFα as early as 15 minutes into reperfusion and upon use of gadolinium chloride to inhibit macrophage function lead to a marked decrease in TNFα production (Naidu et al., 2004). Khimenko *et al,* also demonstrated that an anti-TNFα antibody provided therapeutic benefit to rat lungs, with a 2-hour treatment preventing microvascular damage in lungs exposed to IRI (Khimenko et al., 1998). Andreasson *et al,* also demonstrated that increased TNFα concentration after 30 minutes of EVLP demonstrated reduced patient survival, suggesting a reduction in TNFα could be a good predictor of post-transplant mortality (Andreasson et al., 2017). Elevated CXCL8 levels in lungs have been demonstrated to be a good predictive marker for early graft dysfunction, and has been further demonstrated to be more highly expressed in lungs undergoing EVLP that were then subsequently rejected for use in transplant (Fisher et al., 2001; Andreasson et al., 2017). CXCL8 is a potent neutrophil chemoattractant and has been negatively correlated with lung function (De Perrot et al., 2002).

Therefore, as treatment with hAECs appears to significantly reduce the expression of CXCL8 and TNFα in macrophages and CXCL8 in endothelial cells, this demonstrates the possibility of hAECs as a therapeutic for reducing key IRI cytokines, which could potentially lead to a reduction in lung injury occurring and improving post-transplant outcomes.

Cells isolated from one donor placenta behaved noticeably differently to that of the trend previously observed when used to treat LPS stimulated macrophages. No change in CXCL8 concentration was observed and TNFα production was actively increased upon hAEC-CM treatment. This donor had been taking adalimumab and lansoprazole. Adalimumab works by inhibiting TNFα functions therefore it could be postulated that due to the anti-inflammatory microenvironment provided by this medication, this could have led to the hAECs adopting a pro-inflammatory phenotype. This has been observed in cases where a patient has a chorioamnionitis infection, where hAECs adjusted to a pro-inflammatory phenotype depending on the microenvironment they are exposed to (Gillaux et al., 2011). Therefore, it may be important that hAECs are only isolated from donors that did not undertake anti-inflammatory medications in case this may lead to an alteration in their function.

Pro-inflammatory M1 macrophages play a key role in the early phase of IRI by secreting large amounts of cytokines in response to oxidative stress, including TNFα, which leads to the activation of the endothelium, which ultimately contributes to its breakdown and thus formation of acute lung injury and pulmonary oedema. hAEC treatment have been shown to polarise alveolar M1 macrophages to M2 anti-inflammatory macrophages in a murine lung injury model (Tan et al., 2014). M2 macrophages play a role in immunomodulation, wound healing and tissue repair (Andrewartha & Yeoh, 2019). Our study reflects similar findings, with an upregulation in MRC-1 (CD206), an M2 macrophage marker, upon treatment with hAECs. Although this was not observed upon treatment with hAEC conditioned media and minimally with EVs (Table 4-2). Tan *et al,* also observed an increase in macrophage phagocytosis upon hAEC treatment and a significant upregulation upon hAEC-EV treatment (Tan et al., 2014, 2018). This reflects our findings where we observed an upregulation of phagocytosis by macrophages upon treatment with hAECs compared to HTR cells treatment. An even larger upregulation in phagocytosis was also

observed upon hAEC-EVs treatment. Therefore, findings from our study suggest that hAEC treatment polarises M1 macrophages towards an M2 phenotype. This is demonstrated by the trend of increased phagocytosis, decreased TNFα and CXCL8 production (immunomodulation) and increased MRC1 (CD206) expression, all typical characteristics of M2 macrophages (Figure 4-20). Macrophage inhibition through gadolinium chloride, showed better lung function during the ischemic period and after reperfusion (Fiser et al., 2001). Zhang *et al,* found heme oxygenase-1 (HO-1), which plays a role in M2 macrophage polarisation, can limit liver IRI and Mao *et al,* also observed that injecting M2 macrophages into mice showed reduced renal injury caused by IRI (Zhang et al., 2018; Mao et al., 2020). Therefore, these studies suggest that hAEC treatment leading to the polarisation of macrophages to an M2 phenotype could play an important role for ameliorating IRI.
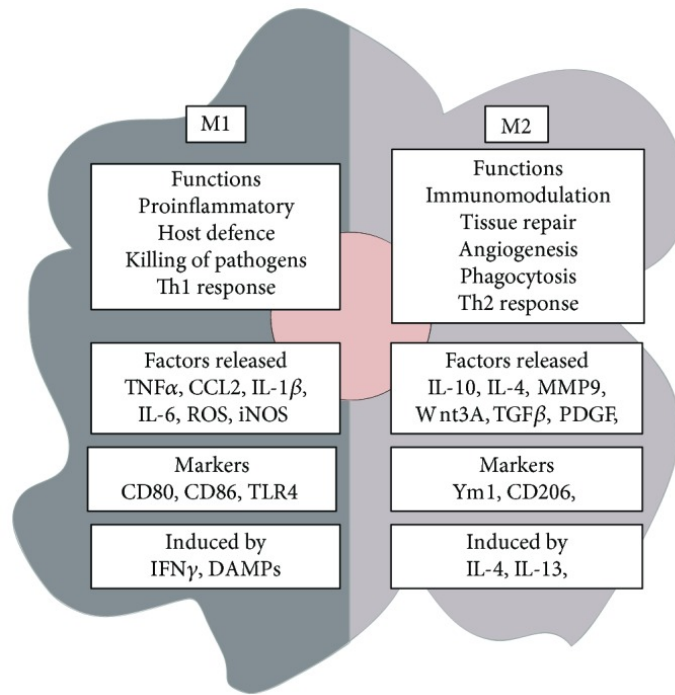
Figure 4-20 M1 and M2 macrophage paradigm of typical phenotypic characteristics.

M1 macrophages have a pro-inflammatory function to defend the host from pathogens, leading to increased production of pro-inflammatory cytokines and ROS. M2 macrophages classically play an immunomodulatory role and aid in tissue repair, phagocytosis and angiogenesis for wound healing. They release anti-inflammatory cytokines and express CD206 (MRC1) (Andrewartha & Yeoh, 2019).

Endothelial cell dysfunction and the transendothelial migration of recipient neutrophils into the airway, by chemotactic factors such as CXCL8, is a classic hallmark of PGD. During ischemia, the endothelium becomes activated by the secretion of TNFα and IL-1β, expressing markers such as ICAM-1 and VCAM-1, and producing ROS (Liu et al., 2011; Morrison et al., 2017; Andreasson et al., 2017). ICAM-1 levels in plasma have been shown to be higher in grade 3 PGD patients pre-operative and at 6, 24, 48, and 72 hours post-transplant. The higher levels of ICAM-1 were also associated with a higher 30-day mortality (Covarrubias et al., 2007). Higher ICAM-1 expression was also observed in lungs that underwent EVLP but were then deemed untransplantable, compared to transplanted lungs (Andreasson et al., 2017). Our study demonstrated the potential of hAECs to markedly reduce ICAM-1 gene expression on HMEC-1 despite continued IL-1β stimulation and sICAM concentration in the supernatants (Table 4-2). We also observed a significant reduction in VCAM-1 gene expression (Table 4-2). The hAEC-conditioned media also led to a decrease in ICAM-1 and VCAM-1 gene expression, as did 5 μg of hAEC-EVs, however this was not as therapeutically beneficial compared to their whole cell counterpart. The upregulation of endothelial activation markers, such as ICAM-1 and VCAM-1, lead to the migration of neutrophils through the endothelium (Schmidt et al., 2011).

Neutrophil infiltration and transendothelial migration during IRI is associated with impaired gas exchange and microvascular leakage (Ng et al., 2006). hAECs significantly reduced neutrophil chemotaxis through IL-1β activated endothelium towards CXCL8, compared to the control HTR cells (Table 4-2). Furthermore, hAEC-EVs also significantly reduced neutrophil transendothelium migration towards CXCL8 compared to the IL-1β positive control (Table 4-2). Less of an effect on neutrophil chemotaxis was observed with the hAEC conditioned media (Table 4-2). This supports the findings in the literature. Li *et al,* also observed a reduction in the chemotaxis of neutrophils towards MIP-2 upon hAEC treatment (Li et al., 2005). Furthermore, a COPD rat model showed reduced neutrophil infiltration into the lungs upon hAEC treatment (Geng et al., 2016). Tan *et al,* also demonstrated hAEC-EVs reduced neutrophil infiltration into bleomycin injured lungs (Tan et al., 2018). This demonstrates the potential for hAECs to limit endothelial activation and neutrophil transendothelial migration, which could potentially ameliorate some of the damaging effects observed in IRI.

In addition to hAECs reducing endothelial activation marker expression and neutrophil transmigration, we also demonstrated that hAECs have the capacity to increase SIPR1 expression and decrease SIPR3 expression on HMEC-1 (Table 4-2). SIP is a lipid that binds to five G protein-coupled receptors (SIPR1-5) to regulate a variety of functions, including playing a key role in endothelial barrier integrity. SIPR1 appears to attenuate IRI in kidneys and is associated with vascular integrity, and SIPR3 appears to be a biomarker for acute lung injury and is associated with vascular permeability (Sun et al., 2012; Perry et al., 2016). Stone *et al,* demonstrated that use of a SIPR1 agonist and SIPR3 antagonist significantly improved lung function and reduced vascular permeability (Stone et al., 2015). Mehaffey *et al,* also demonstrated administering circulating SIP and an inhibitor of SIP clearance during EVLP, significantly improved lung compliance and reduced vascular permeability (Mehaffey et al., 2018). Therefore, hAECs increasing SIPR1 and decreasing SIPR3 expression, could play a further beneficial role in maintaining endothelial integrity and aiding in preventing vascular damage occurring by IRI.

	Macrophages			Endothelial-neutrophil interactions		
	Activation	**Phagocytosis (6 hours)**	**MRC1 expression**	**Endothelium activation**	**Permeability**	**Neutrophil chemotaxis**
hAECs (0.2 x 10^6)	↓ CXCL8 gene (p=0.0290) and protein (p= 0.0465) ↓ TNFα gene (p=0.0158) and protein (p=0.0387) ↓ sICAM (p=0.0190 for 0.5 x 10^6 hAECs)	↑ increased phagocytosis (0.1 x 10^6 showed largest increase)	↑ MRC1 gene expression increased for 0.1 x 10^6 hAECs (ns)	↓ ICAM-1 (ns) ↓ sICAM-1 (ns) ↓ VCAM-1 (p=0.0198) ↓ CXCL8 gene and protein expression (ns)	↑ SIPR1 (ns) ↓ SIPR3 (ns)	↓Neutrophil migration (p=0.0128)
Conditioned media (1:1 dilution)	↓ CXCL8 gene (ns) and protein (p= 0.0001) ↓ TNFα gene (p=0.0445) and protein (p=0.0027)	↑ increased phagocytosis (p=0.0732)	No increase observed	↓ ICAM-1 (ns) ↓ VCAM-1 (p=0.0119) ↓ CXCL8 gene expression (p=0.0119)	↑ SIPR1 (ns) ↓ SIPR3 (ns)	↓Neutrophil migration (ns)
EVs	5 μg: ↓ CXCL8 protein expression (ns) ↓ TNFα protein expression (ns) ↓ sICAM (ns)	↑ increased phagocytosis (largest increase with 20 μg)	↑ MRC1 gene expression increased for all doses (ns)	5 μg: ↓ ICAM-1 (ns) ↓ VCAM-1 (ns) ↓ CXCL8 gene and (ns) ↓ CXCL8 protein expression (p=0.0301)	↑ SIPR3 with 10μg (ns)	↓Neutrophil migration (p=0.0079 for 10 μg)

Table 4-2 Summary of the results of the functional testing of hAECs, conditioned media and EVs on macrophages and endothelial-neutrophil interactions.

Overview of the data collected during the functional testing on macrophage activation, phagocytosis (after 6 hours) and Mannose receptor C Type-1 (MRC1) expression. Additionally, the functional testing on the endothelial activation, permeability and neutrophil transendothelial migration. p numbers included to indicate where significance was achieved.

Ns – not significant. SIPR – sphingosine-1-phosphate receptor. sICAM – soluble ICAM.

4.4.1 Conclusions

To conclude, our functional testing of isolated hAECs and their derivatives have demonstrated their potential to reduce key cytokines involved in donor lung injury and IRI; CXCL8 and TNFα expression in macrophages and endothelial cells. hAECs also demonstrated a trend to polarise pro-inflammatory M1 macrophages, towards an M2 anti-inflammatory phenotype, which are instead associated with tissue repair. Finally, hAECs treatment reduced of activation markers ICAM-1 and VCAM-1 expression, reduced neutrophil transendothelial migration, increased SIPR1 expression and decreased SIPR3 expression. This suggests hAECs are reducing endothelial cell dysfunction. As described previously, macrophages, endothelial cells and neutrophils all play a key role in IRI, which leads to vascular injury and pulmonary oedema formation, resulting in increased risk of PGD and poorer transplant outcomes. Our study demonstrated that hAECs and their derivatives all offer a therapeutic benefit, however we found that hAECs consistently provided a more encompassing therapeutic benefit over their conditioned media and EV counterparts. Therefore, hAECs offer a promising broadly bioactive therapeutic with the ability to target all these key players, thus their administration to the EVLP platform could potentially limit IRI in extended criteria lungs prior to transplant with the potential to improve post-transplant outcomes.

5 Human amniotic epithelial cells in the *ex vivo* lung perfusion platform

5.1 Introduction

Two critical issues currently faced by the field of lung transplantation are the shortage of suitable donor organs available for transplant compared to the number of patients on the active transplant waiting list, and the incidence of PGD which occurs within the first 72 hours post-transplant, caused by donor lung injury.

In 2019-2020, only 21% of potential donor lungs were deemed suitable for transplant (NHSBT, 2020). Despite the selectivity of the criteria and clinicians having a cautious approach to accepting lungs for transplant, PGD still frequently occurs and is a major cause of morbidity and mortality in lung transplant recipients. EVLP provides a promising solution to address these two critical issues, by offering a technique to recondition and evaluate donor lungs prior to transplantation; enabling safe use of lungs that otherwise would be deemed untransplantable. Cypel *et al* demonstrated that following EVLP, 20 of 23 donor lungs deemed high risk for transplant could be successfully transplanted. This resulted in a PGD incidence rate of 15% in the EVLP group compared to 30% in the control group (Cypel et al., 2011). Boffini *et al,* also reported that after carrying out EVLP on 23 out of 75 lungs that were turned down for transplant, 7 were then deemed suitable, increasing the centres activity by 30% (Boffini et al., 2013). Koch *et al,* demonstrated that 9 out of 11 lungs deemed unusable but underwent EVLP could then be considered suitable and successfully transplanted with no significantly different outcomes compared to the control group (Koch et al., 2018). In addition to these studies, there are multiple clinical trials, completed and ongoing, that are assessing the effectiveness of performing EVLP to assess extended criteria donor lungs and to increase lung transplant activity. Of the three completed clinical trials, there were no higher rates of PGD in the EVLP group compared to patients in the standard lung transplant group, and also led to the utilisation of more donor lungs that would otherwise not have been used for transplant (Warnecke et al., 2018; Loor et al., 2018; Fisher et al., 2016).

EVLP was first developed by Steen *et al,* in Lund for the purpose of assessing donor lungs from DCD donors. The technique involves lungs being placed into an evaluation box and connected to a circuit and ventilator. Flow of a perfusate solution,

with optimal osmotic pressures, is pumped through a circuit, passing through an oxygenator to allow for gas exchange and a heating unit to maintain physiological temperatures throughout perfusion (Steen et al., 2001; Wierup et al., 2006). Not only does this technique allow for the evaluation of extended criteria donor lungs to assess if they're suitable to transplant, but it also offers a unique platform to administer therapeutics directly to the lungs.

Multiple traditional therapeutics, antibiotics, receptor agonists/antagonists, gases and gene therapies have been administered to donor lungs while on the EVLP platform (Griffiths et al., 2020). Alternatively, cellular therapies have been attracting recent attention due to their more encompassing therapeutic effect. MSCs and MAPCs have both been successfully administered to donor lungs while on the EVLP platform, demonstrating a reduced production of pro-inflammatory cytokines, an increase in anti-inflammatory cytokines, reduction in oedema formation and reduced cell infiltration into the lungs in the case of the MAPCs (Mordant et al., 2016; Nakajima et al., 2019; McAuley et al., 2014; Martens et al., 2017; La Francesca et al., 2014). These studies highlight the potential for cellular therapies to limit inflammation and donor lung injury prior to transplantation.

Chapter 4 of this thesis demonstrated the potential of hAECs to limit and ameliorate macrophage and vascular endothelial activation and secretion of pro-inflammatory cytokines TNFα and CXCL8, alongside reducing neutrophil chemotaxis through activated endothelium. These are all key processes in development of acute lung injury and the formation of PGD. Therefore, we hypothesised that the administration of hAECs to EVLP could provide a therapeutic benefit in extended criteria lungs that have been turned down for transplant.

5.1.1 Aims and objectives

The aim of this chapter is to evaluate hAECs as a therapeutic for reconditioning lungs through the EVLP platform by:

- Administering hAECs and HTR cells, as a cell treatment control, to a split lung single donor EVLP model for 4 hours and checking the cells would be tolerated.

- Determining any changes in haemodynamics, EVLP physiological parameters (pressure and flow rates), vasculature and weight gain upon administration of hAECs.

- Tracking hAECs within the perfusate and tissue samples to determine whether they engraft in the lungs.

- Determine any biological changes in pro-inflammatory cytokine and oxidative stress expression in the tissue and perfusates upon treatment with hAECs

5.2 Materials and methods

5.2.1 Split lung EVLP model

Human lungs, declined for transplant, were obtained under Human Research Authority Research Ethics Committee approval (REC:16/NE/0230) as part of NHSBT Study 66 entitled 'Further Evaluation of Ex Vivo Lung Perfusion to Improve Transplantation Outcomes'. In order to administer two therapies concurrently, a split lung EVLP model was used, as described in detail below (or see appendix A). The EVLP work was performed in a controlled access laboratory within the NHS Blood and Transplant facility on Holland Drive, Newcastle Upon Tyne.

5.2.1.1 Preparation of homemade Steen solution

Bovine serum albumin (BSA), Dextran 40, 7.5% Sodium Bicarbonate solution, krebs henseleit buffer and 1 M calcium chloride solution (All Sigma Aldrich) were added to 1600 mL Ultrapure water. Once fully dissolved the bottle was topped up to 2000 mL with Ultrapure water. This was filtered using a 0.20 µM polyethersulfone (PES) membrane filter using a vacuum into a sterile plastic 1 litre storage bottle (Fisher Scientific, UK). Homemade Steen solution was stored at 4°C for up to a month before use. For more detail see appendix A.

5.2.1.2 Priming of the circuit

Two Medtronic© circuits were set-up and primed with 1.5 L of homemade Steen solution. The circuit was de-aired and perfusate was left to circulate with 7500 units of heparin at a flow rate of 0.5-1 L/min. The heater-cooler unit was attached to the oxygenator on the circuit and turned to 38°C to warm the circulating perfusate. 7% CO_2/N_2 gas was also connected to the oxygenator. A blood gas measurement was taken using CG4+ cartridge and iSTAT machine (Abbott Laboratories, USA) to ensure appropriate pH of 7.3-7.5 and CO_2 concentration of 3-5. If pH was below this threshold, Tromethamine (THAM) solution was used to increase pH.
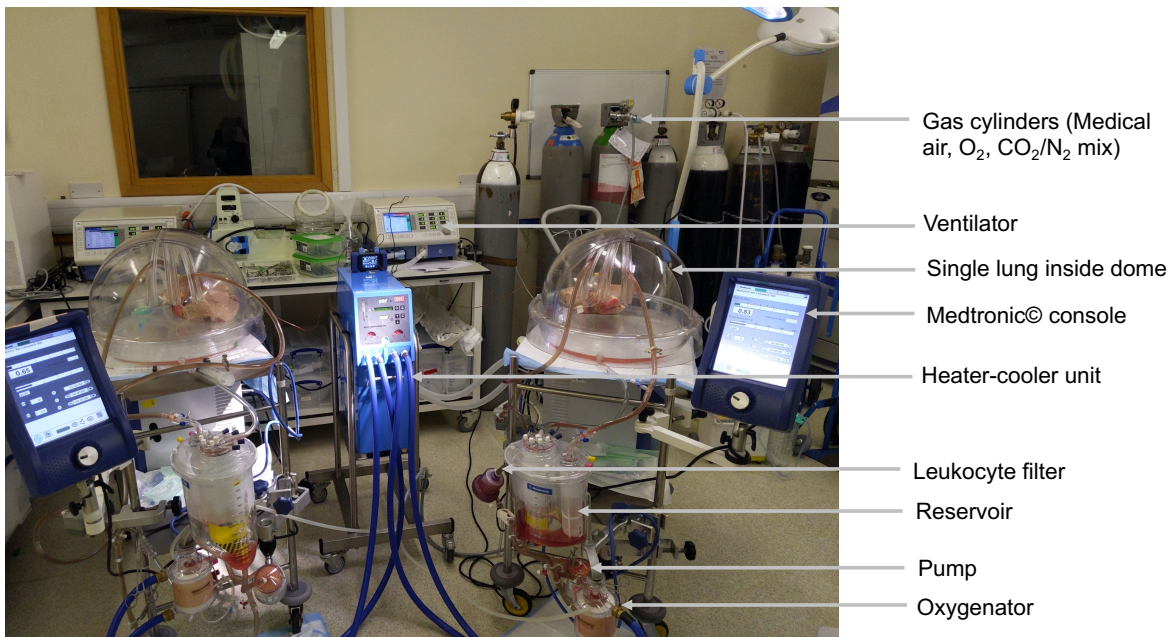
Figure 5-1 Split lung *ex vivo* lung perfusion.

The left and right lungs are split and connected to separate Medtronic© circuits and ventilator. The lungs are perfused concurrently, allowing for a treatment and control arm.

5.2.1.3 *Preparation of the lungs and perfusion procedure*

The lungs were split whilst inflated by cannulating (XVIVO, Sweden) the left and right branches of the pulmonary artery (PA) and pulmonary vein. The trachea was then dissected down to the carina and clamped before the left bifurcation, then cut to deflate the left lung. An adult endotracheal tube (ET) tube was then inserted and secured in place with ties. The right lung was then deflated, and a second ET tube inserted. After the lungs were split, they were weighed. Each lung was connected to a Medtronic© circuit (Medtronic, The Netherlands) at a flow rate of 20% cardiac output (CO) initially, then over 15 minutes this was gradually increased to 40% CO. Pressure transducers, provided by the Medtronic© circuit, were primed using perfusate then connected to the cannulas and the Medtronic© console. Once the lungs reached a temperature of 32°C, the ventilator was attached to the lungs with settings of PEEP of 5, Pinsp of 15, flow of 19 and O_2 of 21. Tidal volume and respiratory rate (breaths per minute) were determined by the ideal body weight (IBW) of the donor, then divided by 45% or 55% for left and right lungs respectively. Tidal volume and breaths per minute were slowly increased as the temperature of the lungs increased but did not exceed the minute volume or maximum perfusate flow rate as determined by the IBW. Regular blood gas measurements were taken

144

throughout perfusion, to ensure normal range of parameters. Physiology and ventilation settings were also recorded throughout perfusion.

1. Check Ideal body weight (IBW) as per formula and note maximum minute volume

	40	45	50	55	60	65	70	75	80	85	90	95	100
Donor Ideal Body Weight / kg	40	45	50	55	60	65	70	75	80	85	90	95	100
Maximum Minute Volume L/min	4	4.5	5	5.5	6	6.5	7	7.5	8	8.5	9	9.5	10
Maximum Perfusate Flow L/min	2.8	3.15	3.5	3.85	4.2	4.55	4.9	5.2	5.6	5.95	6.3	6.65	7

Note minute volume must not exceed 1.5X the perfusate flow

2. Dial tidal volume and respiratory rate to achieve the target minute volume and target V_T/kg for the appropriate donor IBW

If Donor IBW 60kg or greater increase minute volume by 1L/min for each degree from 32 to 37 degrees keeping Peak airway Pressure less than $20cmsH_2O$

If Donor IBW 59kg or less increase minute volume by 1L/min for each 2 degrees from 32 to 37 degrees keeping Peak Airway Pressure less than $20cmsH_2O$

Target Minute Volume	Breaths/min	40kg	45kg	50kg	55kg	60kg	65kg	70kg	75kg	80kg	85kg	90kg	95kg	100kg	Target V_T ml/kg
1L/min	5						200	200	200	200	200	200	200	200	
32°C	8	120	120	120	120	120									2-3 ml/kg
2L/min	8									300	300	300	300	300	
33°C	10			200	200	200	200	200							3-4 ml/kg
34°C	12	170	170	170	170										
3L/min	10					300	300	300	300	300	300	300	300	300	
34°C	12			250	250	250	250	250	250	250					3-5 ml/kg
36°C	15	200	200	200	200	200	200								
4L/min	10								400	400	400	400	400	400	
35°C	12				330	330	330	330	330	330	330	330	330	330	3-5 ml/kg
37°C	15	260	260	260	260	260	260	260	260	260	260				
5L/min	10	MAX	MAX							500	500	500	500	500	
36°C	12						420	420	420	420	420	420	420	420	4-6 ml/kg
37°C	15			330	330	330	330	330	330	330					
						MAX	MAX								
6L/min	10										600	600	600	600	
37°C	12							500	500	500	500	500	500	500	5-7 ml/kg
	15					400	400	400	400	400					
						MAX	MAX								
7L/min	12										580	580	580	580	
37°C	15						470	470	470	470					6-7 ml/kg
								MAX	MAX						
8L/min	12												670	670	
37°C	15									530	530	530	530		6-7 ml/kg
											MAX	MAX			

Figure 5-2 Tidal volume and respiratory rate based on ideal body weight (IBW).

The tidal volume and respiratory rate (breaths per minute) were calculated based off the IBW of the lung donor, these were gradually increased as the temperature of the lungs increased (Fisher et al., 2016).

5.2.1.4 Preparation and administration of hAECs and HTR cell line

Whilst the lungs were being connected to the EVLP rig and perfused stably for 30 minutes, 150×10^6 hAECs (pooled from 5 donors) and HTR cells were thawed rapidly at 37°C then spun at 300 g for 10 minutes. The CellTracker™ Red CMTPX Dye (Thermofisher, USA) was brought to room temperature then reconstituted to a stock concentration of 10 mM in DMSO then diluted for a working concentration of 25 μM in UltraCULTURE™ media. The cells were resuspended in the CMTPX dye working concentration and incubated at 37˚C for 30 minutes in the dark. The cells/dye mix was topped up with UltraCULTURE™ media then spun at 300 g for 10 minutes and finally resuspended in 50 mL of homemade Steen solution. The leukocyte filter on the Medtronic© circuit was clamped off prior to the administration

of the cells. For the initial optimising experiments, 25 million cells were administered every 10 minutes to ensure no changes in lung physiology. Post-optimisation, the cells were then infused via syringe slowly into each lung circuit through a 3-way tap, over 10 minutes. The lungs were then perfused for 2-4 hours post cell-administration.

5.2.2 Sample collection during EVLP

Perfusate samples and tissue biopsies were taken during the EVLP. 10 mL of perfusate was collected at sequential time points, then centrifuged at 1000 g for 10 minutes to remove cells and debris. The perfusate was then frozen at -80°C in 1 mL aliquots, for long term storage. 100 mL of perfusate from each circuit was collected post EVLP and kept at 4°C in the dark until flow cytometry was performed.
Tissue biopsies were collected pre and post EVLP using Proximate™ linear tissue cutter (Ethicon Inc, USA) to maintain patency of the lung and placed in RNAlater™ Stabilization Solution (ThermoFisher Scientific) or 10% neutral buffered formalin (Cell pathologies, UK). RNAlater™ samples were stored at 4°C for 24 hours then frozen at -80°C for long term storage. Formalin biopsies were left to fix for 24-48 hours before being processed by the Cellular Pathology Node at the RVI, Newcastle Upon Tyne Hospitals, into paraffin embedded blocks. Post perfusion tissue biopsies were also fixed in 4% paraformaldehyde (PFA) for 24 hours at 4°C, then transferred to PBS with 0.1% sodium azide and stored at 4°C until further processing.

5.2.3 Flow cytometry

Flow cytometry was performed on the 100 mL post-perfusate samples taken from each circuit to track the number of HTR and hAECs in the perfusate. The perfusate samples from each circuit were spun at 350 g for 10 minutes then resuspended in 50 mL of FACS buffer (PBS with 2% FBS). 500 μL of each sample was taken and further diluted 1:2 with FACS buffer, then 50 μL of CountBright™ Absolute counting beads (Thermofisher Scientific) was added. In a separate FACS tube, 500 μL of each sample was taken and stained with 25 μL CD11b-FITC (Themofisher Scientific), for 30 minutes, in the dark on ice. This stained sample was washed twice in FACS buffer then all samples were run on the BD LSRFortessa™ X-20 (BD biosceinces, USA). FlowJo software was used to gate and analyse the data. Cell concentration was

determined using the following calculation, then adjusted for dilutions made to the perfusate samples:

$$\frac{number\ of\ cell\ events}{number\ of\ bead\ events} \times \frac{number\ of\ beads\ added}{volume\ of\ sample}$$

5.2.4 ELISA on perfusate samples

Perfusate samples were collected during EVLP for downstream ELISA. For the cell optimisation studies, perfusate samples were collected at pre, 15, 25, 35, 45, 55, 65, 90 and 120 minutes relative to when the lungs were attached to the circuit. CX CL8 and TNFα ELISA was performed on each sample as described in chapter 2.6. The post-optimisation perfusate samples were collected pre perfusion, at the time of cell administration and then hourly. CXCL8, TNFα, IL-6 and IL-10 ELISAs were then performed on these perfusate samples as described in chapter 2.6. The final concentration of each sample was then adjusted to donor predicted total lung capacity (TLC). This was calculated based on the donors gender and height (Stocks & Quanjer, 1995) and adjusted to according to the weight of each lung.

5.2.5 Real time PCR on lung tissue biopsies

Lung tissue samples collected pre and post EVLP were stored in RNAlater for 24 hours at 4°C, then transferred to -80°C until RNA extraction was performed. RNA isolation was performed as described in chapter 2.4.1 with 20 mg of tissue using the RNeasy® Mini kit (Qiagen). 1000 ng of isolated RNA was then used to synthesis cDNA as described in chapter 2.4.2. Finally real time qPCR was carried out, as described in chapter 2.4.3, using TaqMan® primers for CXCL8, TNFα, IL-10 and IL-6. The housekeeping gene was briefly optimised using primers for GAPDH, HPRT-1, RPLP0, β-actin and 18S (Figure 5-3). RPLP0 and GAPDH both showed stability with a difference of 0.17 and 0.19 in cycle threshold (CT) values between pre and post tissue biopsies respectively. Therefore, RPLP0 was used as the housekeeping gene.
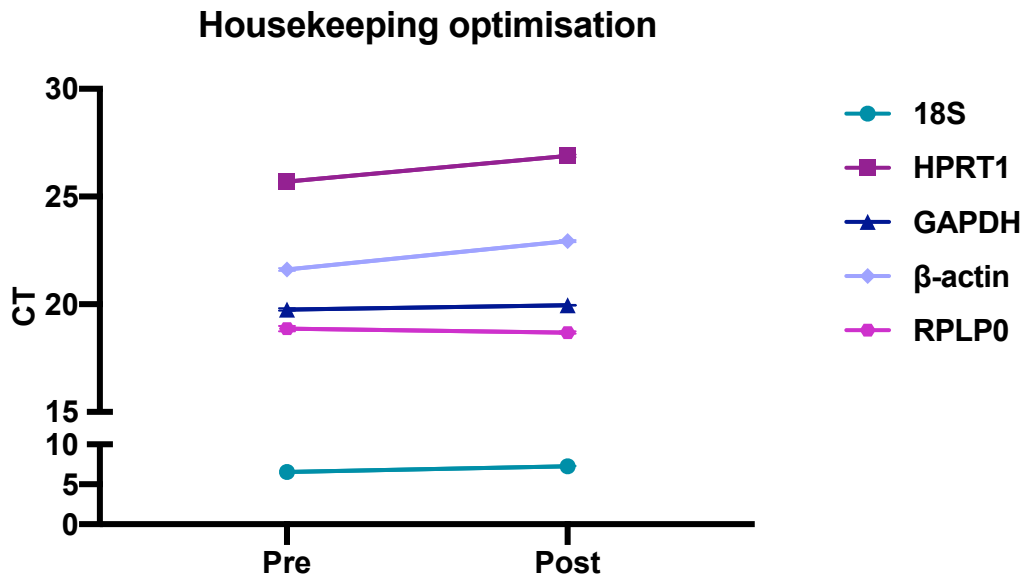
Figure 5-3 Optimising the housekeeping gene to be used to evaluate pre and post EVLP tissue.

RNA was extracted from untreated pre and post EVLP tissue and subsequently converted to cDNA. Housekeeping genes 18S, HPRT-1, GAPDH, β-actin and RPLP0 were evaluated for use.

5.2.6 Histology on lung tissue

Tissue samples collected pre and post EVLP for each lung were fixed with 10% formalin before being embedded in paraffin and then used to carry out H&E staining and immunofluorescence for markers CXCL8 and 3-nitrotryosine (3-NT). Post-EVLP samples fixed in 4% PFA were used to carry out multiphoton imaging for cell tracking.

5.2.6.1 H&E on lung vasculature

Paraffin embedded lung tissue was cut at a thickness of 4 μm on to Superfrost Plus™ slides (ThermoFisher Scientific). H&E staining was then performed as described in chapter 2.3.2. Imaging of the tissue was carried out using an Olympus upright Microscope with the CellSense software.

5.2.6.2 Immunofluorescence staining

Antibody concentrations and antigen retrieval used to carry out immunofluorescence (IF) on the lung tissue was optimised by Mr Chong Yun Pang. Paraffin embedded lung tissue was cut at a thickness of 4 μm on to Superfrost Plus™ slides. IF staining was performed as described in chapter 2.3.2, using CXCL8 and 3-NT primary

antibodies and AlexaFluor488 and Dylight650 secondary antibodies. Imaging was carried out using the Zeiss AxioImager (Zeiss, Germany).

5.2.6.3 Multiphoton imaging

Prior to fixation with 4% PFA, a small section of post-EVLP lung tissue was flushed with 2.5 mg/mL 3,3'-Dioctadecyloxacarbocyanine Perchlorate (DiO) Dye (ThermoFisher Scientific) through the artery to dye the vasculature. Once the lung tissue was fixed, two-photon imaging was performed, which allows for deeper visualisation of tissue than conventional confocal microscopy, with a maximum penetration depth of 1 mm, enabling 3D visualisation of the tissue. This involves two photons combining their energy during excitation of the fluorophore to allow for low-energy infrared photons, which penetrates tissue more deeply. Multiphoton imaging was carried out using the Zeiss LSM800 NLO Multiphoton microscope with Airyscan detector. This work was carried out in collaboration with Dr Glyn Nelson from the Newcastle University Bioimaging Unit.

5.3 Results

5.3.1 Donor and perfusion information

The lungs used in this study were declined by all UK centres for clinical lung transplantation, largely due to poor function or smoking history, then consented to research prior to retrieval. Five donor lungs were used as part of this study, two for cell administration optimisations and three to assess hAECs as a therapeutic, with the HTR cell line used as a control (Table 5-1). Unintentionally, the donors were mostly female, with just one male donor and all were DBD donors. Additionally, all donors had an extensive smoking history. Bi-lateral consolidation in the lower lobes was observed on the chest x ray for donors 1 and 2. Donor 3, upon visual inspection by the cardiothoracic retrieval team was found to also have consolidation in the lower lobes (Table 5-1). The PaO_2 at 100% FiO_2 varied from 15.16 - 70.02 kPa between donors. The lungs were split for each donor and then underwent EVLP with either the HTR-8/SVneo cell line or hAECs (Table 5-2).

Donor	Age	Sex	Bodyweight (kg)	Height (cm)	Donation type	Smoker (Y/N)	Reason for decline	Consolidation observed
1	36	Female	60	170	DBD	Y	Function	Y
2	59	Female	51	159	DBD	Y	Smoking history/function	Y
3	54	Female	65	157	DBD	Y	Function/ Inspection	Y
4	50	Female	88	166	DBD	Y	Smoking history	N
5	48	Male	70	181	DBD	Y	Smoking history/drug abuse/cause of death	N

Table 5-1 Donor information about lungs used in this study.

Donors 1 and 2 were used for cell administration optimisation studies and donors 3-5 were used to compare hAECs vs HTR cells. Y/N – Yes/No; DBD – donation after brainstem death.

Donor		Cells administered	CIT (hours)	EVLP duration (mins)	Weight pre (g)	Weight post (g)
1	**Right**	HTR cell line	15	120	1076	1251
	Left	Untreated			425.5	692.5
2	**Right**	hAECs	11	120	349.5	788.5
	Left	Untreated			391.5	995.5
3	**Right**	hAECs	15	180	383	1574.5
	Left	HTR cell line			363	1328.8
4	**Right**	hAECs	5	240	517.5	1880
	Left	HTR cell line			481	1317
5	**Right**	hAECs	3	120	380.9	1984
	Left	HTR cell line			333.5	2595

Table 5-2 Perfusion information for each donor used in this study.

Each lung was split, and cells were administered randomly to each lung as listed above. EVLP duration was determined post cell administration. CIT – cold ischemic time.

5.3.2 Optimising cell administration during EVLP

Firstly, we aimed to determine whether administering cells to the lungs would be tolerated or instead lead to any adverse physiological or biological changes. This could include a blockage of the capillaries, oedema, or an adverse cytokine production upon administration of the cells to the perfusate. Following from the studies by Mordant *et al* and Martens *et al,* who administered 150×10^6 umbilical cord derived MSCs and MAPCs respectively to achieve therapeutic benefit, therefore we started by administering 150×10^6 to determine any therapeutic benefit of hAECs (Mordant et al., 2016; Martens et al., 2017). Mordant *et al,* also found intravascular delivery through the pulmonary artery led to more retention of MSCs compared to intrabronchial administration (Mordant et al., 2016). Therefore, we proceeded to also administer the cells through the perfusate via the pulmonary artery. The HTR-8/SVneo cell line is a trophoblastic cell line derived from the chorionic villi of the human placenta. These cells possess no anti-inflammatory or inflammatory properties observed in our previous *in vitro* studies and due to also being derived from the placenta, we deemed these a suitable cell control to administer to the lungs.

Firstly, we started by investigating whether the HTR cell line would be tolerated by the lungs by administering 150×10^6 cells to a single lung. Cells were administered slowly over 60 minutes, with 25×10^6 cells being administered to the perfusate every 10 minutes. This was done in order to closely monitor any changes that occur upon every administration, insuring that introducing more cells into the lung vasculature would be tolerated at every step. No adverse changes were seen in the PAP upon administration of the HTR cells over the 60 minutes, furthermore no dramatic decrease in flow rate of the perfusate was observed upon administration (Figure 5-4). Weight gain pre and post perfusion of each lung was not significantly different between the untreated or HTR cell treated lungs. This indicates no adverse changes were occurring in PA pressure despite this being the route of administration, blockages leading to changes in flow rate or large weight gains observed which would indicate oedema formation upon treatment with the HTR cells.

Following on from this, we repeated this experiment but instead using 150×10^6 hAECs administered slowly over 60 minutes (Figure 5-5). Similarly, we also did not observe any substantial changes in PAP or flow rate. A peak in flow rate was observed between 10 and 20 minutes but this was not during a 10-minute

administration timepoint so unlikely to be caused by the hAECs but more likely due to a change within the rig itself. Although a larger weight gain was observed, this was no more than the untreated lungs and so does not indicate that the cells were leading to oedema formation.

To determine any adverse pro-inflammatory cytokine production that may occur upon initial administration of the HTR cell line or hAECs indicating a lack of tolerance by the lungs, TNFα and CXCL8 concentrations were measured in the perfusate (Figure 5-6). As discussed previously, TNFα and CXCL8 are key biomarkers to successful EVLP and lung transplant success respectively and were therefore chosen as good indicators of determining successful tolerance of the cells during EVLP. For both the HTR cell line and the hAECs, TNFα concentration was no higher than the untreated lungs. In fact, upon administration of the hAECs, the TNFα concentration was initially observed to be higher in that lung than the untreated lung but then showed limited increase in concentration in the perfusate in comparison to the untreated lung, which continued to increase. This was also observed with the CXCL8 concentration in the perfusate. The HTR cells did observe an increase in CXCL8 gradually over time but this was also observed with the untreated control lungs.

There were no significant concerns observed in physiology or TNFα and CXCL8 concentration, therefore it appeared the dose of 150 x 10^6 HTR cells or hAECs administered to the perfusate through the pulmonary artery is tolerated by a single lung.
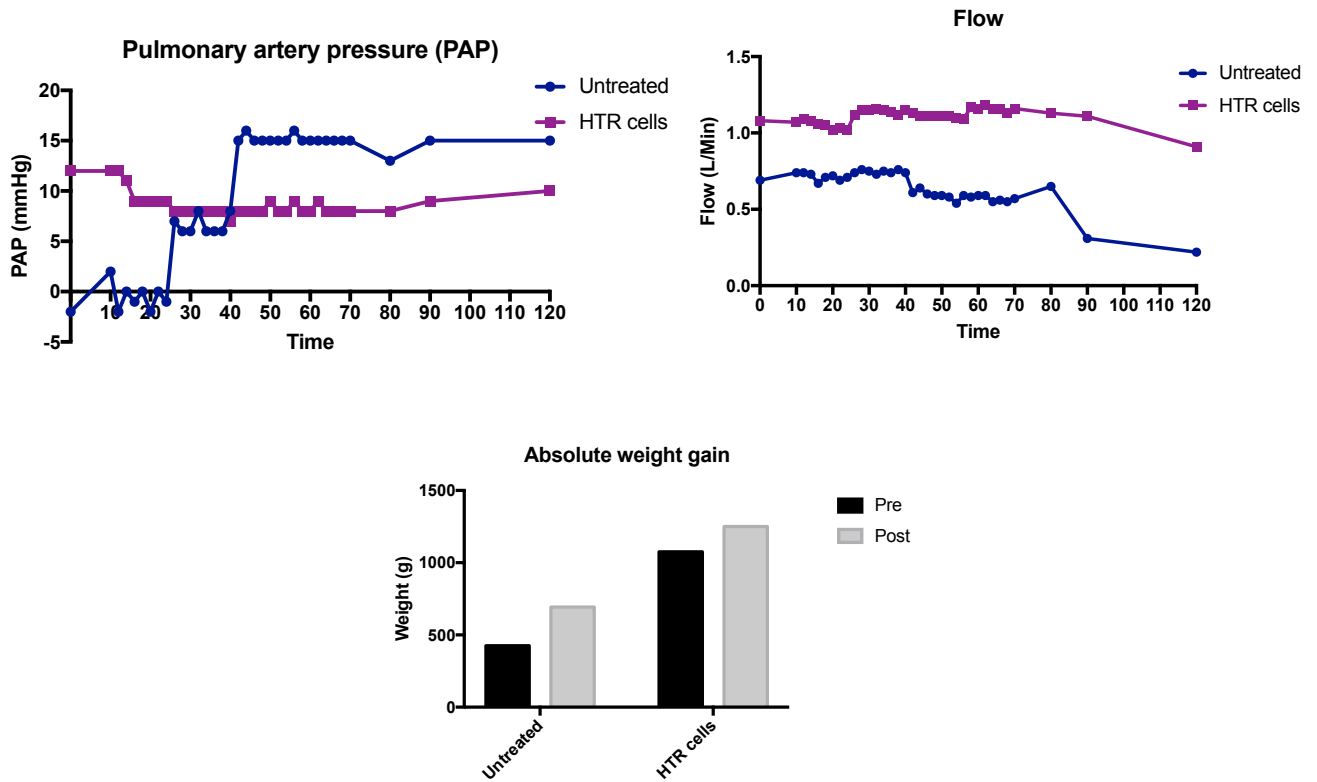
Figure 5-4 Physiological changes observed during the administration of the HTR-8/SVneo cell line during EVLP.

To determine whether a dose of 150 x 10^6 HTR cells would be tolerated by a single lung during EVLP, 25 x 10^6 cells were added every 10-minutes slowly over a 60-minute time-period to the perfusate entering the lungs through the pulmonary artery. Pulmonary artery pressure (PAP) and flow rate of the perfusate was closely monitored for the hour of administration and the hour following. Absolute weight gain was also measured to determine any potential oedema formation. N=1.
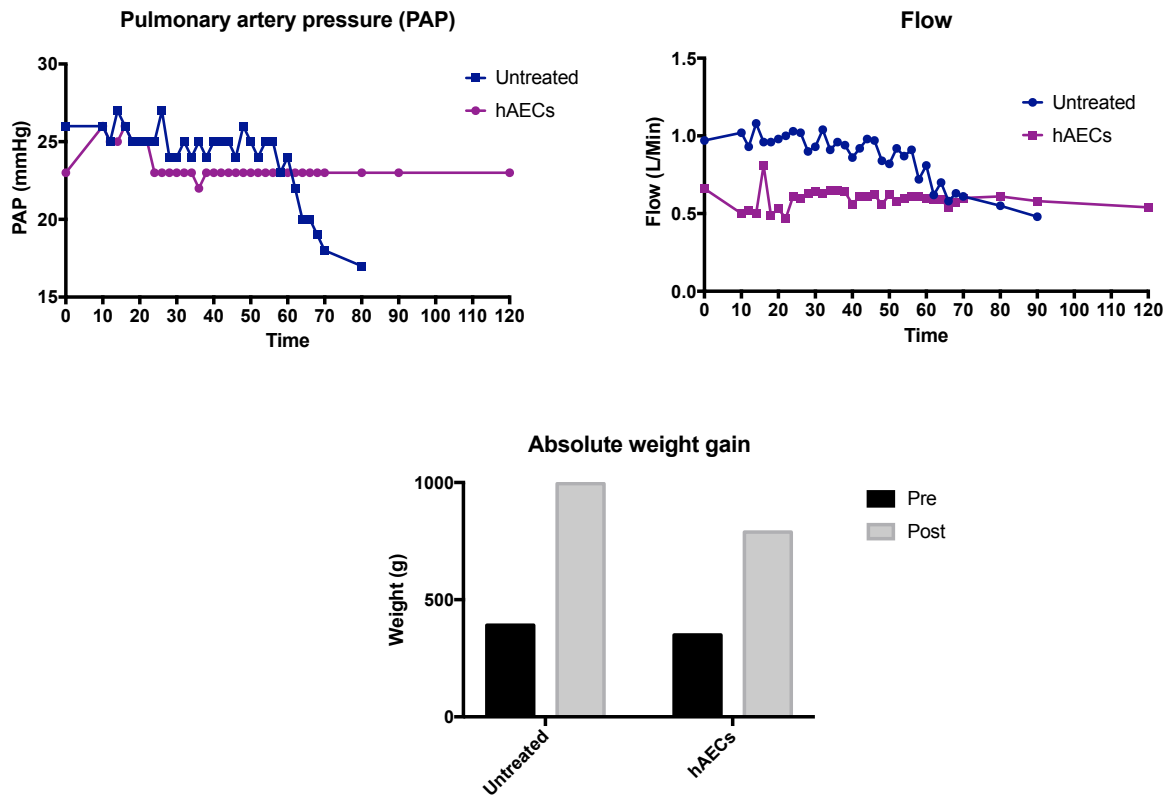
Figure 5-5 Physiological changes observed during the administration of hAECs during EVLP.

To determine whether a dose of 150×10^6 hAECs would be tolerated by a single lung during EVLP, 25×10^6 cells were administered every 10-minutes slowly to the perfusate over a 60-minute time-period, entering the lung through the pulmonary artery. Pulmonary artery pressure (PAP) and flow rate were measured closely for 2 hours Weight of the lungs was measured pre and post perfusion to determine the absolute weight gain. N=1.
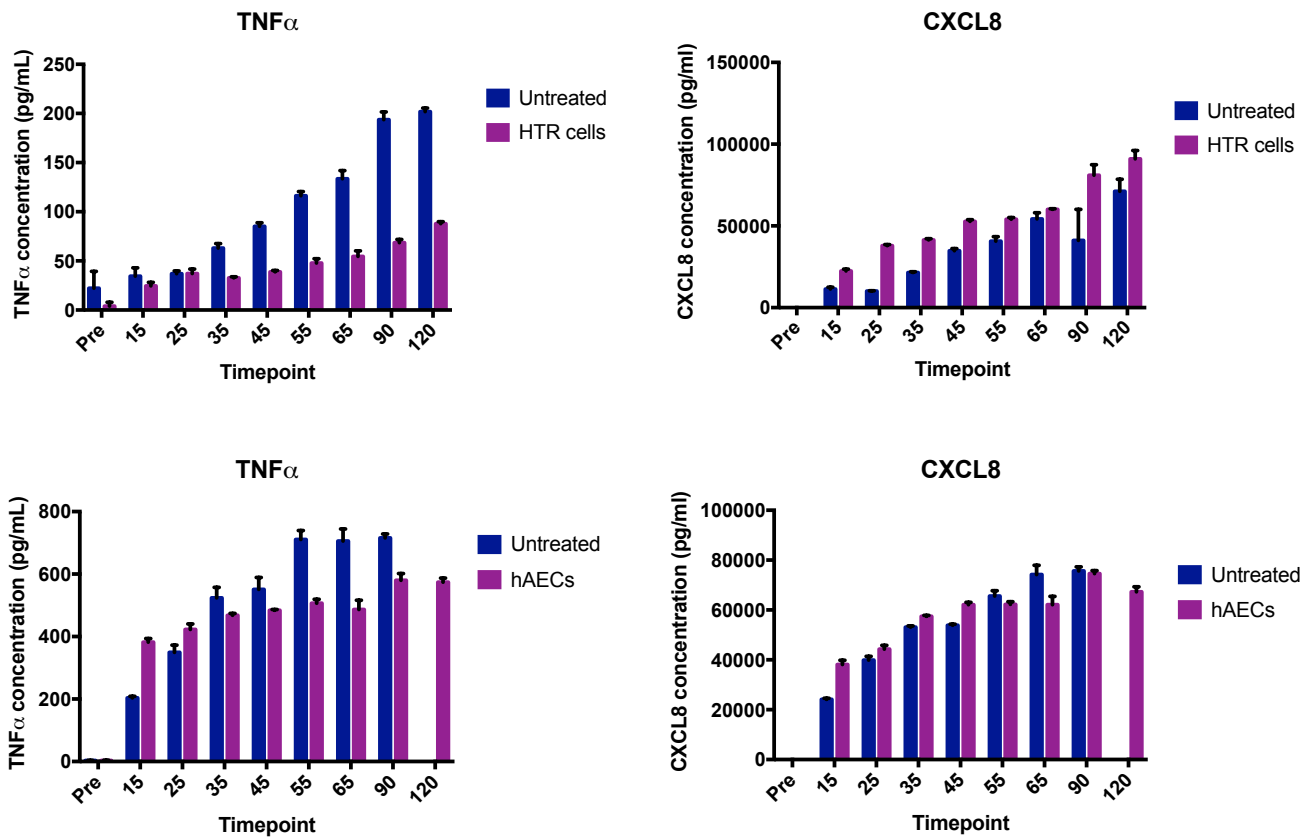
Figure 5-6 TNFα and CXCL8 concentration in the perfusate measured during the optimisation of cell administration during EVLP.

Any significant changes in TNFα and CXCL8 in the perfusate were quantified through ELISA and used to determine the tolerance of cell administration into a single lung. Due to the untreated lung significantly deteriorating during the optimising hAEC administration experiment, a final perfusate at 120 minutes could not be collected. Final concentration values were adjusted to total lung capacity (TLC) for each lung (pg/mL). N=1 for each cell administration.

5.3.3 Physiological parameters during hAEC-treated lungs

A split lung model was used to determine the therapeutic benefits of hAECs during EVLP. 150×10^6 HTR cells, or hAECs, were manually administered to each single lung slowly over 10 minutes, to try to prevent blockage of the capillaries. Physiological parameters were measured throughout perfusion, although this was not believed to be the main therapeutic mechanism behind hAECs. The weight of the lungs was measured pre and post EVLP for both lungs (Figure 5-7). For both the HTR cell line and hAEC treated lungs an increase in weight was observed post perfusion. However, the percentage weight gain increase during perfusion was not significant between the hAECs or HTR cell treatments, suggesting the hAECs do not prevent perfusate accumulation in the lungs. This could suggest oedema formation, which weight gain can indicate, was still occurring despite hAEC treatment. PAP and flow rate of the perfusate through the lungs remained steadier in the hAEC treated lungs, this was more variable in the HTR treated lungs (Figure 5-8).

Blood gases were measured throughout on the perfusate to evaluate any changes in pH, lactate formation and gas exchange. pH decreased and lactate steadily increased throughout perfusion for all lungs despite treatment (Figure 5-9). PaO_2 appeared to increase for the hAEC treated lungs and $PaCO_2$ did appear to be lower for all hAEC treated lungs, compared to the HTR treated lungs. This could indicate that hAEC treatment could be leading to lung function improvement through better gas exchange within the lungs.
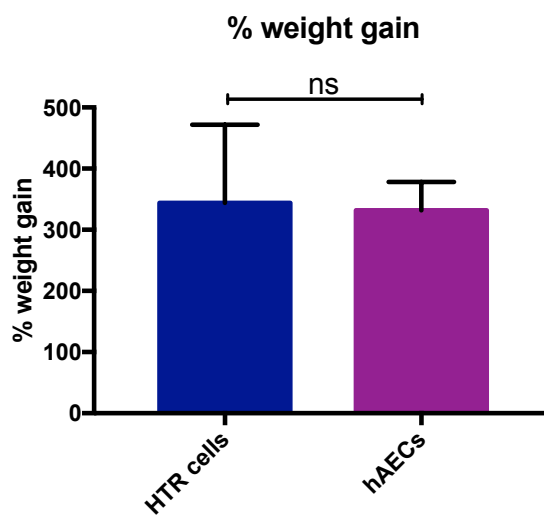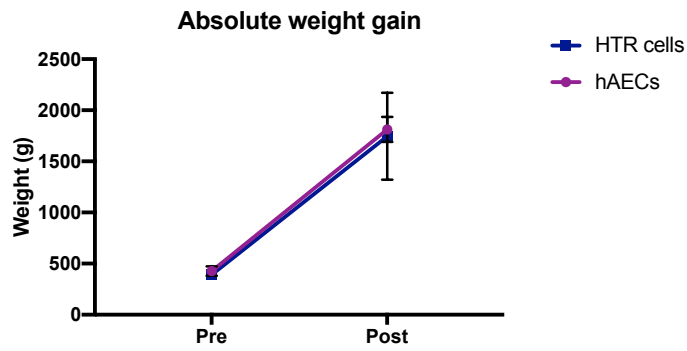
Figure 5-7 Weight gain of lungs during EVLP after treatment with hAECs or the HTR/SVneo-8 cell line.

Each single lung was weighed pre and post EVLP. An increase in absolute weight gain was observed for both treatments post-EVLP. Percentage (%) weight gain increase was not significant between the HTR or hAEC treatments. Statistical significance was determined using a paired T-Test. N=3.
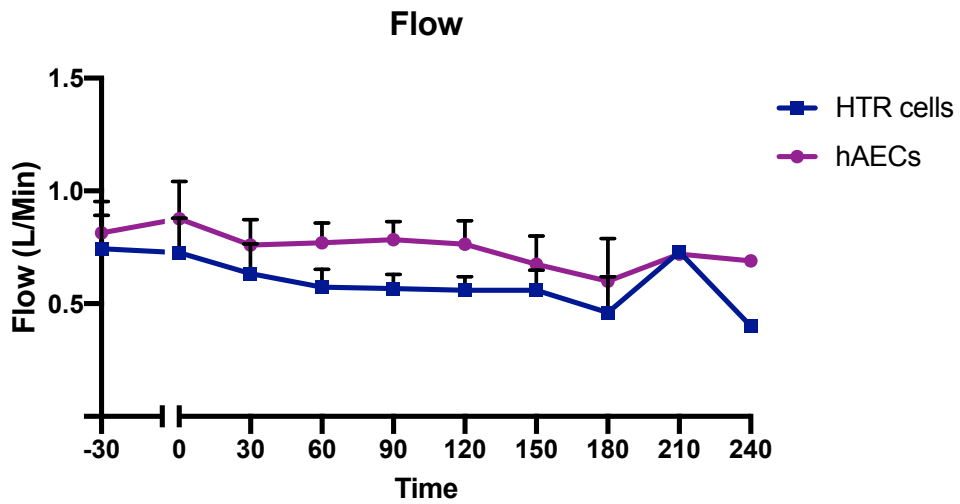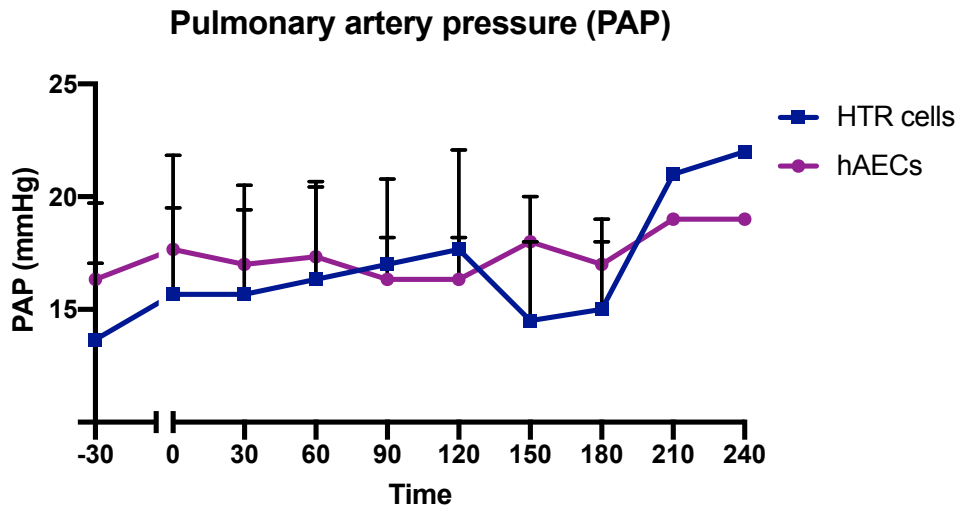
Figure 5-8 Pulmonary artery pressure and perfusate flow rate of lungs during EVLP.

HTR cells or hAECs were administered to the perfusate slowly over 10 minutes, entering the lungs through the pulmonary artery. Pulmonary artery pressure (PAP) and flow rate of the perfusate were monitored every 30 minutes. N=3.
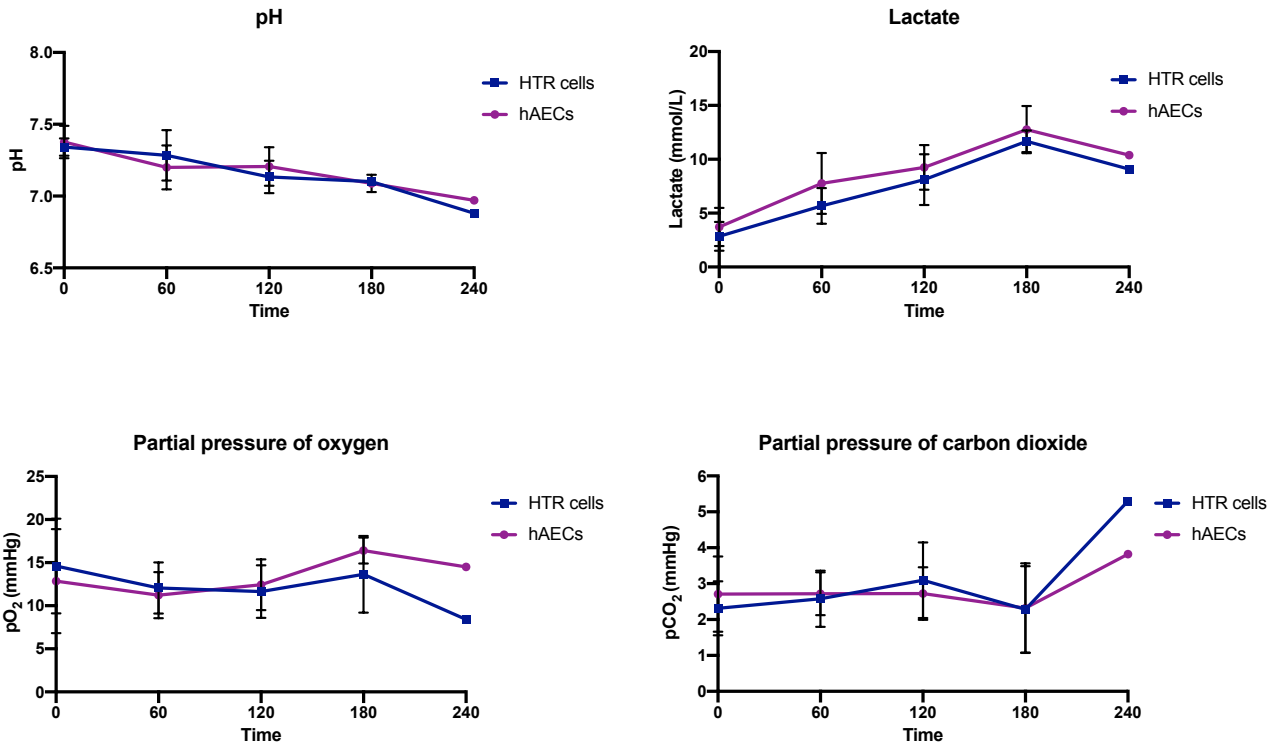
Figure 5-9 Blood gases measured in the perfusate during EVLP.

Blood gases were taken every hour from the perfusate during EVLP for each lung, measuring pH, lactate levels, Partial pressure of oxygen (PaO_2) and Partial pressure of carbon dioxide ($PaCO_2$). N=3.

5.3.4 Protein analysis of perfusates from hAEC-treated lungs

Perfusate samples were collected from each lung every hour during EVLP. An ELISA for the markers TNFα, CXCL8, IL-6 and IL-10 was carried out to determine any preliminary immunomodulatory effects that may be occurring from hAEC treatment. Figure 5-10, plots the concentration of these markers over time of perfusion, demonstrating a reduction in TNFα, CXCL8 and IL-6 concentration with hAEC treatment. IL-10 concentrations appeared to be lower throughout perfusion apart from the T240 timepoint. However, limited conclusions can be drawn from this data as not all donor lungs were able to be perfused for the full 240 minutes. Therefore, the T120 timepoint was plotted, as all donor lungs perfused for 120 minutes (Figure 5-11). TNFα concentration was observably lower in the hAEC-treated lungs demonstrated by the lack of significance to the T0 timepoint (p= 0.0549) unlike the HTR cells which were significantly higher than the T0 timepoint (p= 0.0448). CXCL8 concentration was marginally decreased in the hAEC treated lungs compared to the HTR cell treated lungs although not significant. The hAEC treated lungs at T120 had significantly increased CXCL8 concentration compared to the paired T0 timepoint (p= 0.0052), but this was also observed with the HTR cells (p= 0.0043). Overall, IL-10 concentration appeared to be lower in the hAEC treated lungs, compared to the HTR treated lungs at 120 minutes. Similarly, to CXCL8 concentration, IL-6 concentration at 120 minutes was marginally decreased upon hAEC treatment, but both treatments observed an upregulation in IL-6 production after 120 minutes of perfusion (p= 0.0410, p= 0.0422).

When samples were plotted post-EVLP for each lung, compared to T0 at the start of perfusion, differences in the CXCL8, IL-6 and IL-10 concentrations became more apparent (Figure 5-12). TNFα concentration was still observably lower in the post EVLP perfusate collected from the hAEC treated lungs. CXCL8 concentration was decreased in the hAEC treated lungs and showed reduced significance to the T0 timepoint, compared to the HTR cell line treated lungs (p=0.0159 and p=0.0046 respectively). IL-10 concentration was observably increased in hAEC treated lungs, although not significant. Finally, IL-6 concentration was decreased in the hAEC treated lungs compared to the HTR treated lungs. Both hAECs and the HTR cell treated lungs showed increased IL-6 concentration in the perfusates post perfusion

161

compared to T0, however this neared significance for the HTR cells (p=0.0711) unlike the hAEC treated lungs (p=0.2430).
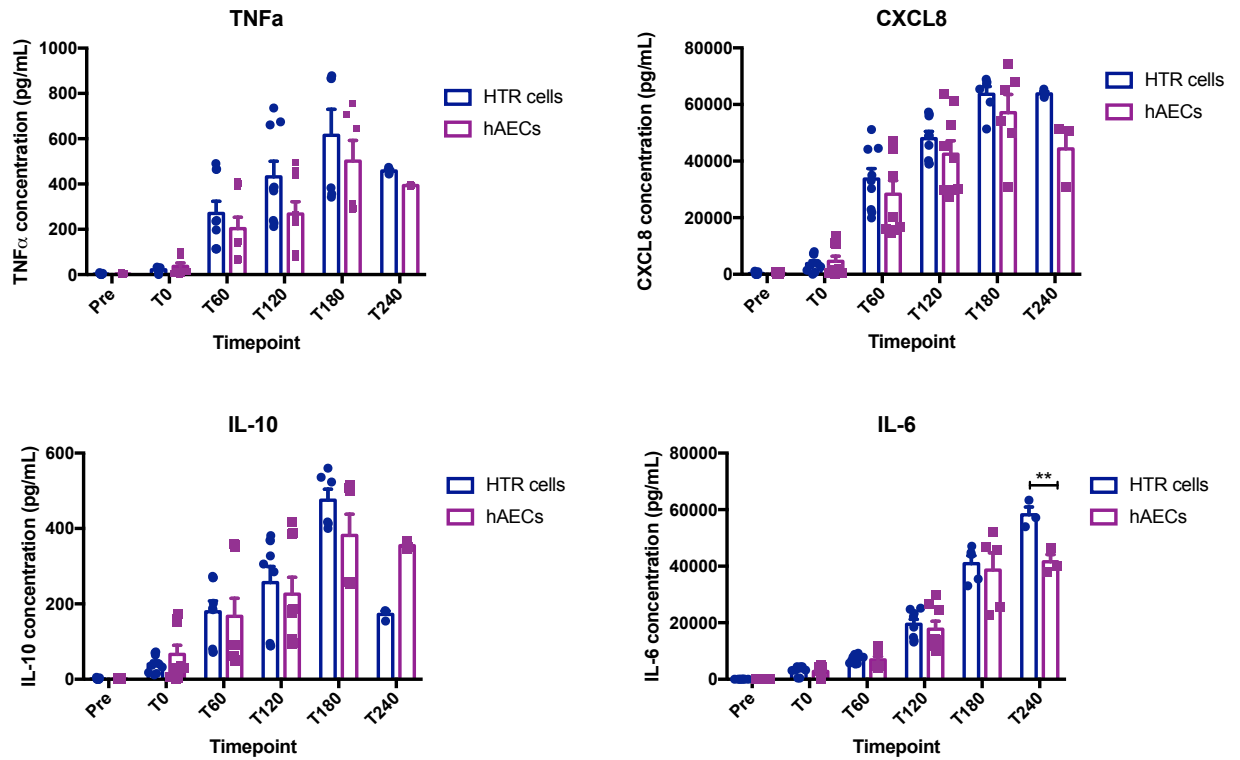
Figure 5-10 Concentration of TNFα, CXCL8, IL-10 and IL-6 during EVLP in hAEC or HTR cell treated lungs.

Perfusate samples were collected from each lung every hour during perfusion. TNFα, CXCL8, IL-10 and IL-6 concentration were determined through ELISA to determine any change in expression over time upon treatment with hAECS. IL-6 concentration was significantly reduced after 240 minutes (p=0.0075), however limited conclusions can be drawn compared to the other timepoints, as only one donor reached this timepoint. Final concentrations were corrected for TLC for each lung (pg/mL). Statistical significance was determined by a Two-way ANOVA. N=3. **
p<0.01
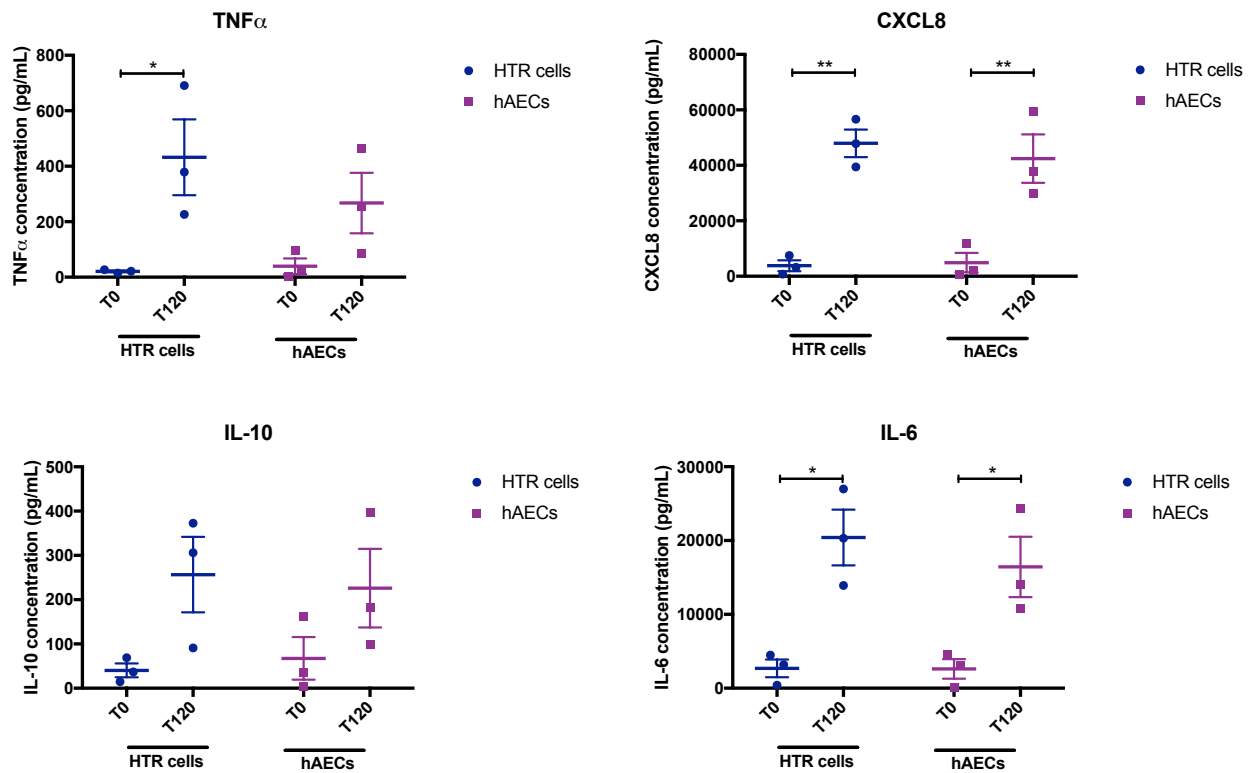
Figure 5-11 Concentration of TNFα, CXCL8, IL-10 and IL-6 at 120 minutes during EVLP.

Perfusate samples were collected just prior to administration of cells (T0) and 120 minutes during perfusion (T120) and concentration of TNFα, CXCL8, IL-10 and IL-6 were determined through ELISA. Final concentration values were adjusted to TLC for each lung (pg/mL). Statistical significance was determined through a two-way ANOVA. N=3. $*p<0.05$, $**$ $p<0.01$.

164
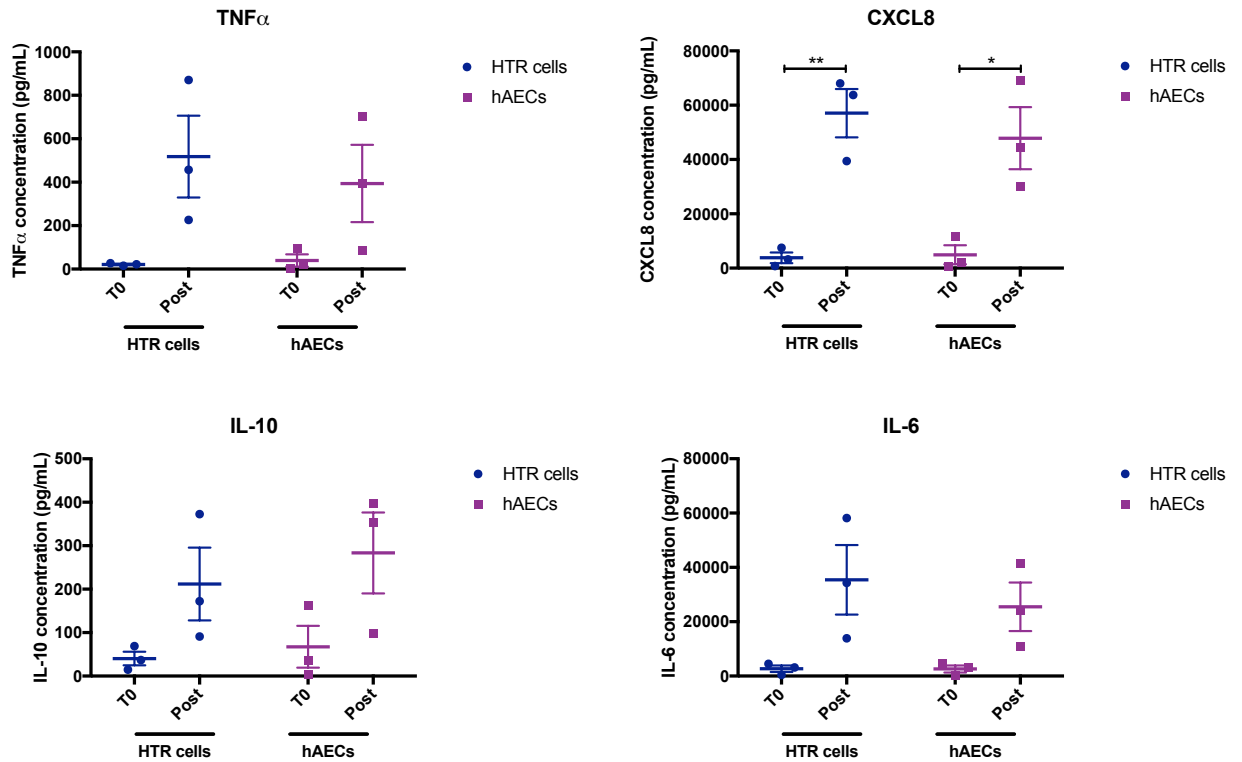
Figure 5-12 Concentration of TNFα, CXCL8, IL-10 and IL-6 pre-cell administration compared to post EVLP.

Perfusate samples were collected just prior to the administration of cells (T0) and post perfusion for the respective lung donor. Concentration of TNFα, CXCL8, IL-10 and IL-6 in the perfusates was then determined through ELISA. CXCL8 concentration increased post perfusion in the HTR cell treated lungs (p=0.0046) and the hAEC treated lungs (p=0.0159). Final concentrations were corrected for TLC for each lung (pg/mL). Statistical significance was determined by a Two-way ANOVA. N=3. ∗p<0.05, ∗∗ p<0.01.

5.3.5   Gene expression of pre- and post-EVLP lung tissue

Tissue biopsies were collected pre and post perfusion for each donor and stored in RNAlater until subsequent gene analysis. Gene expression of TNFα, CXCL8, IL-10 and IL-6 were determined in the tissue to reflect the concentrations examined in the perfusates (Figure 5-13). TNFα gene expression was significantly decreased in the hAEC treated lungs compared to the HTR treated lungs post perfusion (p=0.0415). For CXCL8, the gene expression was visibly reduced in the hAEC treated lungs compared to the HTR treated lungs, however this was not significant. Interestingly, IL-10 gene expression was markedly lower in the hAEC treated lungs compared to the HTR cell line treated lungs (p=0.2271). This could be explained by a more pro-inflammatory environment in the HTR cell line treated lungs, indicated by the increased CXCL8 and TNFα gene expression compared to the hAEC treated lungs, leading to the upregulation of the anti-inflammatory IL-10 response. IL-6 gene expression did not appear to decrease, however there appeared to be one donor that showed much higher expression compared to the other two donors and so may be an outlier limiting observations. Therefore, more repeats are needed to make a clear conclusion about IL-6 gene expression in hAEC treated lungs.
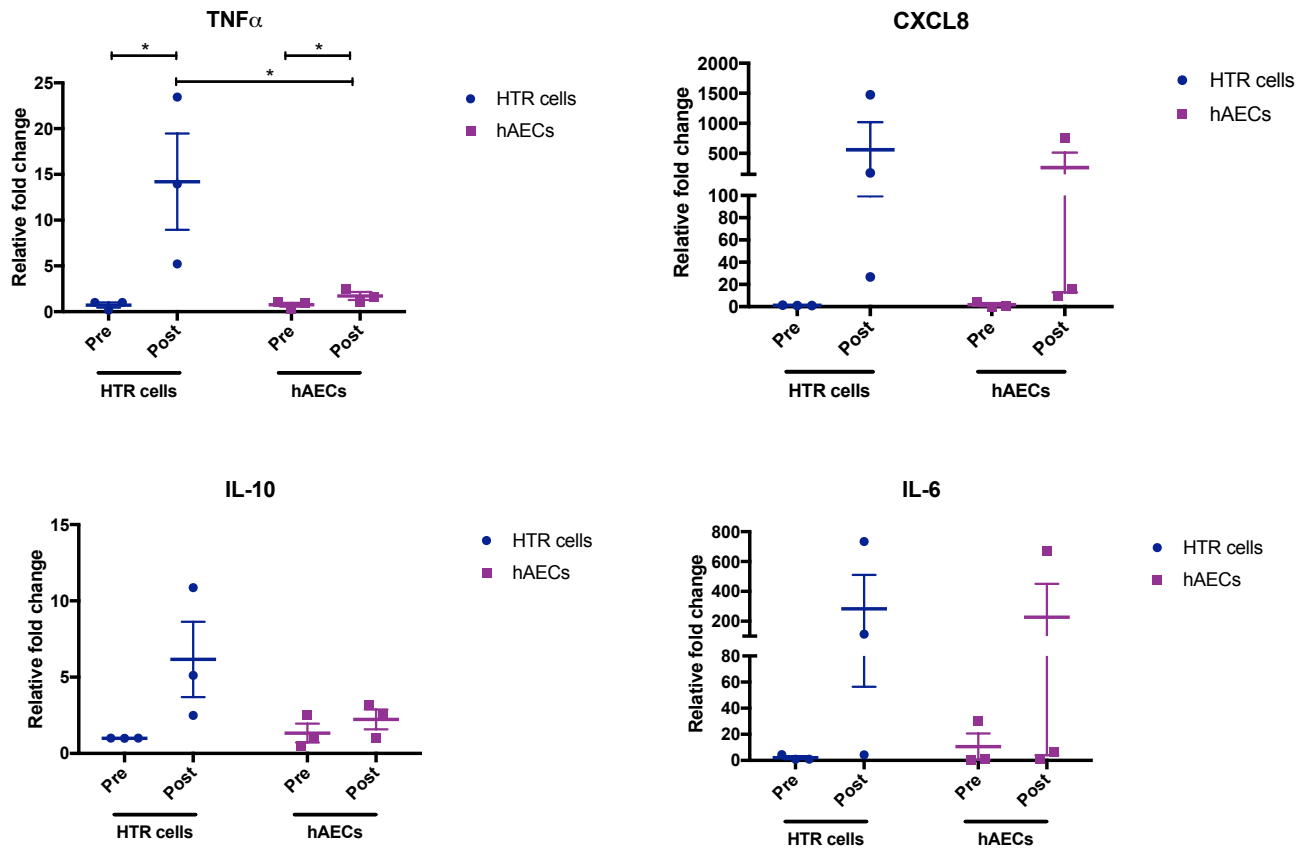
Figure 5-13 Gene expression in hAEC or HTR cell line treated lungs pre and post EVLP.

Lung biopsies were collected pre and post perfusion after hAEC or HTR cell line treatment for 4 hours and stored in RNAlater, then underwent real time PCR to determine TNFα, CXCL8, IL-10 and IL-6 gene expression. Statistical significance was determined by a two-way ANOVA. N=3. .∗p<0.05.

167

5.3.6 Immunofluorescence staining on lung tissue

Immunofluorescence was carried out on tissue collected pre and post EVLP for each lung that underwent hAEC or HTR cell treatment, for CXCL8 and 3-nitrotyrosine (3-NT). Dr Sarah Thompson showed as part of her PhD thesis that 3-NT can be widely expressed by the lungs, which is a marker for peroxynitrite a downstream product of the nitric oxide synthase pathway, an important pathway generating ROS in IRI. Furthermore, she demonstrated 3-NT and CXCL8 staining in lung tissue can show strong co-localisation, which, for our study, was useful for identifying if the lungs were undergoing oxidative stress and inflammation during EVLP with hAEC treatment. The immunofluorescence staining carried out using this lung tissue was done in collaboration with PhD student Mr Chong Yun Pang. In the tissue collected post EVLP, CXCL8 staining was much weaker in the hAEC treated lungs in comparison to the HTR cell treated lungs. Furthermore, there was very little 3-NT staining in the hAEC treated lungs, whereas this was much more highly expressed in the HTR cell treated lungs in comparison (Figure 5-14). The HTR cell treated lungs also showed clear co-localisation of CXCL8 and 3-NT. (Figure 5-14)
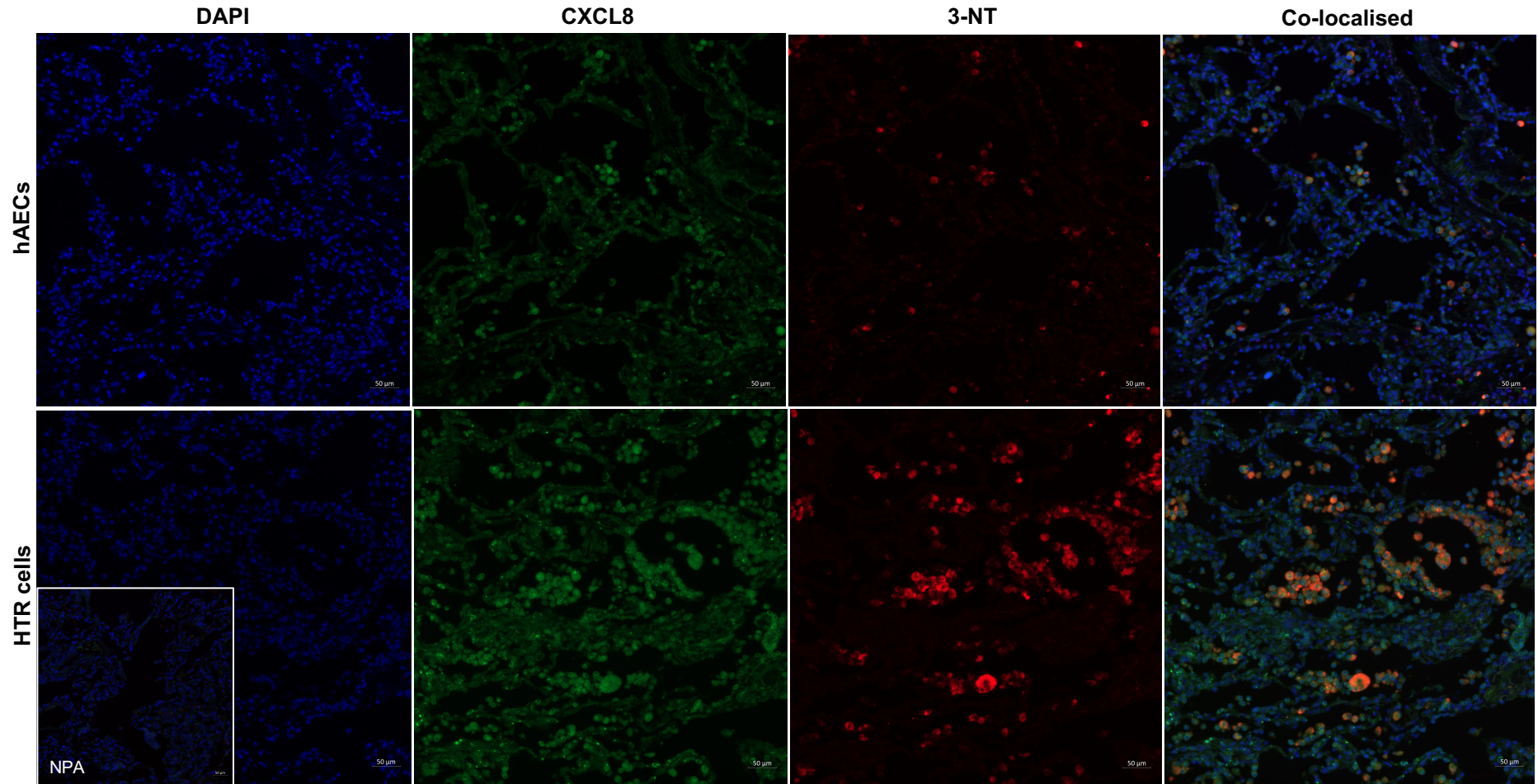
Figure 5-14 CXCL8 and 3-NT staining on hAEC and HTR cell treated lungs.

Immunofluorescent staining was carried out on lung tissue collected post-EVLP that underwent hAEC and HTR cell treatment for the markers CXCL8 and 3-nitrotyrosine (3-NT). Green = CXCL8, red = 3-NT, blue = DAPI. A no primary antibody control (NPA) on the lung was included. Scale: 50 µM. Three images were taken for each section. Representative of N=3

5.3.7 H&E staining of lung vasculatures

H&E staining was performed on lung tissue treated with hAECs or HTR cells, collected pre and post EVLP, to determine the pathology of the lung vasculature (Figure 5-15). Overall, the lung tissue to airspace ratio was improved in the post EVLP lung tissue, compared to the pre EVLP lung tissue. In donors 4 and 5, the lungs that were treated with the hAECs appeared to be less inflamed and more airspace to tissue ratio could be observed compared to the HTR treated. For both treatments, more cell infiltration was observed post EVLP compared to tissue collected pre EVLP. Some of the cell infiltrations, had macrophage morphology, suggesting macrophages are becoming activated during EVLP.
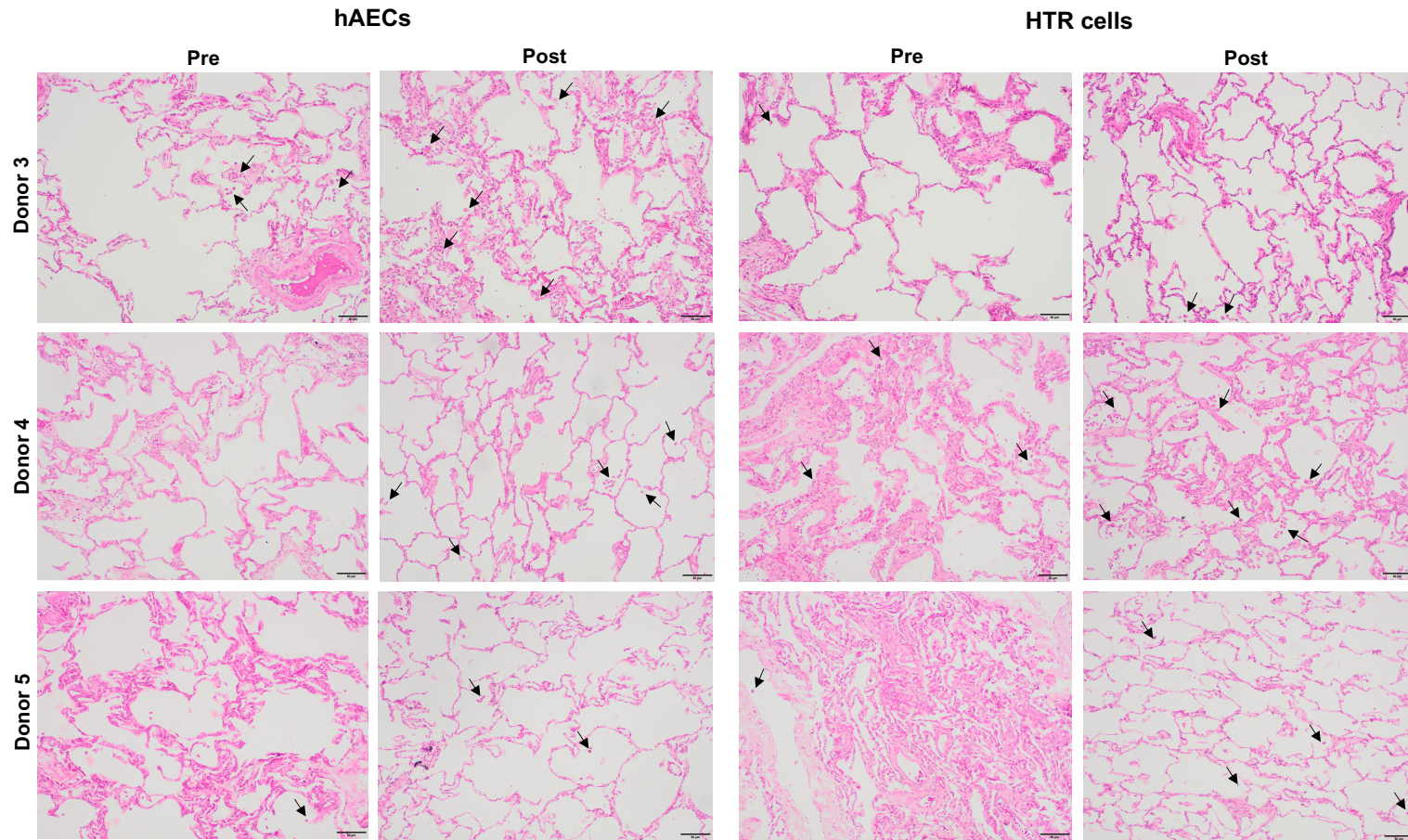
Figure 5-15 H&E staining on pre and post EVLP tissue.

Tissue for the 3 donors was collected pre and post EVLP for each lung that underwent hAEC or HTR cell treatment. H&E staining was carried out to reveal the vasculature. Cell infiltration in labelled with black arrows. Scale: 50μM (x10 magnification). N=3.

5.3.8 Cell tracking using flow cytometry on post-EVLP perfusates

In order to observe whether any cells could be detected in the perfusate, the cells were stained with CellTracker™ Red CMTPX Dye prior to perfusion then 100 mL of perfusate was collected at the end of perfusion and run on the LSRFortessa™ X-20. Quantification was determined using the CountBright™ Absolute counting beads. Cells in the perfusate were also stained for CD11b-FITC to determine if a granulocyte population was also being collected in the perfusate. CD11b population was gated on the 488/530-30 channel and percentage positive cell expression was plotted (Figure 5-16). CMTPX Red and the CountBright™ Absolute counting beads were gated on the 561/610-20 channel (Figure 5-16). The number of positive CMTPX Red cells were higher in the HTR cell line treated lungs compared to the hAEC treated lungs for each paired donor (p=0.0031), suggesting more hAECs could be engrafting into the lungs (Figure 5-17A). CD11b expression for the hAEC treated lungs appeared to be higher than the HTR treated lungs (Figure 5-17B).
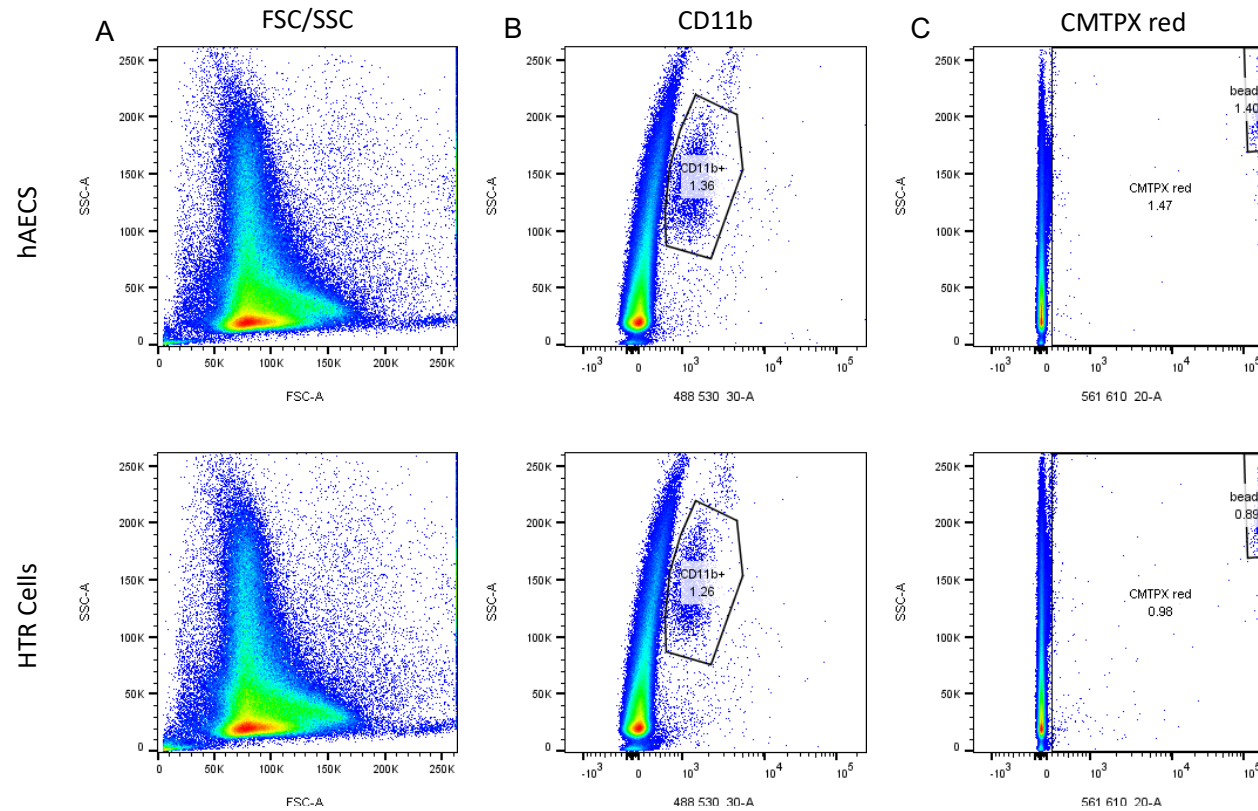
Figure 5-16 Flow cytometry plots for quantifying the number of hAECs and HTR cells and CD11b expression in the perfusate.

HTR cells and hAECs were stained with CellTracker™ Red CMTPX Dye prior to EVLP. 100 mL of perfusate was collected post EVLP, then run on the LSRFortessa™ X-20. (A) Forward scatter (FSC) vs side scatter (SSC) was plotted to demonstrate size and granularity of our perfusate samples for hAEC and HTR cell treated lungs. (B) CD11b-FITC positive population was gated against SSC for hAEC and HTR cell treated lung perfusates. (C) The CMTPX red positive population was gated against SSC and the distinct CountBright™ Absolute counting bead population were separately gated within to quantify the amount of CMTPX red staining.
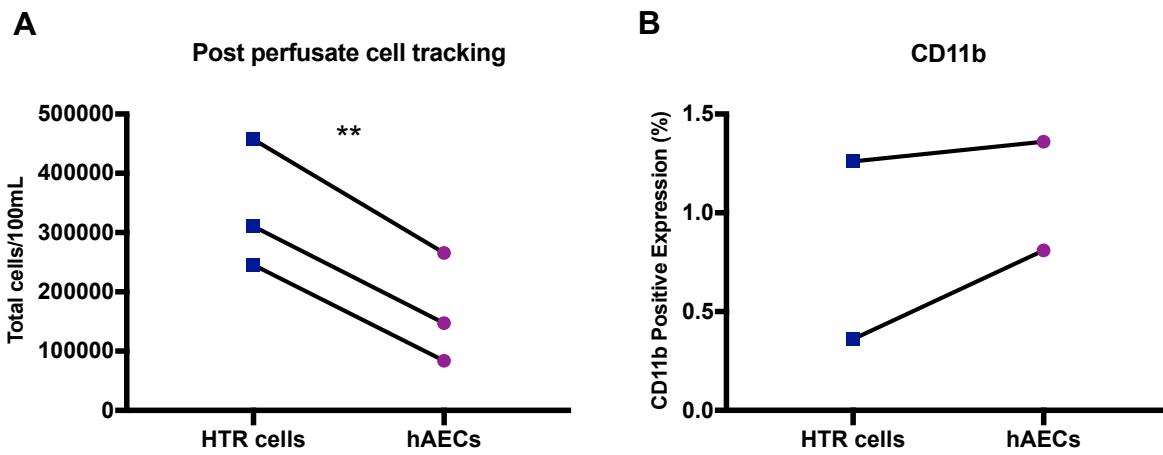
Figure 5-17 Number of labelled cells post EVLP and CD11b expression.

100 mL of perfusate was collected post-perfusion after hAEC or HTR cell treatment to each lung. (A) The number of HTR cells and hAECs labelled with CMTPX dye prior to perfusion, per 100 mL perfusate collected post EVLP, were quantified using the CountBright™ Absolute counting beads then adjusted according to dilutions. N=3. (B) CD11b positive expression was gated in two donor lung pairs treated with hAECs or HTR cells. N=2. Statistical significance was determined through a paired t- test. ∗∗ $p<0.01$.

5.3.9 Multiphoton microscopy for presence of cells

Post-EVLP lung tissue biopsies were flushed with DiO dye through the artery to dye the vasculature, prior to being fixed with 4% PFA. Two photon microscopy was then carried out on this tissue to locate any CellTracker™ Red CMTPX positive staining within the vasculature. Multiphoton imaging was carried out on lung tissue collected at 2 hours (120 minutes) and 4 hours (240 minutes). A "tilescan" was performed on the lung tissue, which involves taking 5 by 5 images on the surface of the tissue, then stitching these together to form one larger more comprehensive image (Figure 5-18). This revealed more hAECs with CMTPX positive staining were visible in the lung tissue collected from the lungs that underwent 4 hours of EVLP, compared to the 2 hours, suggesting that over time more hAECs infiltrated into the lung. Strong CMTPX red positive staining could be seen in all the samples, however this was larger in size than anticipated in some cases, suggesting the hAECs could be clumping together. Unfortunately, the DiO dye also appeared to bind to the cells when flushed through the lungs at the end of perfusion, demonstrated by the co-localisation of the two stains. A "Z-stack" was also performed on the lung tissue, which involves the microscope taking images whilst slicing down through the tissue, providing images within the tissue rather than just surface staining in the tilescan. Penetration into the tissue varies depending on the tissue thickness, for our study on average it varied from 100-200 slices. In the representative Z-stack which uses stronger magnification images, more of the lung vasculature is visible with the DiO Dye (Figure 5-19). Both the hAECs and the HTR cells appear to look like they're located in alveolar space within the vasculature. A "plane" image, a singular image taken at a stronger magnification and for a longer period of time, more clearly demonstrated the cells are homing into the lung parenchyma and particularly between the interstitium of the alveoli (Figure 5-20).
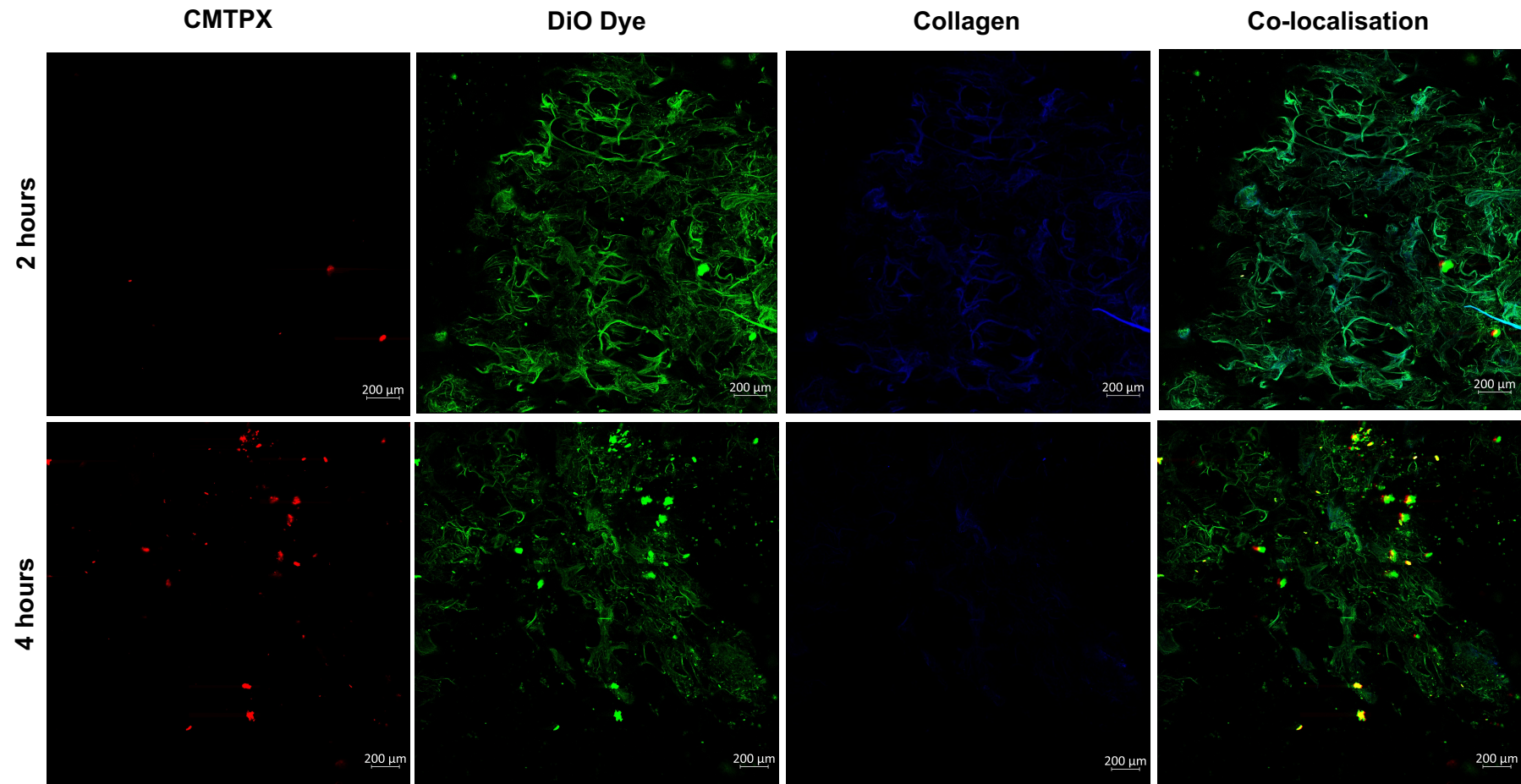
Figure 5-18 Multiphoton microscopy "tilescan" performed on lung tissue treated with hAECs for 2 and 4 hours.

Lung tissue taken from 2 and 4 hours post EVLP, were stained with 3,3'-Dioctadecyloxacarbocyanine Perchlorate (DiO) Dye to stain the vasculature. A tilescan was carried out, where 5 by 5 images were taken on the surface of the tissue and stitched together. This revealed that the CellTracker™ Red CMTPX red positive staining on the hAECs were penetrating the lungs. Scale: 200μM. N=2.

176
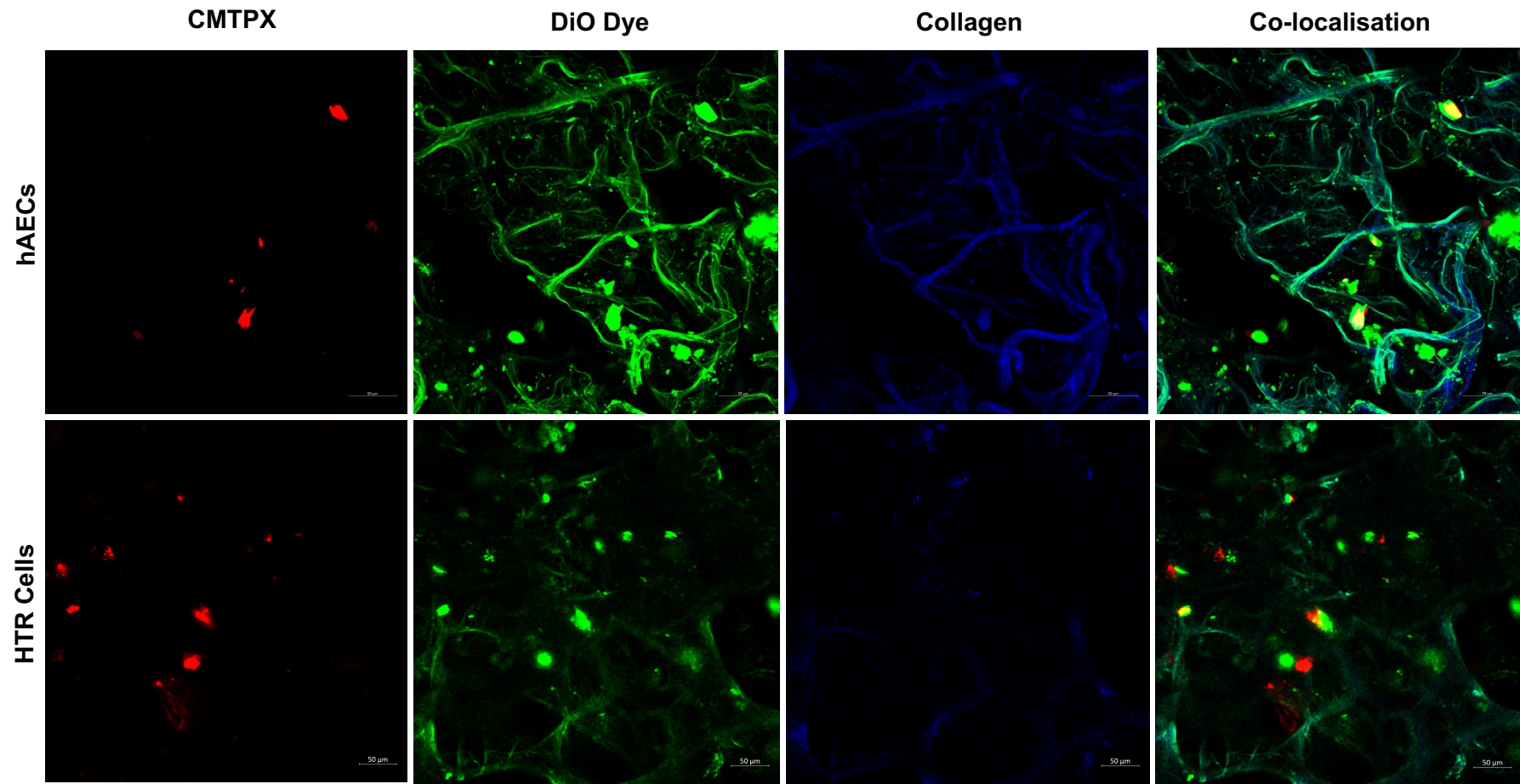
Figure 5-19 Multiphoton microscopy "Z stack" performed on lung tissue treated with hAECs or HTR cells.

Tissue from lungs that underwent EVLP with hAECs or HTR cells were stained with 3,3'-Dioctadecyloxacarbocyanine Perchlorate (DiO) Dye. A "Z-Stack" was used to penetrate the lung tissue. This shows that CellTracker™ Red CMTPX red positive staining on the hAECs are located within the airspace around the alveolar. This could also be observed with the HTR cells. Scale: 50μM. Representative of N=2.

177

CMTPX

DiO dye

Collagen

Co-localisation
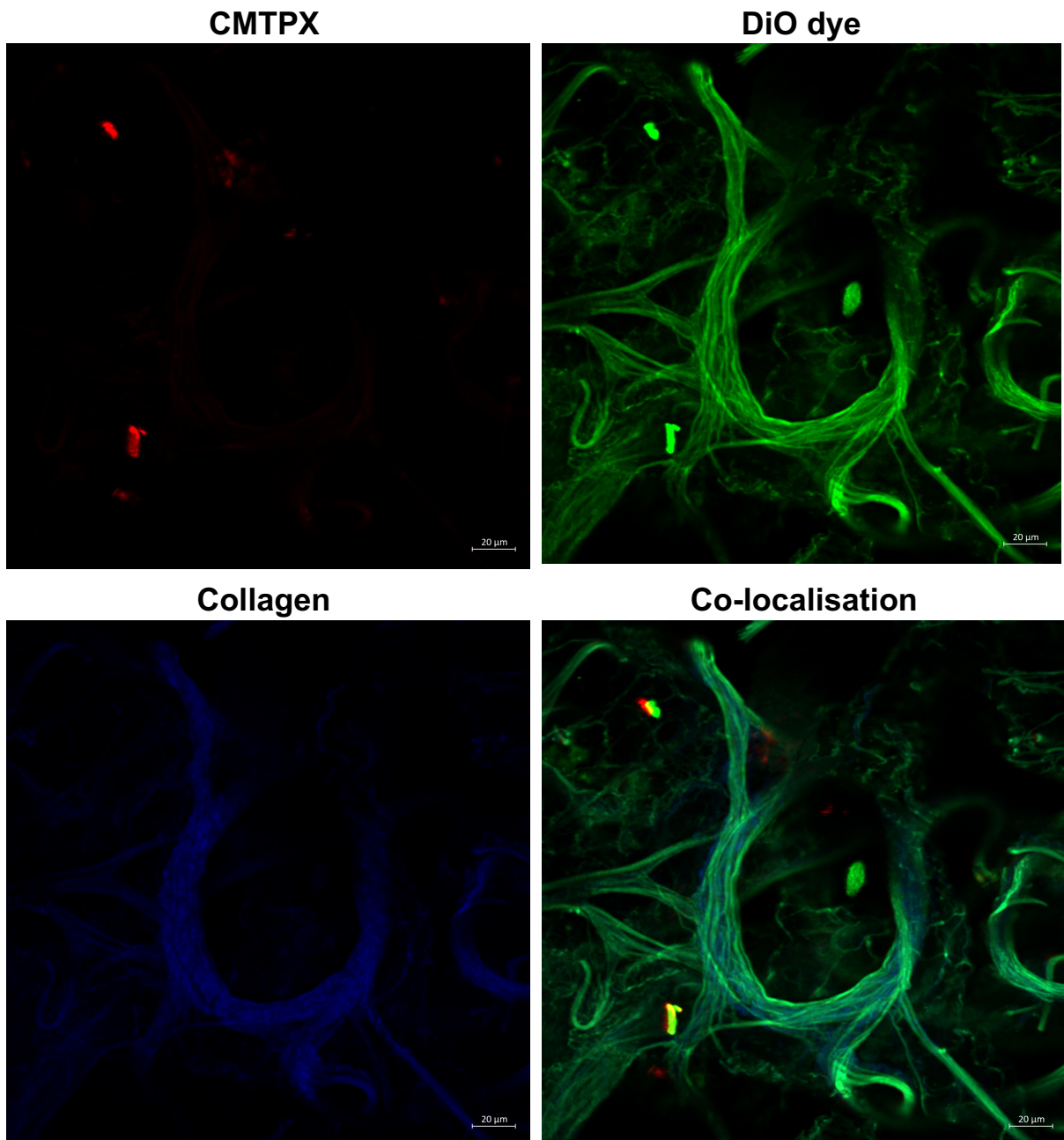
Figure 5-20 Multiphoton microscopy on lung tissue post EVLP.

A singular image was taken at a higher magnification and for a longer time on lung tissue, 4 hours post EVLP, to generate a more defined image. This more clearly demonstrates the hAECs are engrafting into the interstitium around the alveoli, rather than penetrating the tissue itself. Scale: 20μM. N=1.

5.4 Discussion

Lung transplantation offers the only therapeutic option left for end stage lung disease, however there is a disparity between the number of suitable donor lungs available and the growing number of patients on the waiting list. The number of patients on the active lung transplant waiting list has increased by 17% since 2012, with an annual waiting list mortality of 10% reported in the past few years in the UK (NHSBT, 2019, 2020, 2021). EVLP has emerged as a promising technique to recondition and assess extended criteria donor lungs prior to transplant and offers hope of increasing the number of donor lungs available for transplant (Andreasson, Dark, et al., 2014). In addition to this, PGD is a major cause of morbidity and mortality faced post-transplant, incidence rates vary but Diamond *et al* reported an incidence of 16.8% in the case of severe grade 3 PGD in a multicentre study (Diamond et al., 2017). Whitson *et al,* reported those with grade 3 PGD had a survival rate of less than 25% in 10 years (Whitson et al., 2007). The pathology behind PGD is multifactorial, with several points along the transplant process arising potential risk factors for developing PGD and subsequent lung injury. IRI is believed to be one of the mechanisms behind the formation of PGD. Whilst EVLP shows promise to increase the number of donor organs available for transplant by assessing potential donor lungs, it also provides a platform to administer therapeutics. These therapeutics could be used to potentially recondition extended criteria donor lungs, which could further increase the pool of donor lungs and target IRI to potentially reduce the risk of PGD. Furthermore, EVLP provides an ideal platform for assessing the working benefit of the therapeutic and is ideal for preventing any deleterious off target effects which could occur with systemic administration.

Our previous research outlined in chapter 4, demonstrated the capacity for the hAECs to reduce IRI related mechanisms *in vitro*. Therefore, we aimed to administer the hAECs to a split lung model, as this allowed for us to use the HTR-8/SVneo cell line as a control cell type. This is the first EVLP study where cells were administered to both lungs in a split lung model, this was to ensure any changes seen were due to the hAECs, as our studies demonstrated that the HTR cells had no therapeutic benefit or anti-inflammatory properties despite also being derived from the placenta. Mordant *et al,* administered umbilical cord MSCs to porcine lungs using three doses of 50×10^6, 150×10^6 and 300×10^6 cells and found 150×10^6 to be the optimally tolerated dose (Mordant et al., 2016). We administered 150×10^6 and found this dose

of hAECs was also tolerated with no physiological or biological (CXCL8 and TNFα) detriment. Furthermore, Mordant *et al,* demonstrated that intravascular administration resulted in more retention of the MSCs into the lung parenchyma compared to intrabronchial administration (Mordant et al., 2016). Retention of the hAECs was intended to initiate more of a therapeutic benefit, therefore we followed this same method of administration by adding the cells to the perfusate prior to the pulmonary artery thus they would enter the vasculature. Multiphoton imaging revealed that the administration of hAECs in this manner during this study was also indeed resulting in their retention into the lung parenchyma, particularly observing them between the interstitium of the alveoli.

The hAECs did not seem to cause any detrimental effects nor beneficial effects to the physiological parameters of the lungs including PAP or flow rate of the perfusate through the lungs. The haemodynamic changes upon administration were minimal, although marginal improvements in PaO_2 and $PaCO_2$ could be observed, suggesting over time the hAECs could improve gas exchange during EVLP. However, Papagianis *et al* found administering hAECs to the ventilation of pre-term lambs for a week did not appear to show any significant improvements in gas exchange compared to the saline control (Papagianis et al., 2021).

IRI is one of the modalities behind the acute lung injury observed in PGD. IRI involves a cascade of events that start during the cold ischemic period and progress into the reperfusion of the blood flow to the organ. One aspect behind this cascade of events involves an initial activation of macrophages, later followed by neutrophil migration through the endothelium (Sharma et al., 2007; Naidu et al., 2004). TNFα is a pro-inflammatory cytokine that is largely secreted by the alveolar macrophages and shown to have a key role in orchestrating the pro-inflammatory cascade of IRI through stimulating further release of chemokines, increasing endothelium permeability, and ultimately playing a role in the activation of neutrophils. TNFα expression has been noted at both early and late stages of IRI (Eppinger et al., 1997; Maxey et al., 2004). Rats that received anti- TNFα and anti-IL-1β therapy demonstrated significantly reduced vascular injury, neutrophil infiltration and cytokine release (Krishnadasan et al., 2003). Our study has now demonstrated that treatment with hAECs during EVLP leads to a significant reduction in gene expression of this key initiator, compared to the HTR cell treated lungs, with reduced TNFα levels also

observed within the perfusate. Our group has previously demonstrated how lower TNFα levels in the perfusate collected during EVLP could be predictive of 1-year post-transplant survival (Andreasson et al., 2017). Therefore, hAEC treatment resulting in a marked decrease in TNFα, could not only potentially limit the extent of IRI but also potentially indicate improved transplant survival.

IL-6 and CXCL8 have also been implicated to have a role in PGD and post-transplant outcomes, with both being associated with increased risk of grade 3 PGD, IL-6 being associated with longer hospital stays and CXCL8 with more use of ECMO and prolonged ventilation (Verleden et al., 2018; Almenar et al., 2009). hAEC treatment during EVLP has shown a trend of reduced levels of CXCL8 and IL-6 in the perfusate and tissue biopsies, although more repeats are required to determine significance. Notably CXCL8, a neutrophil chemoattractant, expression in the immunofluorescence was markedly less visible in the hAEC treated lungs compared to the HTR cell line treated lungs. Furthermore, the CXCL8 staining observed with the HTR cell line treated lungs in certain areas was colocalised with 3-NT, which is an oxidative stress marker. ROS production is a hallmark of IRI and is largely produced by endothelial cells, neutrophils, and alveolar macrophages in the lungs. Ultimately it leads to the activation and degranulation of neutrophils. Therefore, the reduction observed in CXCL8 production and 3-NT observed in the hAEC treated lungs could suggest a reduction in inflammation and oxidative stress, which could potentially limit neutrophil activation and migration into the vasculature. More studies are required to determine which cells are expressing both the CXCL8 and 3-NT markers, to determine if hAECs may be homing to those specific cells within the tissue.

Cell therapies administered during EVLP have shown promise as therapeutics to recondition lungs prior to transplant. Umbilical cord derived MSCs administered to porcine lungs have been shown to decrease in pro-inflammatory CXCL8, IL-18 and IFNγ production whilst increasing anti-inflammatory IL-4 production. They also observed better lung pathology and less oedema formation (Mordant et al., 2016; Nakajima et al., 2019). Bone marrow derived MSCs administered during EVLP were shown to resolve pulmonary oedema in lungs deemed unsuitable for transplant (McAuley et al., 2014). Alternatively, MAPCs that have been administered to porcine lungs led to a significant decrease in TNFα, IL-1β and IFNγ production in the BAL (Martens et al., 2017). When administered to human lungs turned down for transplant

for 4 hours, the MAPCs resulted in decreased histologic inflammation and cell infiltration. Similarly to our study, they observed a decrease in IL-10 expression in the tissue after 4 hours, which could be explained by the reduction in inflammation they observed upon MAPC treatment and may also be the explanation behind our observation (La Francesca et al., 2014). Although further research is required, hAECs show similar promise to these cell therapies by reducing pro-inflammatory cytokine expression, oxidative stress and improved airspace to tissue ratio in the lungs, but they also offer a therapeutic with minimal ethical issues, ample supply and little need for rapid expansion.

5.4.1 Conclusions

In conclusion, hAECs administration can be tolerated when administered via the PA to a split lung EVLP model and they appear to be retained within the lung parenchyma. hAEC treatment during EVLP showed a significant reduction in TNFα in the tissue and a reduction can also be observed in the perfusate, alongside CXCL8 and IL-6. Oxidative stress marker, 3-NT expression was also largely reduced in hAEC treated lungs. This suggests that administering hAECs to the EVLP platform could limit IRI and recondition lungs deemed unsuitable for transplant, potentially allowing for the expansion of the lung donor pool and reducing the risk PGD occurrence.

6   Discussion, conclusions and future directions

6.1   General discussion

Lung transplantation is the only intervention left for patients with end-stage lung disease, however there is currently a low utilisation rate of donor lungs as many are deemed unsuitable (NHSBT, 2020). Post-transplantation, recipients are then faced with the risk of PGD, a form of acute lung injury that forms within 72 hours and is a significant cause of early morbidity and mortality (Morrison et al., 2017). EVLP can in part be used to address these issues, by offering clinicians a way to assess extended criteria donor lungs in an isolated normothermic environment prior to transplantation, thus allowing for more utilisation of lungs that otherwise might have been deemed unsuitable. Further to this, EVLP offers a platform for the delivery of therapeutics directly to the organ to target lung injury that may have been caused during the donation process, to try to minimise PGD formation post-transplantation.

We hypothesised that hAECs or their subsequently derived conditioned media and EVs, could be a potential cell based therapeutic that could be administered to the EVLP platform to recondition lungs deemed unsuitable for transplant whilst also limiting the formation of PGD post transplantation.

hAECs are derived from the epiblast during embryo formation and so retain many of the pluripotent stem cell characteristics and due to their role in foetal-maternal tolerance they possess immunomodulatory properties, making them attractive as a potential cell therapy (Izumi et al., 2009; Lefebvre et al., 2000). In Chapter 3, we were able to set up a hAEC serum-free isolation process using healthy term-placentae from the Royal Victoria Infirmary, Newcastle upon Tyne Hospitals Trust. Achieving high yields of 132.4×10^6 cells on average, with >90% viability. Flow cytometric analysis on the isolated cells revealed on average there was 94% EpCAM expression. These yields and purity were comparable with what was reported in the literature, and reflected similar results to Murphy *et al*, of which our isolation process was based off (Gramignoli et al., 2016; Murphy et al., 2010; Tabatabaei et al., 2014; Miki et al., 2010; Gomez, 2008; Gottipamula & Sridhar, 2018; Motedayyen et al., 2017).

Exosomes isolated from hAECs have also attracted recent attention as a therapeutic with the literature reporting they also provide an immunomodulatory properties that

can alleviate injury and aid in lung repair (Tan et al., 2018). EVs are secreted by cells into the extracellular space and are involved in cell signalling and communication. They can be isolated through differential ultracentrifugation to yield exosomes, microvesicles and apoptotic bodies from cell cultures (Doyle & Wang, 2019; Théry et al., 2006). Our study attempted to isolate EVs through differential ultracentrifugation using conditioned media from hAECs cultured for 4 days in UltraCULTURE™ medium. Characterisation of exosomes can be done through a variety of protocols, with several being used to confirm exosome isolation. Bead based-flow cytometry demonstrated an average expression of 80% CD9, 60% CD81 and 40% CD63 on the isolated hAEC-EVs, which are tetraspanin exosome markers. The expression of these markers were lower than that reported by Tan *et al*, but higher than Sheller *et al,* for CD9 expression (Tan et al., 2018; Sheller et al., 2016). Furthermore, in TEM we could observe the classic cup shape typical of exosome morphology and these fell within the typical range of 30-150 nm (Doyle & Wang, 2019). Although these findings are suggestive that we were isolating exosomes in our EV preps, we are lacking NTA or DLS data which would determine the size and distribution of our EV preps. This would aid in confidently confirming if our population was made up of mostly exosomes.

PGD pathogenesis is multifactorial with several points along the lung transplantation process where lung injury can arise, but the major mechanism behind PGD is believed to be resultant from IRI (Morrison et al., 2017). IRI does appear to occur in a biphasic pattern, with the initial phase involving the activation of alveolar macrophages and the latter, the activation and migration of neutrophils leading to severe vascular damage, pulmonary oedema and reduced lung functioning (Ng et al., 2006; Diamond & Christie, 2010). Currently, there are a lack of established treatments to target or prevent PGD in lung transplantation. Therefore, a broadly bioactive therapeutic to target multiple aspects of PGD would be desirable. Our study aimed to determine if hAECs or their derivatives could be such a therapeutic.

In Chapter 4, when hAECs and their derivatives were used to treat pro-inflammatory M1 macrophages derived from the THP-1 cell line, we observed a significant decrease in CXCL8 and TNFα expression when treated with hAECs compared to the controls. This was also observed with the conditioned media and EVs, although not as prominently. Phagocytosis upon hAEC treatment was upregulated compared to

the HTR cell treated macrophages, this was also prominently observed with the hAEC-EVs. Macrophage phagocytosis and reduction in TNFα expression were suggestive of an M2 macrophage phenotype. M2 macrophages play a role in immunomodulation and tissue repair (Andrewartha & Yeoh, 2019). It is well established in the literature that hAECs immunomodulate macrophages in a variety of lung injury models and that normal macrophage functioning is required for them to exert their immunomodulatory effects (Murphy et al., 2012; Geng et al., 2016; Zhu et al., 2017; Melville et al., 2017). In particular, Tan *et al,* who demonstrated that hAECs polarised M1 macrophages to an M2 phenotype and observed increasing phagocytosis (Tan et al., 2014). hAEC-EVs have also been reported to increase phagocytosis and polarise M1 macrophages towards an M2 phenotype, supporting our findings (Tan et al., 2018). Use of M2 macrophages, through polarisation by HO-1 of resident macrophages or direct administration to organs has been shown to limit injury caused by IRI (Mao et al., 2020; Zhang et al., 2018). This suggests that our findings that hAECs immunomodulate macrophages towards an M2 phenotype could be important in reducing IRI formation.

Endothelial adhesion molecules ICAM-1 and VCAM-1 play an important role in neutrophil adhesion and migration. Our group demonstrated IL-1β produced during EVLP leads to the upregulation of these adhesion molecules (Andreasson et al., 2017). Therefore, we explored hAEC treatment of IL-1β activated HMEC-1 cells. This showed a trend towards the downregulation of ICAM-1 expression and a significant reduction in VCAM-1 expression. Hashimoto *et al,* reported that sICAM-1 and sVCAM-1 production within the perfusate after 1 hour of EVLP was significantly associated with a higher incidence of PGD post transplantation (Hashimoto et al., 2017). CXCL8, a potent neutrophil chemoattractant, expression was also reduced upon hAEC treatment. A decrease in expression of this marker was also observed with the hAEC conditioned media treated IL-1β activated HMEC-1 cells but not the hAEC-EVs. Neutrophil migration through an IL-1β activated HMEC-1 endothelial monolayer was significantly lower in the hAEC and hAEC-EV treatments compared to the positive controls. The literature also supports our findings that hAECs reduce chemotaxis and infiltration (Li et al., 2005; Geng et al., 2016). hAEC-EVs have also been reported to reduce neutrophil infiltration and myeloperoxidase activity (Tan et al., 2018). A hallmark of PGD is the infiltration of neutrophils into the interstitium and airway of the lungs (Morrison et al., 2017). Therefore, combatting neutrophil

chemotaxis into the lungs, adhesion and subsequent migration into the lung interstitium would be a start in ameliorating the injury observed in PGD.

Our study has demonstrated the capacity of hAECs to immunomodulate these key targets in IRI and have the potential to address the inflammation observed. We also observed that hAECs seemed to show the most encompassing and strongest therapeutic effect in these *in vitro* experiments compared to their derivatives. Therefore, we determined that administering the hAECs during EVLP could potentially recondition lungs turned down for transplant due to poor organ function.

This was the first study that involved the use of hAECs during EVLP. In chapter 5, we demonstrated that hAECs and HTR cells were tolerated with the lungs showing no adverse events during administration through the PA in the perfusate. This is a preliminary study, that requires more repeats but demonstrates the capacity for hAECs to reduce pro-inflammatory markers TNFα, CXCL8 and IL-6 expression. We also observed reduced expression IL-10 gene expression post perfusion which combined with the decreased pro-inflammatory marker expression could suggest that hAECs treatment is resulting in a less inflammatory environment. Furthermore, the IF staining demonstrated that oxidative stress 3-NT marker and CXCL8 co-localisation was largely reduced in the hAEC treated lungs compared to the HTR cell lungs, suggesting that the lungs are less inflamed with hAEC treatment, which could explain the low IL-10 expression observed in the tissue. However therapeutically, AdhIL-10 has been administered to the EVLP platform to provide better gas exchange and reduced pro-inflammatory cytokine expression (Machuca et al., 2017). Therefore, more repeats and further integration of the data is required to determine why IL-10 gene expression is lower in the hAEC treated lungs and what this could mean for lung injury. The hAECs appeared to engraft into the lung parenchyma and appeared to improve airspace-to-tissue ratio. Airspace-to-tissue ratio improvement has also been observed in BPD lungs after hAEC treatment (Zhu et al., 2017).

The use of EVLP as a therapeutic platform has been widely explored with a variety of potential therapies varying from established and novel pharmaceutical agents, gases, gene therapies and cell therapies, as discussed as part of a review article carried out during this study (Griffiths et al., 2020) (Appendix B). The aim of all these studies is the same, to target PGD generally or the IRI mechanism in order to recondition and

186

repair acute lung damage. As there is a lack of established treatments clinically used to treat PGD, administering therapies through EVLP prior to transplantation may hold the answer. Due to the complex multifactorial process of PGD, use of cell therapies may provide the edge as they target multiple aspects of PGD by being able to interact with host cells, release immune modulating paracrine factors and even regulate endothelial permeability. The administration of MSCs and MAPCs to the EVLP platform has been thoroughly evaluated in the literature, demonstrating the capacity of cell therapies to improve lung functioning and injury (Mordant et al., 2016; Nakajima et al., 2019; McAuley et al., 2014; Martens et al., 2017; La Francesca et al., 2014). Our study offers similar therapeutic findings to those described in the literature, this could provide an alternative cell therapy which is free of ethical issues and does not require rapid expansion, which poses a risk of transformation which could lead to cancer in immunosuppressed transplant patients, two issues often faced by these other cell therapies. Therefore, hAECs could potentially be used as a therapeutic to improve lung function and limit lung injury in extended criteria donors. Although it should be remembered that these findings are preliminary (only n=3) and that more repeats and further interrogation of inflammation and tissue injury markers are required to understand the therapeutic mechanism behind hAECs within EVLP.

Figure 6-1 provides a summary of the targets in which the hAECs appear to act upon, which play a role in the mechanism behind IRI. Overall, this study has observed that hAECs can immunomodulate these processes and demonstrated the potential that hAECs could have when delivered to the EVLP platform to improve lung injury, potentially expanding the donor lung pool and PGD outcomes post-transplantation.
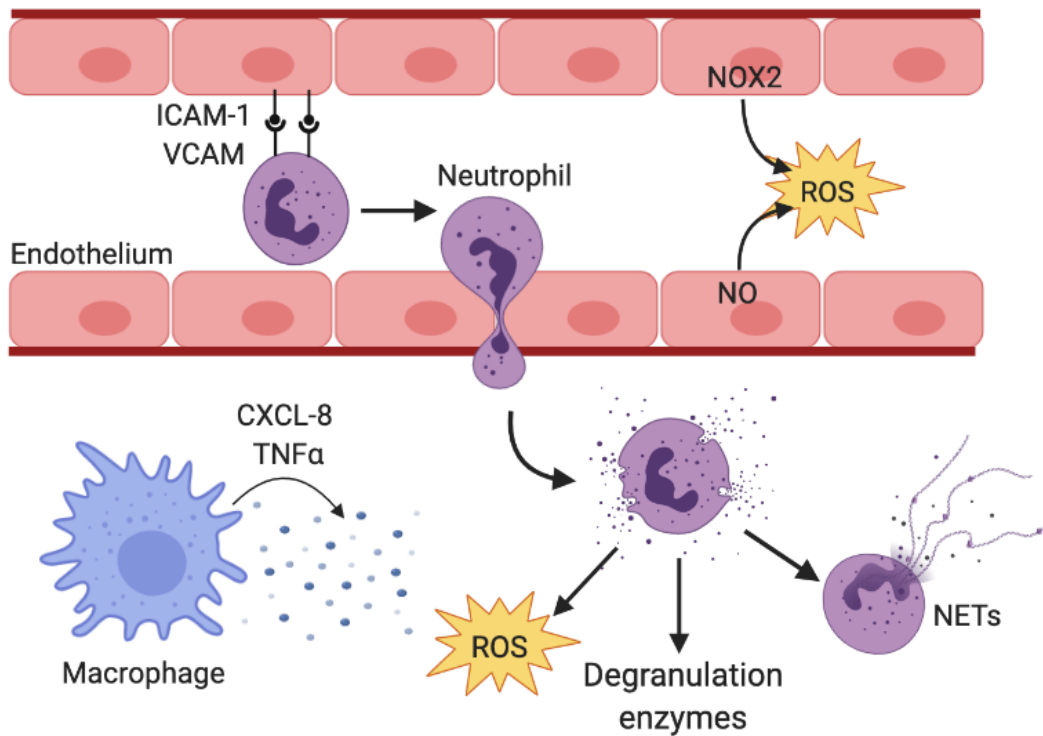
Figure 6-1 Summary of the targets of hAECs that play a role in IRI.

Ischemia reperfusion injury (IRI) triggers a cascade of events, including the formation of reactive oxygen species (ROS), endothelial cell activation, neutrophil migration through the endothelium and alveolar macrophage activation, leading to vascular damage and poor lung functioning. hAEC treatment has been demonstrated in this study either through *in vitro* or *ex vivo* studies to polarise M1 pro-inflammatory macrophages towards an anti-inflammatory M2 phenotype, reduce in neutrophil chemotaxis through an endothelial monolayer, decrease oxidative stress, ICAM-1 and VCAM-1 expression on endothelial cells and reduce chemokine and cytokine production.

6.2   Limitations of the study

The most significant limitation to this study was the small sample size, only three donors were used to determine the effect of hAECs on lung reconditioning during EVLP. In addition to this, one donor, likely due to cause of death, perfused for only 2 hours, hindering any therapeutic comparisons to the other two donors. Our original aim was to use five lung pairs, all reaching 4 hours of perfusion. Unfortunately, this was not possible due to competition for lung donors and only using appropriate lung donors who were not deemed transplantable standard but also not so damaged they could not undergo EVLP. Most substantially, the ongoing COVID-19 pandemic hindered the number of lungs available to research, with an initial total stop to laboratory research occurring in March – July 2020 at the university, and it wasn't possible until October 2020 to start to receive lungs for research again. This initial halt to research also impacted some of the *in vitro* assays that could no longer be carried out as intended too, such as in chapter 3, the isolation of hAEC-EVs could not undergo NTA to determine distribution and size, as this required another laboratory group's equipment, who were also affected by the COVID-19 pandemic.

The *in vitro* functional assays carried out on hAECs and their derivatives on targeting IRI related mechanisms in chapter 4, were limited by their simplification of the multifactorial processes all interacting in the lungs during IRI. We determined the therapeutic benefit of hAECs and their derivatives on isolated cell types, which limits the conclusions that can be drawn based on the mechanisms behind hAECs but this could be in part addressed by our EVLP studies.

The use of THP-1 derived macrophages and HMEC-1 cells used for our functional assays are widely used in the literature. However, they are not fully representative of primary alveolar macrophages or lung endothelium. To improve our understanding on hAEC therapeutic mechanisms in lungs, use of these primary cell types would be more informative.

In chapter 5, the EVLP model faced a few complications and limitations that are still in the process of being addressed. Initially for our optimisation of cell administration assays to assess lung tolerance we only had one ventilator and so custom designed tubing to allow simultaneous ventilation to both lungs from this one ventilator was used. However, this means the air will follow the path of least resistance meaning the

lung with better functioning may be preferred. This was addressed with two ventilators used for our latter study. Our pressure monitoring situation was limited by our equipment's lack of sensitivity, meaning we observed substantial changes in PA pressure which may not be accurately reflecting what is actually occurring within the lungs and so endothelial sheer stress may be occurring, which could explain the fluid taken in by all the donor lungs. Moving forward, a more sensitive pressure monitoring system needs to be put in place, and one that measures the left atrial pressure would also be preferential.

Treatment time with the hAECs during EVLP aimed to be 4 hours but was sometimes cut short before one or both lungs started to deteriorate from pulmonary oedema. Particularly in the case of donor 5. Longer treatment times may be needed to have a more apparent therapeutic benefit of hAECs, for example 6 to 8 hours of perfusion. Our study starts to demonstrate the potential of hAECs after a shorter period of time in contrast to much of the literature, which uses systemic administration of hAECs on chronic injury models to observe their therapeutic benefits. Therefore, future studies should aim to extend these perfusion times.

Most significantly, this EVLP model lacks the capacity of transplantation of the lungs, due to the use of human organs. Therefore, this limits the clinical outcomes that can be concluded post-transplant, that may have been derived from pre-treating the lungs with hAECs via EVLP. A porcine model of EVLP and subsequent transplantation could be used in the future to address this, to determine more longer-term lung function and recipient responses from hAEC treatment.

6.3   Future directions

As this was only a preliminary study which aimed at determining the feasibility of hAECs in the reconditioning of lungs using the EVLP platform, further experiments will be required to substantiate their therapeutic benefit. Once these further experiments have been obtained, this could open up a number of avenues to explore. Firstly, a larger panel of cytokines, chemokines and DAMPs could be explored, using more robust and sensitive methods such as RNA sequencing in the lung tissue and meso-scale discovery (MSD) assays on the perfusate samples. Further to this, the cell infiltration observed in the H&E staining of the lungs could be explored, determining which cells are infiltrating the lungs and in the case of any

macrophages whether they are of an M1 or M2 phenotype. Work on the IF staining involving the CXCL8 and 3-NT co-localisation could also be further substantiated to determine which cells are co-expressing these markers, furthering our understanding of which cells hAECs are having an apparent effect.

Following on from this study, hAEC-EVs could be administered to the EVLP platform after also showing promise in our *in vitro* functional assays. Delivering EVs over the cells could allow for benefit of larger doses being used with no risk of vascular damage and less risk of any potential long-term effects in immunosuppressed patients that could arise post-transplant due to cell engraftment. Potentially the EVs may get taken in by native lung cells and therefore provide a longer therapeutic capacity leading into post-transplantation. By also administering hAEC-EVs, we could determine if the EVs provide a greater therapeutic benefit compared to their whole cell counterpart during EVLP by comparing lung outcomes and carrying out MSD and RNA sequencing assays to determine their effect on inflammatory outputs. EVs could also be primed by using altering culture methods, for example culturing the hAECs in IL-1β, which is a potent biomarker of lung functioning and EVLP success established by our group (Andreasson et al., 2017), could provide more targeted therapeutics for specific pathways.

We have established a split lung model that offers an opportunity to directly assess therapeutics against a concurrently perfused control lung. Therefore, this model can be used to assess other therapeutics outside of cell therapies, including targeted drugs or receptor antagonist/agonists. For example, Miss Jenny Gilmour is exploring the potential for an SIPR1 agonist and SIPR3 antagonist administered during EVLP to improve lung integrity, as part of her PhD project. Furthermore, we've demonstrated the potential of hAECs and their derivatives to provide a therapeutic benefit towards IRI, therefore the cells and EVs are also being explored for other organs that face this form of injury, including the kidneys and heart during *ex vivo* normothermic perfusion, by our group.

6.4   Concluding remarks

EVLP has allowed for the assessment of extended criteria donor lungs addressing some of the shortage of organs available for transplant. Yet despite this, patients are still facing prolonged periods on the transplant waiting list resulting in high mortality

rates and then upon transplantation, face a further risk of PGD formation. The work here has aimed to address these clinical problems faced in the field of lung transplantation today by developing a therapeutic in order to improve the lives of those who are in need of a lung transplant.

7   References

Abdo, R.J. (2016) Treatment of diabetic foot ulcers with dehydrated amniotic membrane allograft: a prospective case series. *Journal of Wound Care*. 25 (Sup7), S4–S9.

Aeba, R., Griffith, B.., Kormos, R.., Armitage, J.., Gasior, T.., Fuhrman, C.., Yousem, S.. & Hardesty, R.. (1994) Effect of Cardiopulmonary Bypass on Early Graft Dysfunction in Clinical Lung transplantation. *The Annals of Thoracic Surgery*. 57715–22.

Alipour, R., Motedayyen, H., Sereshki, N., Rafiee, M., Alsahebfosul, F. & Pourazar, A. (2020) Human Amniotic Epithelial Cells Affect the Functions of Neutrophils. *International journal of stem cells*.

Almenar, M., Cerón, J., Gómez, M.A.D., Peñalver, J.C., Jiménez, M.A.J. & Padilla, J. (2009) [Interleukin 8 concentrations in donor bronchoalveolar lavage: impact on primary graft failure in double lung transplant]. *Archivos de bronconeumologia*. 45 (1), 12–15.

Andreasson, A., Dark, J.H. & Fisher, A.J. (2014) Ex vivo lung perfusion in clinical lung transplantation-State of the art. *European Journal of Cardio-thoracic Surgery*. 46 (5), 779–788.

Andreasson, A., Karamanou, D.M., Gillespie, C.S., Özalp, F., Butt, T., Hill, P., Jiwa, K., R.Walden, H., Green, N.J., Borthwick, L.A., Clark, S.C., Pauli, H., Gould, K.F., Corris, P.A., Ali, S., Dark, J.H. & Fisher, A.J. (2017) Profiling inflammation and tissue injury markers in perfusate and bronchoalveolar lavage fluid during human ex vivo lung perfusion. *European Journal of Cardio-thoracic Surgery*. 51 (3), 577–586.

Andreasson, A., Karamanou, D.M., Perry, J.D., Perry, A., Özalp, F., Butt, T., Morley, K.E., Walden, H.R., Clark, S.C., Prabhu, M., Corris, P.A., Gould, K., Fisher, A.J. & Dark, J.H. (2014) The effect of ex vivo lung perfusion on microbial load in human donor lungs. *The Journal of Heart and Lung Transplantation*. 33 (9), 910–916.

Andreasson, A.S.I., Borthwick, L.A., Gillespie, C., Jiwa, K., Scott, J., Henderson, P., Mayes, J., Romano, R., Roman, M., Ali, S., Fildes, J.E., Marczin, N., Dark, J.H. & Fisher, A.J. (2017) The role of interleukin-1β as a predictive biomarker and potential therapeutic target during clinical ex vivo lung perfusion. *Journal of Heart and Lung Transplantation*. 36 (9), 985–995.

Andrewartha, N. & Yeoh, G. (2019) Human Amnion Epithelial Cell Therapy for

Chronic Liver Disease. *Stem Cells International*. 20191–10.

Baker, E.K., Malhotra, A., Lim, R., Jacobs, S.E., Hooper, S.B., Davis, P.G. & Wallace, E.M. (2019) Human amnion cells for the prevention of bronchopulmonary dysplasia: a protocol for a phase I dose escalation study. *BMJ open*. 9 (2), e026265–e026265.

Baradaran-Rafii, A., Aghayan, H.R., Arjmand, B. & Javadi, M.A. (2007) Amniotic Membrane Transplantation. *Iran J Ophthalmic Res*. 2 (1), 58–75.

Barnes, B.J. & Somerville, C.C. (2020) Modulating Cytokine Production via Select Packaging and Secretion From Extracellular Vesicles. Frontiers in Immunology 11 p.1040.

Berenguer, J., Lagerweij, T., Zhao, X.W., Dusoswa, S., van der Stoop, P., Westerman, B., de Gooijer, M.C., Zoetemelk, M., Zomer, A., Crommentuijn, M.H.W., Wedekind, L.E., López-López, À., Giovanazzi, A., Bruch-Oms, M., van der Meulen-Muileman, I.H., Reijmers, R.M., van Kuppevelt, T.H., García-Vallejo, J.-J., van Kooyk, Y., et al. (2018) Glycosylated extracellular vesicles released by glioblastoma cells are decorated by CCL18 allowing for cellular uptake via chemokine receptor CCR8. Journal of extracellular vesicles 7 (1) p.1446660.

Boffini, M., Ricci, D., Barbero, C., Bonato, R., Ribezzo, M., Mancuso, E., Attisani, M., Simonato, E., Magistroni, P., Mansouri, M., Solidoro, P., Baldi, S., Pasero, D., Amoroso, A. & Rinaldi, M. (2013) Ex vivo lung perfusion increases the pool of lung grafts: analysis of its potential and real impact on a lung transplant program. *Transplantation proceedings*. 45 (7), 2624–2626.

Botha, P., Trivedi, D., Weir, C.., Searl, C.., Corris, P.., Dark, J.. & Schueler, S.V.. (2006) Extended donor criteria in lung transplantation: Impact on organ allocation. *The Journal of Thoracic and Cardiovascular Surgery*. 131 (5), 1154–1160.

Le Bouteiller, P., Solier, C., Pröll, J., Aguerre-Girr, M., Fournel, S. & Lenfant, F. (1999) Placental HLA-G protein expression in vivo: where and what for? *Human reproduction update*. 5 (3), 223–233.

Centurione, L., Passaretta, F., Centurione, M.A., Munari, S. De, Vertua, E., Silini, A., Liberati, M., Parolini, O. & Di Pietro, R. (2018) Mapping of the Human Placenta: Experimental Evidence of Amniotic Epithelial Cell Heterogeneity. *Cell transplantation*. 27 (1), 12–22.

Charles, E.J., Mehaffey, H., Sharma, A.K., Zhao, Y., Stoler, M.H., Isbell, J.M., Lau, C.L., Tribble, C.G., Laubach, V.E. & Kron, I.L. (2017) Lungs donated after

circulatory death and prolonged warm ischemia are transplanted successfully after enhanced ex vivo lung perfusion using adenosine A2B receptor antagonism. *The Journal of Thoracic and Cardiovascular Surgery*. 154 (5), 1811–1820.

Chen, F. & Date, H. (2015) Update on ischemia-reperfusion injury in lung transplantation. *Current opinion in organ transplantation*. 20 (5), 515–520.

Christie, J.D., Bavaria, J.E., Palevsky, H.I., Litzky, L., Blumenthal, N.P., Kaiser, L.R. & Kotloff, R.M. (2018) Primary Graft Failure Following Lung Transplantation. *CHEST*. 114 (1), 51–60.

Christie, J.D., Bellamy, S., Ware, L.B., Lederer, D., Hadjiliadis, D., Lee, J., Robinson, N., Localio, A.R., Wille, K., Lama, V., Palmer, S., Orens, J., Weinacker, A., Crespo, M., Demissie, E., Kimmel, S.E. & Kawut, S.M. (2010) Construct validity of the definition of primary graft dysfunction after lung transplantation. *The Journal of heart and lung transplantation : the official publication of the International Society for Heart Transplantation*. 29 (11), 1231–9.

Christie, J.D., Kotloff, R.M., Pochettino, A., Arcasoy, S.M., Rosengard, B.R., Landis, J.R. & Kimmel, S.E. (2003) Clinical Risk Factors for Primary Graft Failure Following Lung Transplantation. *Chest*. 124 (4), 1232–1241.

Cosgun, T., Iskender, I., Yamada, Y., Arni, S., Lipiski, M., Van Tilburg, K., Walter, W. & Inci, I. (2017) Ex vivo administration of trimetazidine improves post-transplant lung function in pig model. *European Journal of Cardio-thoracic Surgery*. 52 (1), 171–177.

Covarrubias, M., Ware, L.B., Kawut, S.M., De Andrade, J., Milstone, A., Weinacker, A., Orens, J., Lama, V., Wille, K., Bellamy, S., Shah, C., Demissie, E. & Christie, J.D. (2007) Plasma Intercellular Adhesion Molecule-1 and von Willebrand Factor in Primary Graft Dysfunction After Lung Transplantation. *American Journal of Transplantation*. 7 (11), 2573–2578.

Cypel, M., Yeung, J.C., Liu, M., Anraku, M., Chen, F., Karolak, W., Sato, M., Laratta, J., Azad, S., Madonik, M., Chow, C.-W., Chaparro, C., Hutcheon, M., Singer, L.G., Slutsky, A.S., Yasufuku, K., de Perrot, M., Pierre, A.F., Waddell, T.K., et al. (2011) Normothermic Ex Vivo Lung Perfusion in Clinical Lung Transplantation. *New England Journal of Medicine*. 364 (15), 1431–1440.

Cypel, M., Yeung, J.C., Machuca, T., Chen, M., Singer, L.G., Yasufuku, K., de Perrot, M., Pierre, A., Waddell, T.K. & Keshavjee, S. (2012) Experience with the first 50 ex vivo lung perfusions in clinical transplantation. *The Journal of thoracic and*

cardiovascular surgery. 144 (5), 1200–1206.

Daud, S.A., Yusen, R.D., Meyers, B.F., Chakinala, M.M., Walter, M.J., Aloush, A.A., Patterson, G.A., Trulock, E.P. & Hachem, R.R. (2007) Impact of immediate primary lung allograft dysfunction on bronchiolitis obliterans syndrome. *American journal of respiratory and critical care medicine*. 175 (5), 507–513.

Davis, J. (1910) Skin transplantation with a review of 550 cases at the Johns Hopkins Hospital. *John Hopkins Medical Journal*. 15307.

Diamond, J.M., Arcasoy, S., Kennedy, C.C., Eberlein, M., Singer, J.P., Patterson, G.M., Edelman, J.D., Dhillon, G., Pena, T., Kawut, S.M., Lee, J.C., Girgis, R., Dark, J. & Thabut, G. (2017) Report of the International Society for Heart and Lung Transplantation Working Group on Primary Lung Graft Dysfunction, part II: Epidemiology, risk factors, and outcomes—A 2016 Consensus Group statement of the International Society for Heart and Lung Tran. *Journal of Heart and Lung Transplantation*. 36 (10), 1104–1113.

Diamond, J.M. & Christie, J.D. (2010) The contribution of airway and lung tissue ischemia to primary graft dysfunction. *Current opinion in organ transplantation*. 15 (5), 552–557.

Diamond, J.M., Lee, J.C., Kawut, S.M., Shah, R.J., Localio, A.R., Bellamy, S.L., Lederer, D.J., Cantu, E., Kohl, B.A., Lama, V.N., Bhorade, S.M., Crespo, M., Demissie, E., Sonett, J., Wille, K., Orens, J., Shah, A.S., Weinacker, A., Arcasoy, S., et al. (2013) Clinical risk factors for primary graft dysfunction after lung transplantation. *American journal of respiratory and critical care medicine*. 187 (5), 527–534.

Dong, B., Stewart, P.W. & Egan, T.M. (2013) Postmortem and ex vivo carbon monoxide ventilation reduces injury in rat lungs transplanted from non–heart-beating donors. *The Journal of Thoracic and Cardiovascular Surgery*. 146 (2), 429–436.

Dong, B.M., Abano, J.B. & Egan, T.M. (2009) Nitric Oxide Ventilation of Rat Lungs from Non-Heart-Beating Donors Improves Posttransplant Function. *American Journal of Transplantation*. 9 (12), 2707–2715.

Doyle, L.M. & Wang, M.Z. (2019) Overview of Extracellular Vesicles, Their Origin, Composition, Purpose, and Methods for Exosome Isolation and Analysis. *Cells*. 8 (7), 727.

Emaminia, A., Lapar, D.J., Zhao, Y., Steidle, J.F., Harris, D.A., Laubach, V.E., Linden, J., Kron, I.L. & Lau, C.L. (2011) Adenosine A2A Agonist Improves Lung

Function During Ex-vivo Lung Perfusion. *Annals of Thoracic Surgery*. 92 (5), 1840–6.

Eppinger, M.J., Deeb, G.M., Bolling, S.F. & Ward, P.A. (1997) Mediators of ischemia-reperfusion injury of rat lung. *The American journal of pathology*. 150 (5), 1773–1784.

Eppinger, M.J., Jones, M.L., Deeb, G.M., Bolling, S.F. & Ward, P.A. (1995) Pattern of injury and the role of neutrophils in reperfusion injury of rat lung. *The Journal of surgical research*. 58 (6), 713–718.

Feng, X., Deng, T., Zhang, Y., Su, S., Wei, C. & Han, D. (2011) Lipopolysaccharide inhibits macrophage phagocytosis of apoptotic neutrophils by regulating the production of tumour necrosis factor α and growth arrest-specific gene 6. *Immunology*. 132 (2), 287–295.

Ferrari, R.S. & Andrade, C.F. (2015) Oxidative Stress and Lung Ischemia-Reperfusion Injury. *Oxidative medicine and cellular longevity*. 2015590987.

Fiser, S.M., Tribble, C.G., Long, S.M., Kaza, A.K., Cope, J.T., Laubach, V.E., Kern, J.A. & Kron, I.L. (2001) Lung transplant reperfusion injury involves pulmonary macrophages and circulating leukocytes in a biphasic response. *The Journal of Thoracic and Cardiovascular Surgery*. 121 (6), 1069–1075.

Fisher, A., Andreasson, A., Chrysos, A., Lally, J., Mamasoula, V., Exley, C., Wilkinson, J., Qian, J., Watson, G., Lewington, O., Chadwick, T., McColl, E., Pearce, M., Mann, K., McMeekin, N., Vale, L., Tsui, S., Yonan, N., Simon, A., et al. (2016) An observational study of Donor Ex Vivo Lung Perfusion in UK lung transplantation: DEVELOP-UK. *Health Technology Assessment*. 20 (85), 1–276.

Fisher, A.J., Donnelly, S.C., Hirani, N., Haslett, C., Strieter, R.M., Dark, J.H. & Corris, P.A. (2001) Elevated levels of interleukin-8 in donor lungs is associated with early graft failure after lung transplantation. *American journal of respiratory and critical care medicine*. 163 (1), 259–265.

La Francesca, S., Ting, A.E., Sakamoto, J., Rhudy, J., Bonenfant, N.R., Borg, Z.D., Cruz, F.F., Goodwin, M., Lehman, N.A., Taggart, J.M., Deans, R. & Weiss, D.J. (2014) Multipotent adult progenitor cells decrease cold ischemic injury in ex vivo perfused human lungs: An initial pilot and feasibility study. *Transplantation Research*. 3 (1), 1–9.

Geng, L., Chen, Z., Ren, H., Niu, X., Yu, X. & Yan, H. (2016) Effects of an early intervention using human amniotic epithelial cells in a COPD rat model. *Pathology, research and practice*. 212 (11), 1027–1033.

Gennai, S., Monsel, A., Hao, Q., Park, J., Matthay, M.A. & Lee, J.W. (2015) Microvesicles Derived From Human Mesenchymal Stem Cells Restore Alveolar Fluid Clearance in Human Lungs Rejected for Transplantation. *American Journal of Transplantation*. 15 (9), 2404–2412.

Geudens, N., Vanaudenaerde, B.M., Neyrinck, A.P., Van De Wauwer, C., Vos, R., Verleden, G.M., Verbeken, E., Lerut, T. & Van Raemdonck, D.E.M. (2007) The importance of lymphocytes in lung ischemia-reperfusion injury. *Transplantation proceedings*. 39 (8), 2659–2662.

Ghaidan, H., Fakhro, M., Andreasson, J., Pierre, L., Ingemansson, R. & Lindstedt, S. (2019) Ten year follow-up of lung transplantations using initially rejected donor lungs after reconditioning using ex vivo lung perfusion. *Journal of cardiothoracic surgery*. 14 (1), 125.

Gillaux, C., Méhats, C., Vaiman, D., Cabrol, D. & Breuiller-Fouché, M. (2011) Functional Screening of TLRs in Human Amniotic Epithelial Cells. *The Journal of Immunology*. 187 (5), 2766 LP – 2774.

Gilmour, J., Griffiths, C., Pither, T., Scott, W.E. 3rd & Fisher, A.J. (2020) Normothermic machine perfusion of donor-lungs ex-vivo: promoting clinical adoption. *Current opinion in organ transplantation*. 25 (3), 285–292.

Gomez, D.R. (2008) *Human amniotic epithelial cells: isolation and characterisation*.

Gottipamula, S. & Sridhar, K.N. (2018) Large-scale Isolation, Expansion and Characterization of Human Amniotic Epithelial Cells. *International journal of stem cells*. 11 (1), 87–95.

Gramignoli, R., Srinivasan, R.C., Kannisto, K. & Strom, S.C. (2016) Isolation of Human Amnion Epithelial Cells According to Current Good Manufacturing Procedures. *Current Protocols in Stem Cell Biology*. 371E.10.1-1E.10.13.

Grange, C., Bellucci, L., Bussolati, B. & Ranghino, A. (2020) Potential Applications of Extracellular Vesicles in Solid Organ Transplantation. *Cells*. 9 (2), 369.

Griffiths, C., Scott III, W.E., Ali, S. & Fisher, A.J. (2020) Maximizing organs for donation: the potential for ex situ normothermic machine perfusion. *QJM: An International Journal of Medicine*.

Haam, S., Lee, J., Park, M. & Lim, B. (2018) Hydrogen gas inhalation during ex vivo lung perfusion of donor lungs recovered after cardiac death. *The Journal of heart and lung transplantation*. 37 (10), 1271–1278.

Haam, S., Lee, S., Paik, H.C., Park, M.S., Song, J.H., Lim, B.J. & Nakao, A. (2015) The effects of hydrogen gas inhalation during ex vivo lung perfusion on donor

lungs obtained after cardiac death. *European Journal of Cardio-thoracic Surgery*. 48 (4), 542–547.

Haam, S., Noda, K., Philips, B.J., Harano, T., Sanchez, P.G. & Shigemura, N. (2020) Cyclosporin A Administration During Ex Vivo Lung Perfusion Preserves Lung Grafts in Rat Transplant Model. *Transplantation*.

Hadley, E.E., Sheller-Miller, S., Saade, G., Salomon, C., Mesiano, S., Taylor, R.N., Taylor, B.D. & Menon, R. (2018) Amnion epithelial cell-derived exosomes induce inflammatory changes in uterine cells. *American journal of obstetrics and gynecology*. 219 (5), 478.e1-478.e21.

Hammer, A., Hutter, H., Blaschitz, A., Mahnert, W., Hartmann, M., Uchanska-Ziegler, B., Ziegler, A. & Dohr, G. (1997) Amnion Epithelial Cells, in Contrast to Trophoblast Cells, Express All Classical HLA Class I Molecules Together With HLA-G. *American Journal of Reproductive Immunology*. 37 (2), 161–171.

Hardy, J., Webb, W., Dalton, M.J. & Walker, D.J. (1963) LUNG HOMOTRANSPLANTATION IN MAN. *JAMA*. 1861065–74.

Harirah, H.M., Donia, S.E., Parkash, V., Jones, D.C. & Hsu, C.-D. (2002) Localization of the Fas-Fas ligand system in human fetal membranes. *The Journal of reproductive medicine*. 47 (8), 611–616.

Hashimoto, K., Cypel, M., Kim, H., Machuca, T.N., Nakajima, D., Chen, M., Hsin, M.K., Zamel, R., Azad, S., Waddell, T.K., Liu, M. & Keshavjee, S. (2017) Soluble Adhesion Molecules During Ex Vivo Lung Perfusion Are Associated With Posttransplant Primary Graft Dysfunction. *American Journal of Transplantation*. 17 (5), 1396–1404.

Huerter, M.E., Sharma, A.K., Zhao, Y., Charles, E.J., Kron, I.L. & Laubach, V.E. (2016) Attenuation of Pulmonary Ischemia-Reperfusion Injury by Adenosine A2B Receptor Antagonism. *Annals of Thoracic Surgery*. 102 (2), 385–393.

Huppertz, B. (2008) The anatomy of the normal placenta. *Journal of Clinical Pathology*. 61 (12), 1296 LP – 1302.

Izumi, M., Pazin, B.J., Minervini, C.F., Gerlach, J., Ross, M.A., Stolz, D.B., Turner, M.E., Thompson, R.L. & Miki, T. (2009) Quantitative comparison of stem cell marker-positive cells in fetal and term human amnion. *Journal of reproductive immunology*. 81 (1), 39–43.

Jin, Z., Suen, K., Wang, Z. & Ma, D. (2020) Review 2: Primary graft dysfunction after lung transplant-pathophysiology, clinical considerations and therapeutic targets. *Journal of Anesthesia*. 34 (5), 729–749.

Khimenko, P.L., Bagby, G.J., Fuseler, J. & Taylor, A.E. (1998) Tumor necrosis factor-α in ischemia and reperfusion injury in rat lungs. *Journal of applied physiology*. 85 (6), 2005–2011.

King, R.C., Binns, O.A., Rodriguez, F., Kanithanon, R.C., Daniel, T.M., Spotnitz, W.D., Tribble, C.G. & Kron, I.L. (2000) Reperfusion injury significantly impacts clinical outcome after pulmonary transplantation. *The Annals of thoracic surgery*. 69 (6), 1681–1685.

Koch, A., Pizanis, N., Olbertz, C., Abou-Issa, O., Taube, C., Slama, A., Aigner, C., Jakob, H.G. & Kamler, M. (2018) One-year experience with ex vivo lung perfusion: Preliminary results from a single center. *The International Journal of Artificial Organs*. 41 (8), 460–466.

Kolanko, E., Kopaczka, K., Koryciak-Komarska, H., Czech, E., Szmytkowska, P., Gramignoli, R. & Czekaj, P. (2019) Increased immunomodulatory capacity of human amniotic cells after activation by pro-inflammatory chemokines. *European Journal of Pharmacology*. 859172545.

Krenn, K., Klepetko, W., Taghavi, S., Lang, G., Schneider, B. & Aharinejad, S. (2007) Recipient Vascular Endothelial Growth Factor Serum Levels Predict Primary Lung Graft Dysfunction. *American Journal of Transplantation*. 7 (3), 700–706.

Krishnadasan, B., Naidu, B. V, Byrne, K., Fraga, C., Verrier, E.D. & Mulligan, M.S. (2003) The role of proinflammatory cytokines in lung ischemia-reperfusion injury. *The Journal of thoracic and cardiovascular surgery*. 125 (2), 261–272.

Krutsinger, D., Reed, R.M., Blevins, A., Puri, V., De Oliveira, N.C., Zych, B., Bolukbas, S., Van Raemdonck, D., Snell, G.I. & Eberlein, M. (2015) Lung transplantation from donation after cardiocirculatory death: A systematic review and meta-analysis. *Journal of Heart and Lung Transplantation*. 34 (5), 675–684.

Laubach, V.E. & Sharma, A.K. (2016) Mechanisms of lung ischemia-reperfusion injury. *Current opinion in organ transplantation*. 21 (3), 246–252.

Lebreton, F., Lavallard, V., Bellofatto, K., Bonnet, R., Wassmer, C.H., Perez, L., Kalandadze, V., Follenzi, A., Boulvain, M., Kerr-Conte, J., Goodman, D.J., Bosco, D., Berney, T. & Berishvili, E. (2019) Insulin-producing organoids engineered from islet and amniotic epithelial cells to treat diabetes. *Nature Communications*. 10 (1), 4491.

Lederer, D.J., Kawut, S.M., Wickersham, N., Winterbottom, C., Bhorade, S., Palmer, S.M., Lee, J., Diamond, J.M., Wille, K.M., Weinacker, A., Lama, V.N., Crespo, M., Orens, J.B., Sonett, J.R., Arcasoy, S.M., Ware, L.B. & Christie, J.D. (2011)

Obesity and primary graft dysfunction after lung transplantation: The lung transplant outcomes group obesity study. *American Journal of Respiratory and Critical Care Medicine*. 184 (9), 1055–1061.

Lee, J.C., Christie, J.D. & Keshavjee, S. (2010) Primary Graft Dysfunction : Definition , Risk Factors , Short- and Long-Term Outcomes. *Seminars in Respiratory and Critical Care Medicine*. 31 (2), 161–171.

Lee, S., Huen, S., Nishio, H., Nishio, S., Lee, H.K., Choi, B.-S., Ruhrberg, C. & Cantley, L.G. (2011) Distinct macrophage phenotypes contribute to kidney injury and repair. *Journal of the American Society of Nephrology : JASN*. 22 (2), 317–326.

Lefebvre, S., Adrian, F., Moreau, P., Gourand, L., Dausset, J., Berrih-Aknin, S., Carosella, E.D. & Paul, P. (2000) Modulation of HLA-G Expression in Human Thymic and Amniotic Epithelial Cells. *Human Immunology*. 61 (11), 1095–1101.

Li, H., Niederkorn, J.Y., Neelam, S., Mayhew, E., Word, R.A., McCulley, J.P. & Alizadeh, H. (2005) Immunosuppressive factors secreted by human amniotic epithelial cells. *Investigative ophthalmology & visual science*. 46 (3), 900–907.

Lim, R., Hodge, A., Moore, G., Wallace, E.M. & Sievert, W. (2017) A Pilot Study Evaluating the Safety of Intravenously Administered Human Amnion Epithelial Cells for the Treatment of Hepatic Fibrosis. *Frontiers in pharmacology*. 8549.

Lim, R., Malhotra, A., Tan, J., Chan, S.T., Lau, S., Zhu, D., Mockler, J.C. & Wallace, E.M. (2018) First-In-Human Administration of Allogeneic Amnion Cells in Premature Infants With Bronchopulmonary Dysplasia: A Safety Study. *Stem cells translational medicine*. 7 (9), 628–635.

Lin, C.-C., Lu, H., Wu, L.-F., Liang, Y., Chen, B.-C. & Bai, Y.-H. (2016) [The role of sub-transform of macrophages in renal ischemia/reperfusion injury in rats]. *Zhongguo ying yong sheng li xue za zhi = Zhongguo yingyong shenglixue zazhi = Chinese journal of applied physiology*. 32 (4), 338–342.

Lin, H., Chen, M., Tian, F., Tikkanen, J., Ding, L., Cheung, H.Y.A., Nakajima, D., Wang, Z., Mariscal, A., Hwang, D., Cypel, M., Kesgavjee, S. & Liu, M. (2018) α1-Anti-trypsin improves function of porcine donor lungs during ex-vivo lung perfusion. *The Journal of heart and lung transplantation*. 37 (5), 656–666.

Liu, G., Vogel, S.M., Gao, X., Javaid, K., Hu, G., Danilov, S.M., Malik, A.B. & Minshall, R.D. (2011) Src phosphorylation of endothelial cell surface intercellular adhesion molecule-1 mediates neutrophil adhesion and contributes to the mechanism of lung inflammation. *Arteriosclerosis, thrombosis, and vascular*

biology. 31 (6), 1342–1350.

Liu, J., Li, L. & Li, X. (2019) Effectiveness of Cryopreserved Amniotic Membrane Transplantation in Corneal Ulceration: A Meta-Analysis. *Cornea*. 38 (4), 454–462.

Liu, Yao, Liu, Yi, Su, L. & Jiang, S. (2014) Recipient-related clinical risk factors for primary graft dysfunction after lung transplantation: a systematic review and meta-analysis. *PloS one*. 9 (3), e92773.

Lonati, C., Bassani, G.A., Brambilla, D., Leonardi, P., Carlin, A., Maggioni, M., Zanella, A., Dondossola, D., Fonsato, V., Grange, C., Camussi, G. & Gatti, S. (2019) Mesenchymal stem cell-derived extracellular vesicles improve the molecular phenotype of isolated rat lungs during ischemia/reperfusion injury. *The Journal of heart and lung transplantation : the official publication of the International Society for Heart Transplantation*. 38 (12), 1306–1316.

Loor, G., Warnecke, G., Villavicencio, M., Smith, M., Kukreja, J., Ardehali, A., Hartwig, M., Daneshmand, M., Hertz, M., Haverich, A., Madsen, J. & Van Raemdonck, D. (2018) Results of the OCS Lung EXPAND International Trial Using Portable Normothermic OCS Lung Perfusion System (OCS) to Recruit and Evaluate Extended Criteria Donor (ECD) Lungs. *The Journal of Heart and Lung Transplantation*. 37 (4), S147.

Lötvall, J., Hill, A.F., Hochberg, F., Buzás, E.I., Di Vizio, D., Gardiner, C., Gho, Y.S., Kurochkin, I. V, Mathivanan, S., Quesenberry, P., Sahoo, S., Tahara, H., Wauben, M.H., Witwer, K.W. & Théry, C. (2014) Minimal experimental requirements for definition of extracellular vesicles and their functions: a position statement from the International Society for Extracellular Vesicles. *Journal of Extracellular Vesicles*. 3 (1), 26913.

Machuca, T.., Cypel, M., Bonato, R., Yeung, J.., Chun, Y.., Juvet, S., Guan, Z., Hwang, D.., Chen, M., Saito, T., Harmantas, C., Davidson, B., Waddell, T.., Liu, M. & Keshavjee, S. (2017) Safety and efficacy of ex vivo donor lung adenoviral IL-10 gene therapy in a large animal lung transplant survival model. *Human Gene Therapy*. 28 (9), 757–765.

Magatti, M., Vertua, E., Cargnoni, A., Silini, A. & Parolini, O. (2018) The Immunomodulatory Properties of Amniotic Cells: The Two Sides of the Coin. *Cell transplantation*. 27 (1), 31–44.

Mamede, A.C., Carvalho, M.J., Abrantes, A.M., Laranjo, M., Maia, C.J. & Botelho, M.F. (2012) Amniotic membrane: from structure and functions to clinical

applications. *Cell and Tissue Research*. 349 (2), 447–458.

Mao, R., Wang, C., Zhang, F., Zhao, M., Liu, S., Liao, G., Li, L., Chen, Y., Cheng, J., Liu, J. & Lu, Y. (2020) Peritoneal M2 macrophage transplantation as a potential cell therapy for enhancing renal repair in acute kidney injury. *Journal of cellular and molecular medicine*. 24 (6), 3314–3327.

Martens, A., Ordies, S., Vanaudenaerde, B., Verleden, S., Vos, R., Van Raemdonck, D., Verleden, G., Roobrouck, V., Claes, S., Schols, D., Verbeken, E., Verfaillie, C. & Neyrinck, A. (2017) Immunoregulatory effects of multipotent adult progenitor cells in a porcine ex vivo lung perfusion model. *Stem Cell Research & Therapy*. 8 (1), 159.

Maxey, T.S., Enelow, R.I., Gaston, B., Kron, I.L., Laubach, V.E. & Doctor, A. (2004) Tumor necrosis factor-alpha from resident lung cells is a key initiating factor in pulmonary ischemia-reperfusion injury. *The Journal of thoracic and cardiovascular surgery*. 127 (2), 541–547.

Maymó, J.L., Riedel, R., Pérez-Pérez, A., Magatti, M., Maskin, B., Dueñas, J.L., Parolini, O., Sánchez-Margalet, V. & Varone, C.L. (2018) Proliferation and survival of human amniotic epithelial cells during their hepatic differentiation. *PLOS ONE*. 13 (1), e0191489.

McAuley, D.., Curley, G.., Hamid, U.., Laffey, J.., Abbott, J., McKenna, D.., Fang, X., Matthay, M.. & Lee, J.. (2014) Clinical grade allogeneic human mesenchymal stem cells restore alveolar fluid clearance in human lungs rejected for transplantation. *American journal of physiology: Lung cellular and molecular physiology*. 309 (9), L809–L815.

Mehaffey, J.H., Charles, E.J., Narahari, A.K., Schubert, S., Laubach, V.E., Teman, N.R., Lynch, K.R., Kron, I.L. & Sharma, A.K. (2018) Increasing Circulating Sphingosine-1-Phosphate Attenuates Lung Injury During Ex Vivo Lung Perfusion. *Journal of Thoracic and Cardiovascular Surgery*. 156 (2), 910–917.

Mehaffey, J.H., Charles, E.J., Sharma, A.K., Salmon, M., Money, D., Schubert, S., Stoler, M.H., Tribble, C.G., Laubach, V.E., Roeser, M.E. & Kron, I.L. (2017) Ex Vivo Lung Perfusion Rehabilitates Sepsis-Induced Lung Injury. *The Annals of thoracic surgery*. 103 (6), 1723—1729.

Melville, J.M., McDonald, C.A., Bischof, R.J., Polglase, G.R., Lim, R., Wallace, E.M., Jenkin, G. & Moss, T.J. (2017) Human amnion epithelial cells modulate the inflammatory response to ventilation in preterm lambs. *PloS one*. 12 (3), e0173572.

Merry, H.E., Phelan, P., Doak, M.R., Zhao, M., Hwang, B. & Mulligan, M.S. (2015) Role of toll-like receptor-4 in lung ischemia-reperfusion injury. *The Annals of thoracic surgery*. 99 (4), 1193–1199.

Miki, T. (2018) Stem cell characteristics and the therapeutic potential of amniotic epithelial cells. *American journal of reproductive immunology (New York, N.Y. : 1989)*. 80 (4), e13003.

Miki, T., Marongiu, F., Dorko, K., Ellis, E.C.S. & Strom, S.C. (2010) Isolation of amniotic epithelial stem cells. *Current protocols in stem cell biology*. 12 (1), 1E – 3.

Moodley, Y., Ilancheran, S., Samuel, C., Vaghjiani, V., Atienza, D., Williams, Elizabeth D, Jenkin, G., Wallace, E., Trounson, A. & Manuelpillai, U. (2010) Human amnion epithelial cell transplantation abrogates lung fibrosis and augments repair. *American journal of respiratory and critical care medicine*. 182 (5), 643–651.

Moodley, Y., Ilancheran, S., Samuel, C., Vaghjiani, V., Atienza, D., Williams, Elizabeth D., Jenkin, G., Wallace, E., Trounson, A. & Manuelpillai, U. (2010) Human amnion epithelial cell transplantation abrogates lung fibrosis and augments repair. *American Journal of Respiratory and Critical Care Medicine*. 182 (5), 643–651.

Morales, M., Ceysens, G., Jastrow, N., Viardot, C., Faron, G., Vial, Y., Kirkpatrick, C., Irion, O. & Boulvain, M. (2004) Spontaneous delivery or manual removal of the placenta during caesarean section: a randomised controlled trial. *BJOG: An International Journal of Obstetrics & Gynaecology*. 111 (9), 908–912.

Mordant, P., Nakajima, D., Kalaf, R., Iskender, I., Maahs, L., Behrens, P., Coutinho, R., Iyer, R.., Davies, J.., Cypel, M., Liu, M., Waddell, T.. & Keshavjee, S. (2016) Mesenchymal stem cell treatment is associated with decreased perfusate concentration of IL-8 during ex vivo perfusion of donor lungs after 18h preservation. *Journal of Heart and Lung Transplantation*. 35 (10), 1245–1254.

Morrison, M.I., Pither, T.L. & Fisher, A.J. (2017) Pathophysiology and classification of primary graft dysfunction after lung transplantation. *Journal of Thoracic Disease*. 9 (10), 4084–4097.

Motedayyen, H., Esmaeil, N., Tajik, N., Khadem, F., Ghotloo, S., Khani, B. & Rezaei, A. (2017) Method and key points for isolation of human amniotic epithelial cells with high yield, viability and purity. *BMC Research Notes*. 10 (1), 552.

Murphy, S., Rosli, S., Acharya, R., Mathias, L., Lim, R., Wallace, E. & Jenkin, G.

(2010) Amnion epithelial cell isolation and characterization for clinical use. *Current Protocols in Stem Cell Biology*. (SUPPL. 13), 1–25.

Murphy, S. V, Kidyoor, A., Reid, T., Atala, A., Wallace, E.M. & Lim, R. (2014) Isolation, Cryopreservation and Culture of Human Amnion Epithelial Cells for Clinical Applications. *Journal of Visualized Experiments*. (94), 4–11.

Murphy, S. V, Shiyun, S.C., Tan, J.L., Chan, S., Jenkin, G., Wallace, E.M. & Lim, R. (2012) Human amnion epithelial cells do not abrogate pulmonary fibrosis in mice with impaired macrophage function. *Cell transplantation*. 21 (7), 1477–1492.

Naidu, B. V, Woolley, S.M., Farivar, A.S., Thomas, R., Fraga, C.H., Goss, C.H. & Mulligan, M.S. (2004) Early tumor necrosis factor-α release from the pulmonary macrophage in lung ischemia-reperfusion injury. *Cardiothoracic transplantation*. 127 (5), 1502–1508.

Nakajima, D., Chen, F., Yamada, T., Sakamoto, J., Ohsumi, A., Bando, T. & Date, H. (2012) Reconditioning of lungs donated after circulatory death with normothermic ex vivo lung perfusion. *The Journal of heart and lung transplantation : the official publication of the International Society for Heart Transplantation*. 31 (2), 187–193.

Nakajima, D., Cypel, M., Bonato, R., Machuca, T.N., Iskender, I., Hashimoto, K., Linacre, V., Chen, M., Coutinho, R., Azad, S., Martinu, T., Waddell, T.K., Hwang, D.M., Husain, S., Liu, M. & Keshavjee, S. (2016) Ex Vivo Perfusion Treatment of Infection in Human Donor Lungs. *American Journal of Transplantation*. 16 (4), 1229–1237.

Nakajima, D., Watanabe, Y., Ohsumi, A., Pipkin, M., Chen, M., Mordant, P., Kanou, T., Saito, T., Lam, R., Coutinho, R., Caldarone, L., Juvet, S., Martinu, T., Iyer, R.K., Davies, J.E., Hwang, D.M., Waddell, T.K., Cypel, M., Liu, M., et al. (2019) Mesenchymal stromal cell therapy during ex vivo lung perfusion ameliorates ischemia-reperfusion injury in lung transplantation. *The Journal of heart and lung transplantation : the official publication of the International Society for Heart Transplantation*. 38 (11), 1214–1223.

Ng, C.S.H., Wan, S., Arifi, A.A. & Yim, A.P.C. (2006) Inflammatory Response to Pulmonary Ischemia–Reperfusion Injury. *Surgery Today*. 36 (3), 205–214.

NHSBT (2019) *Annual Activity Report 2018-2019*. [Online] [online]. Available from: https://www.odt.nhs.uk/statistics-and-reports/annual-activity-report/ (Accessed 3 March 2020).

NHSBT (2020) *Annual Activity Report 2019 - 2020*. [Online]

NHSBT (2021) *Annual Activity Report 2020-2021*. [Online] [online]. Available from: https://www.odt.nhs.uk/statistics-and-reports/annual-activity-report/ (Accessed 5 August 2021).

Nubile, M., Dua, H.S., Lanzini, T.E.-M., Carpineto, P., Ciancaglini, M., Toto, L. & Mastropasqua, L. (2008) Amniotic membrane transplantation for the management of corneal epithelial defects: an in vivo confocal microscopic study. *British Journal of Ophthalmology*. 92 (1), 54 LP – 60.

Orens, J.B., Boehler, A., De Perrot, M., Estenne, M., Glanville, A.R., Keshavjee, S., Kotloff, R., Morton, J., Studer, S.M., Van Raemdonck, D., Waddel, T. & Snell, G.I. (2003) A review of lung transplant donor acceptability criteria. *Journal of Heart and Lung Transplantation*. 22 (11), 1183–1200.

Papagianis, P.C., Ahmadi-Noorbakhsh, S., Lim, R., Wallace, E., Polglase, G., Pillow, J.J. & Moss, T.J. (2021) The effect of human amnion epithelial cells on lung development and inflammation in preterm lambs exposed to antenatal inflammation. *PLOS ONE*. 16 (6), e0253456.

Park, E.K., Jung, H.S., Yang, H.I., Yoo, M.C., Kim, C. & Kim, K.S. (2007) Optimized THP-1 differentiation is required for the detection of responses to weak stimuli. *Inflammation research : official journal of the European Histamine Research Society ... [et al.]*. 56 (1), 45–50.

Patterson, G.A., Cooper, J.D., Dark, J.H. & Jones, M.T. (1988) Experimental and clinical double lung transplantation. *Journal of Thoracic and Cardiovascular Surgery*. 95 (1), 70–4.

Pelekanos, R.A., Sardesai, V.S., Futrega, K., Lott, W.B., Kuhn, M. & Doran, M.R. (2016) Isolation and Expansion of Mesenchymal Stem/Stromal Cells Derived from Human Placenta Tissue. *Journal of visualized experiments : JoVE*. (112), 54204.

De Perrot, M., Bonser, R.S., Dark, J., Kelly, R.F., McGiffin, D., Menza, R., Pajaro, O., Schueler, S. & Verleden, G.M. (2005) Report of the ISHLT Working Group on Primary Lung Graft Dysfunction part III: Donor-related risk factors and markers. *Journal of Heart and Lung Transplantation*. 24 (10), 1460–1467.

de Perrot, M., Liu, M., Waddell, T.K. & Keshavjee, S. (2003) Ischemia-reperfusion-induced lung injury. *American journal of respiratory and critical care medicine*. 167 (4), 490–511.

De Perrot, M., Sekine, Y., Fischer, S., Waddell, T.K., McRae, K., Liu, M., Wigle, D.A. & Keshavjee, S. (2002) Interleukin-8 release during early reperfusion predicts

graft function in human lung transplantation. *American journal of respiratory and critical care medicine*. 165 (2), 211–215.

Perry, H.M., Huang, L., Ye, H., Liu, C., Sung, S.-S.J., Lynch, K.R., Rosin, D.L., Bajwa, A. & Okusa, M.D. (2016) Endothelial Sphingosine 1-Phosphate Receptor-1 Mediates Protection and Recovery from Acute Kidney Injury. *Journal of the American Society of Nephrology : JASN*. 27 (11), 3383–3393.

Phan, T.G., Ma, H., Lim, R., Sobey, C.G. & Wallace, E.M. (2018) Phase 1 Trial of Amnion Cell Therapy for Ischemic Stroke. *Frontiers in neurology*. 9198.

Possoz, J., Neyrinck, A. & Van Raemdonck, D. (2019) Ex vivo lung perfusion prior to transplantation: an overview of current clinical practice worldwide. *Journal of thoracic disease*. 11 (4), 1635–1650.

Pratama, G., Vaghjiani, V., Tee, J.Y., Liu, Y.H., Chan, J., Tan, C., Murthi, P., Gargett, C. & Manuelpillai, U. (2011) Changes in Culture Expanded Human Amniotic Epithelial Cells: Implications for Potential Therapeutic Applications. *PLOS ONE*. 6 (11), e26136.

Ren, Y., Chen, Y., Zheng, X., Wang, H., Kang, X., Tang, J., Qu, L., Shao, X., Wang, S., Li, S., Liu, G. & Yang, L. (2020) Human amniotic epithelial cells ameliorate kidney damage in ischemia-reperfusion mouse model of acute kidney injury. *Stem cell research & therapy*. 11 (1), 410.

Reyes, K.., Mason, D.., Thuita, L., Nowicki, E.., Murthy, S.., Pettersson, G.. & Blackstone, E.. (2010) Guidelines for Donor Lung Selection: Time for Revision? *The Annals of Thoracic Surgery*. 89 (6), 1756–1765.

Rooney, I.A. & Morgan, B.P. (1992) Characterization of the membrane attack complex inhibitory protein CD59 antigen on human amniotic cells and in amniotic fluid. *Immunology*. 76541–547.

Runic, R., Lockwood, C.J., LaChapelle, L., Dipasquale, B., Demopoulos, R.I., Kumar, A. & Guller, S. (1998) Apoptosis and Fas Expression in Human Fetal Membranes*. *Journal of Clinical Endocrinology and Metabolism*. 83 (2), 660–666.

Schmidt, E.P., Lee, W.L., Zemans, R.L., Yamashita, C. & Downey, G.P. (2011) On, around, and through: neutrophil-endothelial interactions in innate immunity. *Physiology (Bethesda, Md.)*. 26 (5), 334–347.

Sharma, A.K., Fernandez, L.G., Awad, A.S., Kron, I.L. & Laubach, V.E. (2007) Proinflammatory response of alveolar epithelial cells is enhanced by alveolar macrophage-produced TNF-α during pulmonary ischemia-reperfusion injury.

American journal of physiology. Lung cellular and molecular physiology. 293 (1), L105–L113.

Sheller, S., Papaconstantinou, J., Urrabaz-Garza, R., Richardson, L., Saade, G., Salomon, C. & Menon, R. (2016) Amnion-Epithelial-Cell-Derived Exosomes Demonstrate Physiologic State of Cell under Oxidative Stress. *PloS one*. 11 (6), e0157614–e0157614.

Snell, G.I., Yusen, R.D., Weill, D., Strueber, M., Garrity, E., Reed, A., Pelaez, A., Whelan, T.P., Perch, M., Bag, R., Budev, M., Corris, P.A., Crespo, M.M., Witt, C., Cantu, E. & Christie, J.D. (2017) Report of the ISHLT Working Group on Primary Lung Graft Dysfunction, part I: Definition and grading—A 2016 Consensus Group statement of the International Society for Heart and Lung Transplantation. *Journal of Heart and Lung Transplantation*. 36 (10), 1097–1103.

Steen, S., Ingemansson, R., Eriksson, L., Pierre, L., Algotsson, L., Wierup, P., Liao, Q., Eyjolfsson, A., Gustafsson, R. & Sjöberg, T. (2007) First Human Transplantation of a Nonacceptable Donor Lung After Reconditioning Ex Vivo. *Annals of Thoracic Surgery*. 83 (6), 2191–2194.

Steen, S., Sjiberg, T., Pierre, L., Liao, Q. & Algotsson, L. (2001) Transplantation of lungs from non-neart-beating donnor. *The Lancet*. 356825–829.

Stocks, J. & Quanjer, P.H. (1995) Reference values for residual volume, functional residual capacity and total lung capacity. ATS Workshop on Lung Volume Measurements. Official Statement of The European Respiratory Society. *The European respiratory journal*. 8 (3), 492–506.

Stone, M., Zhao, Y., Smith, J., Weiss, M., Kron, I., Laubach, V. & Sharma, A. (2017) Mesenchymal stromal cell-derived extracellular vesicles attenuate lung ischemia-reperfusion injury and enhance reconditioning of donor lungs after circulatory death. *Respiratory research*. 18 (1), 212.

Stone, M.L., Sharma, A.K., Zhao, Y., Charles, E.J., Huerter, M.E., Johnston, W.F., Kron, I.L., Lynch, K.R. & Laubach, V.E. (2015) Sphingosine-1-phosphate receptor 1 agonism attenuates lung ischemia-reperfusion injury. *American journal of physiology. Lung cellular and molecular physiology*. 308 (12), L1245–L1252.

Strom, S. & Gramignoli, R. (2016) Human amnion epithelial cells expressing HLA-G as novel cell-based treatment for liver disease. *Human Immunology*. 77 (9), 734–9.

Sun, X., Singleton, P.A., Letsiou, E., Zhao, J., Belvitch, P., Sammani, S., Chiang,

E.T., Moreno-Vinasco, L., Wade, M.S., Zhou, T., Liu, B., Parastatidis, I., Thomson, L., Ischiropoulos, H., Natarajan, V., Jacobson, J.R., Machado, R.F., Dudek, S.M. & Garcia, J.G.N. (2012) Sphingosine-1-phosphate receptor-3 is a novel biomarker in acute lung injury. *American journal of respiratory cell and molecular biology*. 47 (5), 628–636.

Tabatabaei, M., Mosaffa, N., Nikoo, S., Bozoegmehr, M., Ghods, R., Kazemnejad, S., Rezania, S., Keshavarzi, B., Arefi, S., Ramezani-Tehrani, F., Mirzadegan, E. & Zarnani, A.-H. (2014) Isolation and Partial Characterization of Human Amniotic Epithelial Cells: The Effect of Trypsin. *Avicenna Journal of Medical Biotechnology*. 6 (1), 10–20.

Tahan, A. & Tahan, V. (2014) Placental amniotic epithelial cells and their therapeutic potential in liver diseases. *Frontiers in Medicine*. 1 (48), 1–4.

Talaie, T., DiChiacchio, L., Prasad, N.K., Pasrija, C., Julliard, W., Kaczorowski, D.J., Zhao, Y. & Lau, C.L. (2021) Ischemia-reperfusion Injury in the Transplanted Lung: A Literature Review. *Transplantation direct*. 7 (2), e652–e652.

Tan, J.L., Chan, S.T., Wallace, E.M. & Lim, R. (2014) Human amnion epithelial cells mediate lung repair by directly modulating macrophage recruitment and polarization. *Cell Transplantation*. 23 (3), 319–328.

Tan, J.L., Lau, S.N., Leaw, B., Nguyen, H.P.T., Salamonsen, L.A., Saad, M.I., Chan, S.T., Zhu, D., Krause, M., Kim, C., Sievert, W., Wallace, E.M. & Lim, R. (2018) Amnion Epithelial Cell-Derived Exosomes Restrict Lung Injury and Enhance Endogenous Lung Repair. *Stem Cells Translational Medicine*. 7 (2), 180–196.

Taniguchi, K., Kawai, T. & Hata, K. (2018) 'Placental Development and Nutritional Environment', in *Developmental Origins of Health and Disease (DOHaD)*. [Online]. Springer. pp. 63–73.

Théry, C., Amigorena, S., Raposo, G. & Clayton, A. (2006) Isolation and characterization of exosomes from cell culture supernatants and biological fluids. *Current protocols in cell biology*. Chapter 3Unit 3.22.

Théry, C., Witwer, K.W., Aikawa, E., Alcaraz, M.J., Anderson, J.D., Andriantsitohaina, R., Antoniou, A., Arab, T., Archer, F., Atkin-Smith, G.K., Ayre, D.C., Bach, J.-M., Bachurski, D., Baharvand, H., Balaj, L., Baldacchino, S., Bauer, N.N., Baxter, A.A., Bebawy, M., et al. (2018) Minimal information for studies of extracellular vesicles 2018 (MISEV2018): a position statement of the International Society for Extracellular Vesicles and update of the MISEV2014 guidelines. *Journal of Extracellular Vesicles*. 7 (1), 1535750.

Tikkanen, J.M., Cypel, M., Machuca, T.N., Azad, S., Binnie, M., Chow, C.-W., Chaparro, C., Hutcheon, M., Yasufuku, K., de Perrot, M., Pierre, A.F., Waddell, T.K., Keshavjee, S. & Singer, L.G. (2015) Functional outcomes and quality of life after normothermic ex vivo lung perfusion lung transplantation. *The Journal of heart and lung transplantation : the official publication of the International Society for Heart Transplantation*. 34 (4), 547–556.

Toronto Lung Transplant Group (1986) Unilateral Lung Transplantation for Pulmonary Fibrosis. *New England Journal of Medicine*. 314 (18), 1140–1145.

Valadi, H., Ekström, K., Bossios, A., Sjöstrand, M., Lee, J.J. & Lötvall, J.O. (2007) Exosome-mediated transfer of mRNAs and microRNAs is a novel mechanism of genetic exchange between cells. *Nature cell biology*. 9 (6), 654–659.

Verleden, S.E., Martens, A., Ordies, S., Neyrinck, A.P., Van Raemdonck, D.E., Verleden, G.M., Vanaudenaerde, B.M. & Vos, R. (2018) Immediate post-operative broncho-alveolar lavage IL-6 and IL-8 are associated with early outcomes after lung transplantation. *Clinical Transplantation*. 32 (4), e13219.

Vosdoganes, P., Lim, R., Koulaeva, E., Chan, S.., Acharya, R., Moss, T.J.. & Wallace, E.. (2013) Human amniotic epithelial cells modulate hyperoxia-induced neonatal lung injury in mice. *Cytotherapy*. 151021–1029.

Warnecke, G., Moradiellos, J., Tudorache, I., Kühn, C., Avsar, M., Wiegmann, B., Sommer, W., Ius, F., Kunze, C., Gottlieb, J., Varela, A. & Haverich, A. (2012) Normothermic perfusion of donor lungs for preservation and assessment with the Organ Care System Lung before bilateral transplantation: A pilot study of 12 patients. *The Lancet*. 380 (9856), 1851–1858.

Warnecke, G., Van Raemdonck, D., Smith, M.A., Massard, G., Kukreja, J., Rea, F., Loor, G., De Robertis, F., Nagendran, J., Dhital, K.K., Moradiellos Díez, F.J., Knosalla, C., Bermudez, C.A., Tsui, S., McCurry, K., Wang, I.-W., Deuse, T., Lesèche, G., Thomas, P., et al. (2018) Normothermic ex-vivo preservation with the portable Organ Care System Lung device for bilateral lung transplantation (INSPIRE): a randomised, open-label, non-inferiority, phase 3 study. *The Lancet. Respiratory medicine*. 6 (5), 357–367.

Weber, D., Cottini, S.R., Locher, P., Wenger, U., Stehberger, P.A., Fasshauer, M., Schuepbach, R.A. & Bechir, M. (2013) Association of intraoperative transfusion of blood products with mortality in lung transplant recipients. *Perioperative Medicine*. 2 (10), 1–5.

Whitson, B.., Prekker, M.., Herrington, C.., Whelan, T.P.., Radosevich, D.., Hertz, M..

& Dahlberg, P.. (2007) Primary graft dysfunction and long-term pulmonary function after lung transplantation. *The Journal of heart and lung transplantation*. 26 (10), 1004–1011.

Whitson, B.A., Nath, D.S., Johnson, A.C., Walker, A.R., Prekker, M.E., Radosevich, D.M., Herrington, C.S. & Dahlberg, P.S. (2006) Risk factors for primary graft dysfunction after lung transplantation. *Journal of Thoracic and Cardiovascular Surgery*. 131 (1), 73–80.

Wierup, P., Haraldsson, Å., Nilsson, F., Pierre, L., Scherstén, H., Silverborn, M., Sjöberg, T., Westfeldt, U. & Steen, S. (2006) Ex Vivo Evaluation of Nonacceptable Donor Lungs. *The Annals of Thoracic Surgery*. 81 (2), 460–466.

Wu, Q., Fang, T., Lang, H., Chen, M., Shi, P., Pang, X. & Qi, G. (2017) Comparison of the proliferation, migration and angiogenic properties of human amniotic epithelial and mesenchymal stem cells and their effects on endothelial cells. *International journal of molecular medicine*. 39 (4), 918–926.

Xiao, J., Lin, F., Pan, L., Dai, H., Jing, R., Lin, J. & Liang, F. (2020) [Dexamethasone on alleviating lung ischemia/reperfusion injury in rats by regulating PI3K/AKT pathway]. *Zhonghua wei zhong bing ji jiu yi xue*. 32 (2), 188–193.

Xie, M., Xiong, W., She, Z., Wen, Z., Abdirahman, A.S., Wan, W. & Wen, C. (2020) Immunoregulatory Effects of Stem Cell-Derived Extracellular Vesicles on Immune Cells. Frontiers in Immunology 11 p.13.

Xu, R., Greening, D.W., Zhu, H.-J., Takahashi, N. & Simpson, R.J. (2016) Extracellular vesicle isolation and characterization: toward clinical application. *The Journal of clinical investigation*. 126 (4), 1152–1162.

Yeung, J.., Wagnetz, D., Cypel, M., Rubacha, M., Koike, T., Chun, Y.., Hu, J., Waddell, T.., Hwang, D.., Liu, M. & Keshavjee, S. (2012) Ex vivo adenoviral vector gene delivery results in decreased vector-associated inflammation pre- and post-lung transplantation. *Molecular therapy: the journal of the American Society of Gene Therapy*. 20 (6), 1204–1211.

Zhang, M., Nakamura, K., Kageyama, S., Lawal, A.O., Gong, K.W., Bhetraratana, M., Fujii, T., Sulaiman, D., Hirao, H., Bolisetty, S., Kupiec-Weglinski, J.W. & Araujo, J.A. (2018) Myeloid HO-1 modulates macrophage polarization and protects against ischemia-reperfusion injury. *JCI insight*. 3 (19), .

Zhang, Q., Sun, J., Huang, Y., Bu, S., Guo, Y., Gu, T., Li, B., Wang, C. & Lai, D. (2019) Human Amniotic Epithelial Cell-Derived Exosomes Restore Ovarian Function by Transferring MicroRNAs against Apoptosis. *Molecular therapy.*

Nucleic acids. 16407–418.

Zhao, B., Zhang, Y., Han, S., Zhang, W., Zhou, Q., Guan, H., Liu, J., Shi, J., Su, L. & Hu, D. (2017) Exosomes derived from human amniotic epithelial cells accelerate wound healing and inhibit scar formation. *Journal of Molecular Histology*. 48 (2), 121–132.

Zhu, D., Tan, J., Maleken, A.S., Muljadi, R., Chan, S.T., Lau, S.N., Elgass, K., Leaw, B., Mockler, J., Chambers, D., Leeman, K.T., Kim, C.F., Wallace, E.M. & Lim, R. (2017) Human amnion cells reverse acute and chronic pulmonary damage in experimental neonatal lung injury. *Stem cell research & therapy*. 8 (1), 257.

Zinne, N., Krueger, M., Hoeltig, D., Tuemmler, B., Boyle, E.C., Biancosino, C., Hoeffler, K., Braubach, P., Rajab, T.K., Ciubotaru, A., Rohde, J., Waldmann, K.H. & Haverich, A. (2018) Treatment of infected lungs by ex vivo perfusion with high dose antibiotics and autotransplantation: A pilot study in pigs. *PLoS ONE*. 5 (13), e0193168.

8   Appendices

8.1   Appendix A: Split lung *ex vivo* lung perfusion SOP

Making homemade Steen

List of equipment/consumables needed:

- Fisher Glass Bottles – 2 litre capacity
- Scales
- Funnel
- 0.2 µM PES sterile filters (Fisher Scientific)
- Dextran 40 (Sigma Aldrich)
- Bovine Serum Albumin Fraction V (Fisher Scientific)
- Sodium Bicarbonate Sol. 7.5% (Sigma Aldrich)
- Calcium Chloride Dihydrate (Sigma Aldrich)
- Krebs-Henseleit Buffer with 2000 mg/L Glucose, Without Calcium Chloride and Sodium Bicarbonate (Sigma Aldrich)

To make 2 litres of stock:

1. Fill 2 litre glass bottle to 1800ml with distilled water, and add 140 g of BSA, 10 g of Dextran 40 and 56 mL of 7.5% Sodium Bicarbonate Solution.
2. Mix on magnetic stirrer plate.
3. Add 1 M Calcium Chloride
4. Mix on magnetic plate whilst adding 2 bottles of powdered Krebs-henseleit buffer
5. Top up to 2 litres with distilled water
6. Once fully dissolved, filter through 0.2 µM sterile filter using vacuum into a sterile 1 litre bottle
7. Label with "Homemade Steen", date and initials

Setting up the circuit

- Open two Medtronic© circuit boxes and remove the circuits
- Place the reservoir onto its spike, adjusting so that the reservoir is just lower than the top of the trolley
- Attach pump head to pump and twist till it clicks in place

- Attach oxygenator by holding down tag and attaching to holder just below reservoir spike. Make sure there are no kinks between reservoir, oxygenator and pump at this point – may need to adjust metal clamps/limbs if necessary
- Feed venous tubing and arterial tubing into the dome hood
- Lock the 6 prong-port located on the arterial tubing into the flow holder, making sure that the flow is facing up towards the dome and that the arterial tube is not twisted.
- Clamp smaller arterial tube before 6 prong port and cut if happy it's clamped correctly
- Clamp the small tubing emerging from the top of the oxygenator
- Clamp below the reservoir to pump and from pump to oxygenator, ready for priming the circuit
- Switch Medtronic© console on and zero the flow rate
- Fill the heater/cooler unit using tap water and a funnel, set to 32°C
- Attach heater/cooler to the oxygenator in the circuit
- Attach corrugated ventilator tubing to each of the ventilator ports then to a green Y tube.
- Connect the Y Tube to a ventilator filter, then connect a endotracheal tube to this

Priming of the circuit

1. Add 1.5L of homemade Steen to each circuit using the dome. Add 7500 units of heparin to each circuit into an inlet port on top of the reservoir
2. De-air the circuit by removing the clamp to the pump head once reservoir is filled. Ensure no air bubbles in pump head before de airing oxygenator
3. Set flow rate to 0.5-1 L/min to circulate the perfusat.
4. Connect the CO_2/N_2 gas to each of the oxygenators and turn on
5. When perfusate is above a temperature of 15°C, do a perfusate blood gas analysis. pH should be between 7.3-7.5 and CO_2 between 3-5. Adjust pH using THAM if needed
6. Let the perfusate circulate for 10-15 minutes before connecting the lungs , making sure a blood gas is taken prior for any further corrections

Surgical preparation of the lungs

1. Open hospital box and take out lungs. Cut open the bag and place lungs into the dissection bowl

2. Leave the lungs inflated

3. Locate exactly where the pulmonary artery (PA) splits into the left and right lung branches

4. Cut down the front and back so the PA opens, ensuring enough is left to cannulate both lungs

5. Cut between the left and right branches to separate (bias this towards the left, as the right PA is shorter)

6. Insert yellow cannulas into both PA branches and secure using 1 usp tie

7. Locate left and right pulmonary vein

8. Insert a green cannula inside left atrium (LA)

9. Cut the green LA cannula cuff down to an appropriate size and then suture this securely in place using a 4-0 prolene

10. Repeat the previous two steps with the right half using the white cannula cuff

11. Dissect down the trachea until the carina is located

12. Dissect around the right side of the carina

13. Clamp just before the left bifurcation and cut the trachea just below, the left lung will now deflate

14. Cannulate the left main bronchus by securing a 3-8 straight connector without port in place with a 1 usp tie

15. Remove the clamp of the right bronchus, the right lung will now deflate

16. Cannulate the right main bronchus by securing a 3-8 straight connector without port in place with a 1 usp tie

17. Weigh each lung on the scale and record the starting weights. Using the weights and the calculated IBW of the donor calculate the 20% and 40% cardiac output (CO)

18. Take tissue biopsy

Perfusion procedure

1. Set flow rate for each lung to 20% CO

2. Attach arterial tubing to the PA cannula, wait until return from the venous cuff cannula is visible and then attach this to the venous tubing

3. Adjust positioning of tubing/lungs on dome if necessary to achieve appropriate LA pressure (if getting a siphoning effect, either use a gate clamp or raise venous tubing up the dome)

4. Increase to 40% CO gradually over 15 minutes of perfusion

5. Place temperature probe where possible on the lungs

6. Prime pressure transducers until all air has been removed and the membrane within the balloon is level then attach the transducer to the back of the console and zero

7. Once the lungs reach 32°C, switch on the ventilator

8. Set the tidal volume and breaths per minute based on the appropriate values for lung temperature and IBW

9. Set PEEP to 5, Pinsp to 15, flow to 19 and O2 to 21

10. Once set, attach bronchiole tree to the lungs, note if the lungs appear to be recruiting

11. Adjust the tidal volume and breaths per minute accordingly as the temperature increases (don't go beyond 2-3 L/min)

12. Increase the heater/cooler temperature to 38°C to achieve a lung temperature of 37°C

13. Record ventilation settings and haemodynamics on monitoring sheets

14. Acquire blood gas to ensure measurements are within parameters and gas exchange is occurring

15. Clamp off the leucocyte filter before proceeding with next step

16. Once the hAECs/HTR cells are stained, infuse these slowly into the 3-way tap located after oxygenator slowly over 10 minutes of each circuit

17. Record haemodynamics every 2 minutes up to 20 minutes, then every 10 minutes up to 60 minutes to ensure no adverse effects occur due to the cell administration

18. Take perfusate samples as required and blood gases hourly. Record haemodynamics and ventilation settings every half an hour.

19. Once perfusion has ended, detach lungs by clamping arterial and venous lines then pulling out cannulas from there.

20. Weigh lungs again, noting down weight and take tissue samples from lungs

21. Take 100 mL of perfusate from each circuit into 2 x 50 mL falcons (keep at 4°C until ready for flow cytometry) then drain circuit.

8.2   Appendix B: Publications, Presentations and Awards

Publications:

Griffiths, C., Charlton, C., Scott, W., Ali, S., Fisher, A.J. (2019). Evaluating the immunomodulatory potential of human amniotic epithelial cells as a therapeutic in ex vivo donor lung reconditioning. *Cytotherapy*, Volume 21, Issue 5, S49 - S50. (Abstract only)

C Griffiths, W E Scott, III, S Ali, A J Fisher. (2020). Maximizing organs for donation: the potential for *ex situ* normothermic machine perfusion, *QJM: An International Journal of Medicine*, hcz321.

J Gilmour, C Griffiths, T Pither, W E Scott, A J Fisher. (2020) Normothermic machine perfusion of donor-lungs ex-vivo: promoting clinical adoption. *Current Opinion in Transplantation.* 25(3): 285-292.

L Milross, C Griffiths, A J Fisher. Ex vivo lung perfusion: a platform for donor lung assessment, treatment and recovery. *Transplantology*. (Accepted)

C Griffiths, L Wang, L Bates, M Brown, CY Pang, J Dark, WE Scott, S Ali, AJ Fisher. Evaluating the immunomodulatory properties of human placenta amniotic epithelial cells as a therapeutic in ex vivo lung reconditioning. (Manuscript under preparation.)

Conferences:

<u>November 2018</u>, North East Postgraduate Conference – Oral Presentation
<u>March 2019</u>, British Transplantation Society Conference – Poster Presentation
<u>May 2019</u>, The International Society for Cell and Gene Therapies – Poster Presentation
<u>September 2021</u>, The. Joint Congress of the International Xenotransplantation Association and Cell Transplant and Regenerative Medicine Society – Oral presentation.

Awards:

PhD Exchange Program travel award between Newcastle & Monash Universities.